Cobalt(II) and Manganese(II) Nitrosyl Complexes as Potential HNO/NO^- Donor

A dissertation submitted to the Indian Institute of Technology Guwahati as Partial fulfillment for the degree of Doctor of Philosophy in Chemistry

Submitted by

Shankhadeep Saha

(Roll No. 186122035)

Supervisor

Prof. Biplab Mondal

Department of Chemistry

Indian Institute of Technology Guwahati

Assam, India

June, 2024

Dedicated to My Parents

STATEMENT

I hereby declare that this thesis entitled "**Cobalt(II) and Manganese(II) Nitrosyl Complexes as Potential HNO/NO^- Donor**" is the outcome of research work carried out by me under the supervision of Prof. Biplab Mondal in the Department of Chemistry, Indian Institute of Technology Guwahati, India.

In keeping with the general practice of reporting scientific observations, due acknowledgements have been made wherever the work described is based on the findings of other investigators.

June, 2024

Shankhadeep Saha

IIT Guwahati

भारतीय प्रौद्योगिकी संस्थान गुवाहाटी
INDIAN INSTITUTE OF TECHNOLOGY GUWAHATI
North Guwahati, Assam – 781039, India

Dr. Biplab Mondal
Professor
Department of Chemistry

Phone : + 91-361-258-2317
Fax: + 91-361-258-2349
E-mail: biplab@iitg.ac.in

Certificate

This is to certify that **Mr. Shankhadeep Saha** has been working under my supervision since July, 2018 as a regular Ph.D. student in the Department of Chemistry, Indian Institute of Technology Guwahati. I am forwarding his thesis entitled "**Cobalt(II) and Manganese(II) Nitrosyl Complexes as Potential HNO/NO$^-$ Donor**" being submitted for the Ph.D. degree.

I certify that he has fulfilled all the requirements according to the ordinance of this Institute regarding the investigations embodied in his thesis and this work has not been submitted elsewhere for a degree.

June, 2024 **(Biplab Mondal)**

Acknowledgement

I would like to mention that behind the success of this wonderful journey lies the contribution of many people I have come across at different stages of life. Their unwavering love, boundless inspiration, and expert guidance have been pivotal in making this endeavor possible. This is a humble attempt on my part to gracefully thank all such people who have stood by me during this expedition. My sincere apologies in advance to those I failed to mention at this moment.

First and foremost, I am immensely grateful to my PhD supervisor Prof. Biplab Mondal. His guidance, support and encouragement have been invaluable throughout my time at IIT Guwahati. His expertise and knowledge have been a great source of inspiration. He let me go off and try things on my own, yet was always available when I needed help or advice. I believe, this combination of independence with reliable safety prepared me well for upcoming days. Words cannot suffice the thankfulness I owe to him.

I'm incredibly grateful to my doctoral committee members, Prof. Gopal Das, Dr. Dipankar Srimani, and Dr. Shyam Prosad Biswas for their invaluable guidance and constructive criticism.

My gratitude extends to the Department of Chemistry and Central Instrument Facility, IITG, for providing instrument facilities and IITG for the financial support. My sincere thanks to all the faculty members and non-teaching staff of the Department of Chemistry, IITG, for their unrestrained help.

The last six years I spent in CHEL004 lab was not so easy. Thanks to my past and present lab mates for helping me through this journey. I extend my sincere gratitude to Baisakhi Di, Dibya Da, Rakesh, Bapan, Riya, Sayani, Bristi, Mrinmoy and Risha for their friendship

and help throughout this process. I would like to express my deepest appreciation to Rakesh for mentoring me during my initial years in lab. All thanks to Riya and Sayani, for the all pep-talks over cups of tea and boosting my spirits when I felt low. Their continuous support and warm humor made this journey easier for me.

My deepest gratitude to all my PhD colleagues for their help and support. Special mention to Debjyoti, Santanu, Somnath, Monuranjan and Prangobinda. They made IITG more enjoyable and more memorable.

I would like to express my deepest gratitude to Bidisha for her continuous support, patience and understanding. Her belief in me and my dreams has given me the strength to persevere through challenges and strive for excellence.

Lastly, I would like to thank the most important people in my life, Ma, Baba and Rimi, for their unconditional love, unwavering support and encouragement over the years. I would have never gotten this far without them. Thank you for believing in me.

I am incredibly honored and grateful for the successful submission of my thesis. It has been a beautiful life venture on the beautiful campus of IITG that will be cherished forever.

Shankhadeep Saha

Indian Institute of Technology Guwahati

List of Abbreviations

Abbreviations	Full Form
BPB^{2-}	1,2-*bis*(2-pyridinecarboxamido)benzene dianion
BPI^{-}	1,3-*bis*(2′-pyridylimino)isoindol anion
DTC^{-}	Diethyldithiocarbamate anion
IM	Imidazole
Nu	Nucleophile
OAc^{-}	Acetate anion
$TMTAA^{2-}$	5,7,12,14-tetramethyldibenzotetraaza[14]annulene dianion
TPP^{2-}	Tetraphenylporphyrin dianion
$TTMPP^{2-}$	5,10,15,20-tetrakis(3,4,5-trimethoxyphenyl)porphyrin dianion
ATR FT-IR	Attenuated Total Reflectance-Fourier Transform Infrared Spectroscopy
EPR	Electron Paramagnetic Resonance Spectroscopy
ESI-mass	Electrospray Ionisation Mass Spectrometry
FT-IR	Fourier Transform Infrared Spectroscopy
GC	Gas Chromatography
GC-MS	Gas Chromatography–Mass Spectrometry
NMR	Nuclear Magnetic Resonance Spectroscopy
SC-XRD	Single Crystal X-ray Diffraction
UV-vis	Ultraviolet-Visible Spectroscopy

Contents

Synopsis

The thesis entitled, "**Cobalt(II) and Manganese(II) Nitrosyl Complexes as Potential HNO/NO^- Donor**" is divided into five chapters.

Chapter 1: Introduction

Nitroxyl (HNO/NO^-) is the one electron reduced form of the well-known biological signaling molecule nitric oxide (NO). Although, HNO and NO share structural similarities, their *in-vivo* production and biological reactivity is different.[1] HNO reacts with itself rapidly to yield hyponitrous acid ($H_2N_2O_2$), which further decomposes to nitrous oxide (N_2O) and H_2O.[2] It can readily react with soft nucleophiles like thiols and produce disulfides or sulfinamides.[3] It is very reactive towards metal and metalloproteins resulting in reductive nitrosylation of the metal centre.[4] Due to these high reactivities, handling of HNO becomes difficult as it is produced *in situ* from HNO donors. The time-resolved direct detection and quantification is also very challenging.

While nitroxyl has been linked to biological activities such as cytotoxicity[5-6] and vasodilatation[7-9] like NO, it also has distinct physiological activity like inhibition of aldehyde dehydrogenase.[10-11] HNO precursor compounds show unusual cardiovascular activity which may be used to prepare protective drugs for heart diseases.[12-14] In addition, iron-nitroxyl complexes are important intermediates in NO and nitrite (NO_2^-) reducing enzymes in bacteria and fungi,[15] which perform important functions in global nitrogen cycle.

As a transient species, the intermediacy of HNO in various reactions has long been a subject of debate.[16-17] Many studies have been done on HNO (gas phase) in relation to the combustion of nitrogen containing compounds.[18-20] HNO can be generated by photolysis of methyl nitrite,[21] or by discharging microwave in a mixture of hydrogen gas and NO.[22-23] Nitroxyl in aqueous

phase is first observed as an intermediate during the decomposition of sodiumtrioxodinitrate, $Na_2N_2O_3$, also known as Angeli's salt.[24] Since then, Angeli's salt has been widely used in the generation of nitroxyl at pH 4 to 8.[25] Many alkylsulfonylhydroxylamine acids are used as a source of nitroxyl at higher pH.[26] Hydroxylamine derivatives *e.g.* Piloty's acid[27] and cyanamide[28] are also used for nitroxyl generation. Transition-metal nitrosyl complexes can also produce HNO *via* proton coupled electron transfer pathway (Scheme S1).[29]

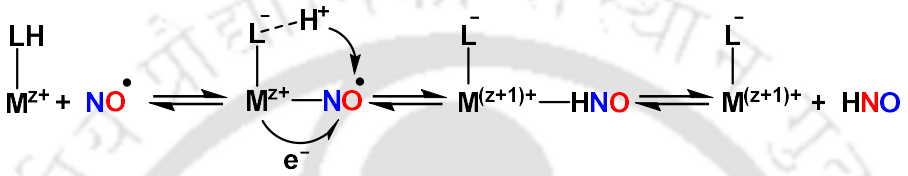

Scheme S1. NO reduction *via* proton coupled electron transfer.

This thesis work is solely focused on the HNO/NO^- release from the transition-metal nitrosyl complexes, especially cobalt(II) and manganese(II)-nitrosyls. A new pathway for HNO/NO^- donation from metal-nitrosyls has been proposed and investigated. The second chapter describes the nitroxyl donation from a cobalt(II)-nitrosyl complex in the presence of sixth ligands like BF_4^- (tetrafluoroborate anion) and DTC^- (diethyldithiocarbamate anion). The third chapter illustrates the reaction of DTC^- with a $\{Co(NO)\}^8$ complex leading to nitroxyl donation. The fourth chapter describes the involvement of neutral imidazole ligand in nitroxyl donation from an electron rich cobalt(II)-nitrosyl complex. In the last chapter, a nitrosyl complex of manganese(II)-porphyrinate was studied as a potential nitroxyl donor.

Chapter 2: Sixth ligand induced HNO/NO^- release by a five-coordinated cobalt(II)-nitrosyl complex having $\{Co(NO)\}^8$ configuration

The precursor complex, $[Co^{II}(BPB^{2-})]$, **2.1** was synthesized and characterized by routine spectroscopic methods.[30] The corresponding nitrosyl complex, $[Co(BPB^{2-})(NO)]$, **2.2**, was

prepared by bubbling NO gas into the dry and degassed methanolic solution of **2.1** and isolated as a green crystalline solid. The nitrosyl complex was characterized both structurally and spectroscopically. The FT-IR spectrum shows nitrosyl stretching frequency at 1662 cm^{-1}. The X-ray crystal structure reveals the bent nature of the coordinated nitrosyl (Figure S1). The oxygen atom associated with the nitrosyl moiety of complex **2.2** occupies two non-equivalent vibrational positions with 50% occupancy each. The observed Co-N-O bond angles in complex **2.2** are 125.2(9)° and 130.2(7)° for Co-N1-O1 and Co-N1-O2, respectively. The N-O bond lengths are 1.045(13) Å and1.119(10) Å for N-O1 and N-O2, respectively.

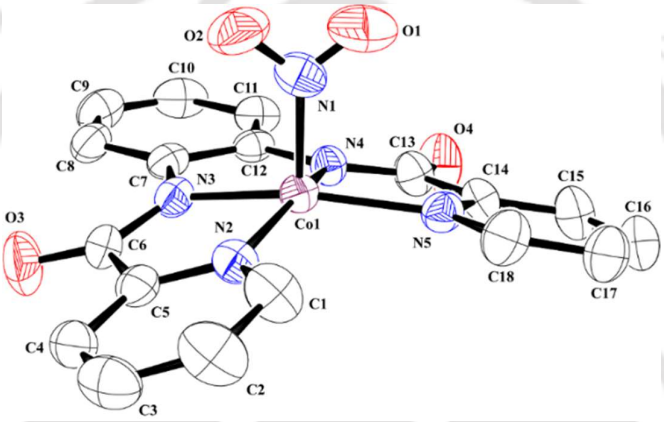

Figure S1. ORTEP diagram of complex **2.2** (40% thermal ellipsoid plot, H-atoms are omitted for clarity).

FT-IR spectral monitoring of the reactivity of complex **2.2** with well-known nitroxyl acceptor, $[Fe^{III}(TPP^{2-})Cl]$ in dry and degassed dichloromethane solution doesn't show any sign of $[Fe(TPP^{2-})(NO)]$ formation even after 24 hours. However, when the reaction was carried out in the presence of one mole equivalent $HBF_4.Et_2O$, the FT-IR spectroscopic study shows the presence of a new stretching frequency at 1698 cm^{-1} suggesting the formation of $[Fe(TPP^{2-})(NO)]$ in the reaction (Figure S2(a)).[31-33] Subjecting the reaction mixture in X-band EPR spectroscopy, an isotropic signal at g ~ 2.04 was observed which also supports the $[Fe(TPP^{2-})(NO)]$ formation (Figure S2(b)).[31-34] Similar results were also observed in presence of imidazole as the sixth ligand.

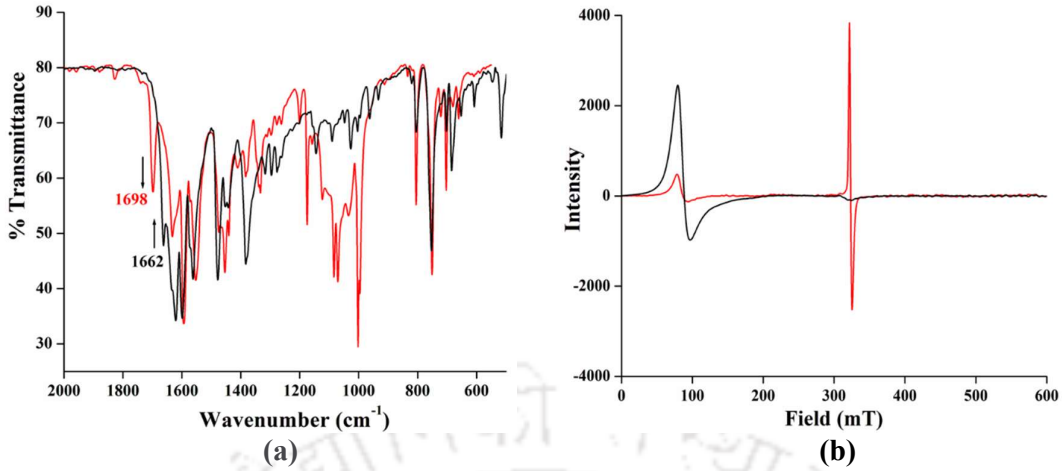

Figure S2. (a) FT-IR (KBr) and (b) X-band EPR (CH_2Cl_2, 77 K) spectroscopic study of the reaction mixture of complex **2.2** and [Fe^{III}(TPP^{2-})Cl] (before HBF_4 addition (black), after HBF_4 addition (red)).

Again, complex **2.2** was made to react with another nitroxyl acceptor, [Fe^{III}(DTC^-)$_3$]. The FT-IR spectrum of the reaction mixture shows a new stretching frequency at 1690 cm^{-1} which is assignable as the nitrosyl stretching of [Fe(DTC^-)$_2$(NO)] complex (Figure S3(a)).[34,35] It is further confirmed by the presence of a signal at g ~ 2.05 in the X-band EPR spectroscopic study (Figure S3(b)).[34,36] It is proposed that [Fe^{III}(DTC^-)$_3$] dissociates during the reaction to give DTC^- which acts as the sixth ligand for complex **2.2** and facilitates the NO^- donation. [Co^{III}(BPB^{2-})(DTC^-)], **2.4** was isolated as the final product which, in turn, supports our proposal.

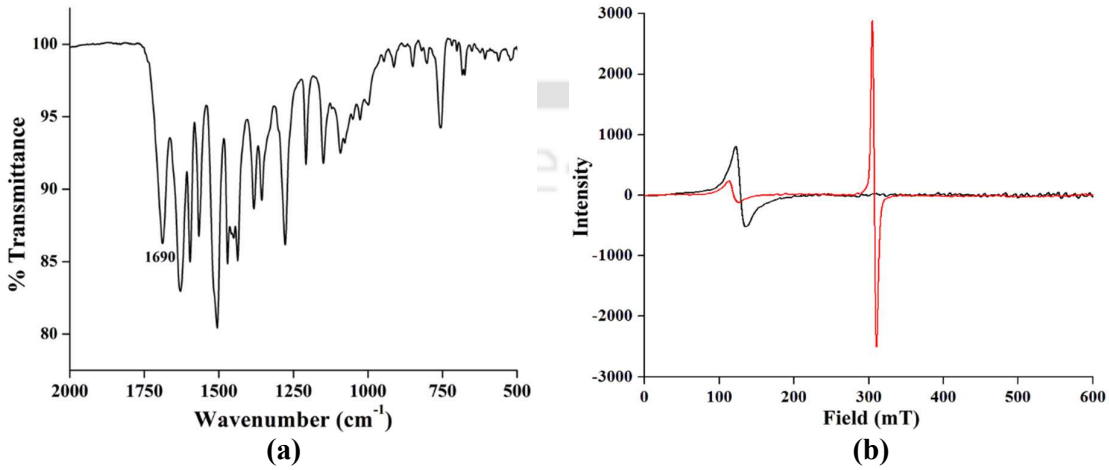

Figure S3. (a) FT-IR (KBr) and (b) X-band EPR (CH_2Cl_2, 77 K) spectroscopic study of the reaction mixture of complex **2.2** and [Fe^{III}(DTC^-)$_3$] (before reaction (black), after reaction (red)).

The gas chromatographic detection of nitrous oxide (N_2O) gas in the headspace of the reaction vessel confirms the HNO release from complex **2.2** in the presence of HBF_4. The characteristic reaction of HNO with PPh_3 was also tested.[37]

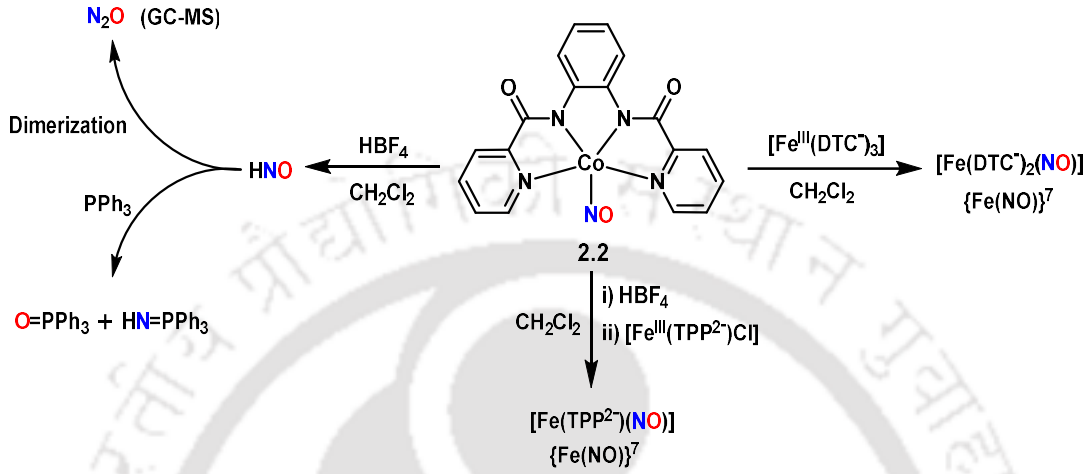

Scheme S2. Overall reactions.

In conclusion, the cobalt-nitrosyl complex, **2.2** was synthesized and characterized spectroscopically and structurally. HNO releasing ability in the presence of a sixth ligand was tested and confirmed using nitroxyl trapping agents such as $[Fe^{III}(TPP^{2-})Cl]$ and $[Fe^{III}(DTC^{-})_3]$. HNO donation was further confirmed using GC-MS and its characteristic reaction with PPh_3.

Chapter 3: Reaction of a cobalt(II)-nitrosyl complex with dithiocarbamate ligand: a potential nitroxyl anion donor

The cobalt-nitrosyl complex, $[Co(BPI^{-})(OAc^{-})(NO)]$, **3.1** was synthesized following a reported procedure.[38] The complex was isolated as a crystalline green solid and characterized using standard spectroscopic techniques as well as single crystal X-ray structure determination. Complex **3.1** shows nitrosyl stretching frequency at 1674 cm^{-1} in KBr. X-band EPR spectroscopic study suggests the diamagnetic nature of the complex, as expected. The X-ray single crystal structure shows that the cobalt centre is penta-coordinated in a distorted square

pyramidal geometry (Figure S4). The oxygen atom of the nitrosyl moiety was found to occupy two symmetry equivalent positions with 50% occupancy each. The observed Co-N-O bond angle is 129.9(3)° and N-O bond length is 1.091(5) Å. Complex **3.1** was found to be quite stable in dichloromethane solution under argon atmosphere.

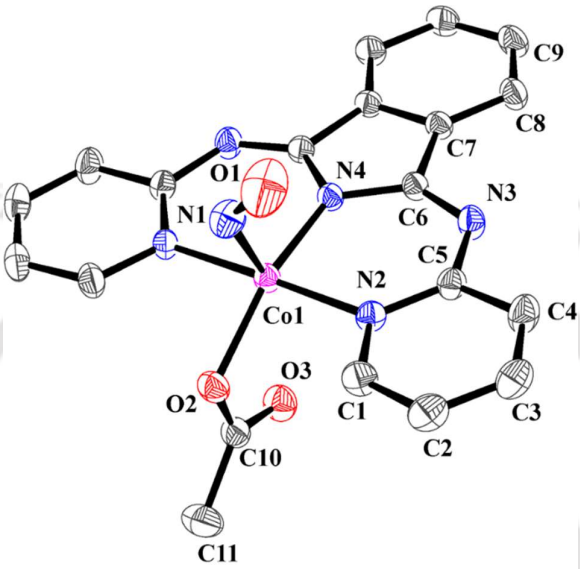

Figure S4. ORTEP diagram of complex **3.1** (30% thermal ellipsoid plot, H-atoms are omitted for clarity).

FT-IR spectroscopic monitoring of the reaction mixture containing complex **3.1** and $[Fe^{III}(TPP^{2-})Cl]$ doesn't show the formation of $[Fe(TPP^{2-})(NO)]$ even after 24 hours. But, upon reaction with $[Fe^{III}(DTC^{-})_3]$, complex **3.1** was found to donate NO^{-}. The FT-IR spectrum of this reaction shows the formation of a stretching frequency at 1688 cm^{-1}, which is the characteristic nitrosyl stretching frequency of $[Fe(DTC^{-})_2(NO)]$ (Figure S5(a)).[34,35] X-band EPR spectroscopic study also suggests the formation of the iron-nitrosyl complex (Figure S5(b)).[34,36] It is believed that DTC^{-} played the role of coordinating ligand and facilitates the release of NO^{-} from complex **3.1**.

To support this, the reaction of complex **3.1** and DTC^{-} (NaDTC) was further studied using various spectroscopic methods. In UV-visible spectroscopic monitoring, addition of one mole equivalent NaDTC (in methanol) to the dry and degassed dichloromethane solution of complex

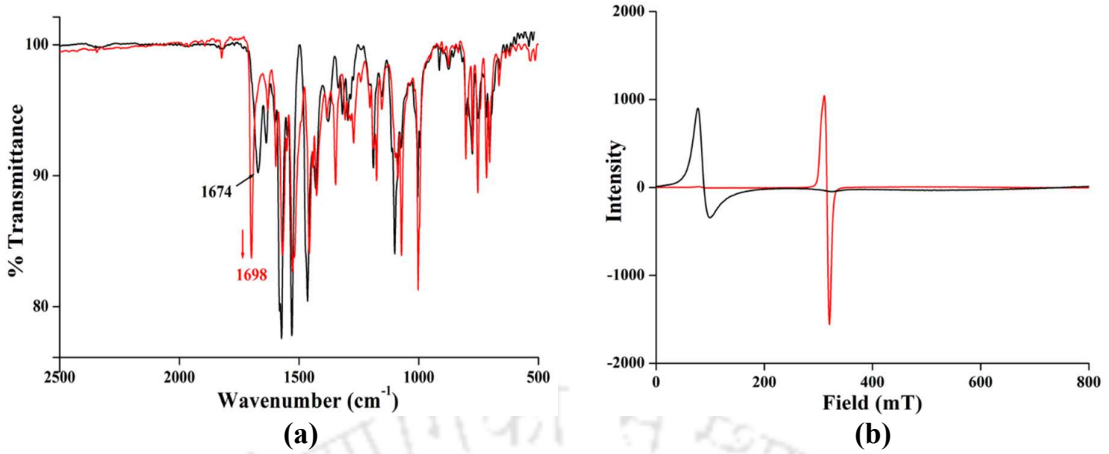

Figure S5. (a) FT-IR (KBr) and (b) X-band EPR (CH_2Cl_2, 77 K) spectra of the reaction mixture of complex **3.1** and [$Fe^{III}(DTC^-)_3$] (before reaction (black), after reaction (red)).

3.1 shows the formation of a new species, complex **3.2** (Figure S6(a)). FT-IR spectroscopic study shows the disappearance of the nitrosyl stretching frequency at 1674 cm^{-1}, and no new stretching frequency associated with any oxidized or reduced analogue of nitrosyl moiety was observed. Complex **3.2** was isolated and characterized spectroscopically as [$Co^{III}(BPI^-)(DTC^-)(OAc)$]. The one-electron oxidation of cobalt centre and the simultaneous disappearance of nitrosyl moiety suggests the NO^- release from complex **3.1** in the presence of DTC^- as sixth ligand. In the presence of $HBF_4.Et_2O$, the complex **3.1** was found to donate HNO which is confirmed by the presence of N_2O in the headspace of the reaction vessel. In the

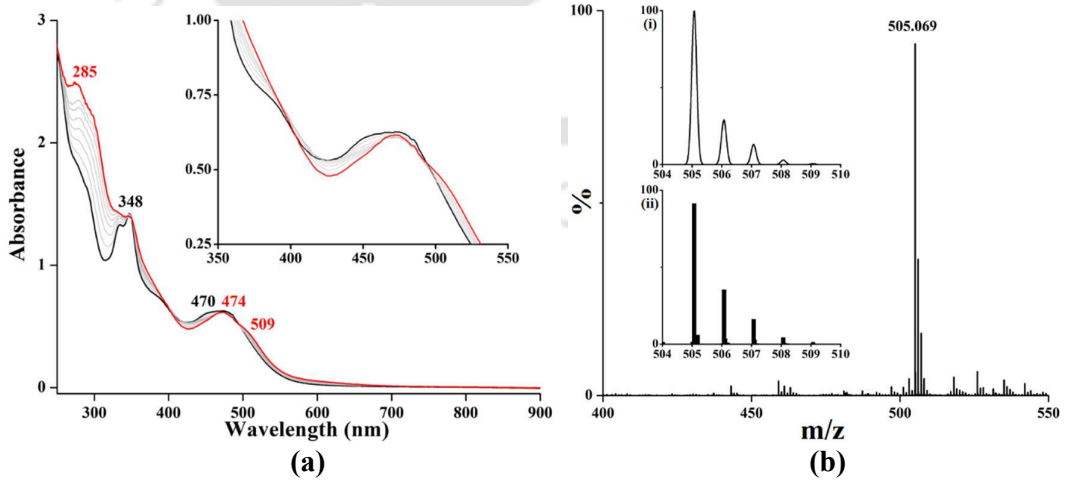

Figure S6. (a) UV-visible spectroscopic study of the reaction of complex **3.1** and NaDTC in CH_2Cl_2 at room temperature [complex **3.1** (black) and after NaDTC addition (red)]. (b) ESI-mass spectrum of complex **3.2** (inset: (i) simulated, (ii) experimental isotopic distribution pattern).

reaction with PPh_3, the formation of azaylide ($Ph_3P{=}NH$) and phosphine oxide ($Ph_3P{=}O$) also observed.

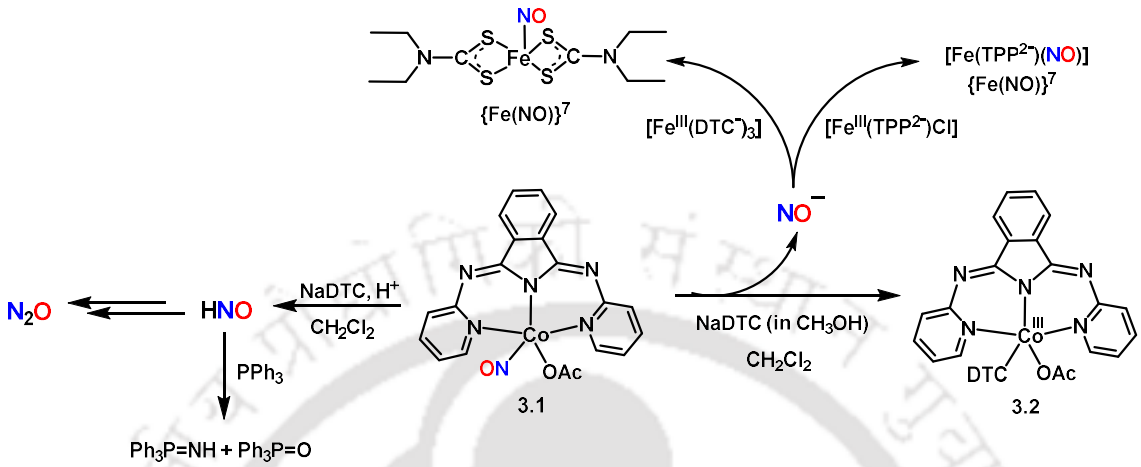

Scheme S3. Overall reactions.

In conclusion, complex **3.1** was found to donate NO^- in the presence of a sixth anionic ligand, DTC^- which is confirmed by the reductive nitrosylation of the nitroxyl trapping iron(III)-complexes. Evolution of nitrous oxide (N_2O) in the presence of proton source and characteristic reaction with PPh_3 also confirm the HNO donation.

Chapter 4: HNO/NO^- release from an electron rich cobalt(II)-nitrosyl complex

The precursor complex, [Co^{II}(TMTAA^{2-})], **4.1** was synthesized and characterized structurally as well as spectroscopically. The nitrosyl complex, [Co(TMTAA^{2-})(NO)], **4.2a** was synthesized by purging NO(g) into the dry and degassed dichloromethane solution of complex **4.1**. Standard spectroscopic characterization supports the formulation of the complex. FT-IR spectrum shows unusually low nitrosyl stretching frequency at 1622 cm^{-1}. The X-ray single crystal structure reveals the bent nature of the nitrosyl moiety with Co-N-O bond angle 125.1(3)° (Figure S7). The Co-N_{NO} and N-O bond lengths are 1.818(3) Å and 1.124(5) Å, respectively. The complex

is found to be diamagnetic as expected.

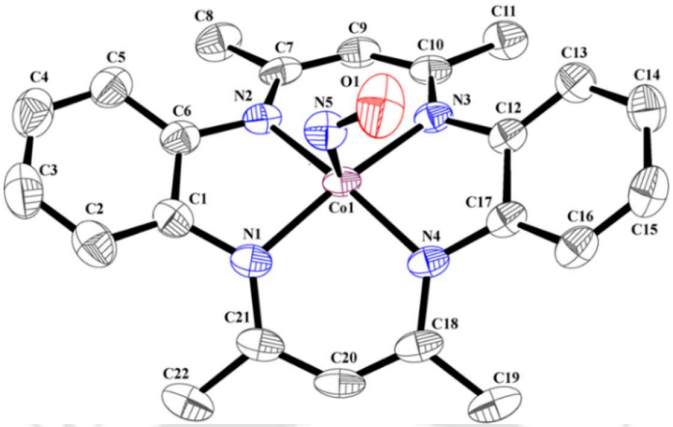

Figure S7. ORTEP diagram of complex **4.2a** (40% thermal ellipsoid plot, H-atoms are omitted for clarity).

The NO^- donation ability of complex **4.2a** was studied by its reaction with [Mn^{III}(TPP)Cl], a very good nitroxyl acceptor.[39] In the presence of a neutral sixth ligand like imidazole (IM), complex **4.2a** was found to donate NO^- to the [Mn^{III}(TPP)Cl]. The FT-IR spectrum of the reaction mixture reveals the presence of nitrosyl stretching frequency at 1759 cm^{-1} confirming the formation of [Mn(TPP)(NO)] (Figure S8).[40] [Mn(TPP)(NO)] was isolated and characterized spectroscopically.

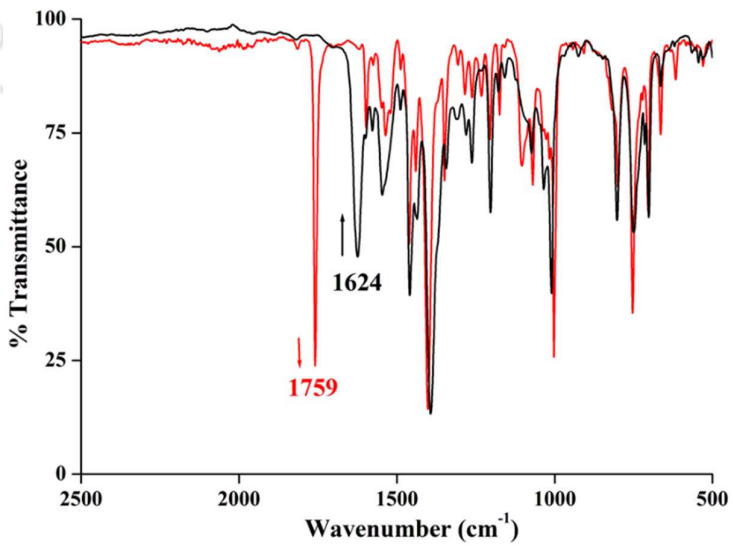

Figure S8. FT-IR (ATR probe) spectrum of the reaction mixture of complex **4.2a** and [Mn^{III}(TPP)Cl] in the absence (black) and presence (red) of imidazole.

The UV-visible spectroscopic study of the reaction of complex **4.2a** with imidazole shows the gradual decrease of intensity of the 399 nm band along with the formation of a new band at 446 nm (Figure S9(a)). The final product was isolated as $[Co^{III}(TMTAA^{2-})(IM)](BPh_4)$, **4.3** which supports the coordination of imidazole to the cobalt centre. X-band EPR spectrum also confirms the presence of Co(III)-centre in complex **4.3**. In ESI-mass spectrum, a signal at m/z = 469.155 (Calculated m/z = 469.155) was observed corresponding to $[Co^{III}(TMTAA^{2-})(IM)]^+$ unit (Figure S9(b)).

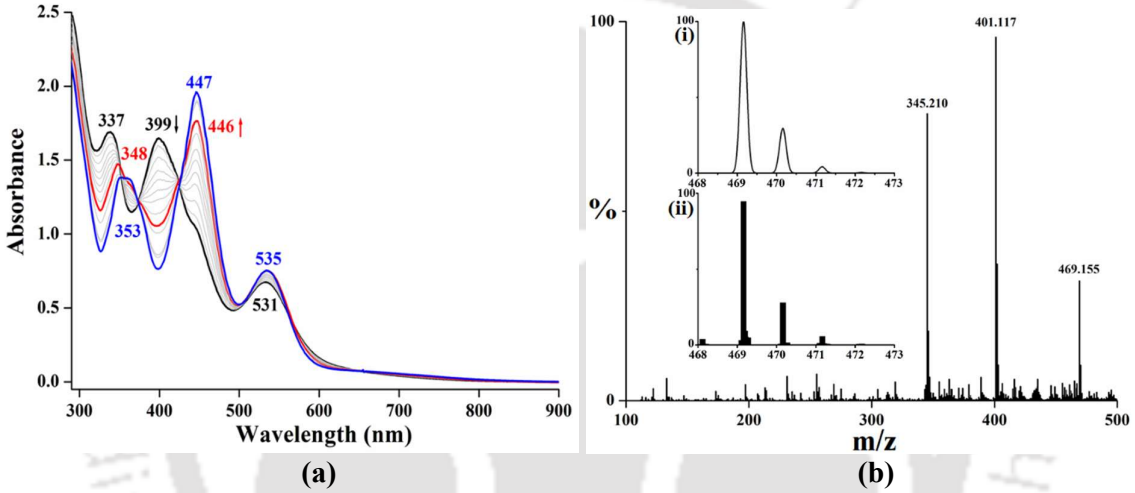

Figure S9. (a) UV-visible spectroscopic study of the reaction of complex **4.2a** and imidazole in CH_2Cl_2 at room temperature [complex **4.2a** (black) and after imidazole addition (red) followed by $NaBPh_4$ addition (blue)]. (b) ESI-mass spectrum of complex **4.3** [inset: (i) simulated, (ii) experimental isotopic distribution pattern.]

The reaction of complex **4.2a** with $[Fe^{III}(TPP^{2-})Cl]$ in the presence of imidazole further confirms the NO^- donation. The FT-IR spectrum of the reaction mixture shows the stretching band at 1698 cm^{-1} confirming the presence of $[Fe(TPP^{2-})(NO)]$ in the reaction medium (Figure S10(a)).[31-33] X-band EPR spectrum of the reaction mixture also supports the same (Figure S10(b)).[31-34]

In the presence of a proton donor, N_2O was produced in the reaction of complex **4.2a** and imidazole which is detected using gas-chromatography. In the reaction with PPh_3, azaylide ($Ph_3P{=}NH$) and phosphine oxide ($Ph_3P{=}O$) were formed, which is confirmed using ^{31}P-NMR.

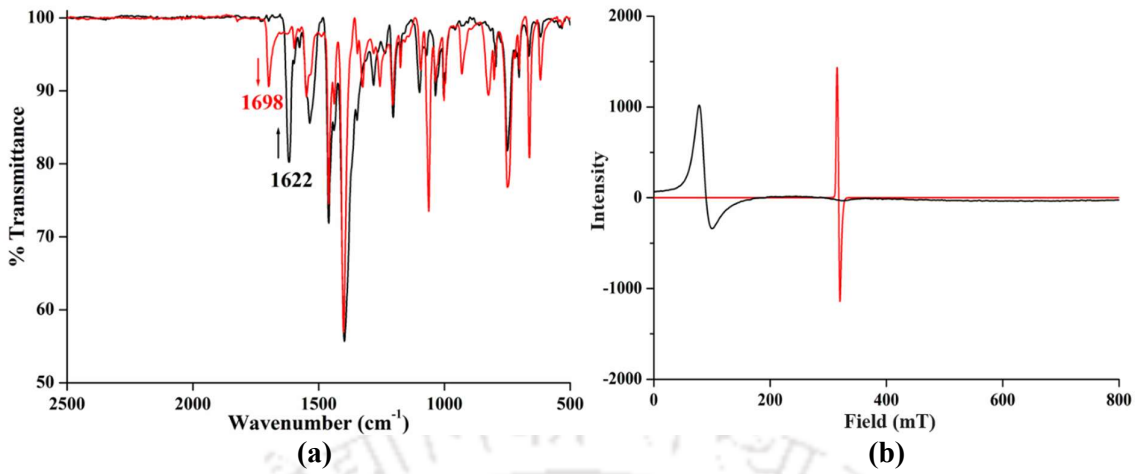

Figure S10. (a) FT-IR (ATR probe) and (b) X-band EPR (CH_2Cl_2, 77 K) spectroscopic study of the reaction mixture of complex **4.2** and [$Fe^{III}(TPP^{2-})Cl$] in the presence of imidazole (before reaction (black), after reaction (red))

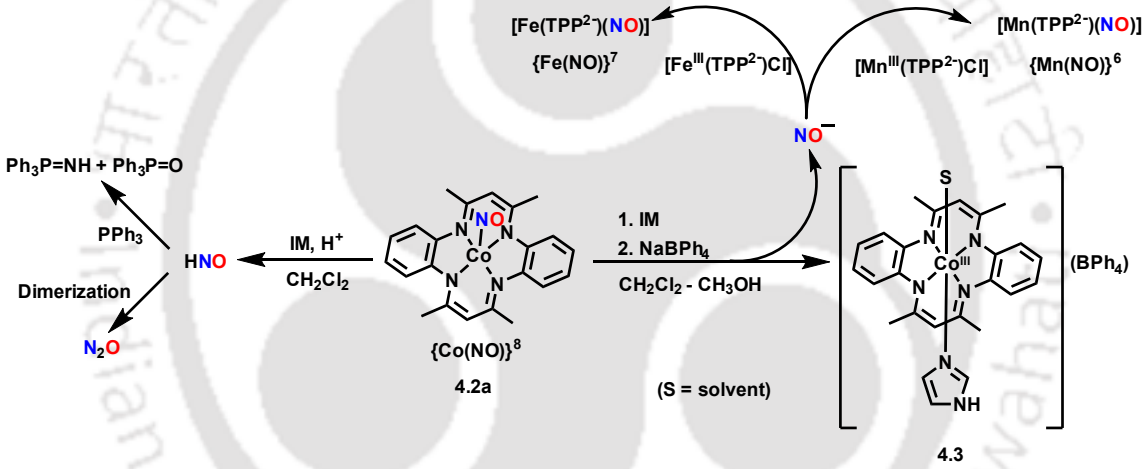

Scheme S4. Overall reactions.

Thus, this work demonstrates NO^- donation from complex **4.2** in the presence of imidazole as the sixth ligand. The NO^- releasing ability was confirmed using [$Mn^{III}(TPP)Cl$] and [$Fe^{III}(TPP^{2-})Cl$]. In presence of H^+, the production of N_2O confirms the HNO release from complex **4.2a**. The formation of azaylide ($Ph_3P=NH$) and phosphine oxide ($Ph_3P=O$) in the reaction with PPh_3 also confirms the same.

Chapter 5: Photo-induced nitroxyl anion/HNO release from a nitrosyl complex of Mn(II)-porphyrinate

The precursor complex, [Mn^{III}($TTMPP^{2-}$)Cl], **5.1** was prepared by following a reported procedure.[41] It was characterized both spectroscopically and structurally. The corresponding nitrosyl complex, [Mn($TTMPP^{2-}$)(NO)], **5.2** was synthesized *via* the reductive nitrosylation of the precursor complex using hydroxylamine.[42] Complex **5.2** was characterized using various spectroscopic techniques such as FT-IR, UV-visible, ^{1}H-NMR, EPR spectroscopy and ESI-mass spectrometry. The FT-IR spectrum shows nitrosyl stretching frequency at 1747 cm^{-1} which shifts to 1740 cm^{-1} upon dissolving it in dichloromethane. The UV-visible spectrum shows characteristic soret band at 416 nm and Q bands at 534 and 562 nm. X-band EPR spectrum and well resolve ^{1}H-NMR spectrum confirm the diamagnetic nature of the complex.

In dry and degassed dichloromethane solution, complex **5.2** was found to be quite stable under argon atmosphere at -40 °C in the absence of light. But upon exposure to visible light, the nitrosyl complex solution changes color from red to green indicating photo-decomposition of the complex. UV-visible spectral monitoring shows rapid decay of the 416 nm band with concomitant formation of a new band at 482 nm suggesting one-electron oxidation of the

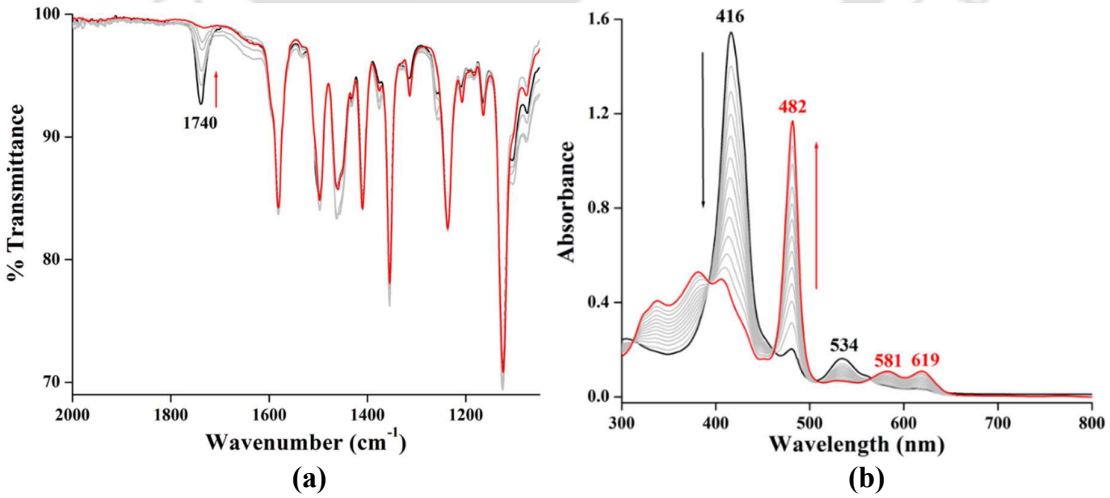

Figure S11. (a) FT-IR (ATR probe) and (b) UV-visible (-40 °C) spectroscopic study of the photo-decomposition of complex **5.2** in CH_2Cl_2 (before (black) and after (red) decomposition).

Mn-centre (Figure S11(b)). FT-IR spectroscopic study of the photo-decomposition in dichloromethane solution also shows gradual disappearance of the nitrosyl stretching frequency at 1740 cm^{-1} (Figure S11(a)).

The green compound was isolated and identified as $[Mn^{III}(TTMPP^{2-})(OH)]$, **5.3**. Addition of methanolic solution of $NaBPh_4$ to the dichloromethane solution of complex **5.2** prior to the exposure in visible light yields complex $[Mn^{III}(TTMPP^{2-})(CH_3OH)_2](BPh_4)$, **5.4** as the decomposition product. The X-ray single crystal structure of complex **5.4** is shown in figure S12. These spectroscopic observations lead to a conclusion that the complex **5.2** releases NO^- in the presence of visible light.

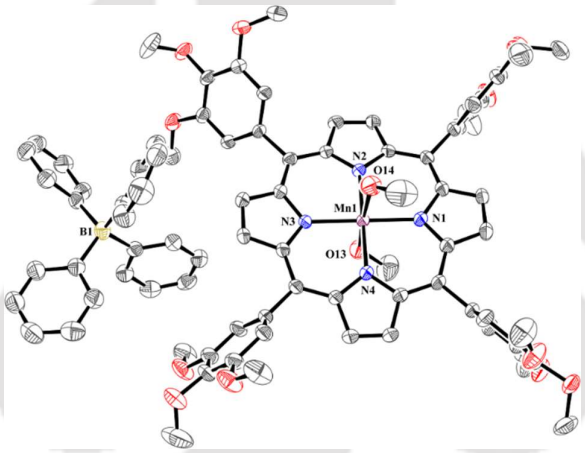

Figure S12. ORTEP diagram of complex **5.4** (40% thermal ellipsoid plot, solvent and H-atoms are omitted for clarity).

The nitroxyl trapping agents, $[Fe^{III}(TPP^{2-})Cl]$ and $[Fe^{III}(DTC^-)_3]$, were used to confirm the NO^- release from complex **5.2**. In the presence of visible light, FT-IR spectrum of the reaction mixture of complex **5.2** and $[Fe^{III}(TPP^{2-})Cl]$ shows the characteristic nitrosyl stretching frequency of $[Fe(TPP^{2-})(NO)]$ at 1698 cm^{-1} while 1747 cm^{-1} stretching signal completely disappeared (Figure S13(a)).[31-33] X-band EPR spectral study also confirms the formation of $[Fe(TPP^{2-})(NO)]$ (Figure S13(b)).[31-34] $[Mn^{III}(TTMPP^{2-})Cl]$, **5.1** was isolated as the final product.

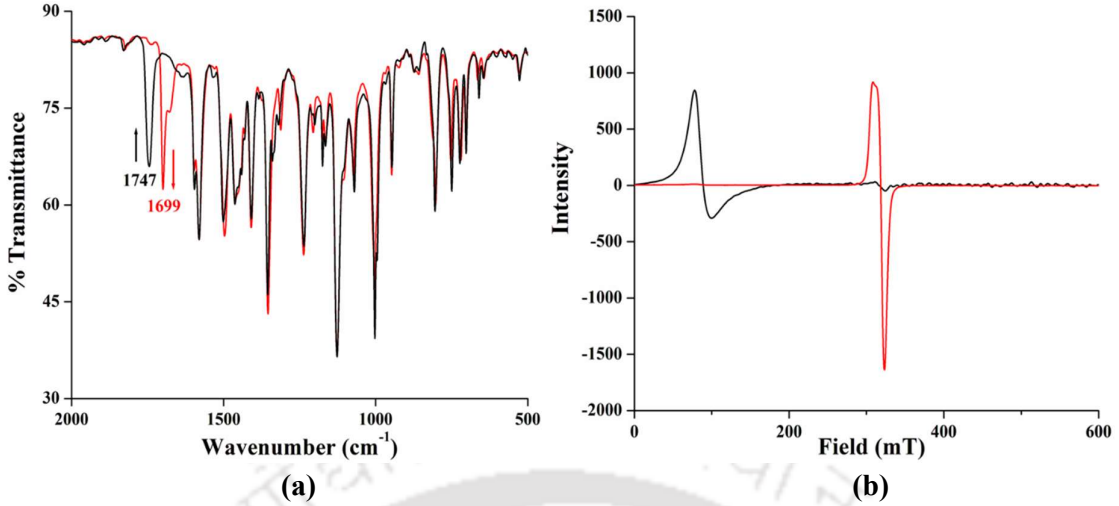

Figure S13. (a) FT-IR (ATR probe) and (b) X-band EPR (CH_2Cl_2, 77 K) spectroscopic study of the reaction mixture of **5.2** and [$Fe^{III}(TPP^{2-})Cl$] (before reaction (black), after reaction (red)).

The reaction of complex **5.2** with [$Fe^{III}(DTC^{-})_3$] also shows a similar result. Upon exposing the reaction mixture of complex **5.2** and [$Fe^{III}(DTC^{-})_3$] to visible light, the formation of the nitrosyl stretching frequency at 1690 cm^{-1} in the FT-IR spectrum suggests the formation of [$Fe(DTC^{-})_2(NO)$] during the reaction (Figure S14(a)).[34-35] A sharp signal at g ~ 2.04 in X-band EPR spectrum also suggests the same (Figure S14(b)).[34,36] [$Mn^{III}(TTMPP^{2-})(DTC^{-})$], **5.5** was isolated as final product.

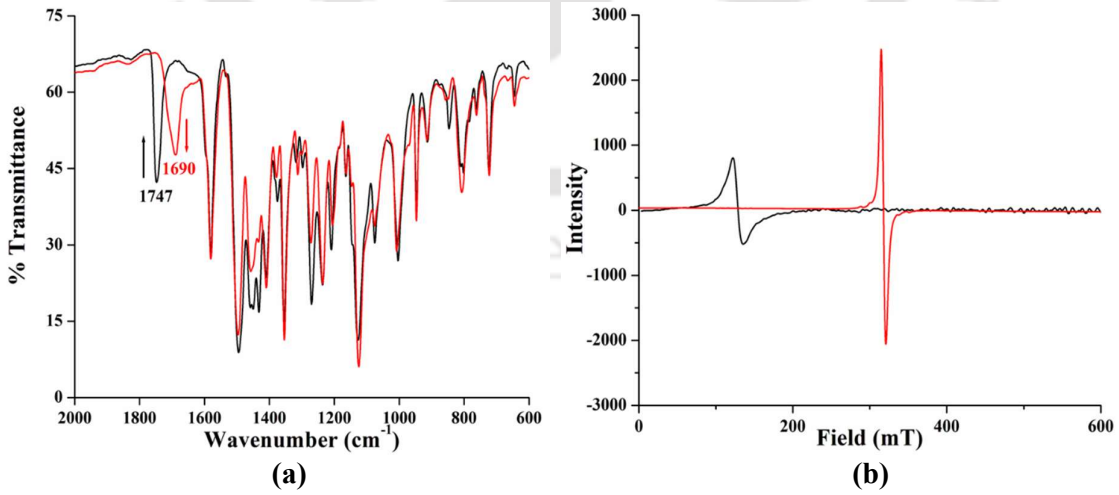

Figure S14. (a) FT-IR (ATR probe) and (b) X-band EPR (CH_2Cl_2, 77 K) spectroscopic study of the reaction mixture of **5.2** and [$Fe^{III}(DTC^{-})_3$] (before reaction (black), after reaction (red)).

In the presence of a proton source, formation of N_2O in the reaction vessel was observed, as expected. In the reaction of complex **5.2** and PPh_3 in presence of H^+, formation of azaylide ($Ph_3P{=}NH$) and phosphine oxide ($Ph_3P{=}O$) was also observed in ^{31}P NMR.[37]

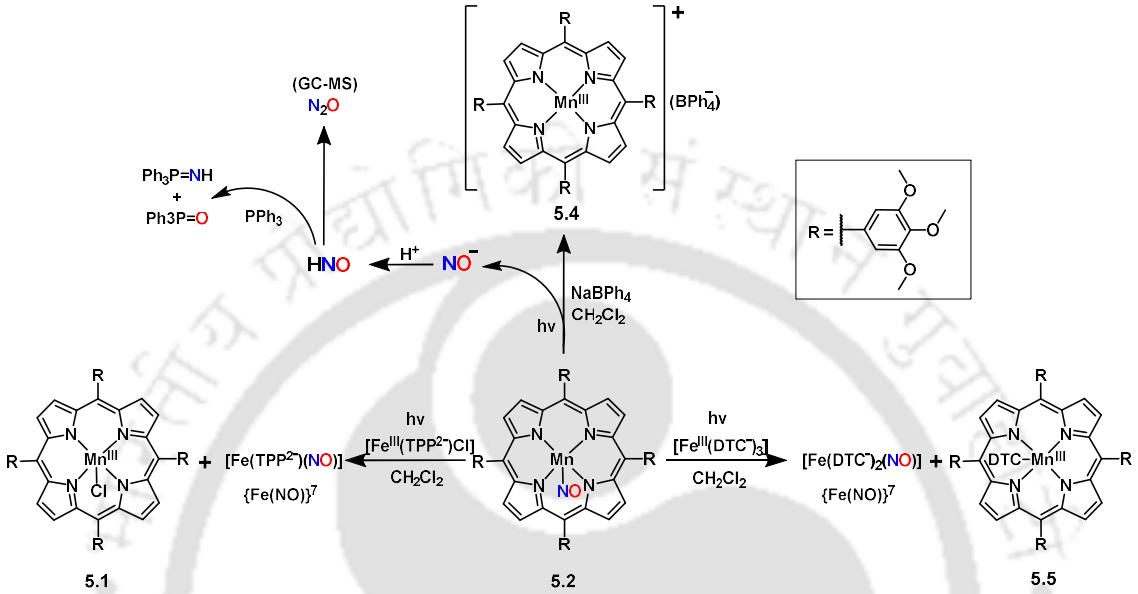

Scheme 5: Overall reactions.

In summary, a manganese-nitrosyl complex, **5.2** was synthesized in an electron-rich porphyrin framework which is found to be decomposing upon exposure to visible light. Spectroscopic analyses suggest one-electron oxidation of Mn-centre during the photo-decomposition with simultaneous release of NO^-. NO^- release was confirmed by its reaction of with $[Fe^{III}(TPP^{2-})Cl]$ and $[Fe^{III}(DTC^-)_3]$. HNO formation was observed in the presence of H^+ which was confirmed from GC-MS and its characteristic reaction with PPh_3.

References:

1. Paolocci, N.; Jackson, M. I.; Lopez, B. E.; Miranda, K.; Tocchetti, C. G.; Wink, D. A.; Hobbs, A. J.; Fukuto, J. M. *Pharmacol. Ther.* **2007**, *113*, 442.
2. Shafirovich, V.; Lymar, S. V. *Proc. Natl. Acad. Sci. U. S. A*. **2002**, *99*, 7340.

3. Wong, Y.; Hyun, J.; Fukuto, J. M.; Shirota, F. N.; DeMaster, E. G.; Shoeman, D. W.; Nagasawa, H. T. *Biochemistry*, **1998**, *37*, 18129.
4. Doyle, M. P.; Mahapatro, S. N.; Broene, R. D.; Guy, J. K. *J. Am. Chem. Soc.* **1988**, *110,* 593.
5. Wink, D. A.; Feelisch, M.; Fukuto, J.; Chistodoulou, D.; Jourd'heuil, D.; Grisham, M. B.; Vodovotz, Y.; Cook, J. A.; Krishna, M.; DeGraff, W. G.; Kim, S. M.; Gamson, J.; Mitchell, J. B. *Arch. Biochem. Biophys*. **1998**, *351*, 66.
6. Lipton, S. A.; Singel, D. J.; Stamler, J. S. *Ann. N.Y. Acad. Sci.* **1994**, *738*, 382.
7. Fukuto, J. M.; Chiang, K.; Hszieh, R.; Wong, P.; Chaudhuri, G. *J. Pharmacol. Exp. Ther.* **1992**, *263*, 546.
8. Fukuto, J. M.; Chiang, K.; Gulati, P.; Chiang, K. T.; Nagasawa, H. T. *Biochem. Biophys. Res. Commun.* **1992**, *187*, 1367.
9. Fukuto, J. M.; Gulati, P. *Biochem. Pharmacol.* **1994**, *47*, 922.
10. Nagasawa, H. T.; Shirota, F. N.; DeMaster, E. G. Biomedical Chemistry. **2000**, pp. 73.
11. Shoeman, D. W.; Shirota, F. N.; DeMaster, E. G.; Nagasawa, H. T. *Alcohol (New York).* **2000**, *20*, 55.
12. Paolocci, N.; Saavedra, W. F.; Miranda, K. M.; Martignani, C.; Isoda, T.; Hare, J. M.; Espey, M. G.; Fukuto, J. M.; Feelisch, M.; Wink, D. A.; Kass, D. A. *Proc. Natl. Acad. Sci. U.S.A.* **2001**, *98*, 10463.
13. Paolocci, N.; Katori, T.; Champion, H. C.; St. John, M. E.; Miranda, K. M.; Fukuto, J. M.; Wink, D. A.; Kass, D. A. *Proc. Natl. Acad. Sci. U.S.A.* **2003**, *100*, 5537.
14. Feelisch, M. *Proc. Natl. Acad. Sci. U.S.A.* **2003**, *100*, 4978.
15. Lehnert, N.; Berto, T. C.; Galinato, M. G. I.; Goodrich, L. E. *The Role of Heme-Nitrosyls in the Biosynthesis, Transport, Sensing, and Detoxification of Nitric Oxide (NO) in Biological Systems: Enzymes and Model Complexes. In The Handbook of*

Porphyrin Science; Kadish K. M.; Smith, K. M.; Guilard, R., Eds.; World Scientific: Hackensack, NJ, **2011**; Vol. 14; Chap. 63, pp 1−247.

16. Raschig, F. *Angew. Chem*. **1928**, *41*, 207.
17. Andrussov, L. *Angew. Chem.* **1928**, *41*, 262.
18. Clough, P. N.; Thrush, B. A.; Ramsay, D. A.; Stamper, J. G. *Chem. Phys. Lett.* **1973**, *23*, 155.
19. Johns, J. W. C.; McKellar, A. R. W. *J. Chem. Phys.* **1977**, *66*, 1217.
20. Anderson, W. R. *Combust. Flame.* **1999**, *117*, 394.
21. Brown, H. W.; Pimentel, G. C. *J. Chem. Phys.* **1958**, *29*, 883.
22. Kohout, F. C.; Lampe, F. W. *J. Am. Chem. Soc.* **1965**, *87*, 5795.
23. Jacox, M. E.; Milligan, D. E. J. *J. Mol. Spectrosc.* **1973**, *48*, 536.
24. Angeli, A. *Gazz. Chim. Ital.* **1903**, *33*, 245.
25. Hughes, M. N.; Cammack, R. *Meth. Enzymol*. **1999**, *301*, 279.
26. King, S. B.; Nagasawa, T. *Meth. Enzymol.* **1999**, *301*, 211.
27. Bonner, F. T.; Ko, Y. H. *Inorg. Chem*. **1992**, *31*, 2514.
28. Nagasawa, H. T.; Demaster, E. G.; Redfern, B.; Shirota, F. N.; Goon, J. W. *J. Med. Chem.* **1990**, *33*, 3120.
29. Ivanovic-Bburmazovic, I.; *The Chemistry and Biology of Nitroxyl (HNO),* Doctorovich, F.; Farmer, P. J.; Marti, M. A. Eds.; Elsevier, **2017**, 67.
30. Chapman, R. L.; Vagg, R. S. *Inorg. Chim. Acta.* **1979**, *33*, 227.
31. Bari, S. E.; Martí, M. A.; Amorebieta, V. T.; Estrin, D. A.; Doctorovich, F. *J. Am. Chem. Soc.* **2003**, *125*, 15272.
32. Doyle, M. P.; Mahapatro, S. N.; Broene, R. D.; Guy, J. K. *J. Am. Chem. Soc*. **1988**, *110*, 593.
33. Miranda, K. M.; Nims, R. W.; Thomas, D. D.; Espey, M. G.; Citrin, D.; Bartberger, M.

D.; Paolocci, N.; Fukuto, J. M.; Feelisch, M.; Wink, D. A. *J. Inorg. Biochem.* **2003**, *93*, 52.

34. Mazumdar, R.; Saha, S.; Samanta, B.; Mondal B. *Inorg. Chem*. **2021**, *60*, 18024.
35. Ileperuma, O. A.; Feltham, R. D. *Inorg. Chem.* **1977**, *16*, 1876.
36. Komarov, A. M.; Reef, A.; Schmidt, H. H. H. W. *Methods in Enzymology*, **2002**, *359*, 18.
37. Reisz, J. A.; Klorig, E. B.; Wright, M. W.; King, S. B. *Org. Lett*. **2009**, *11*, 2719.
38. Gogoi, K.; Saha, S.; Mondal, B.; Deka, H.; Ghosh, S.; Mondal, B. *Inorg. Chem*. **2017**, *56*, 14438.
39. Martí, M. A.; Bari, S. E.; Estrin, D. A.; Doctorovich, F. *J. Am. Chem. Soc*. **2005**, *127*, 4680.
40. Wayland, B. B.; Olson, L. W.; Siddiqui, Z. U. *J. Am. Chem. Soc.* **1976**, *98*, 94.
41. Tong, S. L.; Zhang, J.; Yan, Y.; Hu, S.; Yu, J.; Yu, L. *Solid State Sci.* **2011**, *13*, 1320.
42. Choi, In-K.; Liu, Y.; Wei, Z.; Ryan, M. D. *Inorg. Chem.* **1997**, *36*, 3113.

Chapter 1

Introduction

1.1 General aspect of nitroxyl anion

Nitroxyl (HNO/NO^-; variously called azanone, nitrosyl hydride, etc.) is the redox sibling of the important biological signaling molecule nitric oxide (NO). This one electron reduced and protonated species is considered to be involved in various physiochemical activities.[1] Although NO and HNO shares structural similarities, the endogenous formation and biological role of HNO is distinct from NO which is reflected in its novel chemical and chemicophysical properties.[2] While HNO/NO^- considered as a potent inotropic agent, NO shows more balanced veno/arterial dilation and negligible inotropic response.[3] Lately, HNO is considered to be an important therapeutic agent involved in the prevention of cardiovascular diseases and controlling myocardial contractility.[4] Moreover, it can act as an anti-oxidant and shows anti-cancer properties.[5]

The endogenous production of HNO can be observed in numerous biochemical processes. According to the recent studies, HNO can be produced from NOS itself or its oxidative intermediates like hydroxylamine and *N*-hydroxy-L-arginine.[6,7] HNO can also be produced from the reduction of nitric oxide by mitochondrial cytochrome c, xanthine oxidase, haemoglobin, ubiquinol and manganese superoxide dismutase.[8,9] HNO can also produced from the reaction of S-nitrosothiols with other thiol species.[6,10]

The endogenous formation and biological role of HNO is enigmatic because of its high reactivity towards itself (dimerization), transition metals and soft nucleophiles. HNO rapidly dimerizes to hyponitrous acid ($H_2N_2O_2$; $k_{dim} = 8 \times 10^6\ M^{-1}\ s^{-1}$) which further dehydrates to give nitrous oxide (N_2O).[11] Free HNO also reacts with soft nucleophiles like thiols to produce sulfonamides or disulfides.[12] Besides these sulfur species, HNO can readily react with

metals/metalloproteins. The interaction of HNO with ferric heme was reported earlier, which indicates its ability to react with methemoglobin ($HbFe^{3+}$)/ or metmyoglobin ($MbFe^{3+}$) to form ferrous nitrosyl ($MbFe^{2+}$-NO) complex.[13,14]

Due to this reactive nature, the direct detection and quantification of HNO is very challenging. Several secondary or indirect methods were used to detect HNO. As mentioned earlier, HNO reacts with itself to form hyponitrous acid ($H_2N_2O_2$), which further decomposes to N_2O and H_2O. Thus, in many studies, the presence of N_2O as an end product considered to be a chemical marker for HNO. Furthermore, HNO shows characteristic reaction towards PPh_3 to yield aza-ylide and phosphine oxide. [15] This reaction is also used for the *in situ* detection of HNO. Transition metal complexes like metMb or its synthetic analogues can be used as a trap for HNO and produces EPR active species.[16] Also, fluorescent probes like TEMPO-9-AC or CuDHX1 were developed for HNO detection in biological samples.[17,18]

Unlike the other small molecule nitrogen species like nitrate (NO_3^-), nitrite (NO_2^-), nitric oxide (NO), nitrogen dioxide (NO_2) or ammonia (NH_3), it is impossible to collect, store or quantify HNO conveniently due to the self-reactivity. Hence, HNO donor species are required. Harteck reported the first attempt of laboratory synthesis of HNO by reacting H atom with NO at -196 °C, which yields hygroscopic yellow solid described as $[HNO]_n$.[19] Nowadays, Angeli's salt ($Na_2N_2O_3$) and Piloty's acid (*N*-hydroxybenzenesulfonamide) are mostly used as a source of HNO. Cyanamide, acyl or acyloxy nitroso compounds can also produce HNO under specific reaction conditions. The donation methods are described below.

Angeli's Salt

In 1896, Angelo Angeli synthesized $Na_2N_2O_3$ (sodium trioxodinitrate), which is commercially known as Angeli's salt.[20a] It's a white solid (mp = 284 ºC) isolated from the condensation reaction of hydroxylamine with organic nitrates. This is widely used in chemistry, biology, and

medicinal field as a source of HNO. In aqueous solution, at pH 4 to 8, Angeli's salt gets decomposes and generates singlet HNO.[20b] The first order decomposition rate in aqueous medium is 6.8×10^{-4} s^{-1} at 25 ºC and 4.5×10^{-3} s^{-1} at 37 ºC.[20c] Protonation at the nitroso group of Angeli's salt followed by tautomerization and finally heterolytic N-N bond cleavage yields HNO along with NO_2^- as a by-product.

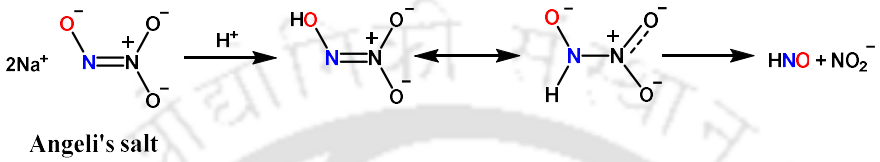

Scheme 1.1. HNO generation from Angeli's salt.

Piloty's Acid

In 1896, *N*-hydroxylbenzenesulfonamide, also known as Piloty's acid was first reported.[21a] It was prepared by the condensation reaction of benzenesulfonyl chloride with hydroxylamine.[21b] Piloty's acid undergo S-N bond heterolysis under basic condition at pH 13 and releases HNO. Benzenesulfinate ion was obtained as a by-product. The first-order decomposition rate at pH 13 is 4.2×10^{-4} s^{-1} at 25 ºC and 1.8×10^{-3} s^{-1} at 37 ºC. These values match well with the Angeli's salt. [21b]

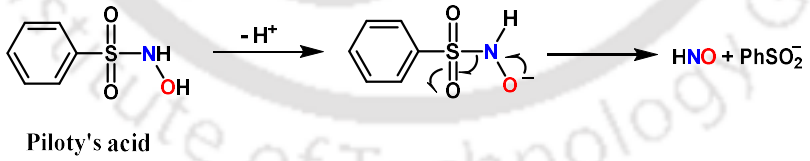

Scheme 1.2. HNO release from Piloty's acid.

Cyanamide

Cyanamide (H_2N-CN) is considered as an antialcoholic drug in Japan, Canada and Europe.[22a] But, the activation of cyanamide is required before utilization. The compound undergoes bioactivation (oxidative) to produce HNO, which is responsible for active site thiol

modification of the ALDH, inhibits the ethanol metabolism.[22b] In the presence of hydrogen peroxide, catalase mediated oxidation of cyanamide results in the formation of *N*-hydroxycyanamide, which further decays to produce nitroxyl and HCN.[22c]

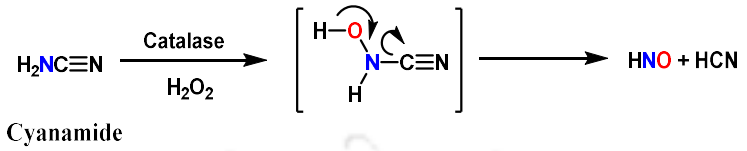

Scheme 1.3. HNO generation from cyanamide.

Acyl Nitroso compounds

These compounds are very reactive species formed during the reaction of N-acyl hydroxylamine derivatives with reagents like Dess-Martin periodinane, tetra-alkyl ammonium periodate, sodium periodate etc.[23] Acyl nitroso compounds readily undergo nucleophilic acyl substitution reaction *via* the formation of a tetrahedral intermediate, which upon decomposition release HNO and corresponding carboxylic acid.

Scheme 1.4. HNO generation from acyl nitroso compound.

Acyloxy Nitroso compounds

These compounds can be easily synthesized by the oxidation of oxime with lead tetraacetate (LTA). Among them, the well known HNO donor 1-nitrosocyclohexyl acetate was prepared *via* the reaction of cyclohexanone oxime with LTA.[24] These nitroso compounds undergo acid or base-catalyzed hydrolysis to give unstable nitroso alcohol, which further decomposes to HNO at biological pH.[24] Corresponding ketone and acid were obtained as a by-product. The HNO donation ability can be modified by modifying the ester group. [24]

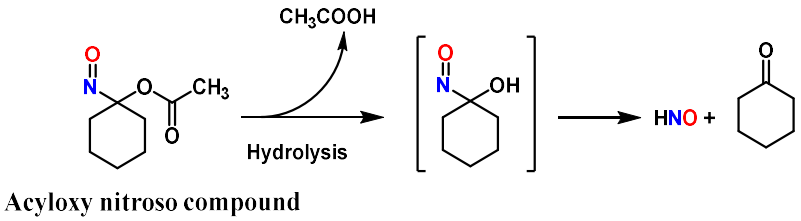

Scheme 1.5. HNO generation from acyloxy nitroso compound.

Although, a number of HNO donors based on organic compounds or inorganic salts have been found effective, but the intrinsic limitations like simultaneous production of undesirable by-products, ineffective release of HNO at physiological pH etc. hinder their widespread utility. For instance, Angeli's Salt, the most commonly used nitroxyl donor, at physiological pH generates HNO and NO_2^- simultaneously. Cyanamide by oxidative activation in the presence of catalase, liberates HNO with the formation of HCN as by-product. Hence, there is a need for more effective HNO donors. As an alternative, metal-bound nitroxyls of suitable electronic configurations could be a good choice for effective release of HNO.

Transition metal mediated HNO formation/release

One-electron reduction of NO requires a potential of about -0.8 (± 0.2) V (vs. NHE) to produce nitroxyl anion ($^3NO^-$), while reduction to $^1NO^-$ is highly unfavourable (-1.7 V vs. NHE).[25] Hence, the reduction of NO is more favourable *via* inner sphere mechanism where proton coupled electron transfer (PCET) takes place. Although, outer sphere electron transfer (OSET) is not favourable due to the high reduction potential, few examples are available in literature. Leipodlt *et al.* reported $[Ru^{II}(NH_3)_6]^{2+}$ mediated direct reduction of NO to NO^-.[26] Lehnert *et al.* also reported NO^- production *via* reaction of free NO with $[Fe(To\text{-}F_2PP)(NO)]^-$ ($To\text{-}F_2PP$ = tetra(*ortho*-difluorophenyl)porphyrin dianion) through outer sphere reaction.[27]

The detoxification of NO through reduction to N_2O was observed in denitrifying bacteria and fungi, which involve NOR enzymes. In *Fusarium oxysporum* (fungi), the reduction takes place

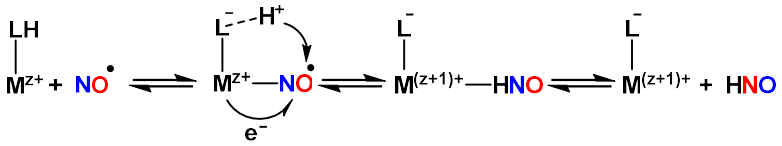

Scheme 1.6. Mechanism for PCET process.

via cytochrome P450 NOR. The proposed mechanism involves the binding of NO to a heme *b* centre with proximal cysteinate ligand coordinated to it at the active site, resulting in the formation of a six coordinated ferric heme-nitrosyl complex which is reduced afterwards by NAD(P)H to corresponding ferrous HNO species.[28]

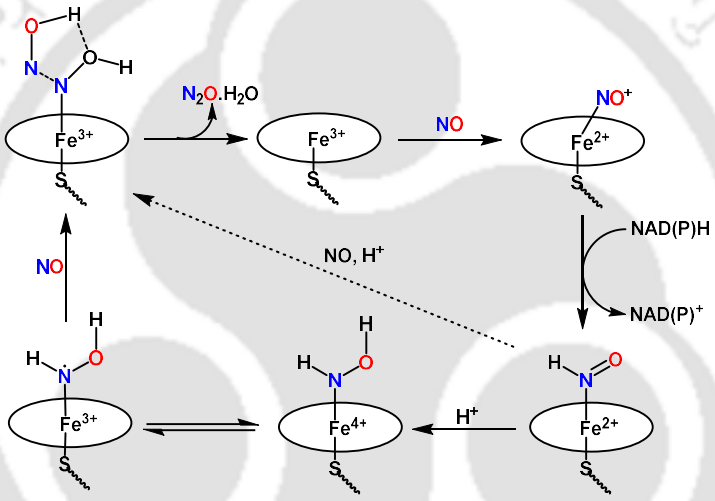

Scheme 1.7. Bacterial nitric oxide reduction using P450 NOR.

In bacterial nitric oxide syntheses (NOS), the Fe^{III}-heme enzyme is found to produce nitroxyl anion (NO^-) in the absence of (6*R*)-tetrahydro-L-biopterin (H_4B). The NO^- release as one of the products was proposed in the H_4B free reduction of *N*-hydroxy-L-arginine (NHA) with NADPH/O_2 or H_2O_2. The formation of NO^- is confirmed using guanylate cyclase as a trapping agent to result in reductive nitrosylation of the heme domain of the enzyme to the corresponding ferrous nitrosyl complex.[29,30]

In plants, the involvement of Fe^{III}-nitroxyl intermediate is proposed in the assimilatory nitrite reductase (NiR) catalyzed reduction of nitrite (NO_2^-) to ammonia (NH_3). The active site

involves a Fe_4S_4 unit. Although, the catalytic reaction was considered to be six electrons transfer process, the exact mechanism is still elusive. The proposed mechanism involves OH^- release from a [Fe^{III}-(NO_2H)] unit forming a [Fe^{III}-(NO^-)] intermediate, which was further reduced and protonated to give a [Fe^{III}-(HNO)] species.[31]

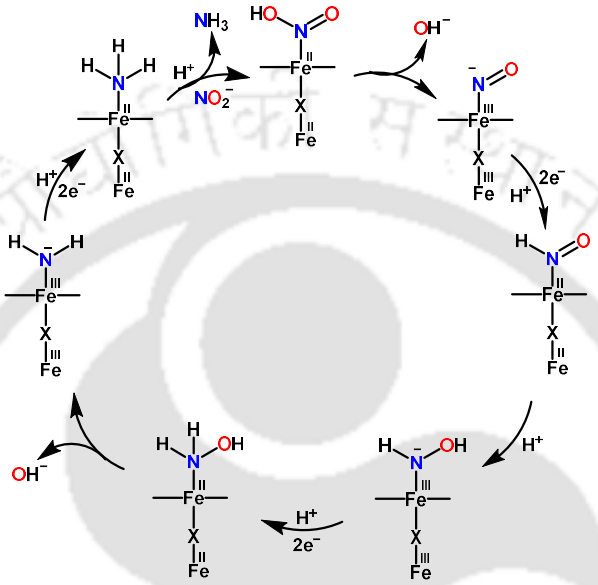

Scheme 1.8. Assimilatory nitrite reductase mechanistic pathway.

As far as the model complexes are concerned, Harrop *et al.* reported a thermally stable {Fe(NO)}^{8} complex, [$Co(Cp^*)_2$][$Fe(LN_4)(NO)$] (LN_4 = (*N*^{1}*E*,*N*^{3}*E*)-*N*^{1},*N*^{3}-bis((1H-pyrrol-2-yl)methylene)propane-1,3-diamine), which was prepared by the reaction of the corresponding {Fe(NO)}^{7} complex with [$Co(Cp^*)_2$] (decamethylcobaltocene) in toluene.[32] Upon reacting with metMb, the {Fe(NO)}^{8} complex reportedly produced MbNO as reductive nitrosylation product. The HNO/NO^- group coordinated with the Fe-centre is responsible for this reaction.

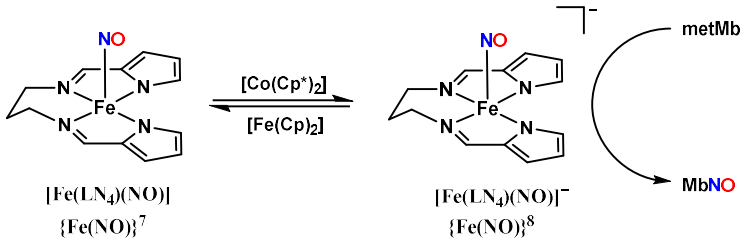

Scheme 1.9.

The same group reported another series of non-heme $\{Fe(NO)\}^7$ complexes, $[Fe(LN_4^R)(NO)]$ (LN_4^R = (*N*^{1}*E*,*N*^{2}*E*)-*N*^{1},*N*^{2}-*bis*((1H-pyrrol-2-yl)methylene)benzene-1,2-diamine); R=C_6H_4 or Ph; and R=4,5-$Cl_2C_6H_2$ or PhCl), which undergo chemical reduction using stoichiometric amount of reductant, provides corresponding $\{Fe(NO)\}^8$ complexes.[33] These $\{Fe(NO)\}^8$ complexes shows HNO-like chemistry when reacted with $[Fe^{III}(TPP^{2-})Cl]$ (TPP^{2-} = tetraphenylporphyrin dianion) and forms $[Fe(TPP^{2-})(NO)]$ *via* reductive nitrosylation.

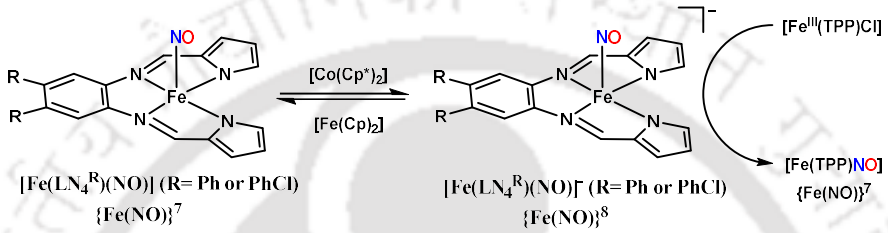

Scheme 1.10.

Lehnert *et al.* reported a high-spin $\{Fe(NO)\}^8$ complex, achieved *via* the electrochemical reduction of the precursor $\{Fe(NO)\}^7$ complex, $[Fe(TMG_3tren)(NO)](OTf)_2$ (TMG_3tren = 1,1,1-tris{2-[*N*2-(1,1,3,3-tetramethylguanidinio)]ethyl}amine, OTf = trifluoromethane sulfonate).[34] They have proposed that depending on the lability of the HNO group, non-heme iron centres can potentially function as HNO synthases in vivo.

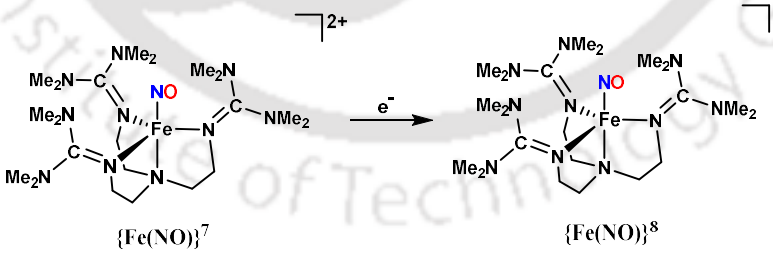

Scheme 1.11.

Goldberg e*t al.* reported a metastable non-heme high-spin iron-nitrosyl complex of $\{Fe(NO)\}^8$ configuration that spontaneously releases N_2O.[35] The $\{Fe(NO)\}^8$ complex was prepared *via* one-electron reduction of precursor complex, $[Fe(NO)(N3PyS)]BF_4$ (N3PyS = *N*-[di(2-

pyridinyl)methyl]-*N*-(2-pyridinylmethyl)amine) using [Co(Cp*)$_2$]. Another pathway has also been reported to prepare the {Fe(NO)}^{8} complex from starting complex [Fe^{II}(CH$_3$CN)(N3PyS)]BF$_4$ using Piloty's acid as a HNO source.

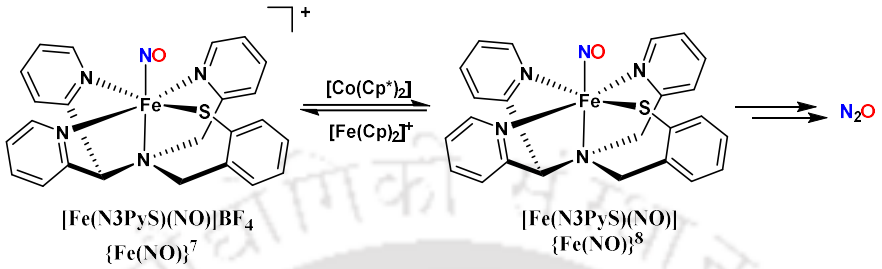

Scheme 1.12.

A non-heme electron deficient {Fe(NO)}^{6} complex, [Fe(NO)(^{TMS}PS2)(^{TMS}PS2H)] (^{TMS}PS2H$_2$ = 2,2′- dimercapto-3,3′-*bis*(trimethylsilyl)diphenyl)phenylphosphine) was reported by Lee *et al.* which undergoes photolysis and forms an intermediate involving intramolecular [SH···ON-Fe] interaction.[36] This intermediate further decomposes to give HNO and involved thiol group coordinates to the Fe-center to result in [Fe(^{TMS}PS2)$_2$]. HNO further reacts with [Mn^{III}(^{TMS}PS3)(DABCO)] (^{TMS}PS3H$_3$ = (2,2′2″-trimercapto-3,3′,3″-tris(trimethylsilyl) triphenylphosphine; DABCO = 1,4-diazabicyclo[2.2.2]octane) to yield [Mn(NO)(^{TMS}PS3)]$^-$ complex of {Mn(NO)}^{6} configuration.

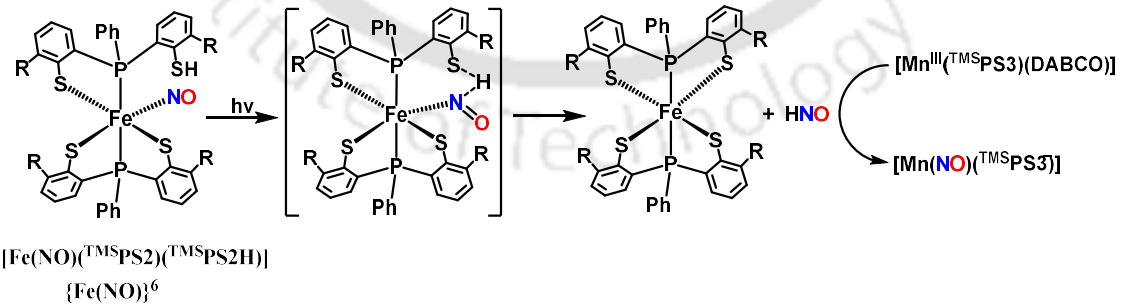

Scheme 1.13.

Richter-addo *et al.* reported a well characterized Fe-heme-HNO model complex synthesized from [(OEP)Fe-(NO)(5-MeIM)](OTf) (OEP = octaethylporphyrinato dianion, 5-MeIM = 5-

methylimidazole) complex.[37] Hydride attack on the precursor $\{Fe(NO)\}^6$ complex generates Fe-HNO product, which was characterized by IR and ^{1}H-NMR spectroscopy. DFT calculation suggests the direct attack of the hydride ion on the N atom of the iron bound nitrosyl.

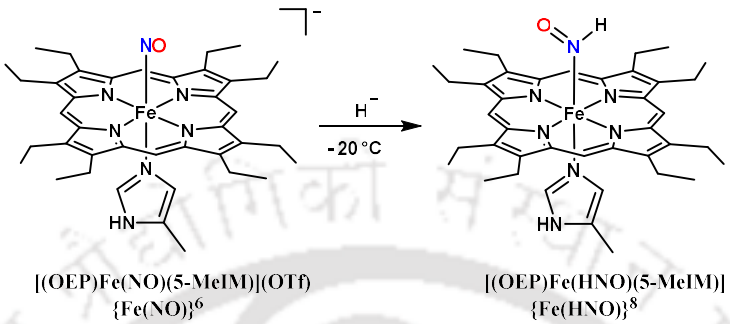

Scheme 1.14.

Very recently, Lehnert *et al.* reported a stable, isolable Fe-heme-HNO model complex of $\{Fe(HNO)\}^8$ configuration using bulky *bis*-picket fence porphyrin and its reactivity towards NO was studied.[38] The $\{Fe(HNO)\}^8$ complex was synthesized from the reaction of initial $\{Fe(NO)\}^6$ complex, [Fe(3,5-Me-BAFP)(MI)(NO)](OTf) (3,5-Me-BAFP^{2-} = 3,5-dimethyl-*bis*aryloxyfence porphyrin; MI = 1-methylimidazole), with 1 equivalent of hydride source. The Fe-HNO complex is stable at low temperature ($t_{1/2}$ = 56 min at −30 °C), can be isolated as solid and can be characterized spectroscopically. The reaction of this Fe-HNO complex with NO results in the formation of N_2O with ~ 90 ± 10% yield, which suggests the involvement of the heme-HNO intermediate for NO reduction in Cyt P450nor.

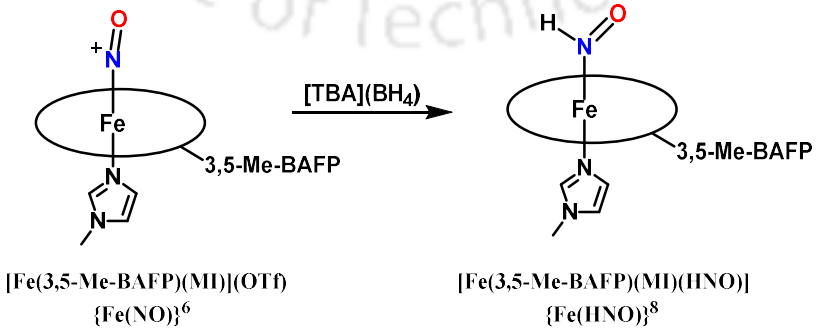

Scheme 1.15.

Thus, except a few, most of the metal nitrosyl based HNO donors are based on iron-nitrosyls. This is perhaps because of the electron rich nature and easy reduction of [Fe^{II}-NO] complexes. However, other metal ions like cobalt are employed to some extent.

Harrop *et al.* reported proton induced NO^- release from a $\{Co(NO)\}^8$ complex, $[Co(LN_4^{PhCl})(NO)]$ (LN_4^{PhCl} = (N^1E,N^2E)-N^1,N^2-*bis*((1H-pyrrol-2-yl)methylene)-4,5-dicholorobenzene-1,2-diamine).[39] In the presence of H^+, the $\{Co(NO)\}^8$ complex release HNO/NO^- which readily reacts with [$Fe^{III}(TPP^{2-})Cl$] to yield corresponding $\{Fe(NO)\}^7$ complex or reacts to PPh_3 leading to the formation of phosphine oxide ($Ph_3P{=}O$) and aza-ylide ($Ph_3P{=}NH$). Absence of any suitable HNO acceptor leads to the formation of $\{Co(NO)_2\}^{10}$ complex.

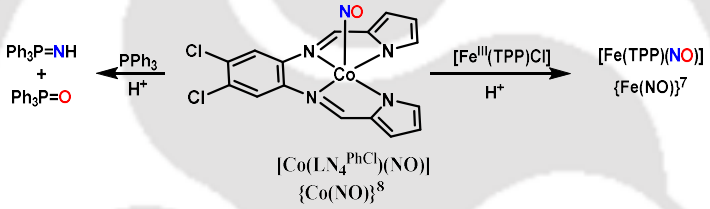

Scheme 1.16.

Later, they have reduced two similar complexes, $[Co(LN_4^{Ph})(NO)]$ and $[Co(LN_4^{PhCl})(NO)]$ to corresponding $\{Co(NO)\}^9$ complex by KC_8 in 18-crown-6 ether.[40] The newly formed $[K(18C6)][Co(LN_4^{Ph/PhCl})(NO)]$ complexes show NO stretching at 1609 and 1617 cm^{-1}, respectively. Upon addition of H^+, the complex releases HNO, which reacts with metMb to give MbNO; [Mn^{III}(Por)] to give [(Por)Mn^{II}-NO]; and PPh_3 to give $Ph_3P{=}NH$ and $Ph_3P{=}O$. The formation of N_2O as a decomposition product also confirms the HNO release.

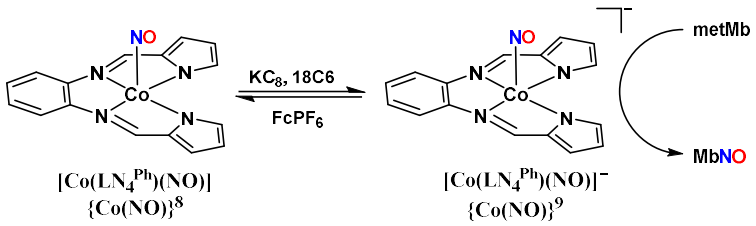

Scheme 1.17.

Low-spin Mn-nitrosyls are considered to have the electronic character of [Mn^{I}-NO^{+}]. Hence, HNO/NO^{-} release from a Mn-nitrosyl is very challenging. Recently, our group reported a Mn-nitrosyl complex, [Mn($TMPP^{2-}$)(NO)] ($TMPP^{2-}$ = 5,10,15,20-tetrakis-4-methoxyphenylporphyrinate dianion) which donates HNO in the presence of HBF_4.[41] The H^{+} polarizes the NO moiety while BF_4^{-} attacks the metal-centre to result in the release of HNO from [Mn($TMPP^{2-}$)(NO)]. The HNO donation was confirmed by its reaction with [Fe^{III}(TPP^{2-})Cl], [Fe^{III}(DTC^{-})$_3$] and PPh_3. Formation of N_2O during the course of the reaction also supports the proposition.

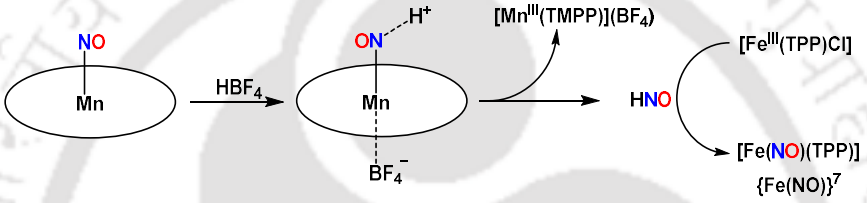

Scheme 1.18.

1.2 Scope of the thesis

The biological metabolism of excess NO in the lower organisms involve the reductive conversion of NO to N_2O by NOR enzymes like P450nor, are often found to proceed through an unstable metal-nitroxyl intermediate. The endogenous formation of iron-nitroxyl intermediates in these metabolic processes and their biological activity were extensively studied. However, the involvement of other transition metal-nitrosyls in this regard is very limited. The high reactivity of nitroxyl towards itself (dimerization) hinders its extensive studies. The production of HNO in situ is restricted to a number of compounds like Angeli's salt and Piloty's acid. Thus, the development of improved HNO donors is needed for both the basic studies and for the better understanding of its endogenous production. The metal-nitrosyl based HNO donation is exclusively studied on the iron-nitrosyl complexes for their biological relevance. However, the HNO donation from other first-row transition metal-nitrosyls is

relatively less explored. Only a few examples other than iron-nitrosyls are known to donate HNO under specific reaction conditions.

This thesis was inspired by our desire to learn more about the release of HNO/NO^- from the first-row transition metal-nitrosyl complexes. This involves the synthesis of cobalt and manganese-nitrosyl complexes using N-donor ligands (heme and non-heme) and their nitroxyl donation ability under suitable reaction condition was also studied. Furthermore, new pathways for nitroxyl donation were also explored.

The low spin $\{Co(NO)\}^8$ complexes are often regarded to have the electronic character of $[Co^{III}\text{-}(NO^-)]$. In addition to that, the higher stability of $\{Co(NO)\}^8$ complexes in contrast to $\{Fe(NO)\}^7$ complexes makes the handling easier in the reaction medium. So, cobalt nitrosyl complexes of $\{Co(NO)\}^8$ configuration can be considered as an efficient HNO/NO^- donor. In chapters 2, 3, and 4, cobalt nitrosyl complexes of three different N-donor ligands were studied. The effect of electronic nature of the ligand over the sixth ligand induced HNO/NO^- donation was also investigated. Chapter 2 includes a $\{Co(NO)\}^8$ complex in an electron deficient ligand framework and its HNO donation ability was tested in the presence of proton and anionic sixth ligands. In Chapter 3, a $\{Co(NO)\}^8$ complex was synthesized with a comparatively electron rich ligand and its NO^- donation ability was tested in the presence of anionic sixth ligands. Chapter 4 focuses on NO^- releasing ability of a highly electron rich $\{Co(NO)\}^8$ complex in the presence of a neutral sixth ligand. In chapter 5, photo-induced HNO/NO^- release from an electron rich manganese-nitrosyl complex of porphyrin ligand framework was studied.

1.3 References

1. Miranda, K. M. *Coord. Chem. Rev.* **2005**, *249*, 433.
2. Paolocci, N.; Jackson, M. I.; Lopez, B. E.; Miranda, K.; Tocchetti, C. G.; Wink, D. A.; Hobbs, A. J.; Fukuto, J. M. *Pharmacol. Ther.* **2007**, *113*, 442.

3. Paolocci, N.; Saavedra, W. F.; Miranda, K. M.; Martignani, C.; Isoda, T.; Hare, J. M.; Espey, M. G.; Fukuto, J. M.; Feelisch, M.; Wink, D. A.; Kass, D. A. *Proc. Natl. Acad. Sci. U.S.A.* **2001**, *98***,** 10463.
4. (a) Paolocci, N.; Katori, T.; Champion, H. C.; St. John, M. E.; Miranda, K. M.; Fukuto, J. M.; Wink, D. A.; Kass, D. A. *Proc. Natl. Acad. Sci. U.S.A.* **2003**, *100*, 5537. (b) Pagliaro, P.; Mancardi, D.; Rastaldo, R.; Penna, C.; Gattullo, D.; Miranda, K. M.; Feelisch, M.; Wink, D. A.; Kass, D. A.; Paolocci, N. *Free Radical Biol. Med.* **2003**, *34*, 33. (c) Wink, D. A.; Miranda, K. M.; Katori, T.; Mancardi, D.; Thomas, D. D.; Ridnour, L.; Espey, M. G.; Feelisch, M.; Colton, C. A.; Fukuto, J. M.; Pagliaro, P.; Kass, D. A.; Paolocci, N. *Am. J. Physiol. Heart Circ. Physiol.* **2003**, *285*, H2264.
5. (a) Lopez, B. E.; Shinyashiki, M.; Han, T. H.; Fukuto, J. M. *Free Radic. Biol. Med.* **2007**, *42*, 482. (b) Augustyniak, A.; Skolimowski, J.; Btaszczyk, A. *Chem. Biol. Interact.* **2013**, *206*, 262.
6. Donzelli, S.; Espey, M. G.; Thomas, D. D.; Mancardi, D.; Tocchetti, C. G.; Ridnour, L. A.; Paolocci, N.; King, S. B.; Miranda, K. M.; Lazzarino, G.; Fukuto, J. M.; Wink, D. A. *Free Radic. Biol. Med.* **2006**, *40*, 1056.
7. Donzelli, S.; Espey, M. G.; Flores-Santana, W.; Switzer, C. H.; Yeh, G. C.; Huang, J.; Stuehr, D. J.; King, S. B.; Miranda, K. M.; Wink, D. A. *Free Radic. Biol. Med.* **2008**, *45*, 578.
8. Fukuto, J. M.; Dutton, A. S.; Houk, K. N. *ChemBioChem.* **2005**, *6*, 612.
9. Bartberger, M. D.; Liu, W.; Ford, E.; Miranda, K. M.; Switzer, C.; Fukuto, J. M.; Farmer, P. J.; Wink, D. A.; Houk, K. N. *Proc. Natl. Acad. Sci. U. S. A.* **2002**, *99*, 10958.
10. Spencer, N. Y.; Patel, N. K.; Keszler, A.; Hogg, N. *Free Radic. Biol. Med.* **2003**, *35*, 1515.
11. Shafirovich, V.; Lymar, S. V. *Proc. Natl. Acad. Sci. U. S. A.* **2002**, *99*, 7340.

12. Wong, Y.; Hyun, J.; Fukuto, J. M.; Shirota, F. N.; DeMaster, E. G.; Shoeman, D. W.; Nagasawa, H. T. *Biochemistry*, **1998**, *37*, 18129.

13. Doyle, M. P.; Mahapatro, S. N.; Broene, R. D.; Guy, J. K. *J. Am. Chem. Soc.* **1988**, *110*, 593.

14. Bazylinski, D. A.; Hollocher, T. C. *Inorg. Chem.* **1985**, *24*, 4285.

15. Reisz, J. A.; Klorig, E. B.; Wright, M. W.; King, S. B. *Org. Lett.* **2009**, *11*, 2719.

16. Xia, Y.; Cardounel, A. J.; Vanin, A. F.; Zweier, J. L. *Free Radic. Biol. Med.* **2000**, *29*, 793.

17. Johnson, G. M.; Chozinski, T. J.; Salmon, D. J.; Moghaddam, A. D.; Chen, H. C.; Mirandan, K. M. *Free Radic. Biol. Med.* **2013**, *63*, 476.

18. Cline, M. R.; Toscano, J. P. *J. Phys. Org. Chem.* **2011**, *24*, 993.

19. Harteck, P. *Berichte der Deutschen Chemischen Gesellschaft*, **1933**, *66*, 423.

20. (a) Angeli, A.; Rimini, E. *Gazz. Chim. Ital.* **1896**, *26*, 17. (b) Bonner, F. T.; Ravid, B. *Inorg. Chem.* **1975**, *14*, 558. (c) Maragos, C. M.; Morley, D.; Wink, D. A.; Dunams, T. M.; Saavedra, J. E.; Hoffman, A.; Bove, A. A.; Isaac, L.; Hrabie, J. A.; Keefer, L. K. *J. Med. Chem.* **1991**, *34*, 3242.

21. (a) Piloty, O. *Ber. Dtsch. Chem. Ges.* **1896**, *29*, 1559. (b) Bonner, F. T.; Ko, Y. H. *Inorg. Chem.* **1992**, *31*, 2514.

22. (a) Fukuto, J. M.; Bianco, C. L.; Chavez, T. A. *Free Radic. Biol. Med.* **2009**, *47*, 1318. (b) Demaster, E. G.; Redfern, B.; Nagasawa, H. T. *Biochem. Pharmacol.* **1998**, *55*, 2007. (c) Nagasawa, H. T.; Demaster, E. G.; Redfern, B.; Shirota, F. N.; Goon, J. W. *J. Med. Chem.* **1990**, *33*, 3120.

23. (a) Christie, C. C.; Kirby, G. W.; McGuigan, H.; Mackinnon, J. W. M. *J. Chem. Soc. Perkin Trans I*, **1985**, 2469. (b) Howard, J. A. K.; Ilyashenko, G.; Sparkes, H. A.; Whiting, A. *Dalton. Trans*. **2007**, *21*, 2108.

24. Sha, X.; Isbell, T. S.; Patel, R. P.; Day, C. S.; King, S. B. *J. Am. Chem. Soc.* **2006**, *128*, 9687.

25. Bartberger, M. D.; Liu, W.; Ford, E.; Miranda, K. M.; Switzer, C.; Fukuto, J. M.; Farmer, P. J.; Wink, D. A.; Houk, K. N. *Proc. Natl. Acad. Sci. U.S.A.* **2002**, *99*, 10958.

26. Leipoldt, J. G.; Eldik, R.; Basson, S. S.; Roodt, A. *Inorg. Chem.* **1986**, *25*, 4639.

27. Goodrich, L. E.; Roy, S.; Alp, E. E.; Zhao, J.; Hu, M. Y.; Lehnert, N. *Inorg. Chem.* **2013**, *52*, 7766.

28. (a) McQuarters, A. B.; Wirgau, N. E.; Lehnert, N. *Curr. Opin. Chem. Biol.* **2014**, *19*, 82. (b) Tosha, T.; Nomura, T.; Nishida, T.; Saeki, N.; Okubayashi, K.; Yamagiwa, R.; Sugahara, M.; Nakane, T.; Yamashita, K.; Hirata, K.; Ueno, G.; Kimura, T.; Hisano, T.; Muramoto, K.; Sawai, H.; Takeda, H.; Mizohata, E.; Yamashita, A.; Kanematsu, Y.; Takano, Y.; Nango, E.; Tanaka, R.; Nureki, O.; Shoji, O.; Ikemoto, Y.; Murakami, H.; Owada, S.; Tono, K.; Yabashi, M.; Yamamoto, M.; Ago, H.; Iwata, S.; Sugimoto, H.; Shiro, Y.; Kubo, M. *Nat. Commun.* **2017**, *8*, 1585.

29. Rusche, K. M.; Spiering, M. M.; Marletta, M. A. *Biochemistry,* **1998**, *37*, 15503.

30. Adak, S.; Wang, Q.; Stuehr, D. J. *J. Biol. Chem.* **2000**, *275*, 33554.

31. Lui, S. M.; Liang, W.; Soriano, A.; Cowan, J. A. *J. Am. Chem. Soc.* **1994**, *116*, 4531.

32. Patra, A. K.; Dube, K. S.; Sanders, B. C.; Papaefthymiou, G. C.; Conradie, J.; Ghosh, A.; Harrop, T. C. *Chem. Sci.* **2012**, *3*, 364.

33. Sanders, B. C.; Patra, A. K.; Harrop, T. C. *J. Inorg. Biochem.* **2013**, *118*, 115.

34. Speelman, A. L.; Lehnert, N. *Angew. Chem. Int. Ed.* **2013**, *52*, 12283.

35. Confer, A. M.; McQuilken, A. C.; Matsumura, H.; Moënne-Loccoz, P.; Goldberg, D. P. *J. Am. Chem. Soc.* **2017**, *139*, 10621.

36. Chiang, C. K.; Chu, K. T.; Lin, C. C.; Xie, S. R.; Liu, Y. C.; Demeshko, S.; Lee, G. H.; Meyer, F.; Tsai, M. L.; Chiang, M. H.; Lee, C. M. *J. Am. Chem. Soc.* **2020**, *142*, 8649.

37. Abucayon, E. G.; Khade, R. L.; Powell, D. R.; Zhang, Y.; Richter-Addo, G. B. *J. Am. Chem. Soc.* **2016**, *138*, 104.

38. Manickas, E. C.; LaLonde, A. B.; Hu, M. Y.; Alp, E. E.; Lehnert, N. *J. Am. Chem. Soc.* **2023**, *145*, 23014.

39. Rhine, M. A.; Rodrigues, A. V.; Bieber Urbauer, R. J.; Urbauer, J. L.; Stemmler, T. L.; Harrop, T. C. *J. Am. Chem. Soc.* **2014**, *136*, 12560.

40. Walter, M. R.; Dzul, S. P.; Rodrigues, A. V.; Stemmler, T. L.; Telser, J.; Conradie, J.; Ghosh, A.; Harrop, T. C. *J. Am. Chem. Soc.* **2016**, *138*, 12459.

41. Mazumdar, R.; Saha, S.; Samanta, B.; Mondal, B. *Inorg. Chem.* **2021**, *60*, 18024.

Chapter 2

Sixth ligand induced HNO/NO^- release by a five coordinated cobalt(II)-nitrosyl complex having $\{Co(NO)\}^8$ configuration

Abstract

Nitroxyl (HNO/NO^-), the one electron reduced analogue of nitric oxide (NO), has been shown to have distinct advantages over NO from pharmacological and therapeutic point of view. However, the roles of nitroxyl in chemical biology have not yet been studied as extensively as NO. Consequently, the examples of HNO donors are still restricted to only few like Angeli's salt, Piloty's acid or acyl and acyloxy nitroso derivatives. However, the intrinsic limitations of all of these hinder their widespread utility. Metal-nitrosyl complexes, though examples are not much, could be an efficient HNO donor. Here, a cobalt nitrosyl complex, **2.2** having $\{Co(NO)\}^8$ configuration has been reported. This complex in the presence of a sixth ligand (BF_4^- (tetrafluoroborate anion), DTC^- (diethyldithiocarbamate anion)) releases/donates HNO/NO^-. This has been confirmed using well-known HNO/NO^- acceptors like $[Fe^{III}(TPP^{2-})Cl]$ and $[Fe^{III}(DTC^-)_3]$. The HNO release has been authenticated further by the detection and estimation of N_2O using GC-MS as well as its reaction with PPh_3.

2.1 Introduction

The interest in HNO chemistry has increased considerably due to its chemical properties and biological relevance.[1,2] HNO is known to react with metalloproteins, thiols, etc. and there is a significant overlap of its reactivity with NO. For instance, HNO and NO, both are reactive towards heme-proteins in both the Fe^{II} and Fe^{III} states.[3-5] It has been demonstrated that the deprotonated form of HNO {*i.e.* nitroxyl (NO^-) ion} has distinct advantages over NO from pharmacological and therapeutic point of view. For example, HNO is known to induce vasorelaxation responses through venous dilation, whereas NO affects the arterial and venous sides.[6] Studies have shown that HNO targets the cysteine residue in sarco/endoplasmic reticulum Ca^{2+}-ATPase and modifies the thiols in phosphorylating phospholamban.[7] This, in turn, removes the inhibition of the Ca^{2+} pump.[8] It has been found that HNO has positive effects on preventing heart failure by targeting various potential agents.[2] It is also known to react with metalloproteins like Cu-Zn-superoxide dismutase (CuZnSOD) and Mn-superoxide dismutase (MnSOD).[9] Thus, to understand the role of HNO in chemical biology, the detailed study of HNO through the design and synthesis of HNO donors is of utmost importance. The examples of HNO donors still remain restricted to only a few such as Angeli's salt, Piloty's acid or acyl and acyloxy nitroso derivatives.[10] However, each of them has some limitations like simultaneous release of undesirable by-products, ineffective release of HNO at physiological pH etc.[11] These actually hinder their widespread utility.

The metal bound nitrosyl complexes with suitable electronic configuration could be an efficient HNO donor. In fact, iron containing NO-synthases are known to release HNO through an iron bound *N*-hydroxy-L-arginine intermediate.[12] In literature, Co-nitrosyl complexes (specifically, non-organometallic complexes) are classified into three main categories, having $\{Co(NO)\}^7$, $\{Co(NO)\}^8$ and $\{Co(NO)\}^9$ configuration based on the Enemark-Feltham notation. In the

$\{Co(NO)\}^7$ systems, the NO is believed to have NO^+ character and hence these can be safely ruled out for nitroxyl/HNO donation. The $\{Co(NO)\}^8$ systems can be considered to have [Co^{III}-NO^-] moiety. There have been a number of examples of $\{Co(NO)\}^8$ complexes in literature, but only a few are known to release HNO. In this direction Harrop and coworkers reported five coordinated $\{Co(NO)\}^8$ system, [$Co(LN_4^{PhCl})(NO)$] (where LN_4^{PhCl} = dianion of (N^1 E,N^2 E)-N^1,N^2-bis(1H-pyrrol-2-yl)methylene)-4,5-dichlorobenzene-1,2 diamine) which upon reduction using KC_8 resulted in the corresponding penta-coordinated $\{Co(NO)\}^9$ complex.[13] The anionic nitroxyl (NO^-) complex was isolated and found to release HNO in the presence of H^+ in organic solvents through the putative formation of [Co^{II}-HNO] intermediate. However, the example of release of HNO or NO^- from $\{Co(NO)\}^8$ complex is in scarce. In fact, no literature report is known except the ones by Harrop *et. al*. where the $\{Co(NO)\}^8$ complex, [$Co(LN_4^{PhCl})(NO)$] was shown to release HNO in the presence of stoichiometric amount of H^+.[14]

This chapter describes the synthesis, characterization of a nitrosyl complex of Co(II) having $\{Co(NO)\}^8$ configuration which in the presence of an anionic sixth ligand releases nitroxyl (HNO/NO^-).

2.2 Results and discussion

The ligand, 1,2-*bis*(2-pyridinecarboxamido)benzene (H_2BPB) was synthesized from 1,2-diaminobenzene and pyridine-2-carboxylic acid using literature procedure.[15] It was characterized using ^1H and ^{13}C-NMR, FT-IR spectroscopy (Exp. Sec., Appendix I, Figures A1.1-A1.3). The precursor complex, [$Co^{II}(BPB^{2-})$], **2.1** was synthesized using an earlier reported method[16] and characterized by spectroscopic analyses (Exp. Sec., Appendix I, Figures A1.4-A1.7). The crystal structure of complex **2.1** has been reported earlier.[17] X-band EPR spectrum confirms the paramagnetic nature of the complex **2.1** *i.e.,* the cobalt centre is in +2 oxidation state. The $\{Co(NO)\}^8$ complex, [$Co(BPB^{2-})(NO)$], **2.2** was prepared by purging NO

gas into a methanol solution of complex **2.1**. Upon keeping under NO environment overnight, dark green crystalline precipitated of complex **2.2** was obtained from the reaction mixture (*ca.* 87% yield). It is fairly stable in air and vacuum in solid state. However, in solution, it is stable only under inert atmosphere. Complex **2.2** was characterized using FT-IR, UV-visible, ^{1}H-NMR spectroscopy, ESI-mass spectrometry and single crystal X-ray structure determination (Appendix I, Figures A1.8-A1.12). Structural studies revealed that the complex **2.2** is a bent nitrosyl (Figure 2.1). The oxygen atom of the nitrosyl moiety in complex **2.2** occupies two non-equivalent vibrational positions with 50% occupancy each. Similar structural feature was previously observed in a high-spin iron-nitrosyl complex.[18] The observed Co-N-O bond angles in complex **2.2** are 125.2(9)° and 130.2(7)° for Co-N1-O1 and Co-N1-O2, respectively. The N-O bond lengths are 1.045(13) Å and 1.119(10) Å for N-O1 and N-O2, respectively. This intrinsic disorder in the crystal structure of complex **2.2** precludes the accurate estimation of the Co-N-O angle and N-O distance. Two different conformers of complex **2.2** are shown in the appendix section (Appendix I, Figure A1.42). Previously reported structurally characterized bent Co-nitrosyls such as [Co(L1)(NO)] (L1 = *N*1-(2,4,6-trimethylbenzyl)-N2-(2-((2,4,6-trimethylbenzyl)amino)ethyl-1,2-diamine)[19] and [Co(BPI)(NO)] (BPI =1,3-*bis*(2′-pyridylimino)isoindol)[20] were found to have Co-N-O bond angle of 124.6(10)° and 132.7(7)° along with N-O bond length of 1.103(9) Å and 1.014(8) Å, respectively. In [Co(LN_4^{PhCl})(NO)], the reported Co-N_{NO} bond length is 1.798(3) Å; N-O bond length 1.172(4) Å and Co-N-O angle is 124.4(3)°.[14] The Co-N_{NO} bond distance in complex **2.2** is found to be 1.791(6) Å. These observed metric parameters match well with the reported ones of analogues complexes.[21]

In FT-IR studies, complex **2.2** exhibits ν_{NO} at 1662 cm^{-1} in KBr. In [Co(LN_4^{PhCl})(NO)], this stretching frequency was reported to appear at 1667 cm^{-1}.[14] The complex **2.2** is EPR silent as the diamagnetic ground state is typical for this class of nitrosyls.[14,22,23]

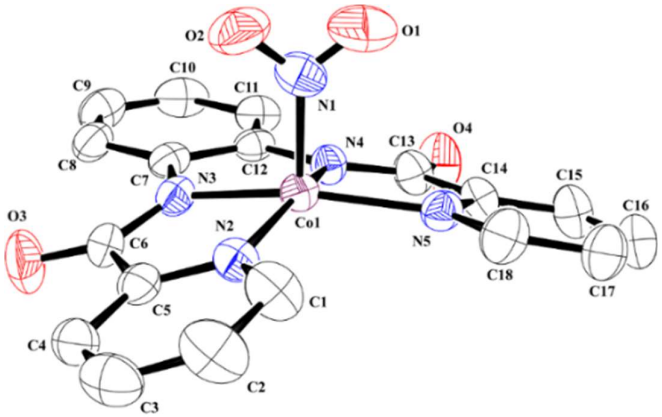

Figure 2.1. ORTEP diagram of complex **2.2** (40% thermal ellipsoid plot, H-atoms are omitted for clarity).

In literature, the potential of $\{Co(NO)\}^8$ complexes as HNO donors are relatively less explored perhaps because of inherent kinetic inertness of low spin d^6 configuration of Co(III).[24] To check the nitroxyl (HNO/NO^-) donor ability of complex **2.2**, it was made to react with the well-established HNO/NO^- acceptor, $[Fe^{III}(TPP^{2-})(Cl)]$ in dry and degassed dichloromethane solution.[14,25] The reaction was monitored by FT-IR spectroscopy. Even after 24 hours of stirring at room temperature, no significant change was observed (Appendix I, Figure A1.24). Then, the reaction was carried out in the presence of one mole equivalent of $HBF_4.Et_2O$. In FT-IR spectral monitoring, the reaction of one mole equivalent of $[Fe^{III}(TPP^{2-})Cl]$ with complex **2.2** in the presence of HBF_4 shows the disappearance of nitrosyl stretching frequency of complex **2.2** at 1662 cm^{-1} with the concomitant formation of a new band at 1698 cm^{-1} (Figure 2.2(a)). This 1698 cm^{-1} stretching frequency is attributed as the nitrosyl stretching of newly formed $[Fe(TPP^{2-})(NO)]$.[3,14,25,26] The reaction was found to be completed in a near quantitative manner. X-band EPR study of the reaction mixture at 77 K shows a sharp signal at g ~ 2.04, which supports the formation of $[Fe(TPP^{2-})(NO)]$ in the reaction medium (Figure 2.2(b)).[3,25,26]

The similar reaction was observed when the reaction was carried out in the presence of $[Fe^{III}(DTC^-)_3]$ without addition of HBF_4 in dry and degassed dichloromethane solution. Upon

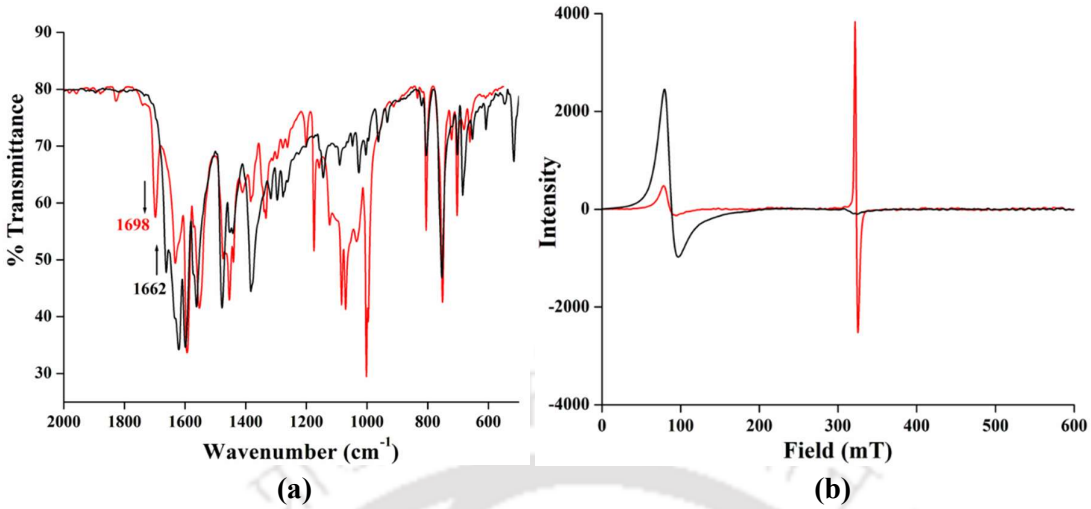

Figure 2.2. (a) FT-IR (KBr) spectra and (b) X-band EPR (CH_2Cl_2, 77 K) spectra of reaction mixture of complex **2.2** and [$Fe^{III}(TPP^{2-})(Cl)$] (black) and after addition of HBF_4 (red).

addition, complex **2.2** was found to donate NO^- to [$Fe^{III}(DTC^-)_3$] to result in [$Fe(DTC^-)_2(NO)$]. In FT-IR spectroscopic study, the reaction mixture of 1 mole equivalent of [$Fe^{III}(DTC^-)_3$] and complex **2.2** shows a stretching frequency at 1690 cm^{-1} while the nitrosyl stretching frequency of complex **2.2** completely disappeared (Appendix I, Figure A1.22). This is attributed to the formation of [$Fe(DTC^-)_2(NO)$] along with [$Co^{III}(BPB^{2-})(DTC^-)$], **2.4** (Eq. 2.1).[27]

$$\mathbf{[Co(BPB^{2-})(NO)] + [Fe^{III}(DTC^-)_3] \longrightarrow [Co^{III}(BPB^{2-})(DTC^-)] + [Fe(DTC^-)_2(NO)]}$$

…Eq. 2.1

The complex **2.4** was isolated and brown crystals were obtained from tetrahydrofuran solution by slow evaporation. The ORTEP diagram is shown in figure 2.3. The cobalt centre is in +3 oxidation state and in a distorted octahedral geometry. Mass spectrometric characterization of complex **2.4** shows a $[M+H]^+$ peak at m/z = 524.063 (Calculated: 524.062) (Appendix I, Figure A1.20).

The formation of [$Fe(DTC^-)_2(NO)$] was further confirmed by subjecting the reaction mixture to X-band EPR spectroscopic studies, which shows a sharp signal at g ~ 2.05 (Appendix I,

Figure A1.23).[25] ESI-mass spectrum of isolated [Fe(DTC$^-$)$_2$(NO)] shows a molecular ion peak at m/z = 351.976 (Calculated: 351.985, after loss of NO unit) (Appendix I, Figure A1.39).

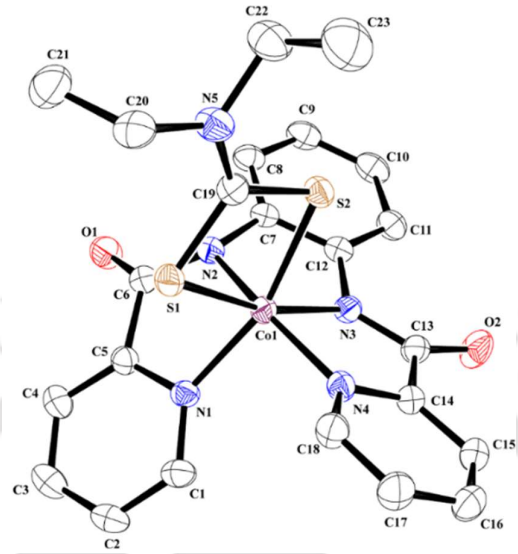

Figure 2.3. ORTEP diagram of complex **2.4** (30% thermal ellipsoid plot, H-atoms and solvent molecules are omitted for clarity).

Earlier, it has been reported that the presence of sixth ligand changes the electronic character of metal bound NO. For example, Enemark *et. al*. has shown that in penta-coordinated cobalt-nitrosyl complex of *bis*-arsenide ligand, increase in the coordination number of the metal ion from 5 to 6 changes the nature of the nitrosyl ligand from NO^+ to NO^-.[28] Recently, it has been reported that five coordinated $\{Mn(NO)\}^6$ complex, in the presence of [Fe^{III}(DTC$^-$)$_3$], releases NO^-.[26] This has been attributed to the fact that [Fe^{III}(DTC$^-$)$_3$] dissociates in solution to [Fe^{III}(DTC$^-$)$_2$]$^+$ and DTC$^-$. This DTC$^-$ then acts as the sixth ligand and binds the Mn-center of $\{Mn(NO)\}^6$ complex, resulting in the release of NO^-. Hence, the observation of release/transfer of NO^- from the complex **2.2** to [Fe^{III}(DTC$^-$)$_3$] leading to the formation of [Fe(DTC$^-$)$_2$(NO)] and [Co^{III}(BPB^{2-})(DTC$^-$)] is logical to be initiated by the coordination of sixth ligand to the cobalt center of complex **2.2**. Though, any end product with BF_4^- coordinated to Co(III)-center was not isolated in case of the reaction of complex **2.2** with [Fe^{III}(TPP^{2-})Cl] in the presence of HBF_4, this reaction presumably proceeds through the same manner.

To check that, the complex **2.2** was made to react with HBF_4. Addition of 1.3 mole equivalent of $HBF_4.Et_2O$ to the dry and degassed dichloromethane solution of complex **2.2** resulted in shifting of UV-visible band from 430 nm to 403 nm (Figure 2.4). In FT-IR spectroscopy, the NO stretching frequency of complex **2.2** at 1662 cm^{-1} disappeared after the addition of HBF_4 (Appendix I, Figure A1.13). Monitoring the reaction in UV-visible spectroscopy at -40 °C did not reveal the formation of any intermediate in the reaction. Isolation and characterization of the final complex, however, revealed the formation of $[Co^{III}(BPB^{2-})](BF_4^-)$, **2.3** having absorption at 403 nm.

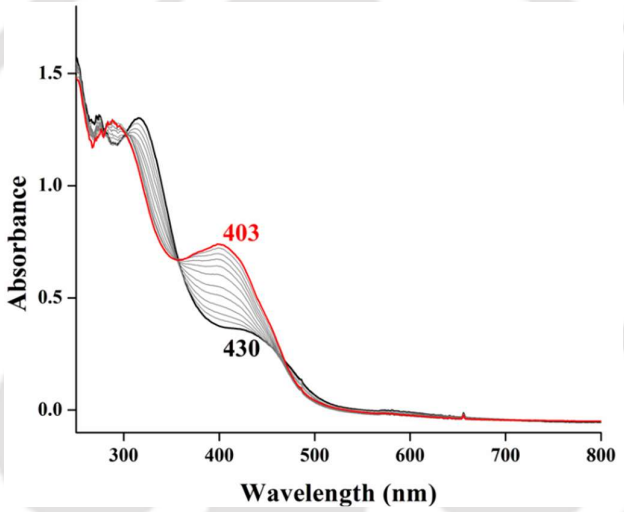

Figure 2.4. UV-visible spectroscopic study of reaction kinetics of complex **2.2** with HBF_4 in CH_2Cl_2 at -40 °C (initial (black) and after addition of HBF_4 (red)).

The presence of BF_4^- unit in the complex **2.3** was confirmed by the appearance of IR stretching at 1084 cm^{-1} (Appendix I, Figure A1.13).[29] X-band EPR study at 77 K indicates the diamagnetic nature of the complex **2.3** as expected (Appendix I, Figure A1.14). ESI-mass spectrometry of complex **2.3** shows a molecular ion peak at m/z = 375.030 (Calculated: 375.029, after loss of BF_4^- unit) (Appendix I, Figure A1.16).[26] Since the final product does not contain NO or it's oxidized or reduced analogue, it is logical to assume that NO is released from complex **2.2**. As the metal ion of complex **2.2** gets oxidized in the process, it is logical to assume that the NO is released as NO^-. It was confirmed by checking the presence of N_2O in the reaction vessel. HNO

rapidly dimerizes (k_{dim} = 8 × 10^6 M^{-1} s^{-1}) to hyponitrous acid, which further decomposes to give N_2O and H_2O.[30] Analyzing the headspace gas of the reaction vessel in gas chromatography confirms the presence of N_2O (Appendix I, Figure A1.27). The yield of N_2O formed in reaction vessel is quantified using GC found to be *ca.* 71%. A calibration curve was prepared using N_2O produced from the alkaline solution of Piloty's acid (Appendix I, Figure A1.28). The presence of N_2O was further confirmed from GC-MS (Appendix I, Figure A1.29).

To understand the role of H^+ and BF_4^-, some control experiments have been conducted. Complex **2.2** was made to react with $NaBF_4$ in dry and degassed methanol medium, which resulted in the formation of complex **2.3** (confirmed from FT-IR spectroscopy, Appendix I, Figure A1.47). In UV-visible spectral monitoring, this reaction shows shifting of band from 420 nm to 398 nm (Appendix I, Figure A1.48). So, it is logical to assume that the presence of BF_4^- as the sixth ligand is the key for the NO^- release.

The HNO formation is further confirmed by its characteristic reaction with triphenylphosphine.[31] Addition of one mole equivalent of HBF_4 to the reaction mixture of triphenylphosphine and complex **2.2** was monitored by ^{31}P-NMR spectroscopy. The ^{31}P-NMR

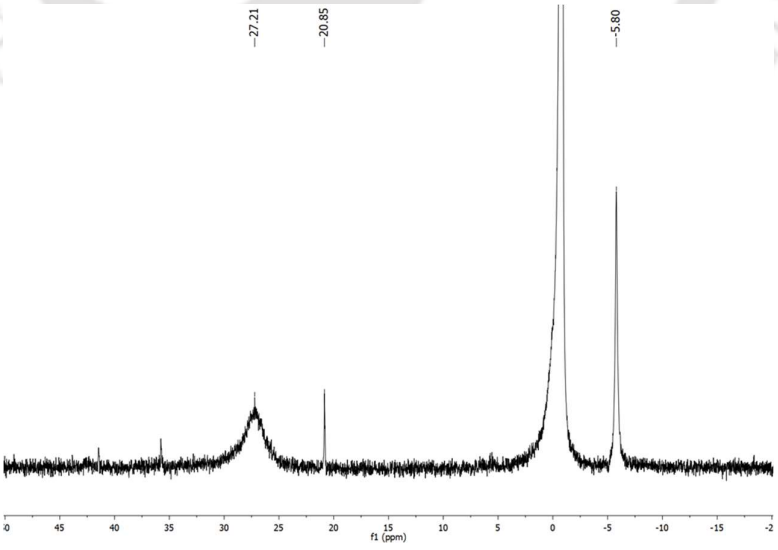

Figure 2.5. ^{31}P-NMR spectrum of the reaction mixture of PPh_3, complex **2.2** and $HBF_4.Et_2O$ in CH_2Cl_2 solution with 0.1 mL DMSO-d_6.

of the reaction mixture reveals the presence of $Ph_3P{=}NH$ (δ_{ppm} = 21.69) and $Ph_3P{=}O$ (δ_{ppm} = 27.95) along with unreacted triphenylphosphine (δ_{ppm} = - 4.95) (Figure 2.5).[25] Subjecting the reaction mixture of complex **2.2** and PPh_3 to ^{31}P NMR in absence of HBF_4 shows signal predominately at δ_{ppm} = - 5.6 (PPh_3) along with a signal at δ_{ppm} = 27.04 ($Ph_3P{=}O$) of very less intensity (Appendix I, Figure A1.25). The less intense signal for the presence of $Ph_3P{=}O$ in this case is attributed to the aerial oxidation of triphenylphosphine.

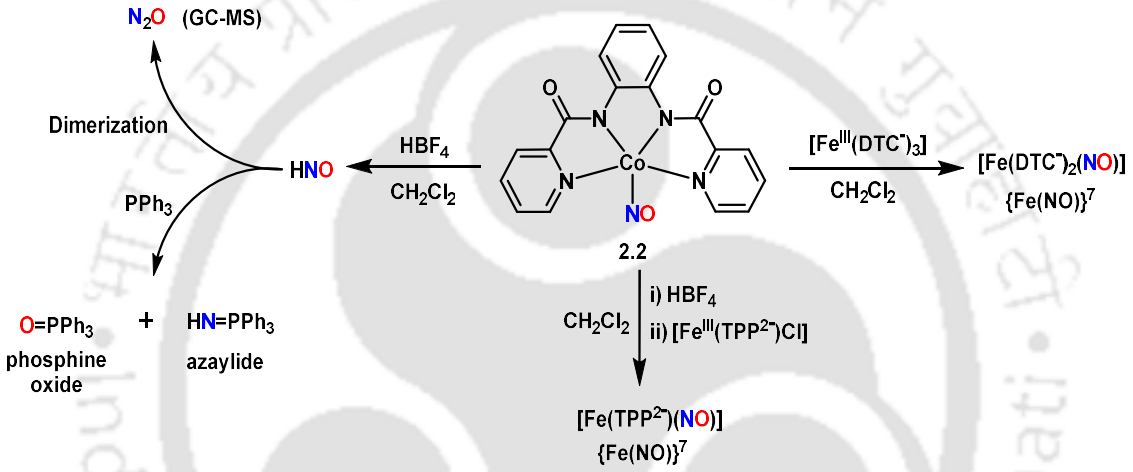

Scheme 2.1. Overall reactions.

2.3 Experimental Section

2.3.1 Materials and Methods

All the reagents were purchased from commercial sources and used as it is without further purification unless specified. Dichloromethane was passed through an alumina column, stored over calcium hydride overnight followed by distillation under N_2. Methanol was dried by distillation with Mg-turnings and iodine. Tetrafluoroboric acid was dried over 4Å molecular sieve under argon. All the reactions were performed under inert atmosphere except mentioned differently. Deoxygenation of solvents and solutions was affected by consecutive vacuum/argon purge cycles. UV-visible spectra were taken on an Agilent Cary 8454

spectrophotometer. FT-IR spectra were recorded as KBr pellets or in a KBr cell using a PerkinElmer spectrophotometer. ^{1}H, ^{13}C, and ^{31}P-NMR studies were done in Bruker Avance III 400 and 500 MHz Varian FT-NMR spectrophotometers. X-band EPR spectra were recorded on a JES-FA200 EPR spectrophotometer with microwave power, 0.998 mW; microwave frequency, 9.14 GHz; and modulation amplitude, 2. Gas chromatograms were obtained on PerkinElmer Clarus® 590.

Single crystals were grown from respective solutions using the slow evaporation and/or reaction diffusion techniques. The intensity data were collected using a Bruker SMART APEX-II CCD diffractometer, equipped with a fine focus 1.75 kW sealed tube Mo Kα radiation (λ = 0.71073 Å), with increasing ω (width of 0.3° per frame) at a scan speed of 3 s/frame. The SMART software was used for data acquisition. Data integration and reduction were undertaken with SAINT and XPREP software.[32] Structures were solved by direct methods using SHELXL[33a] and refined with full-matrix least-squares on F^2 using SHELXL-2019/1.[33b] Structural illustrations were drawn with ORTEP-3 for Windows.[33c]

2.3.2 Syntheses

***N,N'-bis*(2-pyridinecarboxamide)-1,2-benzene (H_2BPB):** The ligand was synthesized using reported procedure.[11] To a stirring pyridine solution of 2-pyridinecarboxylic acid (2.46 g, 20 mmol), 1,2-diaminobenzene (1.08 g, 10 mmol) was added followed by dropwise addition of triphenylphosphite (6.2 g, 20 mmol). The reaction mixture is refluxed for 4 hours at 100 °C. Then the resulting reaction mixture was brought to room temperature and addition of diethylether resulted in precipitation. The precipitate was filtered and washed several times with ethanol and air dried. The ligand (H_2BPB) obtained as white product. Yield: 2.5 g (*ca.* 80%). Elemental analyses for $C_{18}H_{14}N_4O_2$; Calculated (%): C, 67.92; H, 4.43; N, 17.60. Found (%): C, 67.85; H, 4.46; N, 17.58. FT-IR (in KBr): 3316, 1676, 1666, 1593, 1517, 1485, 1449,

1430, 1297, 997, 758, 748 and 689 cm^{-1}. ^{1}H-NMR (400 MHz, $CDCl_3$): δ_{ppm}, 10.26 (s, 2H), 8.56-8.55 (m, 2H), 8.32-8.30 (d, 2H), 7.91-7.87(m, 4H), 7.46-7.44(m, 2H) and 7.32-7.28(m, 2H). ^{13}C-NMR (100 MHz, $CDCl_3$): δ_{ppm}, 162.9, 149.8, 148.1, 137.5, 130.2, 126.4, 126.1, 124.7 and 122.6.

[$Co^{II}(BPB^{2-})$], 2.1: This precursor complex was synthesized using a literature procedure.[12] To a round bottom flask charged with stirring bar, H_2BPB (949 mg, 3 mmol) was added in absolute ethanol (30 mL) and the solution was heated at 80 °C till the ligand dissolves completely. Afterwards, an aqueous solution of $Co(OAc)_2.4H_2O$ (748 mg, 3 mmol) was added into the hot ethanol solution of the ligand. The stirring was continued for 2 hours while precipitation appeared. After cooling down to room temperature, the precipitate was filtered off and washed with cold ethanol and dried. The complex **2.1** was obtained as green solid. Yield: 0.963 g (*ca.* 86%). Elemental analyses for $C_{18}H_{12}N_4O_2Co$; Calculated (%): C, 57.61; H, 3.22; N, 14.93. Found (%): C, 57.68; H, 3.26; N, 14.99. FT-IR (in KBr): 1621, 1596, 1557, 1476, 1451, 1405, 1340, 1277, 1156, 1098, 1031, 757 and 684 cm^{-1}. UV-visible (CH_3OH): 268 nm (ε/M^{-1} cm^{-1}, 1.90×10^4), 312 nm (ε/M^{-1} cm^{-1}, 1.04×10^4) and 403 nm (ε/M^{-1} cm^{-1}, 5.81×10^3). ESI-mass (m/z): Calculated, 375.029; Found, 375.035 (molecular ion peak).

[$Co(BPB^{2-})(NO)$], 2.2: Complex **2.1** (80 mg, 0.2 mmol) was dissolved in dry and degassed methanol. NO gas was bubbled for 5 minutes to this solution. The colour of the solution changes from brown to dark green. After the removal of the excess NO, the product was isolated under continuous argon flash. Dark-green crystals of complex **2.2** were obtained from its methanol solution by slow evaporation. Yield: 71 mg, (*ca.* 87%). Elemental analyses for $C_{18}H_{12}N_5O_3Co$; Calculated (%): C, 53.35; H, 2.98; N, 17.28. Found (%): C, 53.40; H, 2.92; N, 17.36. FT-IR (in KBr): 1662 (ν_{NO}), 1622, 1601, 1573, 1562, 1478, 1376, 1296, 1143, 1090, 1026, 805, 753, 658 and 515 cm^{-1}. UV-visible (CH_2Cl_2): 316 nm (ε/M^{-1} cm^{-1}, 2.30×10^4) and

430 nm (ε/M^{-1} cm^{-1}, 6.13 × 10^4). ^{1}H-NMR (500 MHz, DMSO-d_6): δ_{ppm}, 9.56-9.55 (d, 2H), 8.46-8.43 (m, 2H), 8.28-8.25 (t, 2H), 7.88-7.84(m, 4H) and 6.90-6.87(m, 2H). ESI-mass (m/z): Calculated, 375.029; Found, 375.035 (after loss of NO). Crystal data: complex **2.2**, CCDC No. 2246863, $C_{18}H_{12}N_5O_3Co$, M = 405.26, Monoclinic (P 21), a = 6.2778(2) Å, b = 13.3612(4) Å, c = 9.8714(3) Å, α = 90°, β = 91.582(2)°, γ = 90°, V = 827.69(4) Å^3, Z = 2, D_c = 1.626 g cm^{-3}, μ = 1.068 mm^{-1}, T = 120(2) K, 2920 reflections, 2610 independent, $R(F)$ = 0.0321 [$I > 2\delta(I)$], R(int) = 0.0384, $wR(F2)$ = 0.0692 (all data), GOF = 0.937.

[$Co^{III}(BPB^{2-})$](BF_4^-), 2.3: Complex **2.2** (40 mg, 0.1 mmol) was dissolved in dry and degassed dichloromethane. $HBF_4.Et_2O$ (18 μL, 0.13 mmol) was added and the solution was stirred for 30 minutes. The solvent was removed *in vacuo* and resulting crude was washed multiple time with diethylether. A green precipitate was obtained. Yield: 42 mg (*ca.* 90%). Elemental analyses for $C_{18}H_{12}N_5O_3BF_4Co$; Calculated (%): C, 46.79; H, 2.62; N, 12.13. Found (%): C, 46.86; H, 2.67; N, 12.17. FT-IR (in KBr): 1718, 1618, 1590, 1554, 1476, 1452, 1394, 1277, 1083, 758 and 679 cm^{-1}. UV-visible (CH_3OH): 268 nm (ε/M^{-1} cm^{-1}, 2.06 × 10^4), 312 nm (ε/M^{-1} cm^{-1}, 1.10 × 10^4) and 398 nm (ε/M^{-1} cm^{-1}, 5.94 × 10^3). ^{1}H NMR (500 MHz, CD_3OD): δ_{ppm}, 9.70-9.68 (d, 2H), 8.93-8.91 (q, 2H), 8.38-8.35(t, 2H), 8.25-8.24(d, 2H), 7.98-7.96(t, 2H) and 7.13-7.11(q, 2H). ESI-mass (m/z): Calculated, 375.029; Found, 375.030 (after loss of BF_4^-).

[$Co^{III}(BPB^{2-})(DTC^-)$], 2.4: Mixture of complex **2.2** (40 mg, 0.1 mmol) and [$Fe^{III}(DTC^-)_3$] (65 mg, 0.13 mmol) was taken in a 25 ml round bottom flask and dissolved in dry and degassed dichloromethane. The reaction mixture was stirred for 30 minutes. The precipitate was filtered out washed multiple time with dichloromethane. Green product was obtained. Yield: 42 mg (*ca.* 80%). Elemental analyses for $C_{27}H_{32}N_5O_4S_2Co$; Calculated (%): C, 52.85; H, 5.26; N, 11.41. Found (%): C, 52.80; H, 5.32; N, 11.49. FT-IR (in KBr): 1651, 1618, 1592, 1565, 1525, 1467, 1441, 1352, 1325, 1284, 1206, 1153, 1092, 752 and 673 cm^{-1}. UV-visible (CH_3OH): 292

nm (ε/M^{-1} cm^{-1}, 2.72 × 10^4), 397 nm (ε/M^{-1} cm^{-1}, 1.01 × 10^4) and 590 nm (ε/M^{-1} cm^{-1}, 2.93 × 10^2). ESI-mass (m/z): Calculated, 524.062; Found, 524.063. Crystal data: complex **2.4**, CCDC No. 2279343, $C_{27}H_{32}N_5O_4CoS_2$, M = 613.63, Monoclinic (P 21/c), a = 11.5584(11) Å, b = 20.649(2) Å, c = 12.1832(12) Å, α = 90°, β = 98.591(3)°, γ = 90°, V = 2875.2(5) $Å^3$, Z = 4, D_c = 1.418 g cm^{-3}, μ = 0.784 mm^{-1}, T = 298(2) K, 9717 reflections, 4333 independent, $R(F)$ = 0.0467 [$I > 2\delta(I)$], R(int) = 0.0596, $wR(F2)$ = 0.1143 (all data), GOF = 1.158.

[$Fe^{III}(DTC^-)_3$]: $FeCl_3 \cdot 6H_2O$ (0.27 g, 1 mmol) was dissolved in 10 mL methanol. To this, a methanolic solution of sodium diethyldithiocarbamate trihydrate (0.68 g, 3 mmol in 20 mL) was added slowly. The reaction mixture was stirred for 2 hours, and the solvent was removed using rotavapour. The crude product was recrystallized from boiling toluene to get a dark brown solid. Yield: 0.45 g (*ca.* 82%). Elemental analyses for $C_{10}H_{20}N_3OS_4Fe$; Calculated (%): C, 31.41; H, 5.27; N, 10.99. Found (%): C, 31.48; H, 5.21; N, 11.05. UV-visible (in CH_2Cl_2): 347 nm (ε/M^{-1} cm^{-1}, 1.41 × 10^4), 385 nm (ε/M^{-1} cm^{-1}, 1.15 × 10^4), 510 nm (ε/M^{-1} cm^{-1}, 3.52 × 10^3) and 592 nm (ε/M^{-1} cm^{-1}, 2.85 × 10^3). FT-IR (in KBr): 1494, 1456, 1450, 1434, 1376, 1355, 1296, 1270, 1205, 1142, 1134, 1077, 991, 910, 845, and 784 cm^{-1}. ESI-mass (m/z): Calculated, 500.011; Found, 499.971 $[M]^+$.

[$Fe^{III}(TPP^{2-})(Cl)$]: $FeCl_3 \cdot 6H_2O$ (1.35 g, 5 mmol) and H_2TPP (0.31 g, 0.5 mmol) were dissolved in 20 mL dimethylformamide. The solution was refluxed for 4 hours. It was cooled to room temperature, and water was added to precipitate out the crude solid. It was then filtered and subjected to column chromatography to get a purple solid. Yield: 0.2 g (*ca.* 50%). Elemental analyses for $C_{44}H_{28}N_4ClFe$; Calculated (%): C, 75.07; H, 4.01; N, 7.96. Found (%): C, 75.02; H, 3.95; N, 8.13. UV-visible (CH_2Cl_2): 416 nm (ε/M^{-1} cm^{-1}, 1.32 × 10^5), 509 nm (ε/M^{-1} cm^{-1}, 1.30 × 10^4), 570 nm (ε/M^{-1} cm^{-1}, 5.26 × 10^3) and 690 nm (ε/M^{-1} cm^{-1}, 1.91 × 10^3). FT-IR (in KBr): 1596, 1486, 1442, 1337, 1202, 1175, 1070, 1000, 998, 807, 752, and 704

cm^{-1}.

[Fe(DTC^{-})$_2$(NO)]: Yield: 0.03 g (*ca.* 75%). Elemental analyses for $C_{10}H_{20}N_3OS_4Fe$; Calculated (%): C, 31.41; H, 5.27; N, 10.99, Found (%): C, 31. 37; H, 5. 19; N, 10.93. FT-IR (in KBr): 1690 (ν_{NO}), 1505, 1492, 1457, 1436, 1419, 1382, 1354, 1273, 1202, 1147, 1091, 1075, 1005, 970, 914 and 818 cm^{-1}. UV-visible (CH_2Cl_2): 365, 470 and 635 nm. ESI-mass (m/z): Calculated, 351.986; Found, 351.976 (after loss of NO).

[Fe(TPP^{2-})(NO)]: Yield: 0.06 g (*ca*. 86%). Elemental analyses for $C_{44}H_{28}N_5OFe$; Calculated (%): C, 75.65; H, 4.04; N, 10.03, Found (%): C, 75.61; H, 3.98; N, 10.07. FT-IR (in ATR probe): 2917, 1698 (ν_{NO}), 1596, 1440, 1345, 1263, 1202, 1171, 1158, 1071, 1001, 995, 801, 751, 717, 702, 664 and 530 cm^{-1}. UV-visible (CH_2Cl_2): 412 nm ($\varepsilon/M^{-1}\ cm^{-1}$, 3.12×10^4), 540 nm ($\varepsilon/M^{-1}\ cm^{-1}$, 2.28×10^3) and 611 nm ($\varepsilon/M^{-1}\ cm^{-1}$, 8.17×10^2). ESI-mass (m/z): Calculated, 668.166; Found, 668.172 (after loss of NO).

Reaction of complex 2.2 with $HBF_4.Et_2O$: Complex **2.2** (8 mg, 0.02 mmol) was taken in a Schlenk tube and degassed it properly with argon flash. Dry and degassed dichloromethane was added to it, followed by $HBF_4.Et_2O$ (20 µL, 0.13 mmol) and stirred for 30 minutes. The reaction mixture was dried and the product obtained was characterized using various spectroscopic techniques.

Reaction of complex 2.2 with $HBF_4.Et_2O$ in presence of [Fe^{III}(TPP^{2-})Cl]: Complex **2.2** (40 mg, 0.1 mmol) and [Fe^{III}(TPP^{2-})Cl] (70 mg, 0.1 mmol) were taken in a Schlenk tube and degassed it properly with argon flash. Dry and degassed dichloromethane was added to it and make the complexes soluble by stirring. $HBF_4.Et_2O$ (20 µL, 0.13 mmol) was added to the reaction mixture while stirring and monitor the progress of reaction using spectroscopic techniques.

Reaction of complex 2.2 with [$Fe^{III}(DTC^{-})_3$]: Complex **2.2** (40 mg, 0.1 mmol) and [$Fe^{III}(DTC^{-})_3$] (50 mg, 0.1 mmol) were taken in a Schlenk tube and degassed properly with argon flash. Dry and degassed dichloromethane was added to the tube and stirred. The progress of the reaction was monitored using different spectroscopic techniques. This reaction has been tested out in acetonitrile and methanol medium also.

Reaction of complex 2.2 with $HBF_4.Et_2O$ in presence of triphenylphosphine: A mixture of PPh_3 (0.016 g, 0.062 mmol) complex **2.2** (10 mg, 0.025 mmol) were dissolved in 0.2 mL of dry and degassed dichloromethane under anaerobic conditions. $HBF_4.Et_2O$ (4 µL) was added to this solution and ^{31}P-NMR of the reaction mixture was recorded in DMSO-d_6. ^{31}P-NMR (202 MHz, DMSO-d_6): $\delta_{ppm,}$ 27.95 ($Ph_3P{=}O$), 21.69 ($Ph_3P{=}NH$) and -4.95 (PPh_3).

Determination of the yield of N_2O: N-hydroxybenzenesulfonamide was taken in five 25 mL round bottom flasks in different amounts and degassed using argon/vacuum purge. 10 mL of 0.1 M NaOH solution was added to each flask under the sealed condition. 1 mL of headspace gas from each reaction vessel was subjected to GC. From there, a calibration curve of the concentration of N-hydroxybenzenesulfonamide and peak area at 2.85 minutes (corresponding to N_2O) was drawn.

Complex **2.2** (0.2 g, 0.5 mmol) in 15 mL of dry and degassed dichloromethane was taken in a 25 mL round bottom flask and 87 µL of $HBF_4{\cdot}Et_2O$ was added to it under anaerobic condition. After the completion of the reaction, 1 mL of headspace gas was subjected to GC, and the amount of N_2O was measured from the calibration curve. Yield: *ca.* 71%.

2.4 Conclusion

Thus, in conclusion, a five coordinated Co-nitrosyl complex, **2.2** has been synthesized and characterized spectroscopically as well as structurally. Complex **2.2,** in dichloromethane, in the

presence of HBF_4 releases HNO which has been confirmed by the presence of N_2O in the head-space gas as well as by its characteristic reaction with PPh_3. Complex **2.2** does not react with $[Fe^{III}(TPP^{2-})Cl]$ as such; however, in the presence of one mole equivalent of HBF_4, it has been found to transfer NO^- to $[Fe^{III}(TPP^{2-})Cl]$ resulting in the formation of $[Fe(TPP^{2-})(NO)]$. Additionally, one equivalent of $[Fe^{III}(DTC^-)_3]$ was found to induce the NO^- transfer from complex **2.2,** leading to the formation of $[Fe(DTC^-)_2(NO)]$. All these studies suggest that complex **2.2** can act as a potential NO^- or HNO donor in the presence of anionic sixth ligands in organic solvent.

2.5 References

1. (a) Doctorovich, F.; Bikiel, D. E.; Pellegrino, J.; Suárez, S. A.; Martí, M. A. *Acc. Chem. Res.* **2014**, *47*, 2907. (b) Suarez, S. A.; Neuman, N. I.; Munoz, M.; Alvarez, L.; Bikiel, D. E.; Brondino, C. D.; Ivanovic-Burmazovic, I.; Miljkovic, J. L.; Filipovic, M. R.; Marti, M. A.; Doctorovich, F. *J. Am. Chem. Soc*. **2015**, *137*, 4720.
2. Doctorovich, F.; Bikiel, D.; Pellegrino, J.; Suárez, S. A.; Larsen, A.; Martí, M. A. *Coord. Chem. Rev.* **2011**, *255*, 2764.
3. Bazylinski, D. A.; Hollocher, T. C. *J. Am. Chem. Soc*. **1985**, *107*, 7982.
4. Bazylinsky, D. A.; Goretski, J.; Hollocher, T. C. *J. Am. Chem. Soc*. **1985**, *107*, 7986.
5. Kumar, M. R.; Pervitsky, D.; Chen, L.; Poulos, T.; Kundu, S.; Hargrove, M. S.; Rivera, E. J.; Diaz, A.; Colón, J. L.; Farmer, P. *J. Biochemistry*, **2009**, *48*, 5018.
6. Paolocci, N.; Saavedra, W. F.; Miranda, K. M.; Martignani, C.; Isoda, T.; Hare, J. M.; Espey, M. G.; Fukuto, J. M.; Feelisch, M.; Wink, D. A.; Kass, D. A. *Proc. Natl. Acad. Sci*. **2001**, *98*, 10463.
7. Väänänen, A. J.; Salmenperä, P.; Hukkanen, M.; Rauhala, P.; Kankuri E. *Free Radic. Biol. Med.* **2006**, *41*, 120.

8. Lancel, S.; Zhang, J.; Evangelista, A.; Trucillo, M. P.; Tong, X.; Siwik, D. A.; Cohen, R. A.; Colucci, W. S. *Circ. Res*. **2009**, *104*, 720.
9. (a) Miranda, K. M.; Paolocci, N.; Katori, T.; Thomas, D. D.; Ford, E.; Bartberger, M. D.; Espey, M. G.; Kass, D. A.; Feelisch, M.; Fukuto, J. M.; Wink, D. A. *Proc. Natl. Acad. Sci*. **2003**, *100*, 9196. (b) Liochev, S. I.; Fridovich, I. *Free Radic. Biol. Med.* **2003**, *34*, 1399.
10. (a) Angeli, A.; Angelico, A.; Scurti, *F. Chem. Zentralbl*. **1902**, *73*, 691 (b) Miao, Z.; King, S. B. *Nitric Oxide*, **2016**, *57*, 1.
11. (a) Miranda, K. M. *Coord. Chem. Rev*. **2005**, *249*, 433. (b) Bonner, F. T.; Ko, Y. *Inorg. Chem.* **1992**, *31*, 2514. (c) Paolocci, N.; Jackson, M. I.; Lopez, B. E.; Miranda, K.; Tocchetti, C. G.; Wink, D. A.; Hobbs, A. J.; Fukuto, J. M. *Pharmacol. Ther*. **2007**, *113*, 442.
12. (a) Adak, S.; Wang, Q.; Stuehr, D. J. *J. Biol. Chem.* **2000**, *275*, 33554. (b) Rusche, K. M.; Spiering, M. M.; Marletta, M. A. *Biochemistry*, **1998**, *37*, 15503. (c) Lehnert, N.; Kim, E.; Dong, H. T.; Harland, J. B.; Hunt, A. P.; Manickas, E. C.; Oakley, K. M.; Pham, J.; Reed, G. C.; Alfaro, V. S. *Chem. Rev*. **2021**, *121*, 14682. (d) Sato, M.; Hida, N.; Umezawa, Y. *Proc. Natl. Acad. Sci. U. S. A*. **2005**, *102*, 14515. (e) Chachlaki, K.; Prevot, V. *Br. J. Pharmacol*. **2020**, *177*, 5437.
13. Walter, M. R.; Dzul, S. P.; Rodrigues, A. V.; Stemmler, T. L.; Telser, J.; Conradie, J.; Ghosh, A.; Harrop, T. C. *J. Am. Chem. Soc.* **2016**, *138*, 12459.
14. Rhine, M. A.; Rodrigues, A. V.; Bieber Urbauer, R. J.; Urbauer, J. L.; Stemmler, T. L.; Harrop, T. C. *J. Am. Chem. Soc.* **2014**, *136*, 12560.
15. Barnes, D. J.; Chapman, R. L.; Vagg, R. S.; Watton, E. C. *J. Chem. Eng. Data.* **1978**, *23*, 349.
16. Chapman, R. L.; Vagg, R. S. *Inorg. Chim. Acta.* **1979**, *33*, 227.

17. Liu, Y. Q.; Zeng, X. R. *Acta Cryst.* **2007**, E63, m2547.

18. Haller, K. J.; Johnson, P. L.; Faltham, R. D.; Enemark, J. H.; Ferraro, J. R.; Basile, L. J. *Inorg. Chim. Acta.* **1979**, *33*, 119.

19. Deka, H.; Ghosh, S.; Saha, S.; Gogoi, K.; Mondal, B. *Dalton Trans*. **2016**, *45*, 10979.

20. Gogoi, K.; Saha, S.; Mondal, B.; Deka, H.; Ghosh, S.; Mondal, B. *Inorg. Chem*. **2017**, *56*, 14438.

21. (a) Patra, A. K.; Dube, K. S.; Sanders, B. C.; Papaefthymiou, G. C.; Conradie, J.; Ghosh, A.; Harrop, T. C. A. *Chem. Sci.* **2012**, *3*, 364. (b) Kumar, P.; Lee, Y.-M.; Hu, L.; Chen, J.; Park, Y. J.; Yao, J.; Chen, H.; Karlin, K. D.; Nam, W. *J. Am. Chem. Soc.* **2016**, *138*, 7753. (c) Popp, J.; Riggenmann, T.; Schröder, D.; Ampßler, T.; Salvador, P.; Klüfers, P. *Inorg. Chem*. **2021**, *60*, 15980.

22. (a) McCleverty, J. A. *Chem. Rev*. **1979**, *79*, 53. (b) Duffin, P. A.; Larkworthy, L. F.; Mason, J.; Stephens, A. N.; Thompson, R. M. *Inorg. Chem*. **1987**, *26*, 2034.

23. (a) McCleverty, J. A. *Chem. Rev*. **2004**, *104*, 403. (b) Wyllie, G. R. A.; Scheidt, W. R. *Chem. Rev*. **2002**, *102*, 1067.

24. Huheey, J. E.; Keiter, E. A.; Keiter, R. L. Inorganic chemistry: Principles of structure and reactivity, 4th ed.; Harper Collins College Publishers: New York, **1993**.

25. (a) Bari, S. E.; Martí, M. A.; Amorebieta, V. T.; Estrin, D. A.; Doctorovich, F. *J. Am. Chem. Soc.* **2003**, *125*, 15272. (b) Martí, M. A.; Bari, S. E.; Estrin, D. A.; Doctorovich, F. *J. Am. Chem. Soc*. **2005**, *127*, 4680. (c) Doyle, M. P.; Mahapatro, S. N.; Broene, R. D.; Guy, J. K. *J. Am. Chem. Soc*. **1988**, *110*, 593. (d) Miranda, K. M.; Nims, R. W.; Thomas, D. D.; Espey, M. G.; Citrin, D.; Bartberger, M. D.; Paolocci, N.; Fukuto, J. M.; Feelisch, M.; Wink, D. A. *J. Inorg. Biochem*. **2003**, *93*, 52.

26. Mazumdar, R.; Saha, S.; Samanta, B.; Mondal B. *Inorg. Chem*. **2021**, *60*, 18024.

27. Ileperuma, O. A.; Feltham, R. D. *Inorg. Chem.* **1977**, *16*, 1876.

28. Enemark, J. H.; Feltham, R. D.; Huie, B. T.; Johnson, P. L.; Swedo, K. B. *Inorg. Chem*. **1975**, *14*, 624.

29. Bonadeo, H.; Silberman, E. *J. Mol. Spectrosc.* **1969**, *32*, 214.

30. Shafirovich, V.; Lymar, S. V. *Proc. Natl. Acad. Sci. U. S. A*. **2002**, *99*, 7340.

31. Reisz, J. A.; Klorig, E. B.; Wright, M. W.; King, S. B. *Org. Lett*. **2009**, *11*, 2719.

32. SMART, SAINT and XPREP; Siemens Analytical X-ray Instruments Inc.: Madison, Wisconsin, USA, **1995**.

33. (a) Sheldrick, G. M. *Acta Crystallogr. Sect. A Found. Adv.* **2015***, 71,* 3. (b) Sheldrick, G. M. *Acta Crystallogr. Sect. C Struct. Chem.* **2015**, *71*, 3. (c) Farrugia, L. J. ORTEP-3 for Windows - a version of ORTEP-III with a Graphical User Interface (GUI). *J. Appl. Crystallogr.* **1997**, *30*, 565.

Chapter 3

Reaction of a cobalt(II)-nitrosyl complex with dithiocarbamate ligand: a potential nitroxyl anion donor

Abstract

The distinct chemical properties and reactivity of nitroxyl (HNO/NO^-) over nitric oxide (NO) draw the attention of the researchers significantly. However, the extensive study of HNO is inhibited by its high reactivity towards itself. Hence, for the better understanding of its generation and reactivity, donor compounds are required. Metal-nitrosyl complexes of suitable electronic configuration can act as a potential HNO donor. Here, a penta-coordinated cobalt nitrosyl complex, $[Co(BPI^-)(NO)(OAc^-)]$, **3.1** having $\{Co(NO)\}^8$ configuration has been reported. In the reaction with diethyldithiocarbamate anion (DTC^-), complex **3.1** was found to donate nitroxyl anion (NO^-) to the suitable acceptors such as $[Fe^{III}(TPP^{2-})Cl]$. The HNO release from the complex **3.1** was observed in the presence of H^+, which is confirmed by the detection of nitrous oxide (N_2O) in GC as well as its reaction with PPh_3.

3.1 Introduction

Nitroxyl (HNO), the one electron reduced analogue of nitric oxide (NO), demonstrates unique biological and chemical reactivity compared to its predecessor.[1-3] But its *in-vivo* production and biological activity has not been thoroughly investigated mostly because of its rapid dimerization to N_2O.[4] Furthermore, nitoxyl was found to be very reactive towards soft nucleophiles like thiols[5] and metalloproteins[6], making the isolation and quantification very difficult. In order to thoroughly examine the reactivity of HNO, efficient HNO donors are required. However, HNO donation was limited to some selected compounds like Angeli's salt, Piloty's acid etc.[7-8] Other than that, some reactive intermediates *e.g.* acyl and acyloxy nitroso compounds are often found to donate HNO under specific reaction conditions.[9-10] But the intrinsic limitations of these compounds, such as, concurrent production of biologically toxic by-products or unattainable reaction conditions in physiological medium inhibit their universal applicability. Hence, more efficient donors are needed.

The transition metal-nitrosyls are used as NO donor for quite a long time. Exposure to the external stimuli like heat, light and alteration of the reaction conditions (solvents, pH, etc.) are found to be greatly effective for the release of NO from metal nitrosyls.[11-17] But the release of HNO from a metal nitrosyl complex is much more complicated and requires suitable electronic configuration of the [M-NO] centre as well as suitable ligand frameworks. In this regard, great advancement was made over the last decade. Many electron rich iron-nitrosyl complexes of $\{Fe(NO)\}^8$ configuration were reported to donate HNO.[18-23] An electron deficient $\{Fe(NO)\}^6$ complex was also observed to donate HNO upon exposure to light.[24] The thiol-proton present in the ligand framework plays a crucial role. In contrast, HNO donation from cobalt-nitrosyl complexes is relatively less explored. Although, the cobalt-nitrosyl complexes of $\{Co(NO)\}^8$ configurations are well-known for their $[Co^{III}\text{-}NO^-]$ character, only a few are reported for HNO/NO^- donation. Harrop *et al.* reported the first example of HNO release from a $\{Co(NO)\}^8$

complex in the presence of proton.[25] Subsequently, two more $\{Co(NO)\}^9$ complexes in similar ligand framework were reported by the same group, which also donate HNO to the target complexes.[26] Recently, our group reported a sixth-ligand induced HNO/NO^- donation from a $\{Co(NO)\}^8$ complex.[27] Hence, for the better understanding, more examples of HNO/NO^- donation from cobalt-nitrosyl complexes are needed.

This chapter describes a penta-coordinated cobalt-nitrosyl complex of $\{Co(NO)\}^8$ configuration, which can act as a potential HNO donor. In the presence of an anionic ligand i.e. diethyldithiocarbamate anion (DTC^-), the nitrosyl complex was found to donate NO^- to the target Fe^{III}-complexes. The HNO donation has been tested by its reaction with phosphines. The evolution of N_2O from the reaction mixture also confirms the same.

3.2 Results and discussion

The ligand, 1,3-*bis*(2′-pyridylimino)isoindol (HBPI) was synthesized following a previously reported procedure.[28] The formation of the ligand was confirmed using spectroscopic analyses (Exp. Sec., Appendix II, Figures A2.1-A2.4). The corresponding $\{Co(NO)\}^8$ complex, [$Co(BPI^-)(NO)(OAc^-)$], **3.1** was synthesized using a reported procedure.[29] The structural and spectroscopic characterization match well with the reported one (Exp. Sec., Appendix II, Figures A2.5-A2.8). The ORTEP diagram is shown in figure 3.1. The crystal parameters are given in Appendix II (Table A2.1-A2.3). Complex **3.1** shows characteristic nitrosyl stretching frequency at 1674 cm^{-1} in FT-IR spectrum (Appendix II, Figure A2.5). Two absorption bands at 348 (intra-ligand charge transfer) and 470 nm (LMCT) were observed in the UV-visible spectrum (Appendix II, Figure A2.6). Complex **3.1** remains silent in EPR spectroscopic studies, which is expected for this class of compounds (Appendix II, Figure A2.7).[25,27]

The formal electronic character of $\{Co(NO)\}^8$ complexes are considered as [Co^{III}-NO^-], making them a potential candidate for HNO/NO^- donation. However, the kinetic inertness of

the low-spin cobalt(III)-centre (d^6 electronic configuration) impedes the complex's ability to donate HNO/NO^-. Hence, activation of the cobalt-centre is required.

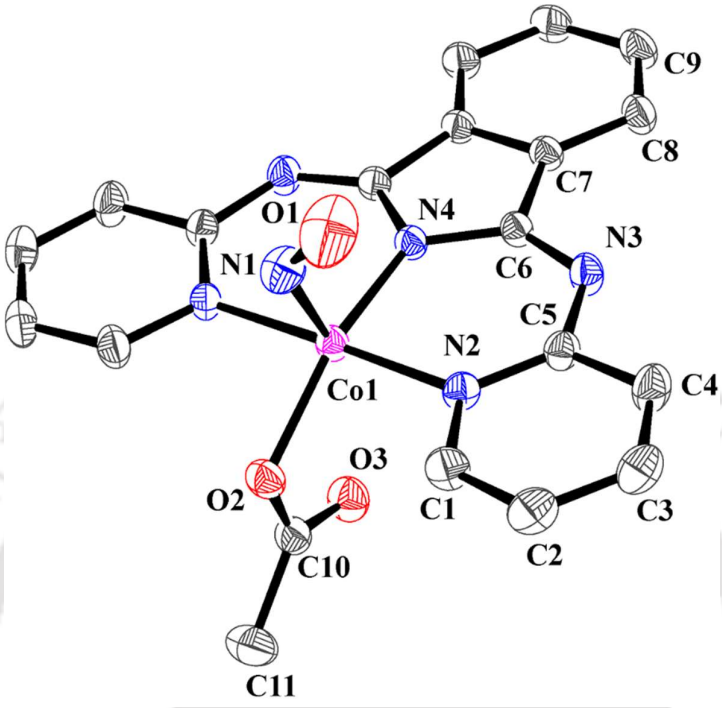

Figure 3.1. ORTEP diagram of complex **3.1** (showing 30% thermal ellipsoid. H-atoms are omitted for clarity).

Earlier, Enemark and coworkers demonstrated that changing the coordination number of the cobalt centre in a penta-coordinated cobalt-nitrosyl complex from five to six results in the change of the electronic nature of the coordinated nitrosyl from NO^+ to NO^-.[30] Based on this observation, an anionic ligand, diethyldithiocarbamate anion (DTC^-) was introduced into the dry and degassed dichloromethane solution of complex **3.1**, where the nitrosyl exhibit NO^- character and the reaction was studied using various spectroscopic techniques. In dry and degassed dichloromethane solution, the complex **3.1** was found to be very stable under argon atmosphere. But, in UV-visible spectroscopy, addition of 1.2 mole equivalent of NaDTC (in methanol) to the dichloromethane solution of complex **3.1** shows gradual change in spectral pattern and finally a new complex, **3.2** was formed (Figure 3.2(a)). The absorption band of complex **3.1** at 470 nm gradually shifted to 474 nm with a shoulder at 509 nm.

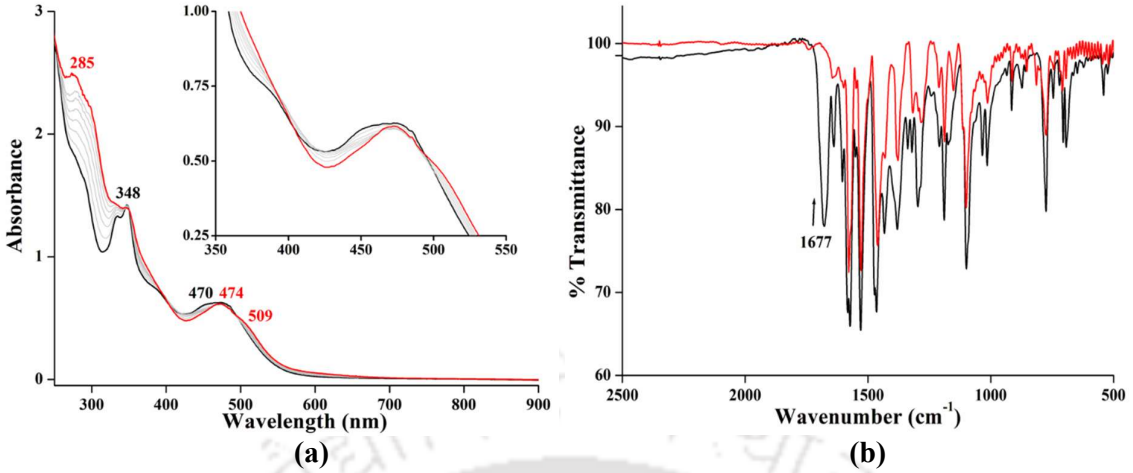

Figure 3.2. (a) UV-visible (CH_2Cl_2, room temperature) and (b) FT-IR (KBr) spectra of complex **3.1** in the absence (black) and presence (red) of NaDTC.

The FT-IR spectral monitoring of the reaction shows the complete disappearance of the nitrosyl stretching frequency at 1674 cm^{-1} (Figure 3.2(b)). No new stretching signal associated with the formation of any oxidized or reduced product of NO was observed, suggesting the release of nitrosyl moiety from complex **3.1**. Recently, it was reported that in the presence of DTC^-, a five-coordinated $\{Co(NO)\}^8$ complex was found to release NO^-.[27] It is proposed that the release of NO^- from the $\{Co(NO)\}^8$ complex is being facilitated by the DTC^- ligand attacking the cobalt centre. Presumably, this reaction also proceeds in the same manner. Isolation of the products and spectroscopic characterization (Appendix II, Figures A2.9-A2.12) confirms the presence of coordinated DTC^- ligand in the newly formed complex **3.2**. The ESI-mass spectrum shows a signal at m/z = 505.069 (Calculated: 505.068) for the $[Co^{III}(BPI^-)(DTC^-)]^+$ unit (Appendix II, Figure A2.12). The EPR silent nature confirms the presence of cobalt(III)-centre in the complex **3.2** (Appendix II, Figure A2.11). All these spectroscopic observations confirm the one electron oxidation of the cobalt-centre and concomitant release of nitrosyl moiety. But, when the headspace gas of the reaction vessel was purged into a dry and degassed dichloromethane solution of $[Fe^{II}(DTC^-)_2]$, no new stretching frequency for the formation of $[Fe(NO)(DTC^-)_2]$ was observed in FT-IR spectrum (Appendix II, Figure A2.13). Therefore, it

is reasonable to assume that the release of NO moiety from the complex **3.1** as NO^-. Formation of any intermediate was not observed, which confirms the concurrent nature of the reaction.

The NO^- donation from complex **3.1** was confirmed by its reaction with well-known nitroxyl acceptor, $[Fe^{III}(TPP^{2-})Cl]$.[25,27,31] The reaction of complex **3.1** and $[Fe^{III}(TPP^{2-})Cl]$ in dry and degassed dichloromethane solution does not lead to any nitrosylation product of the target complex even after 24 hours (Figure 3.3(a), black). But, in the presence of DTC^-, the FT-IR spectrum of the reaction mixture shows a formation of a strong stretching frequency at 1698 cm^{-1} which is characteristic of the $[Fe(TPP^{2-})(NO)]$ complex (Figure 3.3(a), red).[25,27] Studying the same reaction in X-band EPR spectroscopy at 77 K shows the disappearance of the characteristic Fe(III) signal and a new sharp signal at g ~ 2.04 appeared which also confirms the formation of $\{Fe(NO)\}^7$ complex (Figure 3.3(b)).[27,31,32] The $[Fe(TPP^{2-})(NO)]$ was isolated and characterized spectroscopically (Appendix II, Figures A2.16-A2.19).

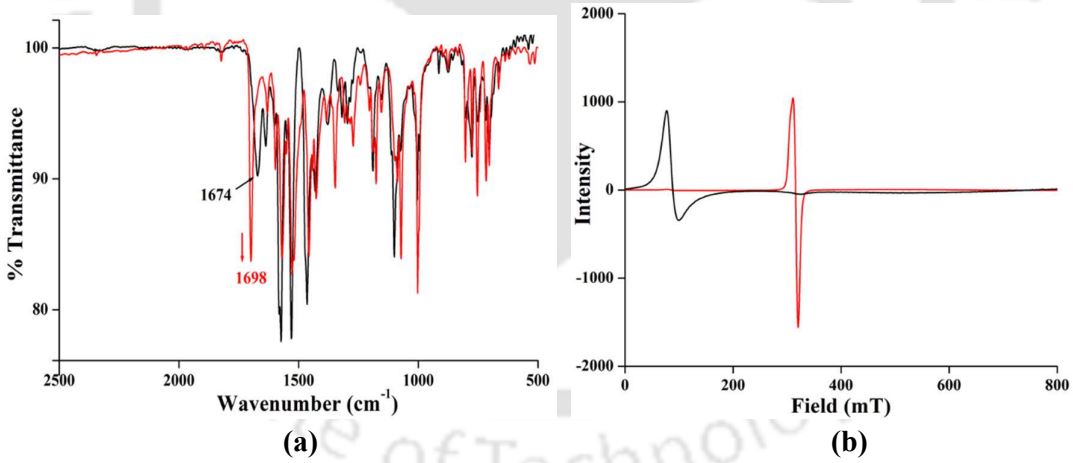

Figure 3.3. (a) FT-IR (KBr) and (b) X-band EPR (CH_2Cl_2, 77 K) spectra of the reaction mixture of complex **3.1** with $[Fe^{III}(TPP^{2-})Cl]$ in absence (black) and presence (red) of NaDTC.

$$[Co(BPI^-)(NO)(OAC^-)]+[Fe^{III}(DTC^-)_3] \rightarrow [Co^{III}(BPI^-)(DTC^-)(OAC^-)]+[Fe(DTC^-)_2(NO)] \quad \text{... Eq. 3.1}$$

The NO^- release was further confirmed by the reaction of complex **3.1** with another nitroxyl acceptor, $[Fe^{III}(DTC^-)_3]$ (Eq. 3.1).[27,33] In FT-IR spectroscopic study, the reaction mixture of

complex **3.1** and $[Fe^{III}(DTC^{-})_3]$ in dichloromethane shows a new stretching frequency at 1688 cm^{-1}, which is characteristic nitrosyl stretching frequency for $[Fe(NO)(DTC^{-})_2]$ complex. This again confirms the reductive nitrosylation of the iron centre of $[Fe^{III}(DTC^{-})_3]$ (Appendix II, Figure A2.14). It is noteworthy that the $[Fe^{III}(DTC^{-})3]$ complex was found to dissociate in the reaction medium, acting as a source of the DTC^{-} ligand itself.[27,33] Hence, the addition of NaDTC is not required. The formation of $[Fe(NO)(DTC^{-})_2]$ was also confirmed from the X-band EPR spectral study at 77 K showing a sharp signal at g ~ 2.05 (Appendix II, Figure A2.15).[27,33,34] The isolated $[Fe(DTC^{-})_2(NO)]$ was characterized spectroscopically (Appendix II, Figures A2.20-A2.23).

The release of HNO was also evidenced by its characteristic reaction with phosphines (PR_3) was tested.[35] The reaction of complex **3.1** and PPh_3 was done in the presence of NaDTC and a suitable proton source (HBF_4). The ^{31}P-NMR spectrum of the reaction mixture shows signals at δ_{ppm} = 21.17 and 32.23 for azaylide ($Ph_3P{=}NH$) and phosphine oxide ($Ph_3P{=}O$), respectively (Figure 3.4).[27,33] The unreacted PPh_3 displays a signal at -5.72 ppm. The signal at 43.25 ppm appears due to the presence of metal-bound PPh_3.[36]

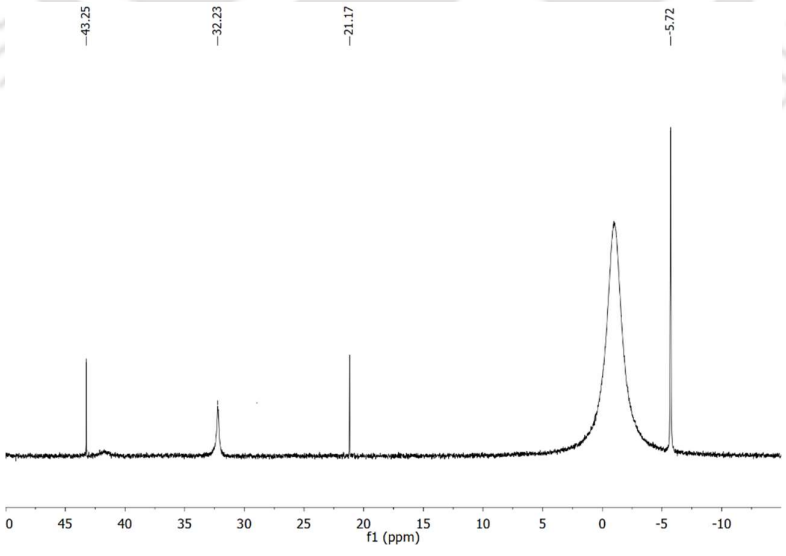

Figure 3.4. ^{31}P-NMR spectrum of the reaction mixture of complex **3.1**, NaDTC and PPh_3 in the presence of H^{+} in CH_2Cl_2 solution with few drops of $CDCl_3$.

Due to rapid dimerization, HNO becomes $H_2N_2O_2$ (hyponitrous acid) and finally decomposes to give N_2O (nitrous oxide) and H_2O.[4] This N_2O formation acts as a chemical marker for the HNO. When the headspace gas of the reaction vessel containing complex **3.1**, NaDTC and HBF_4 (as proton source) in dry and degassed dichloromethane was subjected to gas chromatographic detection, the presence of N_2O was observed (Appendix II, Figure A2.24). The N_2O produced in the reaction was quantified with respect to a standard calibration curve prepared from an alkaline solution of Piloty's acid and found to be *ca.* 66 % (Appendix II, Figure A2.25). A strong signal at m/z = 44 in the GC-MS spectrum also confirms the formation of N_2O (Appendix II, Figure A2.26).

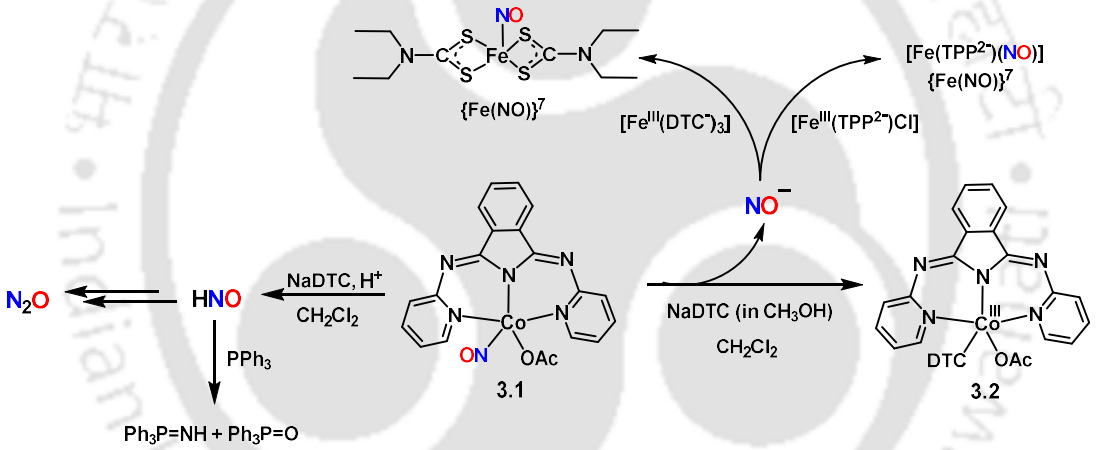

Scheme 3.1. Overall reactions.

3.3 Experimental Section

3.3.1 Materials and Methods

All the reagents were purchased from commercial sources and used as it is without further purification unless specified. Dichloromethane was passed through an alumina column and stored over calcium hydride overnight, followed by distillation under N_2. Methanol was dried by distillation with Mg-turnings and iodine. Tetrafluoroboric acid was dried over 4Å molecular sieves under argon. All the reactions were performed under inert atmosphere except mentioned

differently. Deoxygenation of solvents and solutions was done by consecutive argon/vacuum purge cycles. UV-visible spectra were recorded on an Agilent Cary 8454 spectrophotometer. FT-IR spectra were recorded as KBr pellets or in a KBr cell using a PerkinElmer spectrophotometer. ^{1}H, ^{13}C, and ^{31}P-NMR studies were done in Bruker Avance III 400 and 500 MHz Varian FT-NMR spectrophotometers. X-band EPR spectra were recorded on a JES-FA200 EPR spectrophotometer with microwave power, 0.998 mW; microwave frequency, 9.14 GHz; and modulation amplitude, 2. Gas chromatograms were obtained on PerkinElmer Clarus® 590.

Single crystals were grown from methanol solutions using the slow evaporation technique. The intensity data were collected using a Bruker SMART APEX-II CCD diffractometer, equipped with a fine focus 1.75 kW sealed tube Mo Kα radiation (λ = 0.71073 Å), with increasing ω (width of 0.3° per frame) at a scan speed of 3 s/frame. The SMART software was used for data acquisition. Data integration and reduction were undertaken with SAINT and XPREP software.[37] Structures were solved by direct methods using SHELXL[38a] and refined with full-matrix least-squares on F^2 using SHELXL-2019/1.[38b] Structural illustrations were drawn with ORTEP-3 for Windows.[38c]

3.3.2 Syntheses

1,3-*bis*(2′-pyridylimino)isoindol, HBPI: The ligand was synthesized following a reported procedure with a little modifications.[28] 2-aminopyridine (3.95 g, 42 mmol), 1,2-dicyanobenzene (2.56 g, 20 mmol) and $CaCl_2$ (0.22 g, 2 mmol) were taken in a 100 mL two neck round bottom flask. 30 mL n-butanol was added to it and refluxed for 48 hours. Upon cooling to room temperature, a bright yellow precipitate was observed to form. The precipitate was isolated by filtration and washed several times with ethanol and finally recrystalized from ethanol/water mixture. Yield: 4.72 g (*ca.* 79%). Elemental analyses for $C_{18}H_{13}N_5$; Calculated

(%): C, 72.23; H, 4.38; N, 23.40. Found (%): C, 72.15; H, 4.36; N, 23.50. FT-IR (ATR): ^{1}H-NMR (400 MHz, $CDCl_3$): $\delta_{ppm,}$ 13.98 (s, 1H), 8.62-8.61 (d, 2H), 8.09-8.07 (dd, 2H), 7.78-7.75 (dt, 2H), 7.66-7.64 (dd, 2H), 7.47-7.45 (d, 2H) and 7.13-7.10 (dd, 2H). ^{13}C-NMR (100 MHz, $CDCl_3$): δ_{ppm}, 160.5, 153.7, 147.8, 138.1, 135.8, 131.6, 123.2, 122.6 and 120.2. ESI-mass (m/z): Calculated, 299.117; Found, 300.124 $[M+H]^+$.

[Co(BPI$^-$)(NO)(OAc$^-$)], 3.1: The cobalt-mononitrosyl complex, **3.1** was synthesized using a reported procedure.[29] Ligand HBPI (60 mg, 0.2 mmol), $Co(OAc^-)_2.4H_2O$ (49 mg, 0.2 mmol) were taken in a 15 mL Schlenk tube equipped with a rubber septum. The tube was degassed thoroughly using consecutive argon/vacuum cycles. NO gas was filled into the reaction vessel and 5 mL distilled and degassed methanol was added. Upon keeping the reaction mixture overnight at room temperature, green block shaped crystals of complex **3.1** were obtained and isolated by filtration. Yield: 57 mg (*ca.* 66%). The complex was characterized both structurally and spectroscopically. Elemental analyses for $C_{20}H_{15}N_6O_2Co$; Calculated (%): C, 55.82; H, 3.51; N, 19.53. Found (%): C, 55.88; H, 3.58; N, 19.68. FT-IR (in ATR probe): 2898, 1677 (ν_{NO}), 1638, 1582, 1572, 1529, 1478, 1465, 1433, 1380, 1296, 1189, 1099, 1034, 1014, 774, 705 and 692 cm^{-1}. UV-visible (CH_2Cl_2): 348 nm (ε/ M^{-1} cm^{-1}, 1.24×10^4) and 470 nm (ε/ M^{-1} cm^{-1}, 6.23×10^3). ESI-mass (m/z): Calculated: 387.040; Found: 387.281 (for $[Co(BPI^-)(NO)]^+$ unit).

[Co^{III}(BPI$^-$)(DTC$^-$)(OAc$^-$)], 3.2: Complex **3.1** (86 mg, 0.2 mmol) was taken in a 25 mL round bottom flask equipped with a magnetic stirring bar and degassed *via* continuous argon purge. Distilled and degassed dichloromethane (10 mL) was added to it. A degassed methanolic (5 mL) solution of NaDTC (45 mg, 0.2 mmol) was added to it using a gas tight Hamilton syringe and the reaction mixture was stirred for 2 hours at room temperature. Upon removing the solvent using rotary evaporator, a brown colored solid was isolated and washed with diethyl

ether. Yield: 78 mg (*ca.* 72%). Elemental analyses for $C_{25}H_{25}N_6OS_2Co$; Calculated (%): C, 54.74; H, 4.59; N, 15.32. Found (%): C, 54.67; H, 4.51; N, 15.48. FT-IR (in ATR probe): 2927, 2857, 1580, 1529, 1464, 1431, 1376, 1320, 1287, 1185, 1101, 1013 and 776 cm^{-1}. UV-visible (CH_2Cl_2): 289 nm (ε/M^{-1} cm^{-1}, 5.19×10^4), 349 nm (ε/M^{-1} cm^{-1}, 3.93×10^4) and 476 nm (ε/M^{-1} cm^{-1}, 1.86×10^4). ESI-mass (m/z): Calculated: 505.068; Found: 505.069 (for $[Co(BPI^{-})(DTC^{-})]^{+}$).

$[Fe^{III}(TPP^{2-})Cl]$: The preparation procedure and spectroscopic characterization were described earlier (Exp. Sec., Chapter 2).

$[Fe^{III}(DTC^{-})_3]$: The preparation procedure and spectroscopic characterization were described earlier (Exp. Sec., Chapter 2).

$[Fe(DTC^{-})_2(NO)]$: Yield: 32 mg (*ca.* 85%). Elemental analyses for $C_{10}H_{20}N_3OS_4Fe$; Calculated (%): C, 31.41; H, 5.27; N, 10.99, Found (%): C, 31. 37; H, 5. 19; N, 11.08. FT-IR (in KBr): 1690 (ν_{NO}), 1505, 1492, 1457, 1436, 1419, 1382, 1354, 1273, 1202, 1147, 1091, 1075, 1005, 970, 914 and 818 cm^{-1}. UV-visible (CH_2Cl_2): 365, 470 and 635 nm. ESI-MS (m/z): Calculated: 351.986; Found: 351.976 (after loss of NO).

$[Fe(TPP^{2-})(NO)]$: Yield: 57 mg (*ca.* 82%). Elemental analyses for $C_{44}H_{28}N_5OFe$, Calculated (%): C, 75.65; H, 4.04; N, 10.03, found (%): C, 75.61; H, 3.98; N, 10.07. FT-IR (in KBr): 2920, 1697 (ν_{NO}), 1596, 1440, 1346, 1297, 1202, 1175, 1071, 1002, 995, 803, 752, 718, 703, 664 and 530 cm^{-1}. UV-visible (CH_2Cl_2): 412 nm (ε/M^{-1} cm^{-1}, 3.12×10^4), 540 nm (ε/M^{-1} cm^{-1}, 2.28×10^3) and 611 nm (ε/M^{-1} cm^{-1}, 8.17×10^2). ESI-MS (m/z): Calculated, 668.166; Found, 668.172 (after loss of NO).

Reaction of complex 3.1 with NaDTC: Complex **3.1** (8.6 mg, 0.02 mmol) was taken in a 10

mL round bottom flask and degassed properly *via* argon flush. Dry and degassed dichloromethane (3 mL) was added to it. NaDTC (4.5 mg, 0.02 mmol) was dissolved in minimum amount of methanol (0.5 mL) and added to the dichloromethane solution of complex **3.1**. The reaction was monitored using various spectroscopic techniques.

Reaction of complex 3.1, NaDTC in the presence of [$Fe^{III}(TPP^{2-})Cl$]: Complex **3.1** (43 mg, 0.1 mmol) and [$Fe^{III}(TPP^{2-})Cl$] (70 mg, 0.1 mmol) was taken in a 10 mL round bottom flask and degassed properly *via* continuous argon purge. Dry and degassed dichloromethane (5 mL) was added to it followed by methanolic solution (1 mL) of NaDTC (23 mg, 0.1 mmol). The reaction was monitored using FT-IR spectroscopy.

Reaction of complex 3.1 with [$Fe^{III}(DTC^{-})_3$]: Complex **3.1** (43 mg, 0.1 mmol) and [$Fe^{III}(DTC^{-})_3$] (50 mg, 0.1 mmol) were taken in a 10 mL round bottom flask and degassed properly *via* continuous argon purge. Dry and degassed dichloromethane (5 mL) was added to it and the reaction mixture was stirred at room temperature. The reaction was monitored using FT-IR and X-band EPR spectroscopy.

Test for azaylide and phosphine oxide in ^{31}P-NMR: A mixture of PPh_3 (16 mg, 0.062 mmol) complex **3.1** (10 mg, 0.025 mmol) was dissolved in 0.3 mL of dry and degassed dichloromethane under anaerobic conditions. NaDTC (5.8 mg, 0.025 mmol) dissolved in 0.1 mL dry and degassed methanol was added to it, followed by $HBF_4.Et_2O$ (4.5 µL, 0.03 mmol) and ^{31}P-NMR of the reaction mixture was recorded in $CDCl_3$ after 24 hours. ^{31}P-NMR (202 MHz, $CDCl_3$): $\delta_{ppm,}$ 32.23 ($Ph_3P{=}O$), 21.17 ($Ph_3P{=}NH$) and -5.72 (PPh_3).

Determination of the yield of N_2O: To five degassed Schlenk flask (50 mL) containing different amount of *N*-hydroxybenzenesulfonamide, 0.1 M NaOH solution (10 mL) was added to each under argon atmosphere. 1 mL of headspace gas from each reaction vessel was

subjected to GC. By calculating the peak area at 2.84 minutes (N_2O) for each set, a calibration curve of the concentration of *N*-hydroxybenzenesulfonamide was drawn.

Complex **3.1** (0.22 g, 0.5 mmol) and NaDTC (0.11 g, 0.5 mmol) in 15 mL of dry and degassed dichloromethane was taken in a 10 mL round-bottom flask and 50 µL of $HBF_4 \cdot Et_2O$ was added to it and stirred for 1 hour under argon atmosphere. After that, 1 mL of headspace gas was subjected to GC and amount of N_2O was measured from the calibration curve. Yield: *ca.* 66%.

3.4 Conclusion

Hence, in this chapter, a penta-coordinated cobalt nitrosyl complex, **3.1** was synthesized and studied for nitroxyl donation. In the presence of DTC^- as the sixth ligand, complex **3.1** was found to donate NO^- to the targets like $[Fe^{III}(TPP^{2-})Cl]$ and $[Fe^{III}(DTC^-)_3]$. The reductive nitrosylation product of these target complexes confirms the NO^- release. In the presence of H^+, the NO^- released from complex **3.1** becomes HNO, which is confirmed by the gas chromatographic detection of N_2O in the head-space of the reaction vessel. The HNO donation was further confirmed by its reaction with PPh_3.

3.5 References

1. Irvine, J. C.; Ritchie, R. H.; Favaloro, J. L.; Andrews, K. L.; Widdop, R. E.; Kemp Harper, B. K. *Trends Pharmacol. Sci*. **2008**, *29*, 601.
2. Fukuto, J. M.; Bartberger, M. D.; Dutton, A. S.; Paolocci, N.; Wink, D. A.; Houk, K. N. *Chem. Res. Toxicol.* **2005**, *18*, 790.
3. Miranda, K. M. *Coord. Chem. Rev.* **2005**, *249*, 433.
4. Shafirovich, V.; Lymar, S. V. *Proc. Natl. Acad. Sci. U.S.A*. **2002**, *99*, 7340.
5. Szaciłowski, K.; Chmura, A.; Stasicka, Z. *Coord. Chem. Rev.* **2005**, *249*, 2408.
6. Ford, P. C.; Lorkovic, I. M. *Chem. Rev.* **2002**, *102*, 993.
7. Angeli, A.; Rimini, E. *Gazz. Chim. Ital.* **1896**, *26*, 17.

8. Piloty, O. *Ber. Dtsch. Chem. Ges.* **1896**, *29*, 1559.
9. (a) Christie, C. C.; Kirby, G. W.; McGuigan, H.; Mackinnon, J. W. M. *J. Chem. Soc. Perkin Trans I*, **1985**, 2469. (b) Howard, J. A. K.; Ilyashenko, G.; Sparkes, H. A.; Whiting, A. *Dalton. Trans*. **2007**, *21*, 2108.
10. Sha, X.; Isbell, T. S.; Patel, R. P.; Day, C. S.; King, S. B. *J. Am. Chem. Soc.* **2006**, *128*, 9687.
11. Patra, A. K.; Afshar, R.; Olmstead, M. M.; Mascharak, P. K. *Angew. Chem. Int. Ed.* **2002**, *41*, 2512.
12. Harrop, T. C.; Mascharak, P. K. *Acc. Chem. Res.* **2004**, *37*, 253.
13. Eroy-Reveles, A. A.; Leung, Y.; Beavers, C. M.; Olmstead, M. M.; Mascharak, P. K. *J. Am. Chem. Soc.* **2008**, *130*, 4447.
14. Hsieh, C.-H.; Darensbourg, M. Y. *J. Am. Chem. Soc.* **2010**, *132*, 14118.
15. McQuilken, A. C.; Ha, Y.; Sutherlin, K. D.; Siegler, M. A.; Hodgson, K. O.; Hedman, B.; Solomon, E. I.; Jameson, G. N. L.; Goldberg, D. P. *J. Am. Chem. Soc.* **2013**, *135*, 14024.
16. Jiang, Y.; Hayashi, T.; Matsumura, H.; Do, L. H.; Majumdar, A.; Lippard, S. J.; Moënne-Loccoz, P. *J. Am. Chem. Soc.* **2014**, *136*, 12524.
17. McQuilken, A. C.; Matsumura, H.; Dürr, M.; Confer, A. M.; Sheckelton, J. P.; Siegler, M. A.; McQueen, T. M.; Ivanović-Burmazović, I.; Moënne-Loccoz, P.; Goldberg, D. P. *J. Am. Chem. Soc.* **2016**, *138*, 3107.
18. Patra, A. K.; Dube, K. S.; Sanders, B. C.; Papaefthymiou, G. C.; Conradie, J.; Ghosh, A.; Harrop, T. C. *Chem. Sci.* **2012**, *3*, 364.
19. Sanders, B. C.; Patra, A. K.; Harrop, T. C. *J. Inorg. Biochem.* **2013**, *118*, 115.
20. Speelman, A. L.; Lehnert, N. *Angew. Chem. Int. Ed.* **2013**, *52*, 12283.
21. Confer, A. M.; McQuilken, A. C.; Matsumura, H.; Moënne-Loccoz, P.; Goldberg, D. P.

J. Am. Chem. Soc. **2017**, *139*, 10621.

22. Abucayon, E. G.; Khade, R. L.; Powell, D. R.; Zhang, Y.; Richter-Addo, G. B. *J. Am. Chem. Soc.* **2016**, *138*, 104.
23. Manickas, E. C.; LaLonde, A. B.; Hu, M. Y.; Alp, E. E.; Lehnert, N. *J. Am. Chem. Soc.* **2023**, *145*, 23014.
24. Chiang, C. K.; Chu, K. T.; Lin, C. C.; Xie, S. R.; Liu, Y. C.; Demeshko, S.; Lee, G. H.; Meyer, F.; Tsai, M. L.; Chiang, M. H.; Lee, C. M. *J. Am. Chem. Soc.* **2020**, *142*, 8649.
25. Rhine, M. A.; Rodrigues, A. V.; Bieber Urbauer, R. J.; Urbauer, J. L.; Stemmler, T. L.; Harrop, T. C. *J. Am. Chem. Soc.* **2014**, *136*, 12560.
26. Walter, M. R.; Dzul, S. P.; Rodrigues, A. V.; Stemmler, T. L.; Telser, J.; Conradie, J.; Ghosh, A.; Harrop, T. C. *J. Am. Chem. Soc.* **2016**, *138*, 12459.
27. Saha, S.; Maity, S.; Mazumdar, R.; Samanta, B.; Ghosh, R.; Guha, A.; Mondal, B. *Inorg. Chem.* **2023**, *62,* 17074.
28. (a) Siegl, W. O. *J. Org. Chem*. **1977**, *42*, 1872. (b) Siegl, W. O.; Ferris, F. C.; Mucci, P. A. *J. Org. Chem*. **1977**, *42*, 3442.
29. Gogoi, K.; Saha, S.; Mondal, B.; Deka, H.; Ghosh, S.; Mondal, B. *Inorg. Chem.* **2017**, *56*, 14438.
30. Enemark, J. H.; Feltham, R. D.; Riker-Nappier, J.; Bizot, K. F. *Inorg. Chem.* **1975**, *14*, 624.
31. (a) Bari, S. E.; Martí, M. A.; Amorebieta, V. T.; Estrin, D. A.; Doctorovich, F. *J. Am. Chem. Soc.* **2003**, *125*, 15272. (b) Doyle, M. P.; Mahapatro, S. N.; Broene, R. D.; Guy, J. K. *J. Am. Chem. Soc.* **1988**, *110*, 593. (c) Miranda, K. M.; Nims, R. W.; Thomas, D. D.; Espey, M. G.; Citrin, D.; Bartberger, M. D.; Paolocci, N.; Fukuto, J. M.; Feelisch, M.; Wink, D. A. *J. Inorg. Biochem.* **2003**, *93*, 52.
32. McQuarters, A. B.; Kampf, J. W.; Alp, E. E.; Hu, M.; Zhao, J.; Lehnert, N. *Inorg. Chem.*

2017, *56*, 10513.

33. Mazumdar, R.; Saha, S.; Samanta, B.; Mondal B. *Inorg. Chem*. **2021**, *60*, 18024.
34. Komarov, A. M.; Reef, A.; Schmidt, H. H. H. W. *Methods in Enzymology*, **2002**, *359*, 18.
35. Reisz, J. A.; Klorig, E. B.; Wright, M. W.; King, S. B. *Org. Lett.* **2009**, *11*, 2719.
36. Franco Machado, J.; Cordeiro, S.; Duarte, J. N.; Costa, P. J.; Mendes, P. J.; Garcia, M. H.; Baptista, P. V.; Fernandes, A. R.; Morais, T. S. *Inorg. Chem.* **2024**, *63*, 5783.
37. SMART, SAINT and XPREP; Siemens Analytical X-ray Instruments Inc.: Madison, Wisconsin, USA, **1995**.
38. (a) Sheldrick, G. M. *Acta Crystallogr. Sect. A Found. Adv.* **2015**, *71,* 3. (b) Sheldrick, G. M. *Acta Crystallogr. Sect. C Struct. Chem.* **2015**, *71*, 3. (c) Farrugia, L. J. ORTEP-3 for Windows - a version of ORTEP-III with a Graphical User Interface (GUI). *J. Appl. Crystallogr.* **1997**, *30*, 565.

Chapter 4

HNO/NO^- release from an electron rich cobalt(II)-nitrosyl complex

Abstract

The formal electronic character of $\{Co(NO)\}^8$ complexes is considered to be [Co^{III}-NO^-], which makes them potential candidates for HNO/NO^- donation. But, the kinetic inertness of the low-spin cobalt(III)-centre makes the release of HNO/NO^- very difficult. Only a few $\{Co(NO)\}^8$ complexes are known to donate HNO under specific reaction conditions. A cobalt nitrosyl complex, [$Co(TMTAA^{2-})(NO)$], **4.2a** of $\{Co(NO)\}^8$ configuration has been synthesized in a macrocyclic electron rich ligand framework and characterized. The complex **4.2a** shows unusually low nitrosyl stretching frequency (1622 cm^{-1}) compared to the other reported analogues. In the presence of a neutral imidazole ligand, the complex **4.2a** was found to donate NO^- to [$Mn^{III}(TPP^{2-})Cl$] and [$Fe^{III}(TPP^{2-})Cl$], leading to reductive nitrosylation products. Furthermore, in the presence of H^+, the reaction mixture of complex **4.2a** and imidazole was found to produce N_2O, which in turn confirms the HNO release. This was also evidenced by its characteristic reaction with PPh_3. All these investigations confirm the HNO/NO^- releasing ability of the [$Co(TMTAA^{2-})(NO)$] complex.

4.1 Introduction

Nitric oxide (NO) driven physiological and biochemical processes are often found to be involved with the intermediacy of its one electron reduce analogue known as nitroxyl or HNO/NO^-.[1-5] The endogenous production and biological roles of nitroxyl are still elusive due to its high reactivity towards itself,[6] thiol or thiolate[3] and iron containing proteins.[4] This short-lived species instantly dimerizes and dehydrates to produce nitrous oxide (N_2O), which makes it very difficult to study extensively.[6] The advancement of HNO as a potential therapeutic agent has become a great interest for research. Its medical applications like vasodilation response and more vasodilative effect compared to NO, show its potential as an inotropic agent for the heart failure treatment.[7-8] Although, the source of nitroxyl is limited to a few compounds such as Angeli's salt[9] and Piloty's acid[10], the concurrent release of reactive species and their functionality at strongly alkaline pH (Piloty's acid) hinder their widespread utility. Thus, for the better understanding of the biological reactivity and therapeutic applications of HNO/NO^-, several attempts have been made to prepare metal-nitrosyl based HNO/NO^- donor compounds.[11-21] Using the metal-nitrosyl complexes as sources, the NO release can be triggered by the employment of external stimuli like light, heat or by changing pH etc.[22-28] In contrast, the HNO/NO^- release is comparatively less explored. The metal-HNO reactivity and HNO/NO^- donation are mostly limited to iron-nitrosyl complexes of $\{Fe(NO)\}^8$ configuration due to its highly electron rich nature.[11-17] But, the examples of cobalt nitrosyl complexes as HNO/NO^- donor is still scarce. Among the cobalt nitrosyl complexes of $\{Co(NO)\}^{7/8/9}$ configurations, only the $\{Co(NO)\}^8$ (considering its $[Co^{III}\text{-}NO^-]$ electronic character) and $\{Co(NO)\}^9$ (highly electron-rich nature) complexes were considered to act as potential HNO/NO^- donor. Only a handful number of such complexes are reported. The HNO donation from a cobalt-nitrosyl complex was first reported by Harrop *et al.* which involves the proton induced activity of a $\{Co(NO)\}^8$ complex, $[Co(LN_4^{PhCl})(NO)]$ (LN_4^{PhCl} = dianion of (N^1E,N^2E)-

N^1,N^2-bis(1*H*-pyrrol-2-yl)methylene-4,5-dichlorobenzene-1,2-diamine).[18] Subsequently, two more analogous {Co(NO)}^{8} complexes, [Co(LN_4^{Ph})(NO)] and [Co(LN_4^{PhCl})(NO)] (LN_4^{Ph} = dianion of (N^1E,N^2E)-N^1,N^2-bis(1*H*-pyrrol-2-yl)methylene)benzene-1,2-diamine) were reported by the same group which upon reduction to its corresponding {Co(NO)}^{9} complexes, also act as HNO/NO^- donor.[19] Recently, our group also reported another {Co(NO)}^{8} complex, [Co(BPB^{2-})(NO)] (H_2BPB = 1,2-bis(2-pyridinecarboxamido)benzene) which shows HNO/NO^- releasing ability in the presence of sixth ligands like BF_4^- (tetrafluoroborate anion), DTC^- (DTC^- = diethyldithiocarbamate anion) etc.[21]

This chapter deals with the synthesis and characterization of a cobalt-nitrosyl complex, [Co($TMTAA^{2-}$)(NO)] in an electron rich macrocyclic ligand framework, H_2TMTAA (H_2TMTAA = 5,7,12,14-tetramethyldibenzotetraaza[14]annulene). The presence of a neutral sixth ligand like imidazole facilitates the NO^- donation from the nitrosyl complex, which is monitored *via* the NO^- consumption by well-known HNO/NO^- trapping agents such as [Mn^{III}(TPP^{2-})Cl] and [Fe^{III}(TPP^{2-})Cl].

4.2 Results and discussion

The precursor cobalt(II)-dibenzotetramethyltetraaza[14]annulene complex, [Co^{II}($TMTAA^{2-}$)], **4.1** can be prepared by the template condensation reaction between acetylacetone and 1,2-diaminobenzene in the presence of $Co(OAc)_2.4H_2O$. However, the high reactivity of complex **4.1** towards oxygen and low yield precludes its direct synthesis. Hence, a stepwise synthetic pathway was preferred over the direct one (Scheme 4.1). The ligand, H_2TMTAA was synthesized by the template synthesis method reported earlier using $Ni(OAc)_2.4H_2O$ (Exp. Sec.).[29] Spectroscopic characterization was done to confirm the formation of the ligand (Exp. Sec., Appendix III, Figures A3.1-A3.4). The precursor complex **4.1** was synthesized using a modified method (Exp. Sec.). It was characterized using FT-IR, UV-visible, EPR spectroscopy

along with ESI-mass spectrometry which conclusively supports its formulation (Exp. Sec., Appendix III, Figures A3.5-A3.8). Earlier, Magull *et al.* have reported the single crystal X-ray structure of dimethoxyethane solvated $[Co^{II}(TMTAA^{2-})]$.[30] Later, Zdilla *et al.* reported a solvent free single crystal structure of $[Co^{II}(TMTAA^{2-})]$ which was obtained by slow diffusion of n-pentane into the benzene solution of the complex.[31] In the present case, the single crystals of the complex **4.1** were obtained by layering methanolic solution of $Co(OAc)_2.4H_2O$ over the dichloromethane solution of H_2TMTAA under argon atmosphere (Appendix III, Figures A3.9). The structural parameters match well with the reported ones.[31] The electronic spectrum of complex **4.1** contains a strong absorption band at 367 nm, which can be assigned as the π- π* transition of the ligand. The absorptions at 415, 460, 533 and 582 nm are associated with multiple charge transfer bands.

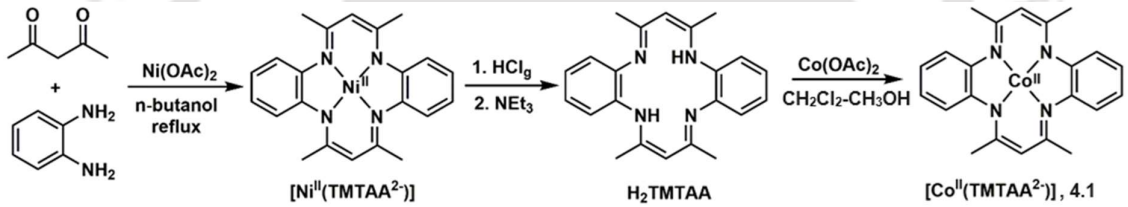

Scheme 4.1. Synthesis of H_2TMTAA ligand and precursor complex **4.1**.

Using the precursor $[Co^{II}(TMTAA^{2-})]$ complex, two conformers of the mononitrosyl cobalt complex, $[Co(TMTAA^{2-})(NO)]$ were synthesized by employing two different synthetic approaches (Exp. Sec.). Purging NO gas into the dry and degassed dichloromethane solution of complex **4.1** gives rise to the mononitrosyl complex **4.2a**. Again, layering of dry and degassed methanolic solution of $Co(OAc)_2.4H_2O$ over dichloromethane solution (degassed) of H_2TMTAA under NO atmosphere yields the mononitrosyl complex **4.2b**. Although both complex **4.2a** and **4.2b** are basically conformers of the same complex, the different synthetic approach affects their crystal structures, which has been discussed later. Both of the complexes were isolated as solid and characterized using standard spectroscopic methods, as well as

structurally (Appendix III, Figures A3.10-A3.14). In FT-IR spectrum, stretching frequencies at 1622 and 1605 cm^{-1} were observed, which are assignable as the nitrosyl stretching frequency of complexes **4.2a** and **4.2b**, respectively (Appendix III, Figures A3.10-A3.11). Floriani *et al.* reported nitrosyl complexes in the same H_2TMTAA ligand framework containing manganese(II) and iron(II) centres which show nitrosyl stretching frequency at 1685 and 1636 cm^{-1}, respectively.[32] These stretching vibrations are considerably lower than the usual range of analogous complexes. Although, cobalt-nitrosyl complexes of $\{Co(NO)\}^8$ configuration typically show nitrosyl-stretching frequency in between 1660-1720 cm^{-1} (Table 4.1), the effect of the presence of electron donating H_2TMTAA ligand in [Co(TMTAA^{2-})(NO)] perhaps responsible for the low nitrosyl stretching frequency. Addition of NO gas to the dry and degassed dichloromethane solution of complex **4.1** displays two new bands at 337 and 399 nm, The 531 nm absorption is associated with charge transfer transitions. The diamagnetic nature of **4.2a** was confirmed from X-band EPR spectroscopy (Appendix III, Figure A3.13), which is further supported by well-resolved ^{1}H-NMR (Appendix III, Figure A3.14).

Table 4.1: List of cobalt-nitrosyl complexes and their respective NO stretching frequencies.

Complex	$\overline{\nu}_{NO}$ (cm^{-1})	Co-N_{NO} (Å)	N-O (Å)	Co-N_{NO}-O (°)	Reference
$[(14\text{-TMC})Co^{III}(NO)]^{2+}$	1715	1.901	1.152	129.35	33a
$[(13\text{-TMC})Co^{III}(NO)]^{2+}$	1716	1.797(4)	1.159(5)	124.4(3)	33b
$[(12\text{-TMC})Co^{III}(NO)]^{2+}$	1712	1.7844(14)	1.155(2)	128.50(13)	33b
[(BPI)Co(NO)(OAc)]	1673	1.828(8)	1.014(8)	132.7(7)	33c
$[Co(LN_4^{PhCl})(NO)]$	1667	1.798(3)	1.172(4)	124.4(3)	18
[Co(BPB)(NO)]	1662	1.791(6)	1.119(10)	130.2(7)	21
$[Co(L_2)(NO)Cl]Cl$	1659	1.765	1.103(9)	124.57(5)	33d
[Co(TMTAA^{2-})(NO)] (**4.2a**)	1622	1.818(3)	1.124(5)	125.1(3)	This work
[Co(TMTAA^{2-})(NO)] (**4.2b**)	1605	1.803(4)	1.138(5)	125.0(3)	

The single crystal structures of the complex **4.2a** and **4.2b** were determined and refined in triclinic P-1 and monoclinic $P2_1/n$ space group, respectively. The ORTEP diagrams of both complexes are shown in figure 4.1. The crystal structures reveal a non-planer saddle shape for

both complexes which arises due to the steric interaction between the benzo and methyl groups of the ligand framework. The asymmetric unit of both crystals comprises of one cobalt-centre, one ligand and one dichloromethane solvent molecule. In complex **4.2b**, the dichloromethane unit has some intrinsic disorder, hence the solvent molecule is squeezed. Both the cobalt-centres are five coordinated, being bonded to four ligand nitrogen atoms in equatorially and one nitrogen atom of the nitrosyl unit axially in a distorted square-pyramidal geometry. The cobalt-centres are elevated from the N4-plane of the ligand towards the nitrosyl unit by 0.258 and 0.248 Å for complex **4.2a** and **4.2b**, respectively. The Co-N-O bond angles are 125.1(3)° (**4.2a**) and 125.0(3)° (**4.2b**). The Co-N_{ligand} bond distances are in the range between 1.902(3) to 1.910(3) Å for complex **4.2a** and 1.892(3) to 1.910(3) Å for **4.2b**. Both the apical Co-N_{NO} bond length appears to be 1.818(3) and 1.803(4) Å for complex **4.2a** and **4.2b**, respectively. The observed N-O bond lengths are 1.124(5) (**4.2a**) and 1.138(5) Å (**4.2b**). All the crystal parameters are in accordance with the previously reported analogous ones (Table 4.1). The N-O bond length of complex **4.2b** is longer compared to that of complex **4.2a** by 0.014 Å; this is in accord to the downshift of the nitrosyl stretching frequency by 17 cm^{-1}. This observation also confirms the stronger NO^- character of the nitrosyl unit in complex **4.2b**. It is worth mentioning that the recrystallization product of complex **4.2b** from dry and degassed dichloromethane solution results in the crystals of complex **4.2a**, suggesting higher thermodynamic stability. Therefore, all the experiments are conducted using complex **4.2a**.

In the literature, low-spin $\{Co(NO)\}^8$ complexes were formally known to exhibit [Co^{III}-NO^-] electronic character. Perhaps, the kinetic inertness of this low spin d^6 Co^{III}-centre prevents its effectiveness as an HNO/NO^- donor.[34] But in the present case, the strong NO^- character of complex **4.2a** may make it a suitable candidate for nitroxyl donation. To check the NO^- donating ability of complex **4.2a**, it was made to react with well-known nitroxyl trapping

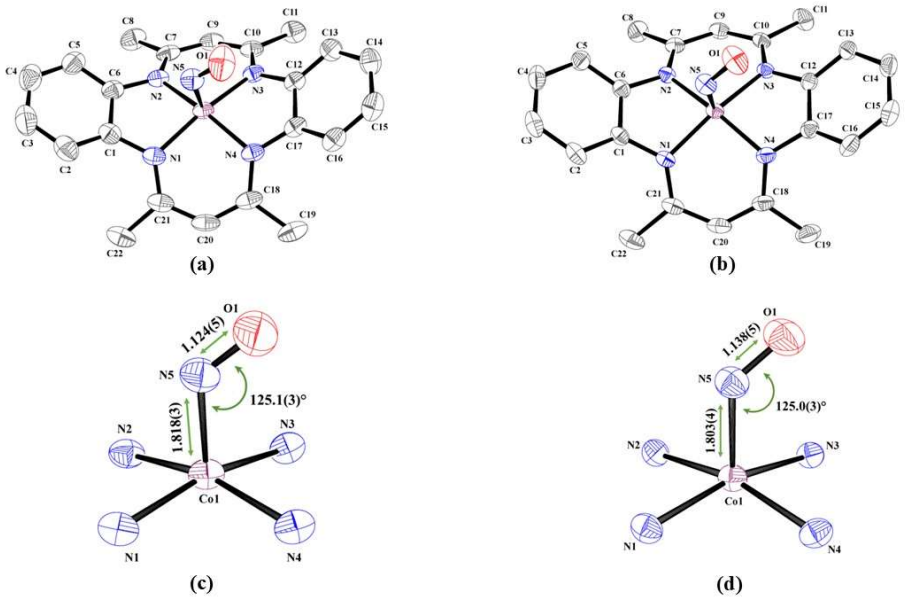

Figure 4.1. ORTEP diagrams of complexes **4.2a** (a) and **4.2b** (b) (H-atoms and solvent are omitted for clarity). The core structures of complexes **4.2a** (c) and **4.2b** (d) with selective bond parameters are also shown.

agents. Manganese(III)-complexes have been used as a HNO/NO^- trapping agent for a long time.[15,35] So, the reaction of complex **4.2a** and [$Mn^{III}(TPP^{2-})Cl$] (1 mole equivalent) in degassed dichloromethane solution was studied using FT-IR spectroscopy. Even after stirring the reaction mixture over 24 hours, the FT-IR spectral pattern remains unchanged (Figure 4.2). Hence, to facilitate the NO^- donation, a sixth ligand was introduced in the reaction mixture. Considering the nitrosyl moiety has strong NO^- character, a neutral sixth ligand was used. Thus, carrying out the same reaction in the presence of imidazole (IM) (1 mole equivalent), shows the formation of a new stretching vibration at 1759 cm^{-1} along with the simultaneous disappearance of 1622 cm^{-1} band in the FT-IR spectral monitoring (Figure 4.2). This 1759 cm^{-1} stretching frequency was identified as the characteristic nitrosyl stretching of the [$Mn(TPP^{2-})(NO)$] complex.[36] The isolation and standard spectroscopic characterization also confirm the formation of the $\{Mn(NO)\}^6$ complex amid the reaction (Appendix III, Figures A3.24-A3.26). The reductive nitrosylation of [$Mn^{III}(TPP^{2-})Cl$] confirms the NO^- donation

from complex **4.2a**.

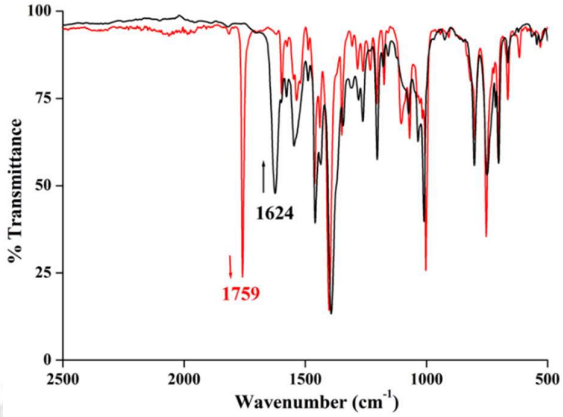

Figure 4.2. FT-IR (ATR) spectral monitoring of the reaction mixture of complex **4.2a** with $[Mn^{III}(TPP^{2-})Cl]$ in the absence (black) and presence (red) of imidazole.

Further evidence of NO^- donation was collected from the reaction of complex **4.2a** with another nitroxyl trapping agent, $[Fe^{III}(TPP^{2-})Cl]$.[18,21,37] Similar to the previous observation, in the absence of imidazole, the reaction of complex **4.2a** and 1 mol equivalent of $[Fe^{III}(TPP^{2-})Cl]$ in dry and degassed dichloromethane solution does not show any evidence for the formation of iron(II)-nitrosyl complex in FT-IR spectral monitoring even after 24 hours (Figures 4.3(a)). But, in the presence of imidazole, the reaction mixture of **4.2a** and $[Fe^{III}(TPP^{2-})Cl]$ shows a new stretching frequency at 1698 cm^{-1} in the FT-IR spectrum, which is attributed to the formation of $[Fe(TPP^{2-})(NO)]$ in the reaction medium (Figures 4.3(a)) with concomitant disappearance of the nitrosyl stretching frequency of **4.2a**. This observation supports the NO^- transfer from complex **4.2a** to $[Fe^{III}(TPP^{2-})Cl]$ during the course of the reaction. Additionally, the X-band EPR spectroscopic study of the reaction mixture shows a sharp isotropic signal at g ~ 2.04, suggesting the presence of $\{Fe(NO)\}^7$ complex (Figure 4.3(b)).[21,37,38] The newly formed $[Fe(TPP^{2-})(NO)]$ complex was isolated and characterized spectroscopically (Appendix III, Figures A3.27-A3.29).

The effect of increasing the coordination number from five to six for a cobalt-nitrosyl complex of $\{Co(NO)\}^8$ configuration in *bis*-arsenide ligand framework was demonstrated by Enemark

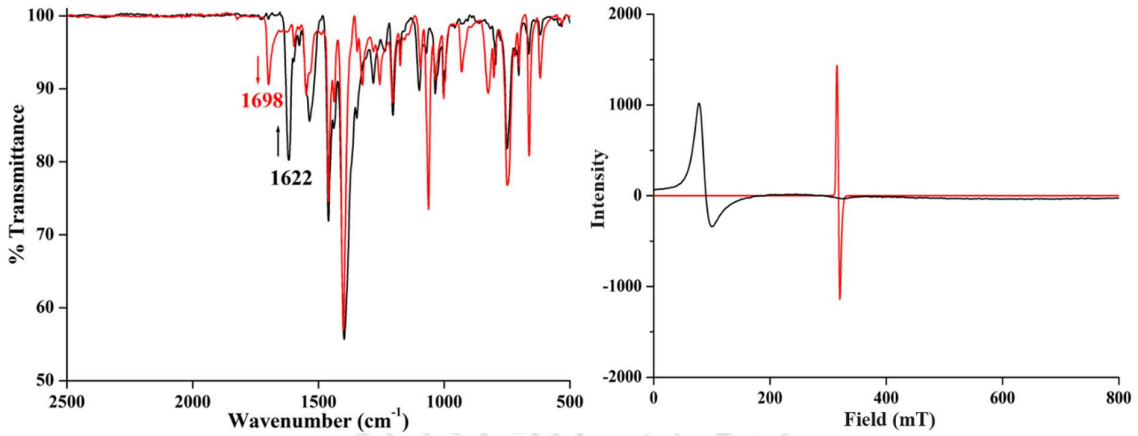

Figure 4.3. (a) FT-IR (ATR probe) and (b) X-band EPR (CH_2Cl_2, 77 K) spectra of the reaction mixture of complex **4.2a** with [$Fe^{III}(TPP^{2-})Cl$] in the absence (black) and presence (red) of imidazole.

et al. where the change in the electronic nature of the nitrosyl moiety from NO^+ to NO^- was observed.[39] In the presence of a sixth anionic ligand like DTC^- (diethyldithiocarbamate anion), the HNO donation from a {Mn(NO)}^{6} complex was also reported.[20] A {Co(NO)}^{8} complex was also found to donate HNO/NO^- in the presence of a sixth ligand (BF_4^-, DTC^- and imidazole) was reported very recently.[21] Hence, it is logical to assume that the imidazole acts as a sixth ligand for complex **4.2a**, which facilitates the NO^- donation to the suitable acceptors like [$Mn^{III}(TPP^{2-})Cl$] and [$Fe^{III}(TPP^{2-})Cl$].

To get further insight, the reaction of imidazole with complex **4.2a** was studied spectroscopically. Addition of 1.2 mole equivalent of imidazole to the dry and degassed dichloromethane solution of complex **4.2a** results in the quenching of the 399 nm band and formation of a new absorption band at 446 nm was observed in UV-visible spectral studies (Figure 4.4(a)). Moreover, the FT-IR spectral monitoring of the reaction of complex **4.2a** and imidazole shows the disappearance of the nitrosyl stretching frequency at 1622 cm^{-1} (Figure 4.4(b)). It is noteworthy that the formation of any oxidized or reduced product of nitrosyl moiety was not observed in the FT-IR spectrum. Subjecting this reaction mixture to X-band EPR spectroscopy results in an EPR silent spectrum suggesting the presence of diamagnetic

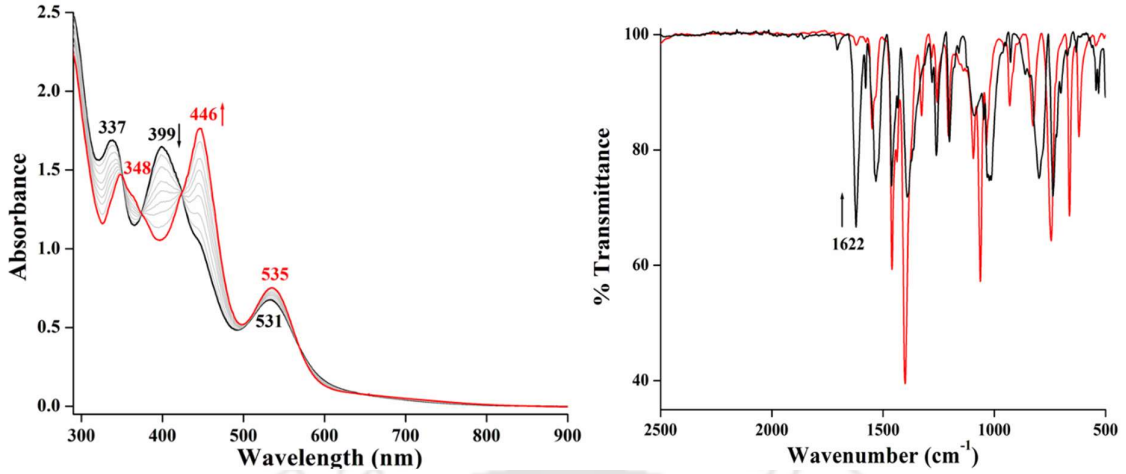

Figure 4.4. (a) UV-visible (room temperature) and (b) FT-IR (ATR probe) spectral monitoring of complex **4.2a** in the absence (black) and presence (red) of imidazole in CH_2Cl_2.

cobalt(III)-centre in the newly formed species (Appendix III, Figure A3.16). These spectroscopic observations suggest the release of nitrosyl unit with concomitant one electron oxidation of the cobalt-centre. Thus, it is reasonable to assume that the release of nitrosyl moiety from complex **4.2** occurred as NO^-.

Addition of 1 mole equivalent of $NaBPh_4$ (in methanol) to the reaction mixture shows a significant change in the spectral pattern in UV-visible spectroscopy (Appendix III, Figure A3.15) confirming the formation of complex $[Co^{III}(TMTAA^{2-})(IM)](BPh_4)$, **4.3**. It was isolated as a brown solid and characterized using various spectroscopic methods (Appendix III, Figures A3.17-A3.20). Although no crystal structure of complex **4.3** was obtained even after several attempts, a molecular ion peak at m/z = 469.155 (Calculated: 469.155) in the ESI-mass spectrum was observed confirming the formation of $[Co^{III}(TMTAA^{2-})(IM)]^+$ unit (Appendix III, Figure A3.20).

The formation of HNO was confirmed by its characteristic reaction with phosphines (PR_3).[40] The reaction of complex **4.2a**, imidazole (1.5 mole equivalent) and PPh_3 (2 mole equivalent) was done in presence of a H^+ (1.5 mole equivalent) and was monitored using ^{31}P-NMR

spectroscopy. The ^{31}P-NMR spectrum of the reaction mixture was recorded after 24 hours which shows the formation of free base aza-ylide (Ph_3P=NH, δ_{ppm} = 21.68) and phosphine oxide (Ph_3P=O, δ_{ppm} = 28.83) (Figure 4.5).[18,20,21] This observation supports the release of NO^- from complex **4.2a**, which becomes HNO in the presence of H^+. Unreacted PPh_3 shows a signal at δ_{ppm}, -5.07. The signal at δ_{ppm}, 36.62 can be attributed to the formation of Ph_3P=NH.HBF_4. This value is in accordance with the previously reported analogous ones.[41]

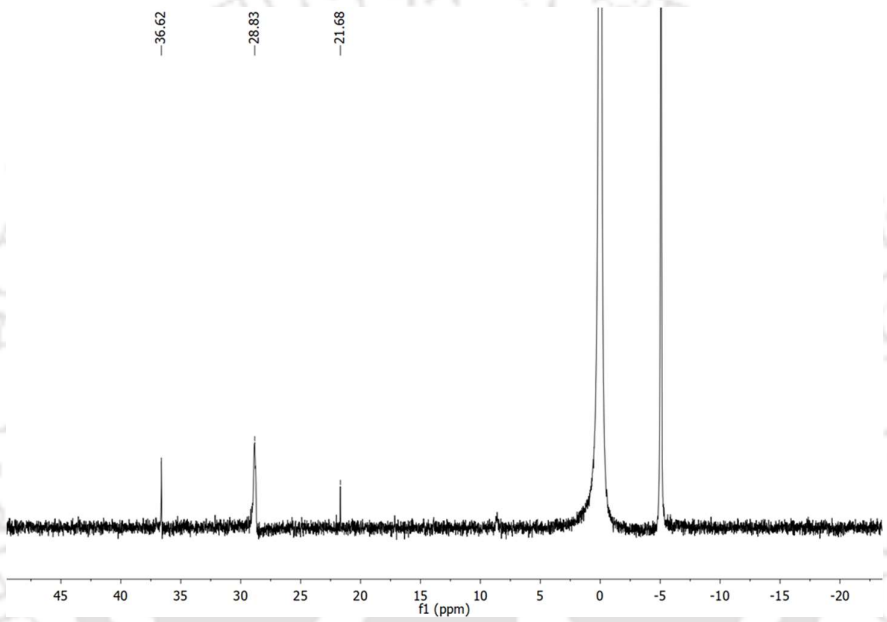

Figure 4.5. ^{31}P-NMR of the reaction mixture of complex **4.2a**, imidazole, PPh_3 and HBF_4 in CH_2Cl_2 solution with 0.1 mL DMSO-d_6.

The NO^- donation from complex **4.2a** was confirmed by testing the presence of N_2O in the headspace gas of the reaction vessel. The N_2O was formed from the decomposition of hyponitrous acid ($H_2N_2O_2$), which is the dimerization product of HNO.[6] In the presence of H^+ in the reaction medium, subjecting the headspace gas of the reaction mixture of complex **4.2a** and imidazole to GC shows a strong signal at 2.77 minutes, suggesting the presence of N_2O (Appendix III, Figure A3.30). The GC-mass spectrum also shows a strong signal at m/z = 44 for N_2O (Appendix III, Figure A3.32). The yield of N_2O was calculated to be *ca.* 65% using GC.

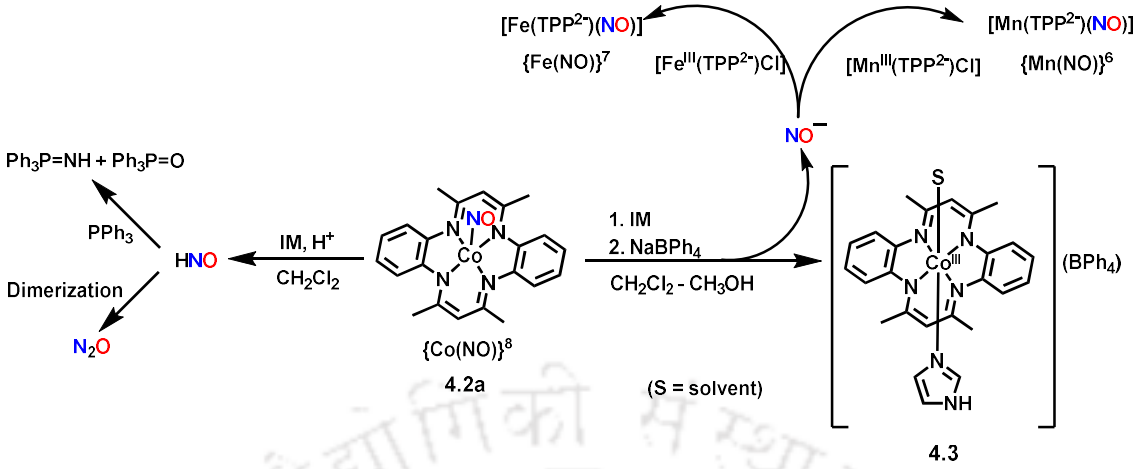

Scheme 4.2. Overall reactions.

4.3 Experimental Section

4.3.1 Materials and Methods

All experiments, unless otherwise specified, were done under argon atmosphere using standard Schlenk techniques on the Schlenk line. All chemicals used were of reagent grade, purchased from commercially available sources and no purification was done unless mentioned. Methanol was distilled using Mg-turnings and iodine. Dichloromethane was purified by passing through a basic alumina column, then storing it over calcium hydride overnight and followed by distillation under inert atmosphere (N_2). All the solvents were stored over molecular sieve (4 Å) for at least two days under argon before use. Molecular sieves were kept at 200 °C for 24 hours for activation and cooled under vacuum. Solvents and solutions were deoxygenated by applying consecutive vacuum/argon purge cycles. All the reactions were performed under inert atmosphere except mentioned differently. UV-visible spectra were taken on an Agilent Cary 8454 spectrophotometer. FT-IR spectra were recorded as KBr pellets or in a KBr cell using a PerkinElmer spectrophotometer. ^{1}H, ^{13}C, and ^{31}P-NMR studies were done in Bruker Avance III 400 and 500 MHz Varian FT-NMR spectrophotometers. X-band EPR spectra were recorded on a JES-FA200 EPR spectrophotometer with microwave power, 0.998 mW; microwave

frequency, 9.14 GHz; and modulation amplitude, 2. Gas chromatograms were obtained on PerkinElmer Clarus® 590.

Single crystals were grown from dichloromethane-methanol solutions using the slow evaporation technique. The intensity data were collected using a Bruker SMART APEX-II CCD diffractometer, equipped with a fine focus 1.75 kW sealed tube Mo Kα radiation (λ = 0.71073 Å), with increasing ω (width of 0.3° per frame) at a scan speed of 3 s/frame. The SMART software was used for data acquisition. Data integration and reduction were undertaken with SAINT and XPREP software.[42] Structures were solved by direct methods using SHELXL[43a] and refined with full-matrix least-squares on F^2 using SHELXL-2019/1.[43b] Structural illustrations were drawn with ORTEP-3 for Windows.[43c]

4.3.2 Syntheses

5,7,12,14-tetramethyldibenzotetraaza[14]annulene (H_2TMTAA): The ligand is prepared following a reported procedure.[1] Briefly, the mixture of 1,2-phenylenediamine (8.92 g, 0.082 mol), 2,4-pentanedione (8.5 mL, 0.085 mol) and $Ni(OAc)_2.4H_2O$ (5 g, 0.02 mol) was refluxed in 125 mL n-butanol for 3 hours in a 250 mL round bottom flask. The reaction mixture was brought to room temperature and 50 mL methanol was added. Keeping this reaction mixture in an ice-bath for 30 minutes results in the formation of crystalline purple-blue solid which was collected by filtration. This purple-blue solid is identified as $[Ni^{II}(TMTAA^{2-})]$ complex. Yield: 6.53 g (*ca.* 80%). Following that, methanolic (100 mL) solution of $[Ni^{II}(TMTAA^{2-})]$ (5 g, 0.012 mol) was prepared in an Erlenmeyer flask and HCl gas bubbled through the solution. The solution became very hot and the color of the solution changed from green to brown. The solution was cooled to room temperature and a white precipitate formed. The precipitate is filtered off and washed with cold methanol. This white solid is identified as H_2TMTAA.2HCl. Yield: 4.35 g (*ca.* 84%). Then, a slurry of H_2TMTAA.2HCl (4.17 g, 0.010 mol) was prepared

with 10 mL methanol in a 50 mL beaker. NEt_3 was added to it dropwise and the color of the slurry became yellow. When the pH of the mixture became 9, a bright yellow precipitate was formed. It was filtered, washed with cold methanol several times and air dried. H_2TMTAA was isolated as a yellow solid. Yield: 2.95 g (*ca.* 86%) Elemental analyses for $C_{22}H_{24}N_4$; Calculated (%): C, 76.71; H, 7.02; N, 16.27. Found (%): C, 76.79; H, 7.06; N, 16.41. FT-IR (in ATR probe): 1610, 1548, 1505, 1460, 1425, 1379, 1353, 1272, 1184, 1109, 1018, 802, 732 and 694 cm^{-1}. ^{1}H-NMR (400 MHz, $CDCl_3$): δ_{ppm}, 12.58 (s, 2H), 6.99 (s, 8H), 4.88 (s, 2H) and 2.13 (s, 12H). ^{13}C-NMR (100 MHz, $CDCl_3$): δ_{ppm}, 158.9, 138.5, 130.5, 123.1, 122.9, 97.9 and 20.9. ESI-mass (m/z): Calculated, 344.200; Found, 345.209 ($[M+H]^+$).

[Co^{II}(TMTAA^{2-})], 4.1: To a 25 mL round bottom flask equipped with a stir bar, dichloromethane (2 mL) solution of H_2TMTAA (68.8 mg, 0.2 mmol) and methanolic (5 mL) solution of $Co(OAc)_2.4H_2O$ (49.8 mg, 0.2 mmol) was added. The reaction mixture was stirred for 2 hours under argon atmosphere which resulted in precipitation. The brown precipitate was filtered off and washed several times with cold methanol. Complex **4.1** was isolated as a dark brown solid. Single crystals of complex **4.1** were obtained by layering a methanolic solution of $Co(OAc)_2.4H_2O$ over a dichloromethane solution of H_2TMTAA. Yield: 62 mg (*ca.* 77%) Elemental analyses for $C_{22}H_{22}N_4Co$; Calculated (%): C, 65.83; H, 5.52; N, 13.96. Found (%): C, 65.78; H, 5.57; N, 14.03. FT-IR (in ATR probe): 1579, 1532, 1517, 1461, 1432, 1388, 1362, 1274, 1199, 1032, 921, 777, 738 and 535 cm^{-1}. UV-visible (CH_2Cl_2): 367 nm ($\varepsilon/M^{-1}\ cm^{-1}$, 7.79×10^4), 415 nm ($\varepsilon/M^{-1}\ cm^{-1}$, 3.35×10^4), 460 nm ($\varepsilon/M^{-1}\ cm^{-1}$, 1.89×10^4), 533 nm ($\varepsilon/M^{-1}\ cm^{-1}$, 9.52×10^3) and 582 nm ($\varepsilon/M^{-1}\ cm^{-1}$, 9.57×10^3). ESI-mass (m/z): Calculated, 401.117; Found, 402.124 ($[M+H]^+$ peak). Crystal data: complex **4.1**, $C_{44}H_{44}Co_2N_8$, M = 802.73, Monoclinic ($P2_1/c$), a = 14.4344(8) Å, b = 16.4066(5) Å, c = 16.2778(7) Å, α = 90°, β = 99.840(4)°, γ = 90°, V = 3798.2(3) Å^3, Z = 4, D_c = 1.404 g cm^{-3}, μ = 0.917 mm^{-1}, T = 293(2) K, 14351 reflections, 6684 independent, $R(F)$ = 0.0453 [$I > 2\delta(I)$], R(int) = 0.0659, $wR(F2)$ =

0.1034 (all data), GOF = 0.998.

[Co(TMTAA^{2-})(NO)], 4.2a: Complex **4.1** (40 mg, 0.1 mmol), was dissolved in dry and degassed dichloromethane (4 mL) solution in a 25 mL round bottom flask equipped with a rubber septum and degassed thoroughly using argon/vacuum cycle. NO gas was purged through this solution for 2 minutes which resulted in a change in color of the solution from brown to dark-red. After standing at room temperature for 30 minutes, excess NO gas was removed by argon flush. Addition of dry and degassed methanol (10 mL) to this solution resulted in precipitation. Complex **4.2a** was isolated as a dark-red solid. The single crystals were obtained by slow evaporation of the dichloromethane solution. Yield: 36 mg (*ca.* 84%) Elemental analyses for $C_{22}H_{22}N_5OCo$; Calculated (%): C, 61.25; H, 5.14; N, 16.23. Found (%): C, 61.36; H, 5.21; N, 16.31. FT-IR (in ATR probe): 2963, 1622 (ν_{NO}), 1578, 1531, 1461, 1391, 1260, 1201, 1089, 1022, 798, 736 and 531 cm^{-1}. UV-visible (CH_2Cl_2): 337 nm (ε/M^{-1} cm^{-1}, 2.75 × 10^4), 399 nm (ε/M^{-1} cm^{-1}, 3.15 × 10^4) and 531 nm (ε/M^{-1} cm^{-1}, 8.62 × 10^3). ^{1}H-NMR (400 MHz, $CDCl_3$): δ_{ppm}, 7.13-7.09 (3, 4H), 6.95-6.90 (3, 4H), 4.55 (s, 2H) and 2.23 (s, 12H). Crystal data: **4.2a**, $C_{23}Cl_2CoN_5OH_{24}$, M = 516.30, Triclinic (P -1), a = 9.1802(8) Å, b = 11.2850(10) Å, c = 12.0488(10) Å, α = 102.415(3)°, β = 94.370(3)°, γ = 104.862(3)°, V = 1166.81(18) Å^3, Z = 2, D_c = 1.470 g cm^{-3}, μ = 0.990 mm^{-1}, T = 296.0 K, 27316 reflections, 4111 independent, $R(F)$ = 0.0702 [$I > 2\delta(I)$], R(int) = 0.0728, $wR(F2)$ = 0.1832 (all data), GOF = 1.095.

[Co(TMTAA^{2-})(NO)], 4.2b: In a reaction tube, dry and degassed dichloromethane (2 mL) solution of H_2TMTAA (68.8 mg, 0.2 mmol) was taken and degassed thoroughly by continuous argon purge. NO gas was bubbled into this solution for 2 minutes. Then, a dry and degassed methanolic (5 mL) solution of $Co(OAc)_2.4H_2O$ (49.8 mg, 0.2 mmol) was layered over it for slow diffusion and after 24 hours, red colored block shaped crystals of complex **4.2b** were

obtained. FT-IR (in ATR probe): 2963, 1605 (ν_{NO}), 1578, 1525, 1452, 1433, 1377, 1264, 1200, 1123, 1027, 751, 732, 529 and 498 cm^{-1}. Crystal data: **4.2b**, $C_{22}H_{22}CoN_5O$, M = 431.37, Monoclinic ($P2_1/n$), a = 7.7663(4) Å, b = 15.5053(8) Å, c = 19.3814(10) Å, α = 90°, β = 90.119(2)°, γ = 90°, V = 2333.9(2) $Å^3$, Z = 4, D_c = 1.228 g cm^{-3}, μ = 0.755 mm^{-1}, T = 298.0 K, 108559 reflections, 4108 independent, $R(F)$ = 0.0566 [$I > 2\delta(I)$], R(int) = 0.0604, $wR(F2)$ = 0.1695 (all data), GOF = 1.164.

[Co^{III}($TMTAA^{2-}$)(IM)](BPh_4), 4.3: Complex **4.2a** (43 mg, 0.1 mmol) was taken in a 15 mL Schlenk tube and degassed by consecutive argon/vacuum cycles. Dry and degassed dichloromethane was added to it resulting in a dark-red solution. Addition of imidazole (10 mg, 0.16 mmol) to this solution caused an immediate color change from red to orange-red. After keeping this reaction mixture at room temperature for 1 hour, methanolic solution of $NaBPh_4$ (68 mg, 0.2 mmol) was added and the reaction mixture was left overnight. Brown precipitation of complex **4.3** was observed which was collected by filtration followed by air drying. Yield: 66 mg (*ca.* 85%) Elemental analyses for $C_{49}H_{46}N_6BCo$; Calculated (%): C, 74.62; H, 5.88; N, 10.66. Found (%): C,74.57; H, 5.93; N, 10.74. FT-IR (in ATR probe): 3121, 2921, 2851, 1548, 1459, 1400, 1326, 1256, 1206, 1093, 1062, 1035, 930, 825, 744, 662 and 619 cm^{-1}. UV-visible (CH_2Cl_2): 355 nm (ε/M^{-1} cm^{-1}, 2.24 × 10^3), 447 nm (ε/M^{-1} cm^{-1}, 3.18 × 10^3) and 535 nm (ε/M^{-1} cm^{-1}, 1.12 × 10^3). ESI-mass (m/z): Calculated, 469.155; Found, 469.155 ([Co($TMTAA^{2-}$)(IM)]$^+$).

[Mn^{III}(TPP^{2-})Cl]: Elemental analyses for $C_{44}H_{28}N_4ClMn$; Calculated (%): C, 75.16; H, 4.01; N, 7.97. Found (%): C, 75.21; H, 4.07; N, 8.06. FT-IR (in ATR probe): 2961, 1596, 1531, 1487, 1440, 1415, 1391, 1342, 1259, 1202, 1071, 1009, 797, 750, 700, 665 and 453 cm^{-1}. UV-visible (CH_2Cl_2): 475 nm (ε/M^{-1} cm^{-1}, 6.6 × 10^4), 579 nm (ε/M^{-1} cm^{-1}, 7.6 × 10^3) and 615 nm (ε/M^{-1} cm^{-1}, 7.6 × 10^3). ESI-mass (m/z): Calculated, 667.169; Found, 667.178 ([Mn(TPP^{2-})]$^+$).

[$Fe^{III}(TPP^{2-})Cl$]: The preparation procedure and spectroscopic characterization were described earlier (Exp. Sec., Chapter 2).

[$Mn(TPP^{2-})(NO)$]: Yield: 58 mg (*ca.* 83%). Elemental analyses for $C_{44}H_{28}N_5OFe$; Calculated (%): C, 75.75; H, 4.05; N, 10.04. Found (%): C, 75.81; H, 4.09; N, 9.95. FT-IR (in ATR probe): 2948, 1760 (ν_{NO}), 1594, 1536, 1486, 1439, 1347, 1261, 1203, 1174, 1068, 1000, 797, 752, 703 and 663 cm^{-1}. UV-visible (CH_2Cl_2): 429 nm ($\varepsilon/M^{-1}\ cm^{-1}$, 8.91×10^4), 548 nm ($\varepsilon/M^{-1}\ cm^{-1}$, 1.04×10^3) and 584 nm ($\varepsilon/M^{-1}\ cm^{-1}$, 5.81×10^3). ESI-mass (m/z): Calculated, 668.177; Found, 668.165 (after loss of NO, protonated).

[$Fe(TPP^{2-})(NO)$]: Yield: 56 mg (*ca.* 80%). Elemental analyses for $C_{44}H_{28}N_5OFe$; Calculated (%): C, 75.65; H, 4.04; N, 10.03. Found (%): C, 75.73; H, 4.13; N, 9.96. FT-IR (in ATR probe): 2917, 1695 (ν_{NO}), 1596, 1440, 1345, 1263, 1202, 1171, 1158, 1071, 1001, 995, 801, 751, 717, 702, 664 and 530 cm^{-1}. UV-visible (CH_2Cl_2): 412 nm ($\varepsilon/M^{-1}\ cm^{-1}$, 3.12×10^4), 540 nm ($\varepsilon/M^{-1}\ cm^{-1}$, 2.28×10^3) and 611 nm ($\varepsilon/M^{-1}\ cm^{-1}$, 8.17×10^2). ESI-mass (m/z): Calculated, 668.166; Found, 668.172 (after loss of NO).

Reaction of complex 4.2a with imidazole: Complex **4.2a** (21 mg, 0.05 mmol) and imidazole (4 mg, 0.06 mmol) were taken in a reaction tube equipped with a magnetic stirring bar and degassed properly *via* consecutive argon/vacuum cycle. Dry and degassed dichloromethane (3 mL) was added to it and the reaction mixture was stirred at room temperature. The reaction progress was monitored using various spectroscopic techniques.

Reaction of complex 4.2a with [$Mn^{III}(TPP^{2-})Cl$] in the presence of imidazole: Complex **4.2a** (43 mg, 0.1 mmol), [$Mn^{III}(TPP^{2-})Cl$] (70 mg, 0.1 mmol) and imidazole (8 mg, 0.12 mmol) was taken in a Schlenk tube and degassed it properly with argon flush. Dry and degassed dichloromethane was added to it and made the complexes soluble by stirring. $HBF_4.Et_2O$ (16 µL, 0.1 mmol) was added to the reaction mixture while stirring and monitored the progress of

reaction using spectroscopic techniques.

Reaction of complex 4.2a with [$Fe^{III}(TPP^{2-}$)Cl] in presence of imidazole: Complex **4.2a** (43 mg, 0.1 mmol), [$Fe^{III}(TPP^{2-}$)Cl] (70 mg, 0.1 mmol) and imidazole (8 mg, 0.12 mmol) was taken in a Schlenk tube and degassed it properly with argon flash. Dry and degassed dichloromethane was added to it and made the complexes soluble by stirring. $HBF_4.Et_2O$ (16 µL, 0.1 mmol) was added to the reaction mixture while stirring and monitor the progress of reaction using spectroscopic techniques.

Determination of the yield of N_2O: N-hydroxybenzenesulfonamide was taken in five 50 mL round-bottom flasks equipped with rubber septum in different measured amounts and degassed using argon/vacuum purge. 10 mL of 0.1 M NaOH solution was added to each flask under the sealed condition. 1 mL of headspace gas from each reaction vessel was subjected to GC. From there, a calibration curve of the concentration of *N*-hydroxybenzenesulfonamide and peak area at 2.77 minutes (corresponding to N_2O) was drawn.

Complex **4.2a** (0.08 g, 0.2 mmol) and imidazole (0.02 g, 0.3 mmol) were dissolved in 10 mL of dry and degassed dichloromethane in a 50 mL round-bottom flask and 32 µL of $HBF_4 \cdot Et_2O$ was added to it under anaerobic condition. After the completion of the reaction, 1 mL of headspace gas was subjected to GC and the amount of N_2O was measured from the calibration curve. Yield: *ca.* 65%.

Preparation of sample for ^{31}P-NMR spectroscopy: Complex **4.2a** (8.6 mg, 0.02 mmol), imidazole (1.5 mg, 0.025 mmol) and PPh_3 (10.4 mg, 0.04 mmol) were taken in an NMR tube and degassed thoroughly using continuous argon purge. Dry and degassed dichloromethane (0.3 mL) was added to it followed by HBF_4 (diluted in dichloromethane) and kept it at room temperature for 2 hours. 0.1 mL of DMSO-d_6 was added to it and the reaction mixture was subjected to ^{31}P-NMR spectrophotometer.

4.4 Conclusion

Thus, in conclusion, a penta-coordinated cobalt mono-nitrosyl complex of $\{Co(NO)\}^8$ configuration in an electron rich ligand framework was successfully synthesized and characterized both spectroscopically and structurally. The different synthetic approaches lead to two different conformers of the nitrosyl complex. The electron donating nature of the ligand influences the electronic nature of the nitrosyl moiety associated with the cobalt centre making the [Co-NO] unit very electron rich. Although the cobalt nitrosyl complex does not act as a nitroxyl donor on its own, in the presence of imidazole as a sixth ligand, this nitrosyl complex was found to donate HNO/NO^-. This is confirmed by its reaction with well-known nitroxyl scavengers like Mn(III) and Fe(III)-heme complexes. The release of the HNO was further confirmed by its reaction with PPh_3 and the evolution of N_2O. These results demonstrate the potential of the $\{Co(NO)\}^8$ complexes as nitroxyl donors.

4.5 Reference

1. Culotta, E.; Koshland, D. E. *Science,* **1992**, *258*, 1862.
2. Fukuto, J. M.; Switzer, C. H.; Miranda, K. M.; Wink, D. A. *Annu. Rev. Pharmacol. Toxicol.* **2005**, *45*, 335.
3. Szaciłowski, K.; Chmura, A.; Stasicka, Z. *Coord. Chem. Rev.* **2005**, *249*, 2408.
4. Ford, P. C.; Lorkovic, I. M. *Chem. Rev.* **2002**, *102*, 993.
5. Miranda, K. M.; Paolocci, N.; Katori, T.; Thomas, D. D.; Ford, E.; Bartberger, M. D.; Espey, M. G.; Kass, D. A.; Feelisch, M.; Fukuto, J. M.; Wink, D. A. *Proc. Natl. Acad. Sci. U. S. A.* **2003**, *100*, 9196.
6. Shafirovich, V.; Lymar, S. V. *Proc. Natl. Acad. Sci. U. S. A.* **2002**, *99*, 7340.
7. Paolocci, N.; Saavedra, W. F.; Miranda, K. M.; Martignani, C.; Isoda, T.; Hare, J. M.; Espey, M. G.; Fukuto, J. M.; Feelisch, M.; Wink, D. A.; Kass, D. A. *Proc. Natl. Acad.*

Sci. U. S. A. **2001**, *98*, 10463.

8. Paolocci, N.; Katori, T.; Champion, H. C.; St. John, M. E.; Miranda, K. M.; Fukuto, J. M.; Wink, D. A.; Kass, D. A. *Proc. Natl. Acad. Sci. U. S. A.* **2003**, *100*, 5537.
9. Angeli, A.; Rimini, E. *Gazz. Chim. Ital.* **1896**, *26*, 17.
10. Piloty, O. *Ber. Dtsch. Chem. Ges.* **1896**, *29*, 1559.
11. Patra, A. K.; Dube, K. S.; Sanders, B. C.; Papaefthymiou, G. C.; Conradie, J.; Ghosh, A.; Harrop, T. C. *Chem. Sci.* **2012**, *3*, 364.
12. Sanders, B. C.; Patra, A. K.; Harrop, T. C. *J. Inorg. Biochem.* **2013**, *118*, 115.
13. Speelman, A. L.; Lehnert, N. *Angew. Chem. Int. Ed.* **2013**, *52*, 12283.
14. Confer, A. M.; McQuilken, A. C.; Matsumura, H.; Moënne-Loccoz, P.; Goldberg, D. P. *J. Am. Chem. Soc.* **2017**, *139*, 10621.
15. Chiang, C. K.; Chu, K. T.; Lin, C. C.; Xie, S. R.; Liu, Y. C.; Demeshko, S.; Lee, G. H.; Meyer, F.; Tsai, M. L.; Chiang, M. H.; Lee, C. M. *J. Am. Chem. Soc.* **2020**, *142*, 8649.
16. Abucayon, E. G.; Khade, R. L.; Powell, D. R.; Zhang, Y.; Richter-Addo, G. B. *J. Am. Chem. Soc.* **2016**, *138*, 104.
17. Manickas, E. C.; LaLonde, A. B.; Hu, M. Y.; Alp, E. E.; Lehnert, N. *J. Am. Chem. Soc.* **2023**, *145*, 23014.
18. Rhine, M. A.; Rodrigues, A. V.; Bieber Urbauer, R. J.; Urbauer, J. L.; Stemmler, T. L.; Harrop, T. C. *J. Am. Chem. Soc.* **2014**, *136*, 12560.
19. Walter, M. R.; Dzul, S. P.; Rodrigues, A. V.; Stemmler, T. L.; Telser, J.; Conradie, J.; Ghosh, A.; Harrop, T. C. *J. Am. Chem. Soc.* **2016**, *138*, 12459.
20. Mazumdar, R.; Saha, S.; Samanta, B.; Mondal, B. *Inorg. Chem.* **2021**, *60*, 18024.
21. Saha, S.; Maity, S.; Mazumdar, R.; Samanta, B.; Ghosh, R.; Guha, A.; Mondal, B. *Inorg. Chem.* **2023**, *62,* 17074.
22. Patra, A. K.; Afshar, R.; Olmstead, M. M.; Mascharak, P. K. *Angew. Chem. Int. Ed.*

2002, *41*, 2512.

23. Harrop, T. C.; Mascharak, P. K. *Acc. Chem. Res.* **2004**, *37*, 253.
24. Eroy-Reveles, A. A.; Leung, Y.; Beavers, C. M.; Olmstead, M. M.; Mascharak, P. K. *J. Am. Chem. Soc.* **2008**, *130*, 4447.
25. Hsieh, C.-H.; Darensbourg, M. Y. *J. Am. Chem. Soc.* **2010**, *132*, 14118.
26. McQuilken, A. C.; Ha, Y.; Sutherlin, K. D.; Siegler, M. A.; Hodgson, K. O.; Hedman, B.; Solomon, E. I.; Jameson, G. N. L.; Goldberg, D. P. *J. Am. Chem. Soc.* **2013**, *135*, 14024.
27. Jiang, Y.; Hayashi, T.; Matsumura, H.; Do, L. H.; Majumdar, A.; Lippard, S. J.; Moënne-Loccoz, P. *J. Am. Chem. Soc.* **2014**, *136*, 12524.
28. McQuilken, A. C.; Matsumura, H.; Dürr, M.; Confer, A. M.; Sheckelton, J. P.; Siegler, M. A.; McQueen, T. M.; Ivanović-Burmazović, I.; Moënne-Loccoz, P.; Goldberg, D. P. *J. Am. Chem. Soc.* **2016**, *138*, 3107.
29. Niewahner, J. H.; Walters, K. A.; Wagner, A. *J. Chem. Educ.* **2007**, *84*, 477.
30. Magull, J.; Simon, A. *Z. Anorg. Allg. Chem.* **1992**, *615*, 81.
31. Dey, S.; Wayland, B. B.; Zdilla, M. J. *Inorg. Chem.* **2019**, *58*, 1224.
32. (a) Franceschi, F.; Hesschenbrouck, J.; Solari, E.; Floriani, C.; Re, N.; Rizzoli, C.; Chiesi-Villa, A. *J. Chem. Soc*., *Dalton Trans*. **2000**, 593. (b) Berno, P.; Floriani, C.; Chiesi-Villa, A.; Guastini, C. *J. Chem. Soc., Dalton Trans.* **1988**, 1409.
33. (a) Kumar, P.; Lee, Y.-M.; Hu, L.; Chen, J.; Park, Y. J.; Yao, J.; Chen, H.; Karlin, K. D.; Nam, W. *J. Am. Chem. Soc.* **2016**, *138*, 7753. (b) Kumar, P.; Lee, Y.-M.; Park, Y. J.; Siegler, M. A.; Karlin, K. D.; Nam, W. *J. Am. Chem. Soc.* **2015**, *137*, 4284. (c) Gogoi, K.; Saha, S.; Mondal, B.; Deka, H.; Ghosh, S.; Mondal, B. *Inorg. Chem.* **2017**, *56*, 14438. (d) Deka, H.; Ghosh, S.; Saha, S.; Gogoi, K.; Mondal, B. *Dalton Trans.* **2016**, *45*, 10979.

34. Huheey, J. E.; Keiter, E. A.; Keiter, R. L. *Inorganic Chemistry: Principles of Structure and Reactivity*, 4th ed.; Harper Collins College Publishers: New York, **1993**.

35. Martí, M. A.; Bari, S. E.; Estrin, D. A.; Doctorovich, F. *J. Am. Chem. Soc.* **2005**, *127*, 4680.

36. Wayland, B. B.; Olson, L. W.; Siddiqui, Z. U. *J. Am. Chem. Soc.* **1976**, *98*, 94.

37. (a) Bari, S. E.; Martí, M. A.; Amorebieta, V. T.; Estrin, D. A.; Doctorovich, F. *J. Am. Chem. Soc.* **2003**, *125*, 15272. (b) Doyle, M. P.; Mahapatro, S. N.; Broene, R. D.; Guy, J. K. *J. Am. Chem. Soc.* **1988**, *110*, 593. (c) Miranda, K. M.; Nims, R. W.; Thomas, D. D.; Espey, M. G.; Citrin, D.; Bartberger, M. D.; Paolocci, N.; Fukuto, J. M.; Feelisch, M.; Wink, D. A. *J. Inorg. Biochem.* **2003**, *93*, 52.

38. McQuarters, A. B.; Kampf, J. W.; Alp, E. E.; Hu, M.; Zhao, J.; Lehnert, N. *Inorg. Chem.* **2017**, *56*, 10513.

39. Enemark, J. H.; Feltham, R. D.; Riker-Nappier, J.; Bizot, K. F. *Inorg. Chem.* **1975**, *14*, 624.

40. Reisz, J. A.; Klorig, E. B.; Wright, M. W.; King, S. B. *Org. Lett.* **2009**, *11*, 2719.

41. Cherryman, J. C.; Harris, R. K.; Davidson, M. G.; Price, R. D. *J. Braz. Chem. Soc.* **1999**, *10*, 287.

42. SMART, SAINT and XPREP; Siemens Analytical X-ray Instruments Inc.: Madison, Wisconsin, USA, **1995**.

43. (a) Sheldrick, G. M. *Acta Crystallogr. Sect. A Found. Adv.* **2015***, 71,* 3. (b) Sheldrick, G. M. *Acta Crystallogr. Sect. C Struct. Chem.* **2015**, *71*, 3. (c) Farrugia, L. J. ORTEP-3 for Windows - a version of ORTEP-III with a Graphical User Interface (GUI). *J. Appl. Crystallogr.* **1997**, *30*, 565.

Chapter 5

Photo-induced nitroxyl anion/HNO release from a nitrosyl complex of Mn(II)-porphyrinate

Abstract

Mn-nitrosyls having $\{Mn(NO)\}^6$ configuration are generally considered to have the electronic character of low spin [Mn^{I}-NO^{+}] owing to which HNO/NO^{-} release from Mn-nitrosyls is not favourable. Although only a handful of $\{Mn(NO)\}^6$ are known to release NO under specific conditions, only one Mn-nitrosyl in 5,10,15,20-tetrakis(4-methoxyphenyl)porphyrin framework is reported to release NO^{-} in the presence of a neutral or anionic sixth ligand. A nitrosyl complex of Mn(II)-porphyrinate, [Mn($TTMPP^{2-}$)(NO)], **5.2** ($TTMPP^{2-}$ = 5,10,15,20-tetrakis(3,4,5-trimethoxyphenyl)porphyrin dianion) has been synthesized and characterized. In the presence of visible light, complex **5.2** in dichloromethane solution at -40 °C was found to release nitroxyl anion (NO^{-}) to [Fe^{III}(TPP^{2-})Cl] and [Fe^{III}(DTC^{-})$_3$] (DTC^{-} = diethyldithiocarbamate anion) to result in the corresponding $\{Fe(NO)\}^7$ complex. Further, when complex **5.2** was stirred with an equivalent amount of HBF_4 under visible light, the presence of N_2O in the headspace gas was observed. This, in turn, suggests that complex **5.2** releases HNO in the presence of H^{+} under visible light. All these studies suggest that complex **5.2** acts as a NO^{-}/HNO donor in the presence of visible light.

5.1 Introduction

The interest in HNO/NO^- chemistry has increased considerably due to its chemical properties and biological relevance.[1,2] To understand the chemical biology of HNO/NO^-, the knowledge of its metal complexes is necessary. HNO is known to react with metallo-proteins, thiols, NO and O_2 and there is a significant overlap of its reactivity with NO. For instance, HNO and NO, both are reactive towards heme-proteins in both the Fe^{II} and Fe^{III} states.[3-5] Thus, to know the actual role of HNO, a careful determination of HNO is very essential. Over the decade, a great advancement has been made towards direct methods of detection and quantification of HNO.[1,2,6-11] The examples of HNO/NO^- donors still remain restricted to only a few such as Angeli's salt, Piloty's acid or acyl and acyloxy nistroso derivatives.[12] However, all of these have some intrinsic limitations like simultaneous formation of undesirable byproducts, ineffective release of HNO at physiological pH etc. These actually hinder their widespread utility. Hence, there is a need for more efficient HNO donors.

The metal bound nitrosyl complexes with suitable electronic configurations have been found to be an efficient HNO donor. In this direction a few examples of $\{Co(NO)\}^8$ complexes and their $\{Co(NO)\}^9$ analogues are reported.[13-18] Mn-nitrosyls having $\{Mn(NO)\}^6$ configuration are generally considered to have the electronic character of low spin [Mn^I-NO^+] owing to which HNO/NO^- release from Mn-Nitrosyls is not favourable. These complexes usually show nitrosyl stretching frequency in FT-IR spectrum in the range of 1730-1770 cm^{-1} (Table – 5.1). Although Mn-nitrosyls are generally considered to have NO^+ character, a handful are known to release NO under specific conditions. For example, Mascharak *et al.* reported two Mn-nitrosyls in a penta-coordinated N5 ligand framework which release NO in the presence of light.[19] Kubaik *et al.* also reported a Mn-nitrosyl in meso-tetrakis(4-methoxyphenyl)porphyrin framework which was found to transfer NO to [$Co^{II}(TPP^{2-})$] in tetrahydrofuran.[20] On the other hand, Lippard and coworkers reported a Mn-nitrosyl in electron rich divalent tropocoronand, (TC-

5,5) ligand system which favours the reduction of the metal bound nitrosyl making it formally $[Mn^{III}\text{-}NO^{-}]^{2+}$.[21] It reacts with excess NO and produce N_2O and $[Mn^{III}(NO_2)(TC\text{-}5,5)]$. Thus, a Mn-nitrosyl complex that can act as an HNO/ NO^- donor is really hard to find.

Recently, our group reported a Mn-nitrosyl in meso-tetrakis(4-methoxyphenyl)porphyrin framework, which releases NO^- in the presence of a neutral or anionic sixth ligand.[22] To our best knowledge, till date, this is the very first example where a Mn-nitrosyl complex acts as HNO/NO^- donor. The scarcity of well-studied Mn-nitrosyls as HNO/NO^- donor in literature may be resolved by modulating the overall electronic properties of these complexes by judicious choice/design of the ligand frameworks. The ligand environment, as a primary criterion, should be electronically flexible to accommodate metal ions in different oxidation states.

This chapter describes a Mn-nitrosyl complex of an electron rich porphyrin ligand which can act as an HNO/NO^- donor in solution in the presence of visible light.

5.2 Results and discussion

The ligand, 5,10,15,20-tetrakis(3,4,5-trimethoxyphenyl)porphyrin (H_2TTMPP) was prepared from 3,4,5-trimethoxybenzaldehyde and pyrrole by following Alder and Longo method.[23] The formation of the ligand was confirmed by ^{1}H-NMR, ^{13}C-NMR, FT-IR, UV-visible spectroscopy and ESI-mass spectrometry (Exp. Sec., Appendix IV, Figures A4.1-A4.5). The precursor complex, $[Mn^{III}(TTMPP^{2-})Cl]$, **5.1** was prepared by following previously reported protocol with small modifications (Exp. Sec.).[24] It was characterized both structurally and spectroscopically (Exp. Sec., Appendix IV, Figures A4.6-A4.10). The spectroscopic data matched well with the previously reported analogous complexes.[24b,25] The single crystal X-ray diffraction study reveals that the manganese-centre is coordinated to four N-atoms of the porphyrin ligand equatorially (Appendix IV, Figure A4.8). The Cl atom was found to occupy

two symmetrically equivalent positions. The structural disorder remains even after growing the crystal for multiple times.

The nitrosyl complex, [Mn(TTMPP^{2-})(NO)], **5.2** was synthesized *via* reductive nitrosylation method using hydroxylamine (Exp. Sec.).[26] It was characterized using UV-visible, FT-IR, EPR, ^{1}H-NMR spectroscopy and ESI-mass spectrometry (Exp. Sec., Appendix IV, Figures A4.11-A4.16). The diamagnetic nature of the complex arises from the antiferromagnetic coupling of unpaired *d* electron of low-spin Mn(II)-centre and the antibonding electron of the nitrosyl moiety. Even after trying for multiple times, we were not able to grow X-ray quality crystals. In FT-IR spectroscopy, complex **5.2** shows nitrosyl stretching frequency at 1747 cm^{-1} in ATR probe, which shifts to 1740 cm^{-1} while measured in dichloromethane solution. In UV-visible spectroscopy, it shows soret band at 416 nm and Q bands at 534 and 562 nm in dichloromethane. These data are in accordance with the reported analogous ones (Table 5.1). In ESI-mass spectrometric study, upon injecting a cold solution (-80 °C) of complex **5.2** in 20% dichloromethane and 80% methanol, a [M+H]$^{+}$ peak at m/z = 1058.440 (Calculated: 1058.302) was observed. The isotopic distribution pattern matches well with the simulated one (Appendix IV, Figure A4.16).

Since we could not grow the single crystal, computational calculations were performed to gain insights into the interaction between NO and Mn-Porphyrin. Based on the geometry optimization at the B3LYP/6-31+G (D, P) level of theory, we determined that NO tends to bind in a linear mode with Mn-porphyrin as seen in figure 5.1. In this linear mode interaction, the bond length of NO elongates to 1.179 Å from its free NO bond length of 1.151 Å. Frontier molecular orbital analysis reveals that the HOMO is predominantly delocalized over the electron-rich porphyrin ligand, while the LUMO+2 orbital is localized over the NO moiety.

In absence of light, the complex **5.2** in dichloromethane solution is very stable at -40 °C under

argon atmosphere. But, upon exposure to visible light, the color of the solution started to change from red to green indicating photo-decomposition of complex **5.2**. UV-visible spectral study of freshly prepared dichloromethane solution of complex **5.2** confirms that the decomposition is associated with the oxidation of the Mn(II)-centre to Mn(III). In fluorescence study (λ_{ex}= 420 nm), complex **1** was found to emit at 651 nm (Appendix IV, Figure A4.39). The soret band at 416 nm gradually decays along with the formation of a new band at 482 nm (Figure 5.2). The soret band at 450-500 nm region is typical for Mn(III)-porphyrin complexes, which suggests the one-electron oxidation

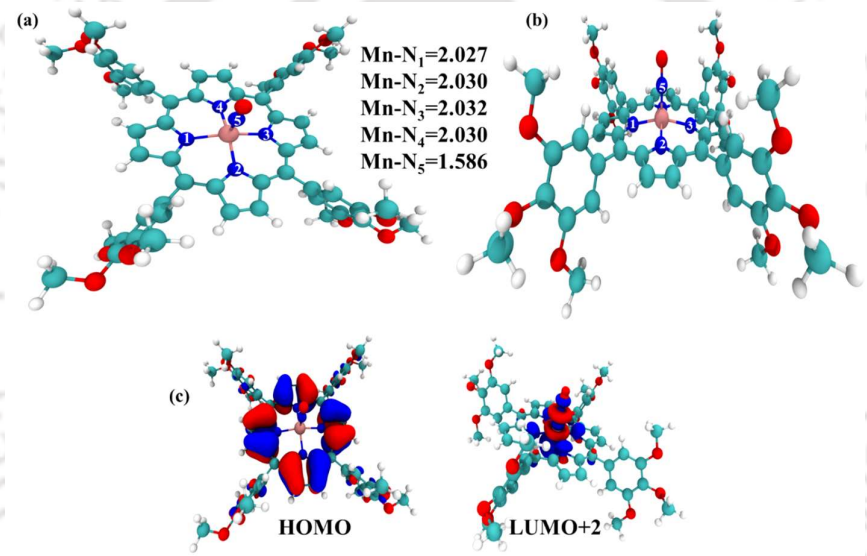

Figure 5.1. Optimized structure of [Mn(TTMPP^{2-})(NO)]: (a) top view, (b) side view. Mn-N distances are indicated in Angstrom (Å). (c) HOMO and LUMO+2 orbitals of the optimized structure.

Table 5.1. List of some selected Mn-nitrosyls of different porphyrin ligand frameworks with their respective nitrosyl stretching frequency (cm^{-1}) and soret band position (nm) in UV-visible spectroscopy.

Mn-nitrosyl Complexes	**$\overline{\nu}_{NO}$ (cm^{-1})**	**Soret band position (nm)**	**References**
[Mn(F_{20}TPP^{2-})(NO)]	1763 (KBr)	415 (THF)	27
[Mn(TPP^{2-})(NO)]	1760 (KBr)	~ 430 (Toluene)	28
[Mn(TMPP^{2-})(NO)]	1755 (KBr)	429 (CH_2Cl_2)	22
[Mn(TTMPP^{2-})(NO)]	1747 (ATR probe)	416 (CH_2Cl_2)	This work

of Mn(II)-centre.[24b,25] Thus, this 482 nm band is attributed to the formation of $[Mn^{III}(TTMPP^{2-})]^{+}$ (green) in the reaction medium. The green complex was worked up and isolated as a solid and recrystallized from dichloromethane-methanol solution (Exp. Sec.). Spectroscopic and structural characterization reveals the final complex as $[Mn^{III}(TTMPP^{2-})(OH)]$, **5.3** (Exp. Sec., Appendix IV, Figures A4.17-A4.21). The crystal structure of complex **5.3** shows a similar structural disorder as complex **5.1**. We presume that, $[Mn^{III}(TTMPP^{2-})]^{+}$, which is formed upon photo-decomposition of complex **5.2** converts into $[Mn^{III}(TTMPP^{2-})(OH)]$ by absorbing moisture during work up process in open air. To confirm, a counter anion BPh_4^- was added to the reaction mixture under anaerobic condition before working up and it was isolated as $[Mn^{III}(TTMPP^{2-})(CH_3OH)_2](BPh_4)$, **5.4**.

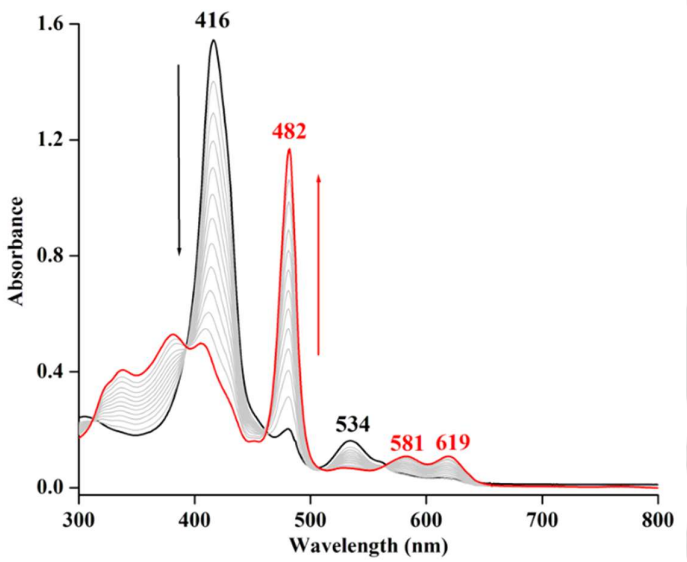

Figure 5.2. UV-visible spectroscopic study of photo-decomposition of complex **5.2** in CH_2Cl_2 at -40 °C (black (initial), red (final)).

It is characterized by UV-visible, FT-IR, EPR spectroscopy and ESI-mass spectrometry (Exp. sec., Appendix IV, Figures A4.22-A4.25). In single crystal x-ray structure determination, the Mn-centre was found to be in a distorted octahedral geometry, coordinated to four N-atoms of $TTMPP^{2-}$ in the equatorial plane and two O-atoms of two methanol units axially. The BPh_4^- unit acts as a counter anion (Figure 5.3).

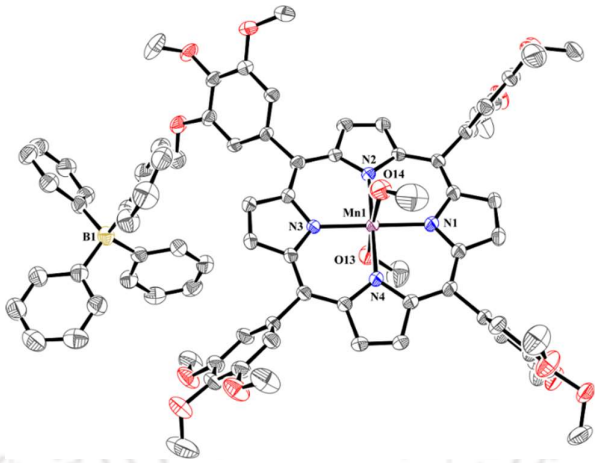

Figure 5.3. ORTEP diagram of complex **5.4** (40% thermal ellipsoid plot, solvent and H-atoms are omitted for clarity).

In FT-IR spectroscopic study, a freshly prepared dichloromethane solution of complex **5.2** upon exposure to visible light shows the gradual disappearance of the nitrosyl stretching frequency at 1740 cm^{-1} (Figure 5.4) and no new stretching frequency was observed which can be attributed to any reduced or oxidized analogue of metal-bound nitrosyl moiety. However, in the absence of light, the solution remains unchanged for several hours at -40 °C. This observation suggests that in the presence of visible light, the release of nitrosyl moiety occurs with a concomitant oxidation of Mn(II)-centre. So, from the UV-visible and FT-IR study, it is logical to assume that nitrosyl moiety must have released from the complex **5.2** as NO^-. It should be noted that for the analogous nitrosyl complexes of Mn-porphyrinates, this behaviour is not common. The presence of the twelve methoxy groups in the ligand framework provides sufficient electron density to the [Mn-NO] centre making it highly reactive. This is evident from the gradual decrease of nitrosyl stretching frequency with increasing electron donating groups in the ligand framework (Table 5.1). In case of [Mn($TMPP^{2-}$)(NO)], the release of NO^- was observed only in the presence of an electron-rich sixth ligand.[22] In addition, for [Co(BPB^{2-})(NO)] complex, it was reported that electron-rich or neutral ligand can induce the release of NO^-.[29] However, in the present case, the release of NO^- happens in the presence of visible light.

It is worth mentioning that after the decomposition of complex **5.2,** the headspace gas of the reaction vessel was purged into the dry and degassed dichloromethane solution of $[Fe^{III}(DTC^{-})_3]$ and the FT-IR spectrum of the solution is recorded (Appendix IV, Figure A4.33). No spectroscopic evidence regarding the formation of $[Fe(NO)(DTC^{-})_3]$ was observed. This observation rules out the possibility of the release of nitric oxide (NO) from complex **5.2**.

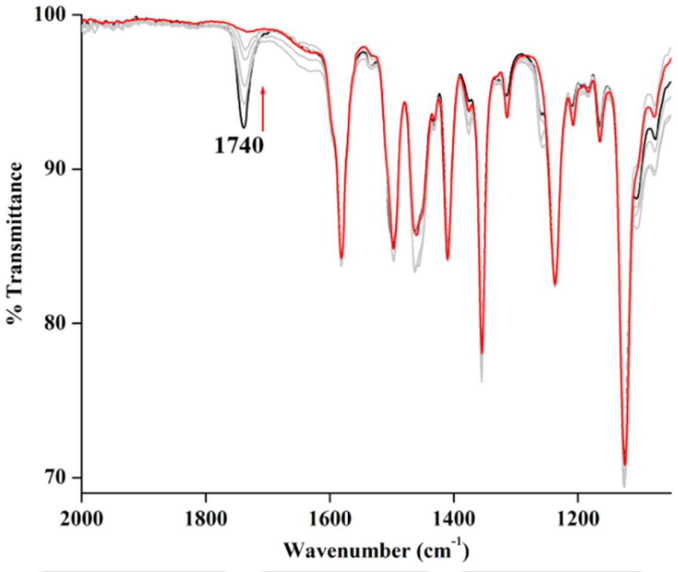

Figure 5.4. FT-IR spectroscopic study of the decomposition of complex **5.2** in CH_2Cl_2 solution in ATR probe [black (initial), red (final)].

The NO^{-} releasing ability of complex **5.2** can be confirmed by it's reaction with well-known HNO/NO^{-} trapping agents like $[Fe^{III}(TPP^{2-})Cl]$[26,29,30] and $[Fe^{III}(DTC^{-})_3]$[22,29]. Nitroxyl anion (NO^{-}) directly attacks these Fe^{III}-centres and leads to the formation of iron-nitrosyls of $\{Fe(NO)\}^7$ configuration, which can be easily identified using FT-IR and X-band EPR spectroscopy. Complex **5.2** was made to expose to visible light in the presence of $[Fe^{III}(TPP^{2-})Cl]$ in dry and degassed dichloromethane solution under inert atmosphere. In FT-IR spectroscopy, the nitrosyl stretching frequency of complex **5.2** at 1747 cm^{-1} completely disappears along with the formation of a new stretching frequency at 1699 cm^{-1} (Figure 5.5(a)). This 1699 cm^{-1} peak is attributed to the nitrosyl stretching frequency of newly formed

[Fe(TPP^{2-})NO] in the reaction medium.[26,29,30] In X-band EPR spectroscopy, the reaction mixture shows a signal with g ~ 2.05 at 77 K, suggesting the formation of [Fe(TPP^{2-})NO] (Figure 5.5(b)). Isolation and characterization of the final products confirm the presence of [Mn^{III}(TTMPP^{2-})Cl], **5.1**, in the reaction mixture, as expected (Eq. 5.1). Complex **5.1** was isolated and characterized using various spectroscopic methods (Exp. Sec., Appendix IV, Figures A4.30-A4.32).

$$\mathbf{[Mn(TTMPP^{2-})(NO)] + [Fe^{III}(TPP^{2-})Cl] \longrightarrow [Mn^{III}(TTMPP^{2-})Cl] + [Fe(NO)(TPP^{2-})]} \quad \text{... Eq. 5.1}$$

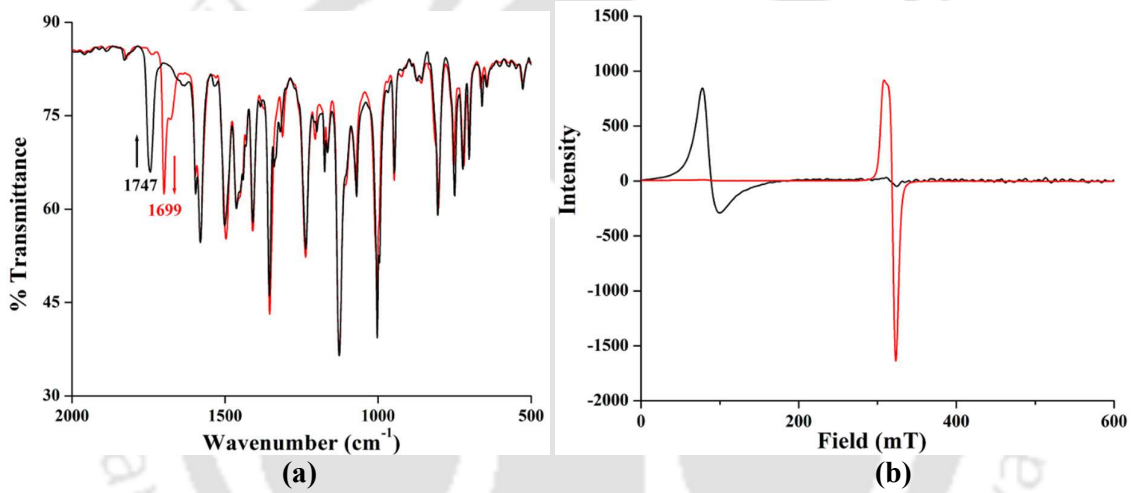

Figure 5.5. (a) FT-IR (ATR probe) and (b) X-band EPR spectrum of the reaction mixture of complex **5.2** and [Fe^{III}(TPP^{2-})Cl] in CH_2Cl_2 before (black) and after (red) exposure to visible light.

$$\mathbf{[Mn(TTMPP^{2-})(NO)]+[Fe^{III}(DTC^{-})_3] \longrightarrow [Mn^{III}(TTMPP^{2-})(\,DTC^{-})]+[Fe(DTC^{-})_2(NO)]} \quad \text{... Eq. 5.2}$$

Similar results were found in the presence of [Fe^{III}(DTC^{-})$_3$]. FT-IR spectroscopic study indicates the formation of a new nitrosyl stretching frequency at 1690 cm^{-1}, with a concomitant decay of stretching frequency at 1747 cm^{-1} (Appendix IV, Figure A4.37). This is attributed to the formation of [Fe(DTC^{-})$_2$(NO)] in the reaction (Eq. 5.2). The X-band EPR spectrum of the reaction mixture in dichloromethane at 77 K also shows a sharp signal at g ~ 2.04, confirming the presence of [Fe(DTC^{-})$_2$(NO)] (Appendix IV, Figure A4.38).[22,29,31] Isolation of the final

products confirms the presence of [Mn^{III}(TTMPP^{2-})(DTC^{-})], **5.5,** in the reaction mixture. Complex **5.5** was characterized spectroscopically (Exp. Sec., Appendix IV, Figures A4.26-A4.29). In ESI-mass spectrometry, it shows $[M+K]^+$ peak at m/z = 1215.746 (Calculated: 1215.293) and the isotopic pattern matches well with the simulated ones. Thus, it is conclusive that complex **5.2** indeed releases NO^- in the presence of visible light, leading to the reductive nitrosylation of the Fe^{III}-centre.

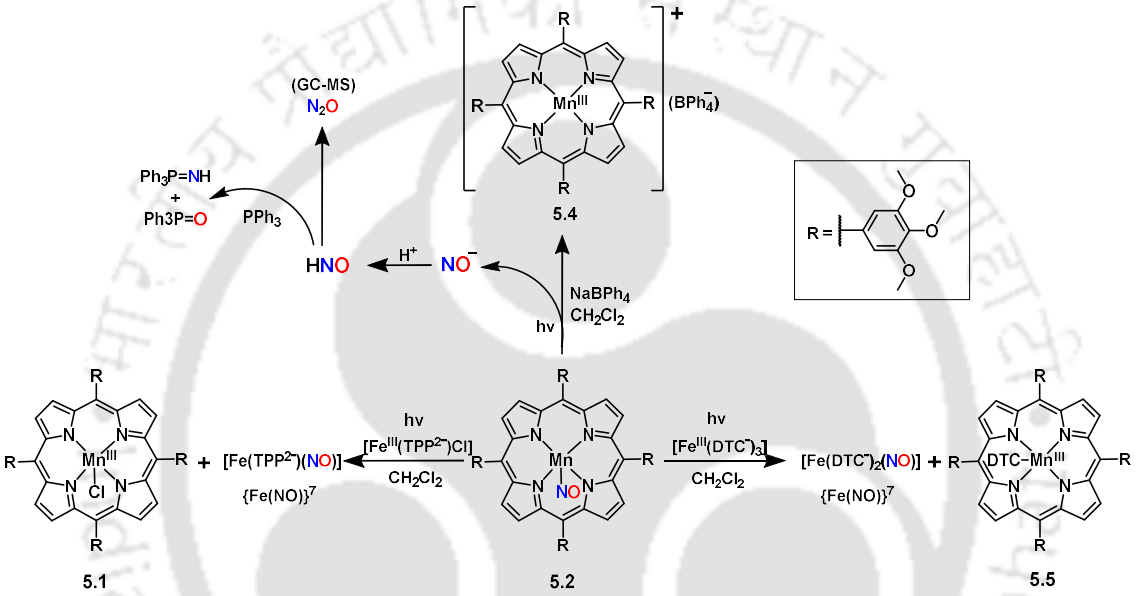

Scheme 2: Overall reactions.

In the presence of a proton source, NO^- readily becomes HNO. This HNO undergoes rapid dimerization ($k_{dim} = 8 \times 10^6\ M^{-1}\ s^{-1}$), which is considered to be an important chemical process for nitroxyl consumption, leading to the formation of hyponitrous acid (HONNOH), which is further decomposed to give N_2O and H_2O.[32] 1.2 equivalent of $HBF_4.Et_2O$ was added to the freshly prepared dichloromethane solution of complex **5.2** and after 1 hour, treatment of the headspace gas of the reaction vessel in gas chromatography confirms the presence of N_2O (Appendix IV, Figure A4.34). In GC-mass spectrum, the signal at m/z = 44 also confirms the same (Appendix IV, Figures A4.35). Quantification of the amount of N_2O produced from complex **5.2** is done using GC. Using alkaline solution of Piloty's acid, a calibration curve was prepared. From

the calibration curve, the yield was found to be about 83% (Appendix IV, Figures A4.36).

Another confirmatory test for the formation of HNO was done by studying its reaction with triphenylphosphine (PPh_3) using ^{31}P-NMR.[33a] In the reaction mixture of complex **5.2** and triphenylphosphine, 1.2 mole equivalent of $HBF_4.Et_2O$ was added and the reaction was monitored by ^{31}P-NMR spectroscopy (Exp. Sec.). Two signals at δ_{ppm} = 22.18 ppm and δ_{ppm} = 26.75 ppm were observed, which suggest the formation of Ph_3P=NH and Ph_3P=O, respectively (Figure 5.6).[15] The signal at δ_{ppm} = 44.26 ppm is attributed to metal-bound triphenylphosphine (Figure 5.6).[33b]

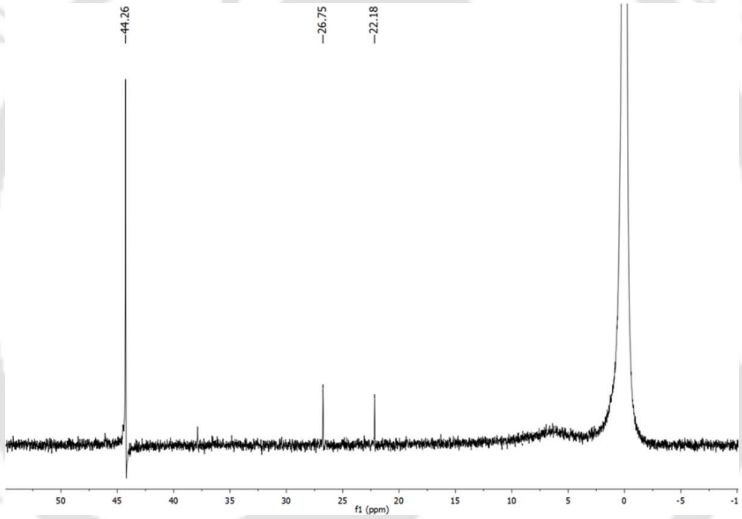

Figure 5.6. ^{31}P-NMR spectrum of the reaction mixture of PPh_3, complex **5.2** and $HBF_4.Et_2O$ in CH_2Cl_2 solution with 0.1 mL DMSO-d_6.

5.3 Experimental Section

5.3.1 Materials and Methods

All experiments, unless otherwise specified, were done under argon atmosphere using standard Schlenk techniques on the Schlenk line. All chemicals used were of reagent grade, purchased from commercially available sources and no purification was done unless mentioned. Methanol was distilled using Mg-turnings and iodine. Tetrahydrofurane was dried by distillation with

sodium and benzophenone. Dichloromethane was purified by passing through a basic alumina column, then storing it over calcium hydride overnight and followed by distillation under inert atmosphere (N_2). All the solvents were stored over molecular sieve (4 Å) for at least 2 days under argon before using. Molecular sieves were kept at 200 °C for 24 hours for activation and cooled under vacuum. Solvents and solutions were deoxygenated by applying consecutive vacuum/argon purge cycles. All the reactions were performed under inert atmosphere except mentioned differently. UV-visible spectra were taken on an Agilent Cary 8454 spectrophotometer. FT-IR spectra were recorded as KBr pellets or in a KBr cell using a PerkinElmer spectrophotometer. ^{1}H, ^{13}C, and ^{31}P-NMR studies were done in Bruker Avance III 400 and 500 MHz Varian FT-NMR spectrophotometers. X-band EPR spectra were recorded on a JES-FA200 EPR spectrophotometer with microwave power, 0.998 mW; microwave frequency, 9.14 GHz; and modulation amplitude, 2. Gas chromatograms were obtained on PerkinElmer Clarus® 590.

Single crystals were grown from dichloromethane-methanol solutions using the slow evaporation technique. The intensity data were collected using a Bruker SMART APEX-II CCD diffractometer, equipped with a fine focus 1.75 kW sealed tube Mo Kα radiation (λ = 0.71073 Å), with increasing ω (width of 0.3° per frame) at a scan speed of 3 s/frame. The SMART software was used for data acquisition. Data integration and reduction were undertaken with SAINT and XPREP software.[34] Structures were solved by direct methods using SHELXL[35a] and refined with full-matrix least-squares on F^2 using SHELXL-2019/1.[35b] Structural illustrations were drawn with ORTEP-3 for Windows.[35c]

5.3.2 Syntheses

5,10,15,20-tetrakis(3,4,5-trimethoxyphenyl)porphyrin (H_2TTMPP): The trimethoxyphenyl substituted porphyrin was synthesized following Alder and Longo

methods.[23] To a 250 mL round bottom flask equipped with a magnetic stir-bar, equimolar amount of 3,4,5-trimethoxybenzaldehyde (3.92 g, 20 mmol) and freshly distilled pyrrole (1.34 g, 20 mmol) was added followed by 75 mL of propionic acid. The mixture was refluxed for 2 hours. The reaction mixture was left overnight at room temperature upon which a purple crystalline solid was precipitated. It was filtered and washed with hot water, followed by hexane. Shiny purple crystals of pure H_2TTMPP were obtained. Yield: 1.17 g (*ca.* 24%). Elemental analyses for $C_{56}H_{54}N_4O_{12}$; Calculated (%): C, 68.98; H, 5.58; N, 5.75. Found (%): C, 69.07; H, 5.49; N, 5.83. FT-IR (in ATR probe): 3311, 2994, 2938, 2835, 1709, 1580, 1501, 1470, 1410, 1360, 1234, 1124, 1078, 1005, 922, 806 and 722 cm^{-1}. ^{1}H-NMR (400 MHz, $CDCl_3$): δ_{ppm}, 8.97 (s, 8H), 7.48 (s, 8H), 4.19(s, 12H), 3.98(s, 24H) and -2.77(s, 2H). ^{13}C-NMR (100 MHz, $CDCl_3$): δ_{ppm}, 151.4, 137.9, 137.5, 120.0, 112.8, 61.33 and 56.4. UV-visible (CH_2Cl_2): 422 nm (ε/M^{-1} cm^{-1}, 4.54×10^5), 463 nm (ε/M^{-1} cm^{-1}, 1.16×10^4), 517 nm (ε/M^{-1} cm^{-1}, 2.09×10^4), 553 nm (ε/M^{-1} cm^{-1}, 8.25×10^3), 592 nm (ε/M^{-1} cm^{-1}, 6.13×10^3) and 648 nm (ε/M^{-1} cm^{-1}, 4.75×10^3). ESI-mass (m/z): Calculated, 975.381; Found, 975.383, $[M+H]^+$.

[Mn^{III}($TTMPP^{2-}$)Cl], 5.1: To a 100 mL round bottom flask equipped with a magnetic stir bar, H_2TTMPP (975 mg, 1 mmol), $Mn(OAc)_2.4H_2O$ (2.45 g, 10 mmol) and KCl (745 mg, 10 mmol) was added followed by 50 mL 1:1 mixture of chloroform-acetic acid. The resulting mixture was refluxed for 12 hours. After brought to room temperature, the reaction mixture was washed with water (3 × 100 mL) and extracted using chloroform (3 × 30 mL). The crude thus obtained was subjected to silica-column and complex **5.1** was isolated as green solid. Yield: 957 mg (*ca.* 90%). Elemental analyses for $C_{56}H_{52}ClMnN_4O_{12}$; Calculated (%): C, 63.25; H, 4.93; N, 5.27. Found (%): C, 63.19; H, 5.01; N, 5.25. FT-IR (in ATR probe): 1580, 1496, 1462, 1409, 1354, 1235, 1124, 1009, 947, 804 and 722 cm^{-1}. UV-visible (CH_2Cl_2): 482 nm (ε/M^{-1} cm^{-1}, 9.34×10^4), 529 nm (ε/M^{-1} cm^{-1}, 5.47×10^3), 583 nm (ε/M^{-1} cm^{-1}, 8.28×10^3) and 619 nm (ε/M^{-1} cm^{-1}, 8.65×10^3). ESI-mass (m/z): Calculated, 1027.296; Found, 1027.296, ($[Mn(TTMPP^{2-})]^+$

ion peak). Crystal data: complex **5.1**, CCDC No. 2349504. $C_{56}H_{52}N_4O_{12}Cl_2Mn$, M = 1098.86, Triclinic (P -1), a = 8.0273(4) Å, b = 12.4667(6) Å, c = 14.3129(7) Å, α = 86.5190(10)°, β = 75.1190(10)°, γ = 88.2800(10)°, V = 1381.60(12) Å^3, Z = 1, D_c = 1.321 g cm^{-3}, μ = 0.400 mm^{-1}, T = 298(2) K, 4862 reflections, 4109 independent, $R(F)$ = 0.0615 [$I > 2\delta(I)$], R(int) = 0.0741, $wR(F2)$ = 0.1998 (all data), GOF = 1.053.

[Mn(TTMPP^{2-})(NO)], 5.2: Complex **5.1** (41 mg, 0.04 mmol) was taken in a 25 ml Schlenk flask and degassed with consecutive vacuum/argon cycles. Dry and distilled tetrahydrofuran (2 mL) was added to it and the green-colored solution was cooled to -40 °C. To this solution, a freshly prepared methanolic solution of hydroxylamine (5 mole equivalent) was added. The color of the solution changes from green to dark red. Precooled dry and degassed methanol (5 mL) is added to this red solution and kept at -40 °C for 24 hours. A reddish-purple colored precipitate of complex **5.2** was obtained. Yield: 31.7 mg (*ca.* 75%). Elemental analyses for $C_{56}H_{52}MnN_5O_{13}$; Calculated (%): C, 63.57; H, 4.95; N, 6.62. Found (%): C, 63.49; H, 5.02; N, 6.70. FT-IR (in ATR probe): 2936, 2833, 1747, 1580, 1499, 1463, 1409, 1355, 1236, 1126, 1004, 946, 802 and 723 cm^{-1}. ^{1}H-NMR (400 MHz, $CDCl_3$): δ_{ppm}, 9.44 (s, 8H), 7.49 (s, 8H), 4.19(s, 12H) and 3.97(s, 24H). UV-visible (CH_2Cl_2): 416 nm (ε/M^{-1} cm^{-1}, 1.20 × 10^5), 534 nm (ε/M^{-1} cm^{-1}, 1.26 × 10^4) and 561 nm (ε/M^{-1} cm^{-1}, 6.90 × 10^3). ESI-mass (m/z): Calculated, 1058.302; Found, 1058.440, $[M+H]^+$.

[Mn^{III}(TTMPP^{2-})(OH)], 5.3: Complex **5.2** (53 mg, 0.05 mmol) was taken in a 15 mL Schlenk tube and degassed properly with consecutive argon/vacuum purge. Addition of dry and degassed dichloromethane to the Schlenk tube results in a red-colored solution. Upon keeping the solution under visible light, the red-colored solution turns green. A green crude product was obtained after the solvent was removed under vacuum. Yield: 47 mg (*ca.* 90%). Crystals were obtained by slow evaporation of dichloromethane solution of the complex. Elemental analyses

for $C_{56}H_{53}MnN_4O_{13}$; Calculated (%): C, 64.37; H, 5.11; N, 5.36. Found (%): C, 64.49; H, 5.06; N, 5.27. FT-IR (in ATR probe): 3435, 2931, 1580, 1497, 1464, 1411, 1355, 1206, 1163, 1124, 1006, 947, 862 and 722 cm^{-1}. UV-visible (CH_2Cl_2): 484 nm (ε/M^{-1} cm^{-1}, 7.44×10^4), 520 nm (ε/M^{-1} cm^{-1}, 7.02×10^3), 577 nm (ε/M^{-1} cm^{-1}, 1.08×10^4), 611 nm (ε/M^{-1} cm^{-1}, 8.82×10^3) and 783 nm (ε/M^{-1} cm^{-1}, 1.33×10^3). ESI-mass (m/z): Calculated, 1027.296; Found, 1027.297 ($[Mn(TTMPP^{2-})]^+$ ion peak, after removal of OH^- group). Crystal data: complex **5.3**, CCDC No. 2349505. $C_{56}H_{54}N_4O_{14}Mn$, M = 1061.97, Triclinic (P -1), a = 7.981(3) Å, b = 12.383(5) Å, c = 14.282(6) Å, α = 85.706(12)°, β = 76.649(12)°, γ = 87.299(13)°, V = 1368.9(9) $Å^3$, Z = 1, D_c = 1.288 g cm^{-3}, μ = 0.309 mm^{-1}, T = 298.0 K, 6126 reflections, 4129 independent, $R(F)$ = 0.0728 [$I > 2\delta(I)$], R(int) = 0.1118, $wR(F2)$ = 0.1998 (all data), GOF = 1.059.

$[Mn^{III}(TTMPP^{2-})(CH_3OH)_2](BPh_4)$, 5.4: Complex **5.2** (53 mg, 0.05 mmol) was taken in a 15 mL Schlenk tube and degassed properly with consecutive argon/vacuum purge. Addition of dry and degassed dichloromethane to the Schlenk tube results in a red-colored solution. Upon keeping the complex solution under visible light, the red-colored solution turns green. To this green solution, dry and degassed methanolic solution of $NaBPh_4$ (1.5 equivalent) was added. After 1 hour of the addition, the solvent was removed under vacuum. Green crude obtained. Yield: 58 mg (*ca.* 86%). Crystals were obtained by layering methanol over chloroform solution of the complex. Elemental analyses for $C_{82}H_{80}BMnN_4O_{14}$; Calculated (%): C, 69.79; H, 5.71; N, 3.97. Found (%): C, 69.85; H, 5.78; N, 3.91. FT-IR (in ATR probe): 2933, 1579, 1492, 1460, 1408, 1353, 1310, 1235, 1163, 1124, 1008, 946, 805, 724 and 704 cm^{-1}. UV-visible (CH_2Cl_2): 482 nm (ε/M^{-1} cm^{-1}, 4.53×10^4), 527 nm (ε/M^{-1} cm^{-1}, 4.47×10^3), 576 nm (ε/M^{-1} cm^{-1}, 1.51×10^4), 614 nm (ε/M^{-1} cm^{-1}, 6.31×10^3) and 710 nm (ε/M^{-1} cm^{-1}, 6.95×10^2). ESI-mass (m/z): Calculated, 1027.296; Found, 1027.296 ($[Mn(TTMPP^{2-})]^+$). Crystal data: complex **5.4**, CCDC No. 2349506 $C_{83}H_{81}BN_4O_{14}Cl_3Mn$, M = 1530.62, Monoclinic (P 21/c), a = 15.425(5) Å, b = 22.911(7) Å, c = 25.451(8) Å, α = 90°, β = 105.144(9)°, γ = 90°, V = 8682(5) $Å^3$, Z = 4, D_c =

1.171 g cm^{-3}, μ = 0.304 mm^{-1}, *T* = 297.00 K, 19273 reflections, 12494 independent, *R*(*F*) = 0.0960 [$I > 2\delta(I)$], *R*(int) = 0.1420, *wR*(*F2*) = 0.2688 (all data), GOF = 1.073.

[$Mn^{III}(TTMPP^{2-})Cl$], 5.1 isolated from the reaction of complex 5.2 and [$Fe^{III}(TPP^{2-})Cl$]: To a 25 mL Schlenk flask equipped with a magnetic stir-bar, complex **5.2** (53 mg, 0.05 mmol) and [$Fe^{III}(TPP^{2-})Cl$] (42 mg, 0.06 mmol) was added and degassed by consecutive Argon/vacuum purge. Dry and degassed dichloromethane was added to it and the reaction mixture was allowed to stir under visible light at -40 °C for 1 hour. After bringing the reaction mixture to room temperature, the solvent was removed under vacuum. The green crude obtained was subjected to column chromatography. Complex **5.1** was obtained as a green solid. Yield: 43 mg (*ca.* 81%). Elemental analyses for $C_{56}H_{52}ClMnN_4O_{12}$; Calculated (%): C, 63.25; H, 4.93; N, 5.27. Found (%): C, 63.19; H, 5.01; N, 5.22. FT-IR (in ATR probe): 1580, 1496, 1462, 1409, 1354, 1235, 1124, 1009, 947, 804 and 722 cm^{-1}. UV-visible (CH_2Cl_2): 482 nm (ε/M^{-1} cm^{-1}, 9.34 × 10^4), 529 nm (ε/M^{-1} cm^{-1}, 5.47 × 10^3), 583 nm (ε/M^{-1} cm^{-1}, 8.28 × 10^3) and 619 nm (ε/M^{-1} cm^{-1}, 8.65 × 10^3). ESI-mass (m/z): Calculated, 1027.296; Found, 1027.296 ($[Mn(TTMPP^{2-})]^+$ ion peak).

[$Mn^{III}(TTMPP^{2-})(DTC^-)$], 5.5 isolated from the reaction of complex 5.2 and [$Fe^{III}(DTC^-)_3$]: To a 25 mL Schlenk flask equipped with a magnetic stir-bar, complex **5.2** (53 mg, 0.05 mmol) and [$Fe^{III}(DTC^-)_3$] (30 mg, 0.06 mmol) was added and degassed by consecutive argon/vacuum purge. Dry and degassed dichloromethane was added to it and the reaction mixture was allowed to stir in the presence of visible light at -40 °C for 1 hour. After bringing the reaction mixture to room temperature, the solvent was removed under *vacuo*. Complex **5.5** was obtained from the reaction mixture by subjecting it to column chromatography. Yield: 52 mg (*ca.* 86%). Elemental analyses for $C_{61}H_{62}MnN_5O_{12}S_2$; Calculated (%): C, 62.29; H, 5.31; N, 5.95. Found (%): C, 62.19; H, 5.41; N, 5.89. FT-IR (in ATR probe): 2925, 1629, 1580, 1498, 1464, 1411, 1355, 1236, 1164, 1124, 1005, 947, 804 and

722 cm^{-1}. UV-visible (CH_2Cl_2): 483 nm (ε/M^{-1} cm^{-1}, 1.21×10^5), 521 nm (ε/M^{-1} cm^{-1}, 1.28×10^4), 576 nm (ε/M^{-1} cm^{-1}, 1.82×10^4), 611 nm (ε/M^{-1} cm^{-1}, 1.50×10^4) and 783 nm (ε/M^{-1} cm^{-1}, 2.77×10^3). ESI-mass (m/z): Calculated, 1215.346; Found, 1215.746, $[M+K]^+$.

$[Fe^{III}(TPP^{2-})(Cl)]$: The preparation procedure and spectroscopic characterization were described earlier (Exp. Sec., Chapter 2).

$[Fe^{III}(DTC^{-})_3]$: The preparation procedure and spectroscopic characterization were described earlier (Exp. Sec., Chapter 2).

$[Fe(TPP^{2-})(NO)]$: Yield: 62 mg (*ca*. 90%). Elemental analyses for $C_{44}H_{28}N_5OFe$; Calculated (%): C, 75.65; H, 4.04; N, 10.03, Found (%): C, 75.61; H, 3.98; N, 10.07. FT-IR (in ATR probe): 2917, 1693 (ν_{NO}), 1595, 1439, 1344, 1297, 1202, 1174, 1071, 1002, 995, 800, 750, 717, 702, 663 and 529 cm^{-1}. UV-visible (CH_2Cl_2): 412 nm (ε/M^{-1} cm^{-1}, 3.12×10^4), 540 nm (ε/M^{-1} cm^{-1}, 2.28×10^3) and 611 nm (ε/M^{-1} cm^{-1}, 8.17×10^2). ESI-mass (m/z): Calculated, 668.166; Found, 668.172 (after loss of NO).

$[Fe(DTC^{-})_2(NO)]$: Yield: 29 mg (*ca*. 76%). Elemental analyses for $C_{10}H_{20}N_3OS_4Fe$; Calculated (%): C, 31.41; H, 5.27; N, 10.99, Found (%): C, 31. 37; H, 5. 19; N, 10.93. FT-IR (in ATR probe): 2976, 1690 (ν_{NO}), 1505, 1457, 1436, 1382, 1355, 1276, 1200, 1146, 1091, 1075, 998, 914 and 848 cm^{-1}. UV-visible (CH_2Cl_2): 365, 470 and 635 nm. ESI-mass (m/z): Calculated: 351.986; Found: 351.976 (after loss of NO).

Reaction of complex 5.2 with $[Fe^{III}(TPP^{2-})Cl]$: Complex **5.2** (106 mg, 0.1 mmol) and $[Fe^{III}(TPP^{2-})Cl]$ (70 mg, 0.1 mmol) were taken in a Schlenk flask and degassed it by applying consecutive vacuum/argon purge. The reaction vessel was cooled to -40 °C and precooled dichloromethane (dry and degassed, 10 mL) was added to it and stirred under visible light. After the reaction mixture was brought to room temperature, the reaction was monitored in FT-

IR and EPR spectroscopic techniques.

Reaction of complex 5.2 with [$Fe^{III}(DTC^{-})_3$]: Complex **5.2** (106 mg, 0.1 mmol) and [$Fe^{III}(DTC^{-})_3$] (50 mg, 0.1 mmol) were taken in a Schlenk flask and degassed it by applying consecutive vacuum/argon purge. The reaction vessel was cooled to -40 °C and precooled dichloromethane (dry and degassed, 10 mL) was added to it and stirred under visible light. After the reaction mixture was brought to room temperature, the reaction was monitored in FT-IR and EPR spectroscopic techniques.

Reaction of complex 5.2 with triphenylphosphine in the presence of $HBF_4.Et_2O$: A mixture of complex **5.2** (10. mg, 0.01 mmol) and PPh_3 (0.08 g, 0.03 mmol) was dissolved in 0.4 mL of dry and degassed dichloromethane under argon atmosphere. To this reaction mixture, $HBF_4.Et_2O$ (2 µL, 1.3 mole equivalent) was added and ^{31}P-NMR was recorded in CD_3CN. ^{31}P-NMR (202 MHz, CD_3CN): $\delta_{ppm,}$ 26.75 ($Ph_3P{=}O$), 22.18 ($Ph_3P{=}NH$) and 44.26 (Metal-bound PPh_3).

Determination of the yield of N_2O: Different amount of N-hydroxybenzenesulfonamide was taken in five 10 mL Schlenk tube and degassed using vacuum/argon purge. 0.1 M NaOH solution (5 mL) was added to each flask under the sealed condition. 1 mL of headspace gas from each reaction vessel was subjected to GC. By calculating the peak area at 2.79 min (corresponding to N_2O) for each set, a calibration curve of the concentration of N-hydroxybenzenesulfonamide was drawn.

Complex **5.2** (0.025 mmol, 0.026 g) in 5 mL of dry and degassed dichloromethane was taken in a 10 mL round-bottom flask and 20 µL of $HBF_4{\cdot}Et_2O$ was added to it under argon atmosphere and stirred for ½ hour in the presence of light. After the completion of the reaction, 1 mL of headspace gas was subjected to GC and the amount of N_2O was measured from the calibration

curve. Yield: *ca.* 83%.

5.4 Conclusion

Thus, the present work demonstrates that upon exposure to visible light, the Mn-nitrosyl complex, **5.2** in dichloromethane solution at -40 °C spontaneously releases NO^-. It was studied using UV-visible and FT-IR spectroscopy. The electron donating tendency of the methoxy substituted porphyrin ligand could be responsible for making the 'Mn-nitrosyl' center more electron rich to show this unusual reactivity in comparison to the previously reported ones. The NO^- release was confirmed using nitroxyl scavengers like $[Fe^{III}(TPP^{2-})Cl]$ and $[Fe^{III}(DTC^-)_3]$. Detection of nitrous oxide (N_2O) using GC in the presence of a H^+ also confirms the same. The formation of azaylide and phosphine oxide in the reaction of complex **5.2** with PPh_3 also supports our proposition. Hence, use of electron rich framework may be a key for HNO/NO^- donation from metal-nitrosyl complexes having $\{Mn(NO)\}^6$ configuration.

5.5 References

1. Doctorovich, F.; Bikiel, D. E.; Pellegrino, J.; Suárez, S. A.; Martí, M. A. *Acc. Chem. Res.* **2014**, *47*, 2907.
2. Doctorovich, F.; Bikiel, D.; Pellegrino, J.; Suárez, S. A.; Larsen, A.; Martí, M. A. *Coord. Chem. Rev*. **2011**, *255*, 2764.
3. Bazylinski, D. A.; Hollocher, T. C. *J. Am. Chem. Soc*. **1985**, *107*, 7982.
4. Bazylinsky, D. A.; Goretski, J.; Hollocher, T. C.; *J. Am. Chem. Soc.* **1985**, *107*, 7986.
5. Kumar, M. R.; Pervitsky, D.; Chen, L.; Poulos, T.; Kundu, S.; Hargrove, M. S.; Rivera, E. J.; Diaz, A.; Colón, J. L.; Farmer, P. J. *Biochemistry*, **2009**, *48*, 5018.
6. Cline, M. R.; Tu, C.; Silverman, D. N.; Toscano, J. P. *Free Radical Biol. Med*. **2011**, *50*, 1274.
7. Reisz, J. A.; Zink, C. N.; King, S. B. *J. Am. Chem. Soc*. **2011**, *133*, 11675.

8. Donzelli, S.; Espey, M. G.; Flores-Santana, W.; Switzer, C. H.; Yeh, G. C.; Huang, J.; Stuehr, D. J.; King, S. B.; Miranda, K. M.; Wink, D. A. *Free Radical Biol. Med*. **2008**, *45*, 578.
9. Dobmeier, K. P.; Riccio, D. A.; Schoenfisch, M. H. *Anal. Chem.* **2008**, *80*, 1247.
10. Rosenthal, J.; Lippard, S. J. *J. Am. Chem. Soc.* **2010**, *132*, 5536.
11. Zhou, Y.; Liu, K.; Li, J.-Y.; Fang, Y.; Zhao, T.-C.; Yao, C. *Org. Lett.* **2011**, *13*, 1290.
12. Miao, Z.; Bruce King, S. *Nitric Oxide*, **2016**, *57*, 1.
13. Walter, M. R.; Dzul, S. P.; Rodrigues, A. V.; Stemmler, T. L.; Telser, J. C.; Ghosh, A.; Harrop, T. C. *J. Am. Chem. Soc*. **2016**, *138*, 12459.
14. Sanders, B. C.; Rhine, M. A.; Harrop, T. C. *Struct. Bond*. **2014**, *160*, 57.
15. Rhine, M. A.; Rodrigues, A. V.; Bieber Urbauer, R. J.; Urbauer, J. L.; Stemmler, T. L.; Harrop, T. C. *J. Am. Chem. Soc.* **2014**, *136*, 12560.
16. Vaire, M. Di; Ghilardi, C.A.; Sacconi, L. *Inorg. Chem.* **1976**, *15*, 1555.
17. Thyagarajan, S.; Incarvito, C. D.; Rheingold, A. L.; Theopold, K. H. *Inorg. Chim. Acta* **2003**, *345*, 333.
18. Tomson, N. C.; Crimmin, M. R.; Petrenko, T.; Rosebrugh, L. E.; Sproules, S.; Boyd, W. C.; Bergman, R. G.; DeBeer, S.; Toste, F. D.; Wieghardt, K. *J. Am. Chem. Soc*. **2011**, *133*, 18785.
19. (a) Eroy-Reveles, A. A.; Leung, Y.; Mascharak, P. K. *J. Am. Chem. Soc.* **2006**, *128*, 7166. (b) Eroy-Reveles, A. A.; Leung, Y.; Beavers, C. M.; Olmstead, M. M.; Mascharak, P. K. *J. Am. Chem. Soc.* **2008**, *130*, 4447.
20. Zavarine, I. S.; Kini, A. D.; Morimoto, B. H.; Kubiak, C. P. *J. Phys. Chem. B*, **1998**, *102*, 7287.
21. Franz, K. J.; Lippard, S. J. *J. Am. Chem. Soc.* **1998**, *120*, 9034.
22. Mazumdar, R.; Saha, S.; Samanta, B.; Mondal B. *Inorg. Chem*. **2021**, *60*, 18024.

23. Alder, D.; Longo, F. R.; Finarelli, J. D.; Goldmacher, J.; Assour, J.; Korsakoff, L. *J. Org. Chem.* **1967**, *32*, 476.

24. (a) Tong, S. L.; Zhang, J.; Yan, Y.; Hu, S.; Yu, J.; Yu, L. *Solid State Sci.* **2011**, *13*, 1320. (b) da Silva, V. S.; Vieira, W. C. d. S.; Meireles, A. M.; Ucoski, G. M.; Nakagaki, S.; Idemoria, Y. M.; DeFreitas-Silva, G. *New J. Chem.* **2017**, *41*, 997.

25. Chen, X.; Duez, Q.; Tripodi, G. L.; Gilissen, P. J.; Piperoudis, D.; Tinnemans, P.; Elemans, J. A. A. W.; Roithová, J.; Nolte, R. J. M. *Eur. J. Org. Chem.* **2022**, *2022*, e202200280.

26. Choi, In-K.; Liu, Y.; Wei, Z.; Ryan, M. D. *Inorg. Chem.* **1997**, *36*, 3113.

27. Mondal, B.; Borah, D.; Mazumdar, R.; Mondal, B. *Inorg. Chem.* **2019**, *58*, 14701.

28. Wayland, B. B.; Olson, L. W.; Siddiqui, Z. U. *J. Am. Chem. Soc.* **1976**, *98*, 94.

29. Saha, S.; Maity, S.; Mazumdar, R.; Samanta, B.; Ghosh, R.; Guha, A.; Mondal, B. *Inorg. Chem.* **2023**, *62,* 17074.

30. (a) Bari, S. E.; Martí, M. A.; Amorebieta, V. T.; Estrin, D. A.; Doctorovich, F. *J. Am. Chem. Soc.* **2003**, *125*, 15272. (b) Martí, M. A.; Bari, S. E.; Estrin, D. A.; Doctorovich, F. *J. Am. Chem. Soc*. **2005**, *127*, 4680. (c) Doyle, M. P.; Mahapatro, S. N.; Broene, R. D.; Guy, J. K. *J. Am. Chem. Soc*. **1988**, *110*, 593. (d) Miranda, K. M.; Nims, R. W.; Thomas, D. D.; Espey, M. G.; Citrin, D.; Bartberger, M. D.; Paolocci, N.; Fukuto, J. M.; Feelisch, M.; Wink, D. A. *J. Inorg. Biochem*. **2003**, *93*, 52.

31. Komarov, A. M.; Reef, A.; Schmidt, H. H. H. W. *Methods in Enzymology*, **2002**, *359*, 18.

32. Shafirovich, V.; Lymar, S. V. *Proc. Natl. Acad. Sci. U. S. A*. **2002**, *99*, 7340.

33. (a) Reisz, J. A.; Klorig, E. B.; Wright, M. W.; King, S. B. *Org. Lett*. **2009**, *11*, 2719. (b) Rentsch, D.; Hany, R.; von Philipsborn, W. *Magn. Reson. Chem.* **1997**, *35*, 832.

34. SMART, SAINT and XPREP; Siemens Analytical X-ray Instruments Inc.: Madison,

Wisconsin, USA, **1995**.

35. (a) Sheldrick, G. M. *Acta Crystallogr. Sect. A Found. Adv.* **2015**, *71,* 3. (b) Sheldrick, G. M. *Acta Crystallogr. Sect. C Struct. Chem.* **2015**, *71*, 3. (c) Farrugia, L. J. ORTEP-3 for Windows - a version of ORTEP-III with a Graphical User Interface (GUI). *J. Appl. Crystallogr.* **1997**, *30*, 565.

Conclusion

This dissertation addresses our attempt to understand the potential of Co(II) and Mn(II) nitrosyl complexes as nitroxyl (HNO/NO^-) donors. A series of nitrosyl complexes were synthesized by varying the ligand framework (from electron deficient to electron rich) with a central metal ion (e.g. Co^{2+} and Mn^{2+}). The ability of these metal-nitrosyl complexes to act as HNO/NO^- donors under different reaction conditions was discussed in chapters 2 to 5. The potential of cobalt-nitrosyl complexes as nitroxyl donors was extensively discussed in chapters 2 to 4, whereas chapter 5 addresses the manganese-nitrosyl complex, which led to some significant observations. For instance, in chapter 2, the nitroxyl releasing ability of a $\{Co(NO)\}^8$ complex in presence of anionic sixth ligands like BF_4^- and DTC^- was observed, which is the first example of such kind of reaction. Chapter 3 describes our in detailed findings of the reaction between a $\{Co(NO)\}^8$ complex and DTC^- anion, which also leads to the NO^- donation. In chapter 4, a neutral imidazole ligand mediated NO^- release from a highly electron rich $\{Co(NO)\}^8$ complex was studied. All of these sixth ligand mediated nitroxyl release from cobalt-nitrosyl complexes are found to be concomitant in nature. The kinetic inertness of low-spin d^6 cobalt-centre of $\{Co(NO)\}^8$ complexes makes the release of HNO very difficult. Our recent findings on the methodology for HNO/NO^- release from $\{Co(NO)\}^8$ complexes will contribute significantly to the existing knowledge of nitroxyl donation from cobalt-nitrosyl complexes.

Lastly, in chapter 5, photo-induced HNO donation from the nitrosyl complex of Mn(II)-porphyrinate was investigated. The formal $[Mn^I\text{-}NO^+]$ electronic character of the $\{Mn(NO)\}^6$ complex makes them unsuited for HNO donation. However, by modulating the ligand framework appropriately, the $\{Mn(NO)\}^6$ complex can also act as an HNO donor. Upon exposure to the visible light, the $\{Mn(NO)\}^6$ complex was found to donate NO^-. Although

many photo-induced NO release from $\{Mn(NO)\}^6$ complexes were reported earlier, this is the only example of HNO/NO^- release. The incorporation of more electron donating groups in the ligand framework makes it electron rich, which in turn affects the reactivity of the [Mn-NO] centre, leading to the HNO donation.

This thesis work is focused on developing simpler methods for releasing HNO/NO^- from transition metal nitrosyl complexes, mostly Co- and Mn-nitrosyls. The idea behind working with $\{Co(NO)\}^8$ complexes is its native [Co^{III}-NO^-] electronic character. Most of the previously reported metal-nitrosyls (e.g $\{Fe(NO)\}^8$ systems) required 1-electron reduction for nitroxyl release or developing NO^- character over the coordinated nitrosyl moiety, which is energy demanding. In contrast, for $\{Co(NO)\}^8$ complexes, the presence of sixth ligand (anionic or neutral) can make the five-coordinated metal-nitrosyl centre more accessible for HNO/NO^- donation. Furthermore, the number of metal nitrosyl complexes that can release NO^- upon photoactivation, which has been demonstrated in the case of $\{Mn(NO)\}^6$ complex in this thesis, is very rare. This type of complexes can be explored for photodynamic therapy.

Despite having widespread medical applications for HNO, the complex systems, that were discussed in this work can not be utilized for medicinal purposes as they are. The limitation lies in the non-aqueous nature of these metal nitrosyl complexes. However, fine-tuning of the ligand framework may allow these complexes to release HNO in an aqueous medium. This will certainly open up a new avenue to test their medicinal applications. Development of such ligand frameworks is currently in progress in our laboratory.

Appendix I

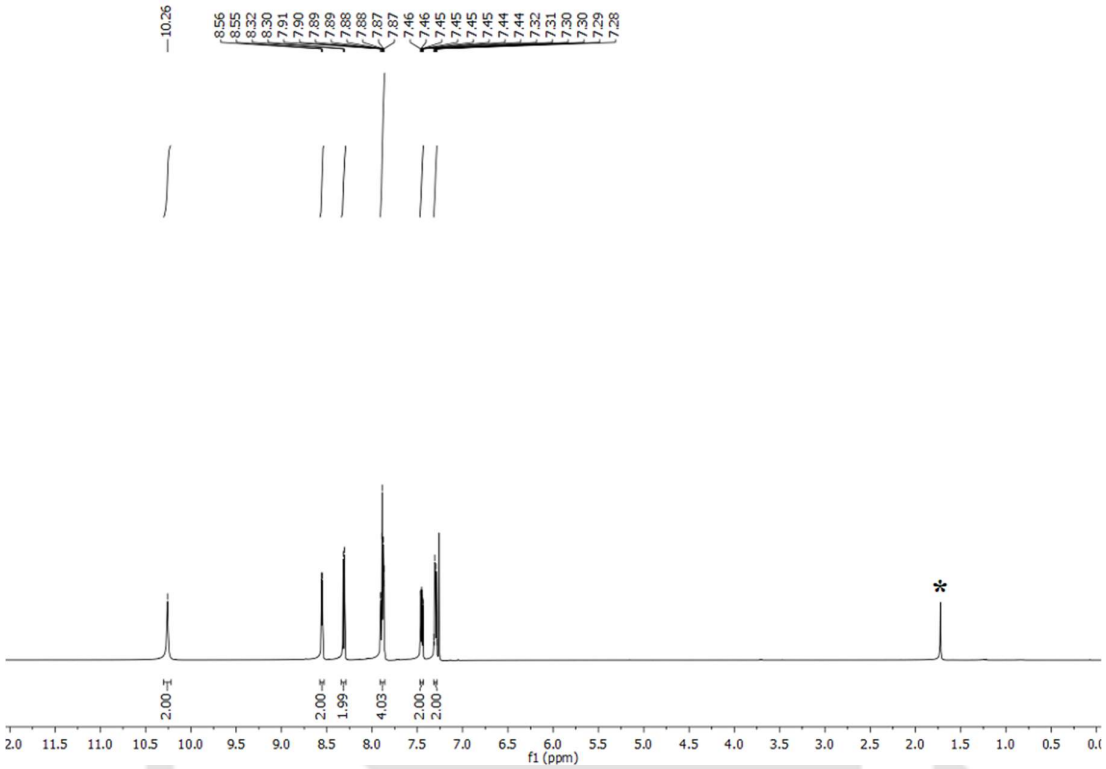

Figure A1.1. ^{1}H-NMR spectrum of H_2BPB in $CDCl_3$ (* = solvent).

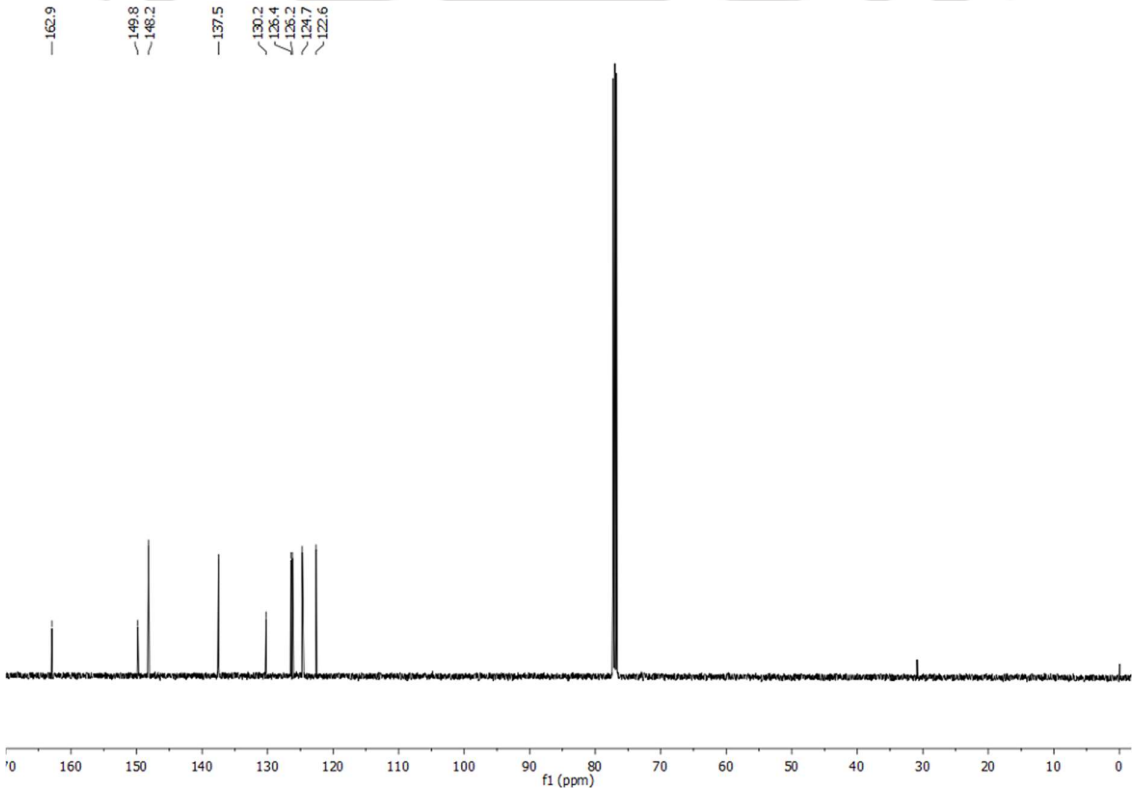

Figure A1.2. ^{13}C-NMR spectrum of H_2BPB in $CDCl_3$.

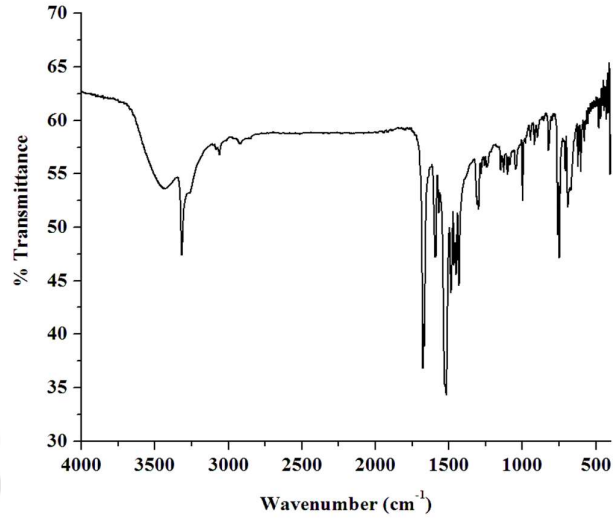

Figure A1.3. FT-IR spectrum of H_2BPB in KBr.

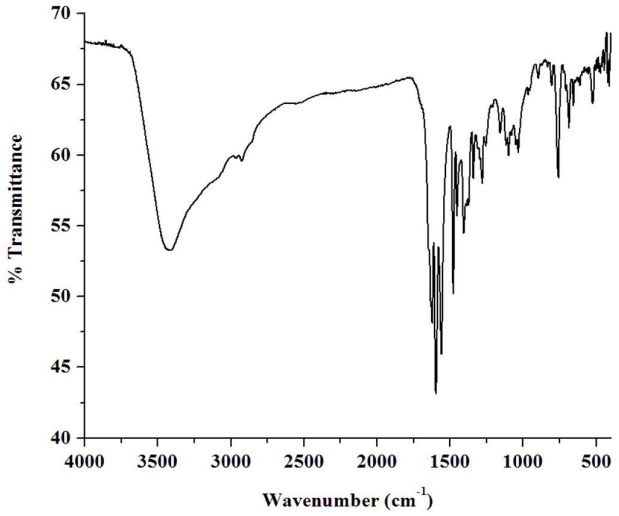

Figure A1.4. FT-IR spectrum of complex **2.1** in KBr.

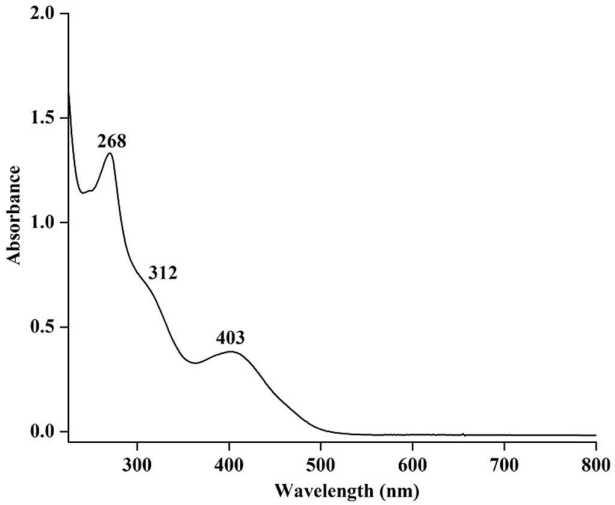

Figure A1.5. UV-visible spectrum of complex **2.1** in CH_3OH at room temperature.

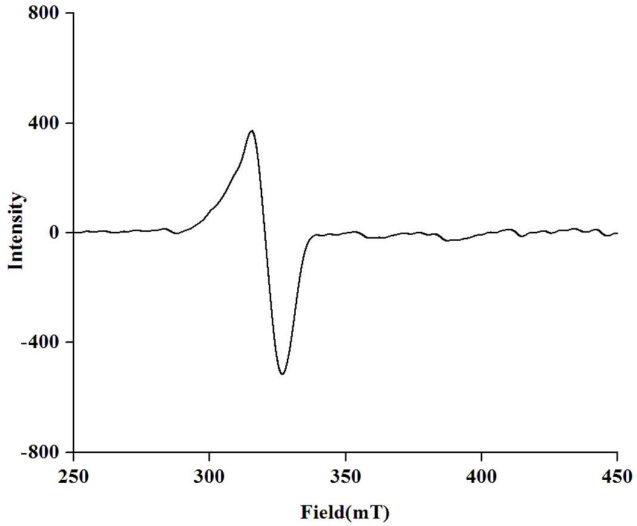

Figure A1.6. X-band EPR spectrum of complex **2.1** in CH_2Cl_2 at 77 K.

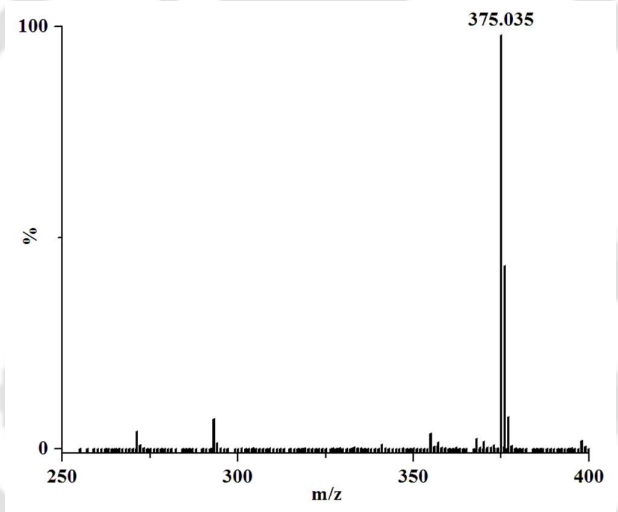

Figure A1.7. ESI-mass spectrum of complex **2.1** in CH_3OH **(**Calculated: 375.029; Found: 375.035).

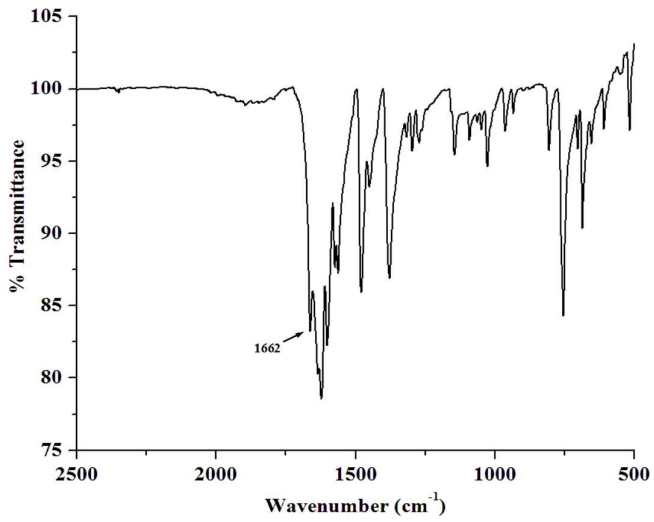

Figure A1.8. FT-IR spectrum of complex **2.2** in KBr.

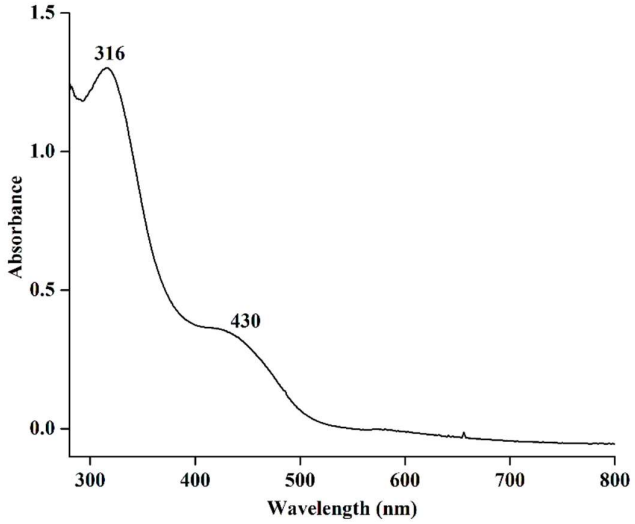

Figure A1.9. UV-visible spectrum of complex **2.2** in CH_2Cl_2 at room temperature.

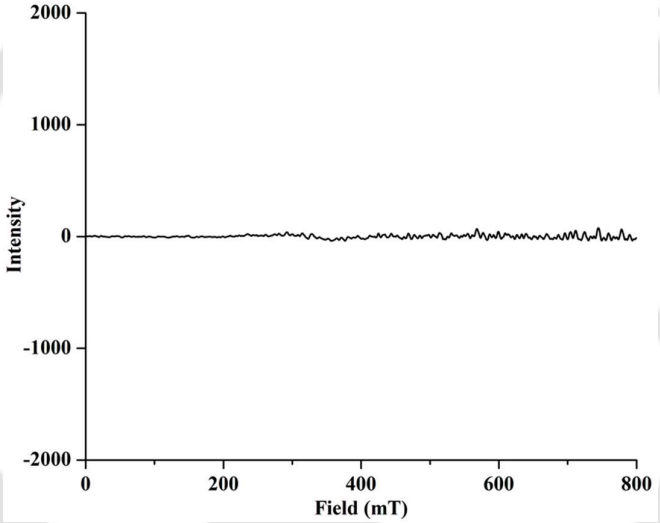

Figure A1.10. X-band EPR spectrum of complex **2.2** in CH_2Cl_2 at 77 K.

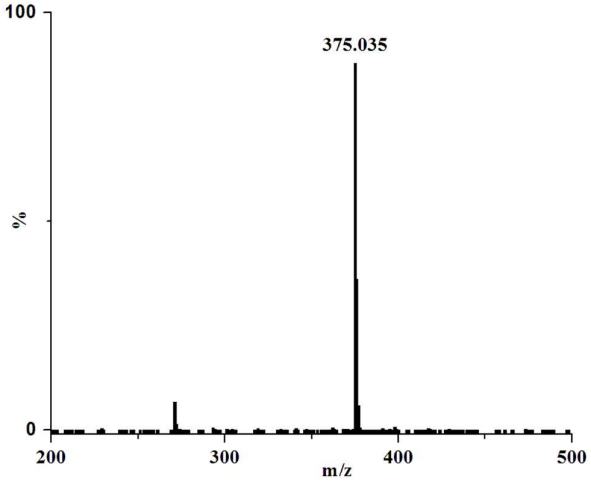

Figure A1.11. ESI-mass spectrum of complex **2.2** in CH_3OH (Calculated, 375.029; Found, 375.035, after loss of NO).

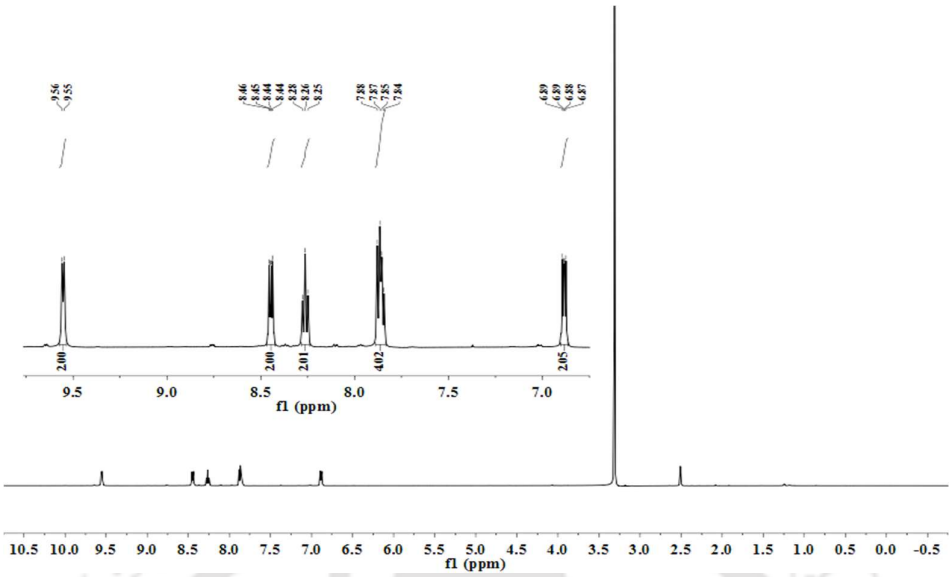

Figure A1.12. ^{1}H-NMR spectrum of complex **2.2** in DMSO-d_6.

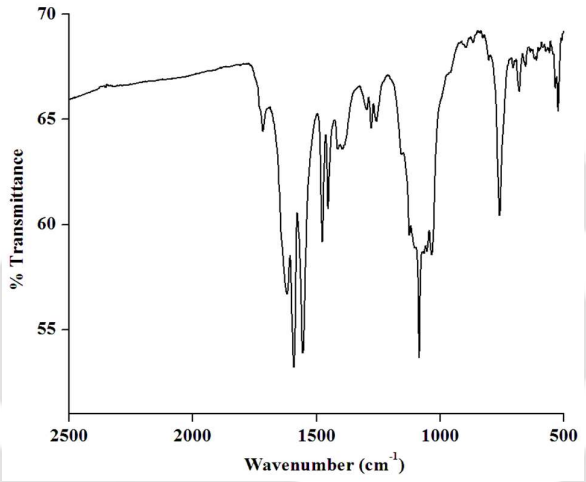

Figure A1.13. FT-IR spectrum of complex **2.3** in KBr.

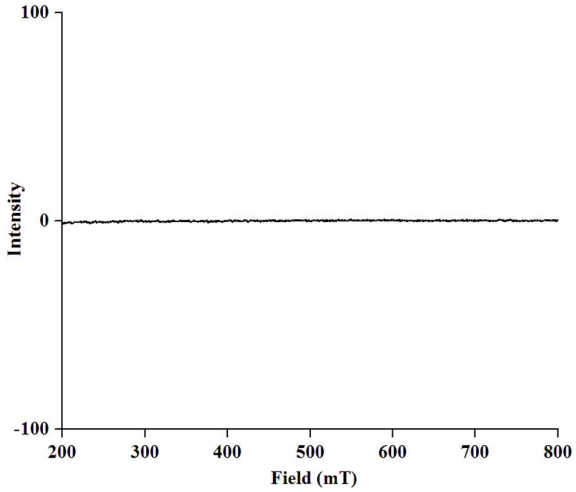

Figure A1.14. X-band EPR spectrum of complex **2.3** in CH_2Cl_2 at 77 K.

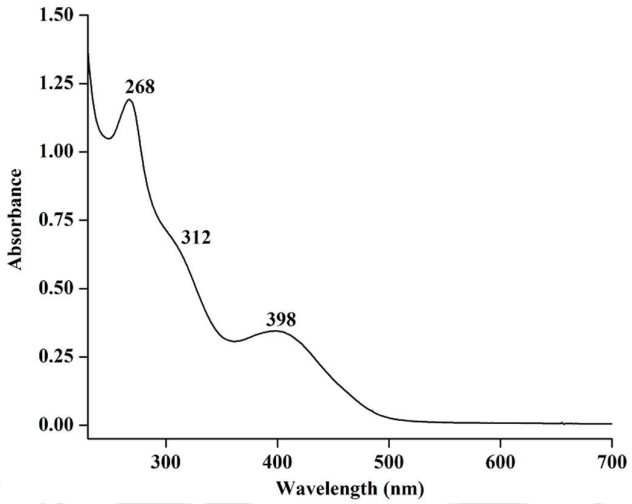

Figure A1.15. UV-visible spectrum of complex **2.3** in CH_3OH at room temperature.

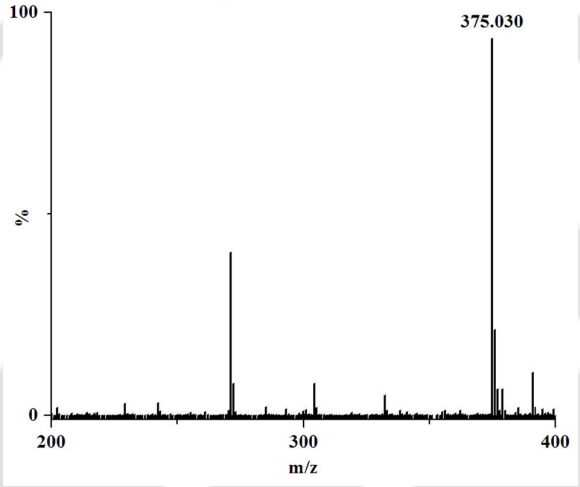

Figure A1.16. ESI-mass spectrum of complex **2.3** in CH_3OH (Calculated: 375.029; Found: 375.030, after loss of BF_4^- unit).

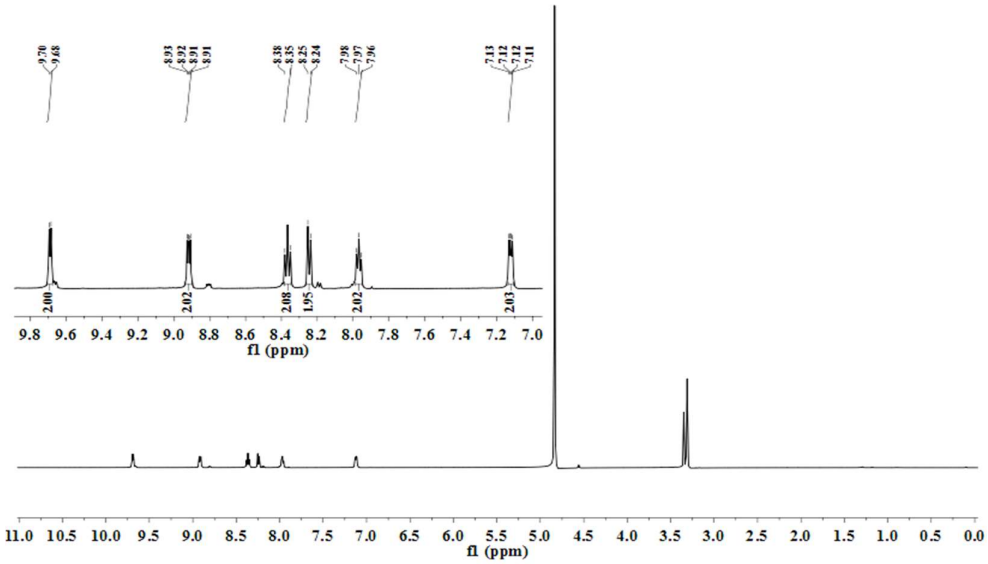

Figure A1.17. ^{1}H-NMR spectrum of complex **2.3** in CD_3OD.

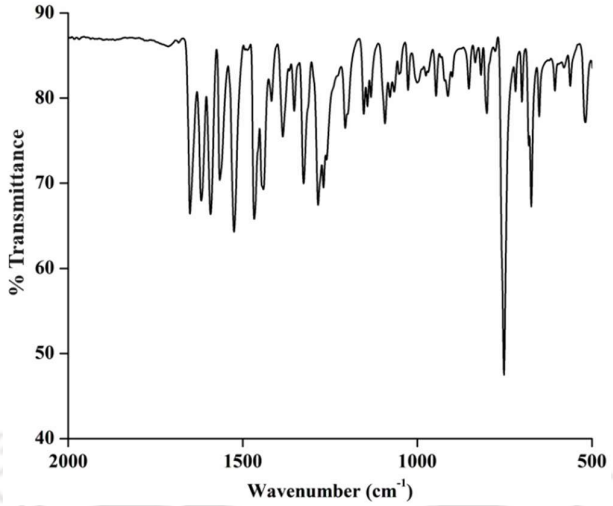

Figure A1.18. FT-IR spectrum of complex **2.4** in KBr.

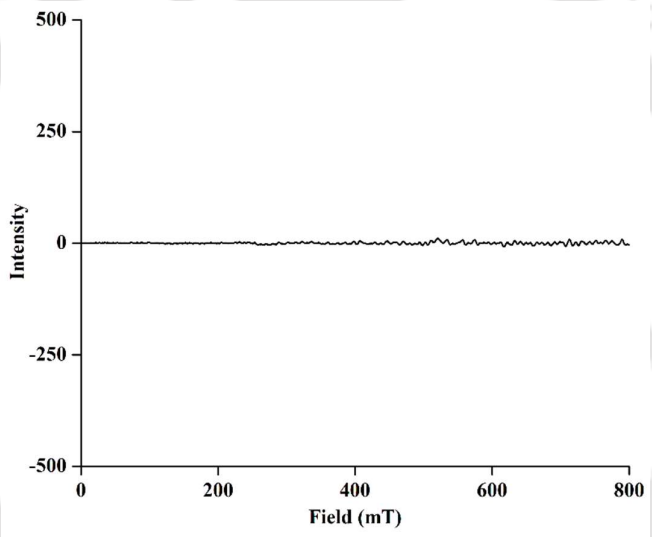

Figure A1.19. X-band EPR spectrum of complex **2.4** in CH_2Cl_2 at 77 K.

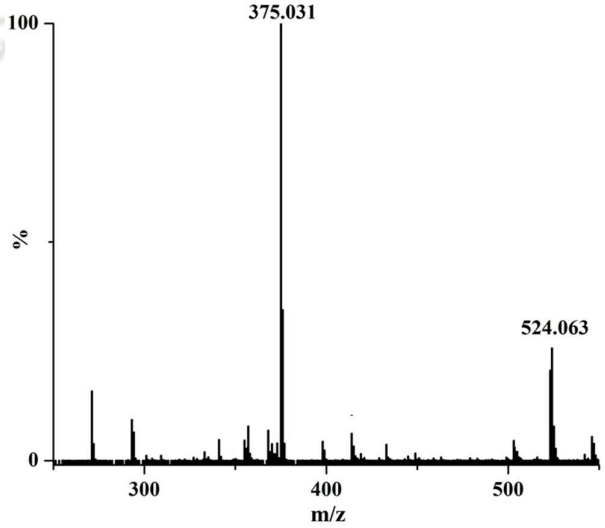

Figure A1.20. ESI-mass spectrum of complex **2.4** (Calculated: 524.063; Found: 524.063 $[M+H]^+$).

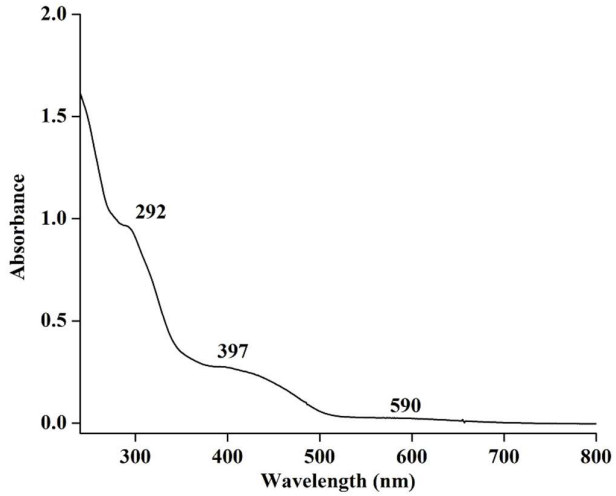

Figure A1.21. UV-visible spectrum of complex **2.4** in CH_3OH at room temperature.

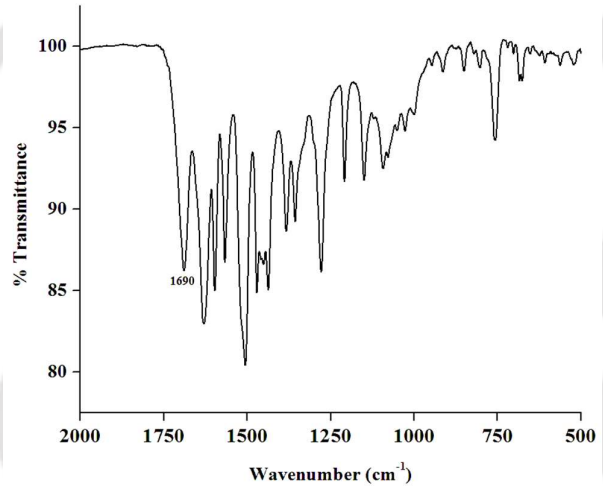

Figure A1.22. FT-IR spectrum of the reaction mixture of $[Fe^{III}(DTC^{-})_3]$ and complex **2.2** after 1 hour in KBr.

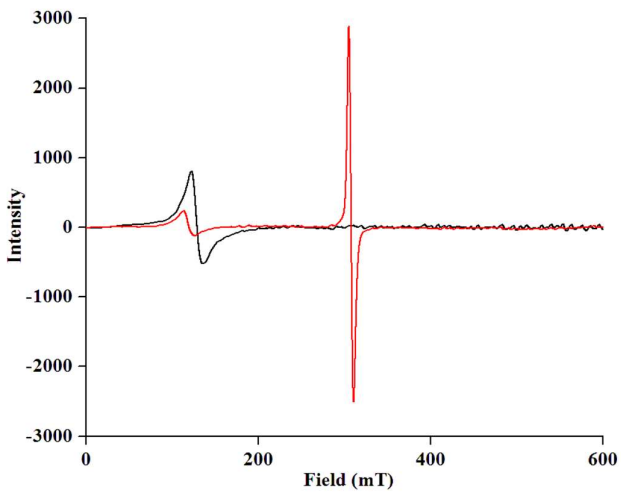

Figure A1.23. X-band EPR spectra of the reaction of $[Fe^{III}(DTC^{-})_3]$ and complex **2.2** in CH_2Cl_2 at 77 K (Initial (black) and final (red)).

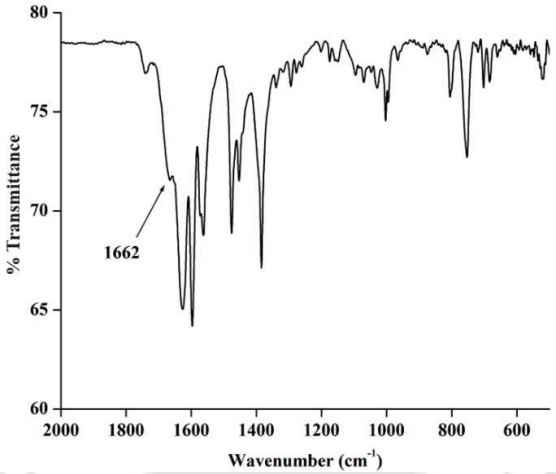

Figure A1.24. FT-IR spectrum of reaction mixture of complex **2.2** and [$Fe^{III}(TPP^{2-})Cl$] after 24 hours in KBr.

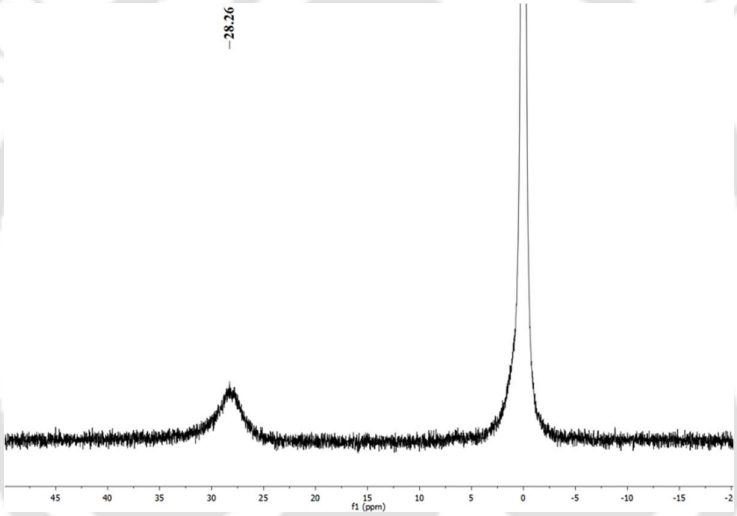

Figure A1.25. ^{31}P-NMR spectrum of the reaction mixture of phosphine oxide, complex **2.2** and $HBF_4.Et_2O$ in CH_2Cl_2 solution with 0.1 mL DMSO-d_6.

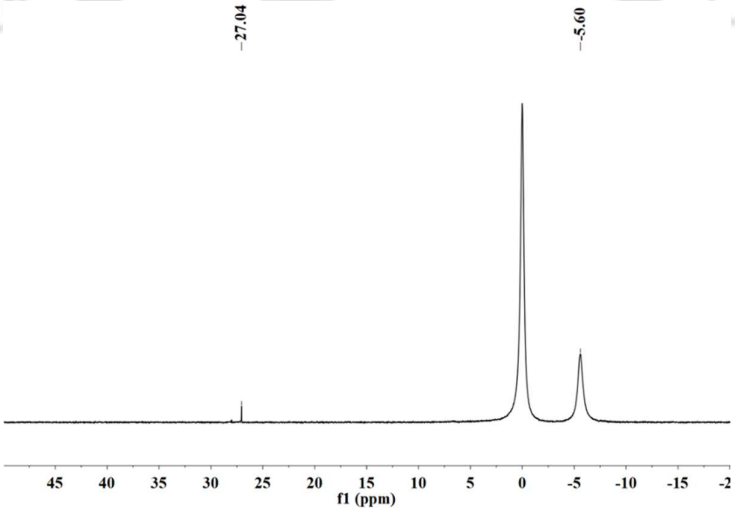

Figure A1.26. ^{31}P-NMR spectrum of the reaction mixture of PPh_3 and complex **2.2** in CH_2Cl_2 solution with 0.1 mL DMSO-d_6.

Result File : D:\GC Data\N2O 2.rst
Sequence File : D:\GC Data\N2O 2.seq

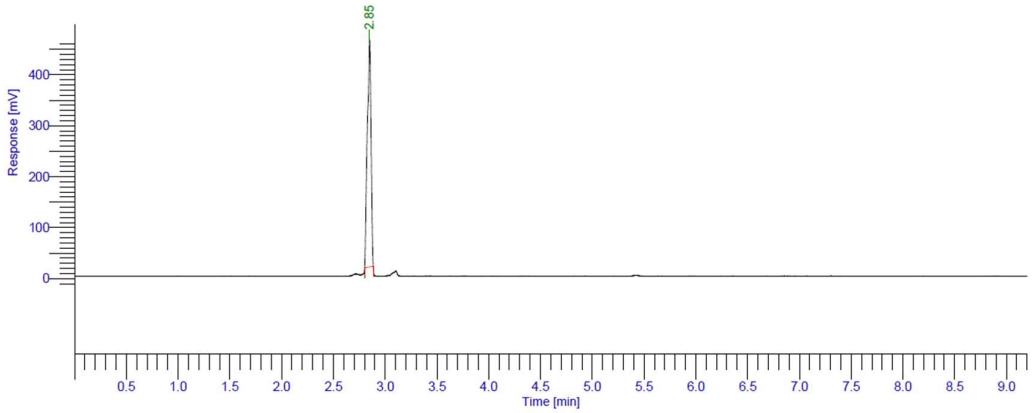

Dept. of Chemistry, IIT Guwahati

Peak #	Component Name	Time [min]	Area [uV*sec]	Height [uV]	Area [%]
1		2.849	1115043.36	445312.67	100.00
			1115043.36	445312.67	100.00

Figure A1.27. Gas chromatograms of headspace gas of the reaction mixture of complex **2.2** and HBF_4 (retention time = 2.85 minutes).

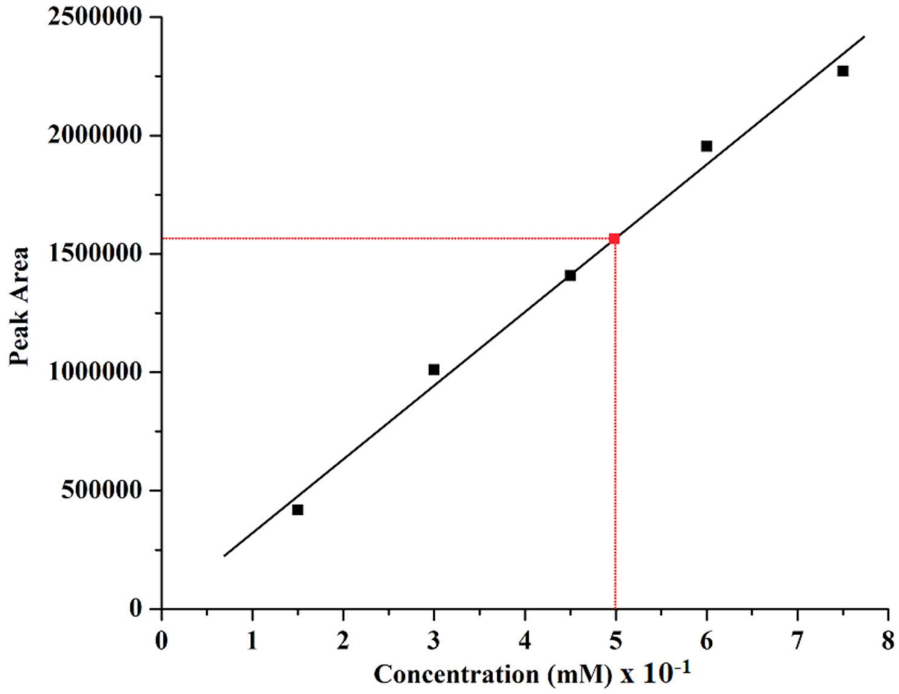

Figure A1.28. GC calibration curve for determination of amount of N_2O (red dot corresponds to the sample).

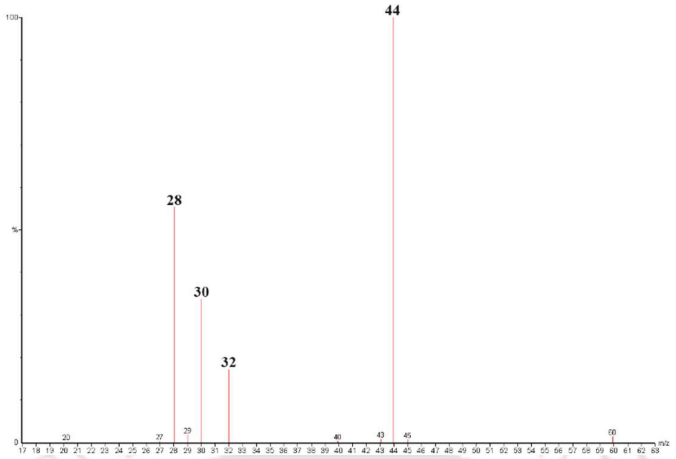

Figure A1.29. GC-mass spectrum of the headspace gas of the reaction mixture of complex **2.2** and HBF_4.

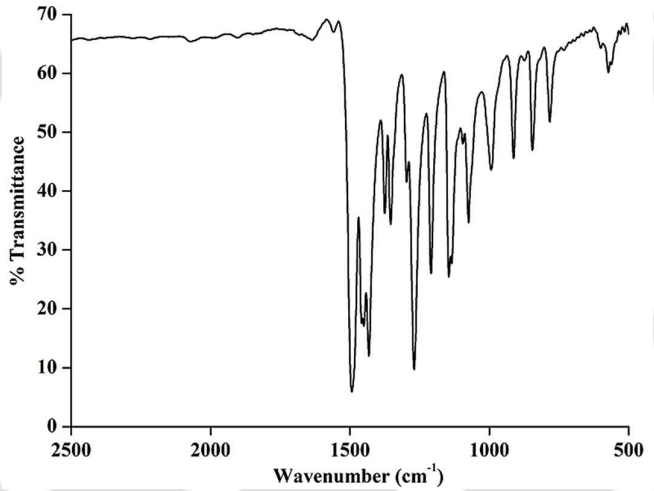

Figure A1.30. FT-IR spectrum of complex $[Fe^{III}(DTC^{-})_3]$ in KBr.

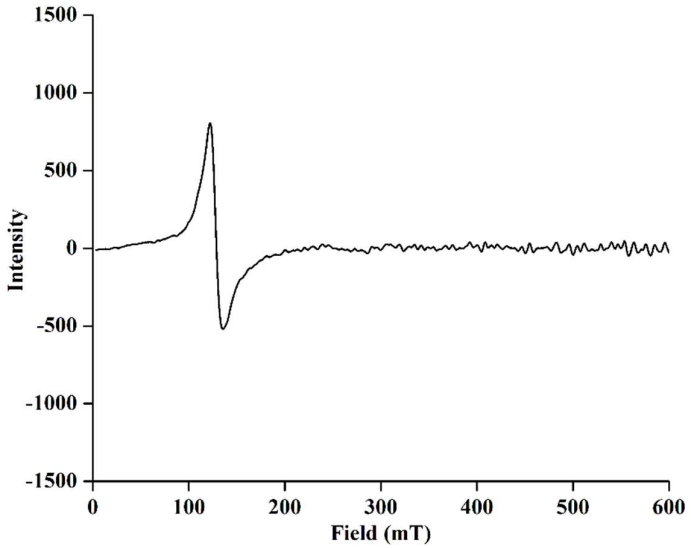

Figure A1.31. X-band EPR spectrum of $[Fe^{III}(DTC^{-})_3]$ in CH_2Cl_2 at 77 K.

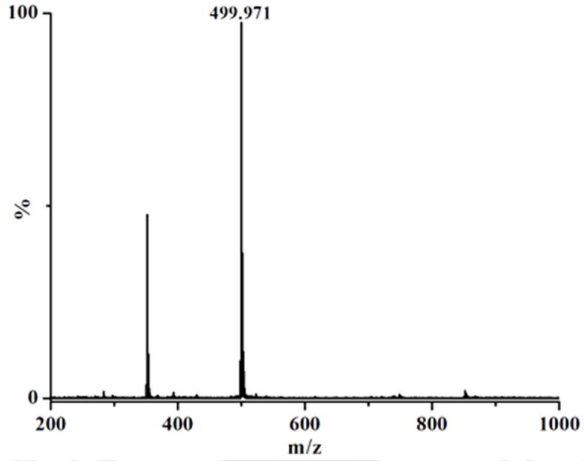

Figure A1.32. ESI-mass spectrum of $[Fe^{III}(DTC^{-})_3]$ in CH_3CN (Calculated: 500.011; Found: 499.971).

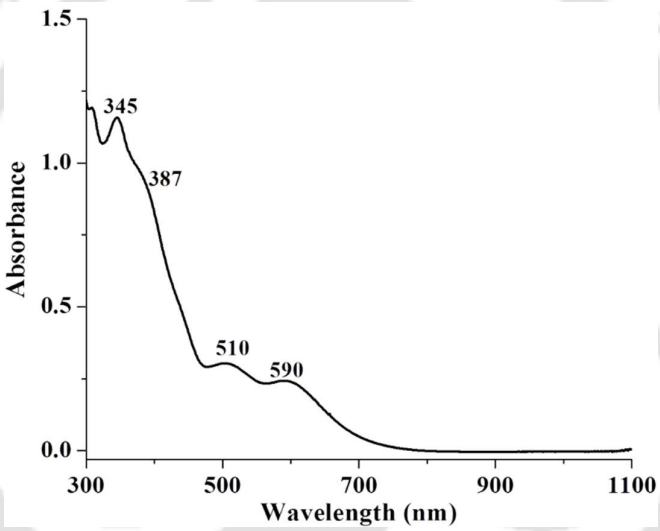

Figure A1.33. UV-visible spectrum of $[Fe^{III}(DTC^{-})_3]$ in CH_2Cl_2 at room temperature.

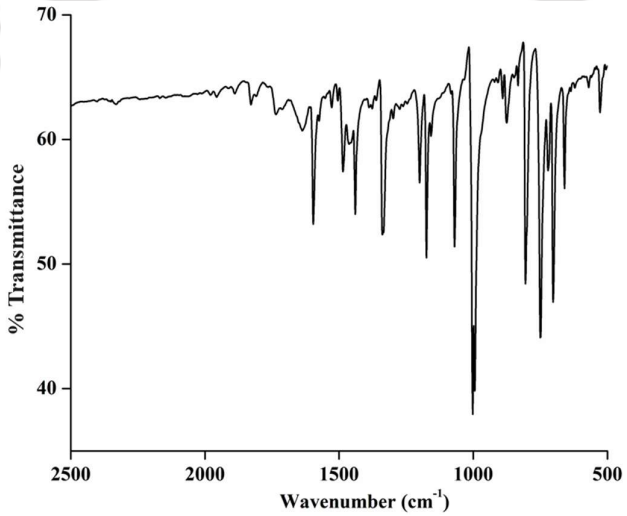

Figure A1.34. FT-IR spectrum of $[Fe^{III}(TPP^{2-})Cl]$ in KBr.

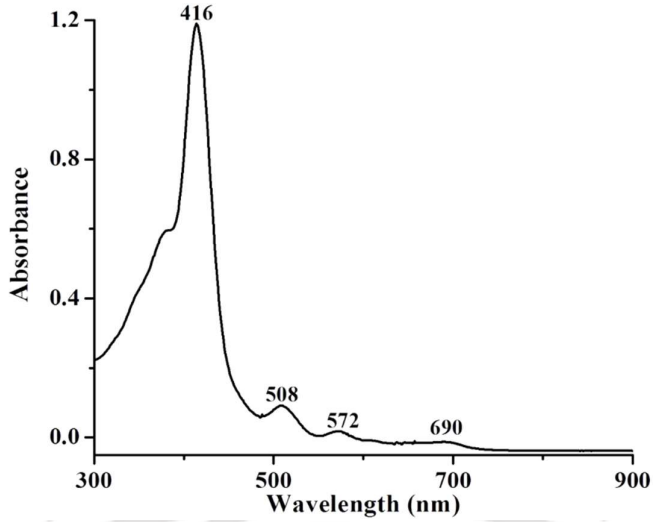

Figure A1.35. UV-visible spectrum of [$Fe^{III}(TPP^{2-})Cl$] in CH_2Cl_2 at room temperature.

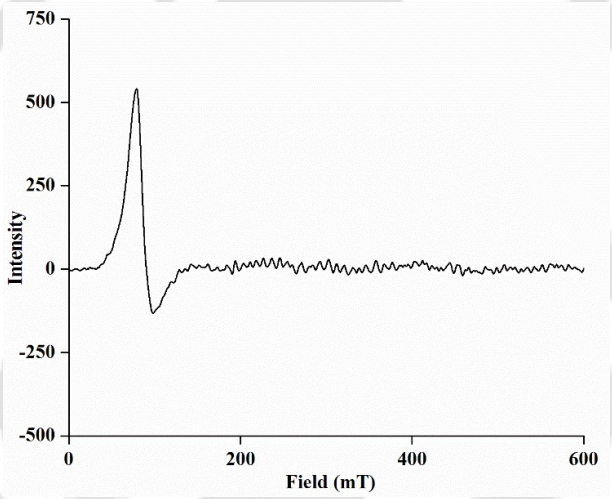

Figure A1.36. X-band EPR-spectrum of [$Fe^{III}(TPP^{2-})Cl$] in CH_2Cl_2 at 77 K.

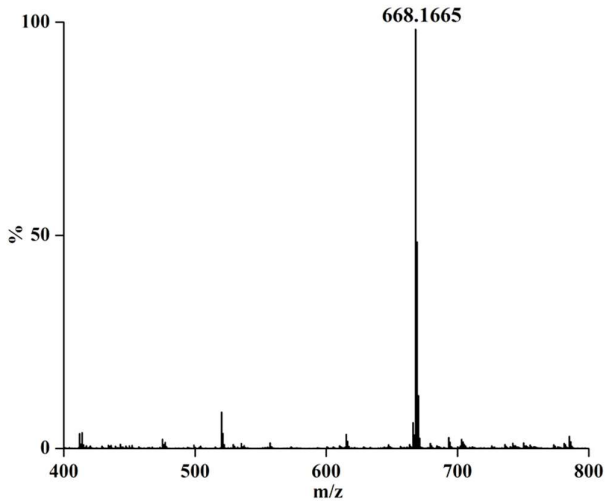

Figure A1.37. ESI-mass spectrum of [$Fe^{III}(TPP^{2-})Cl$] in CH_3OH (Calculated: 668.166; Found: 668.166, after loss of Cl^-).

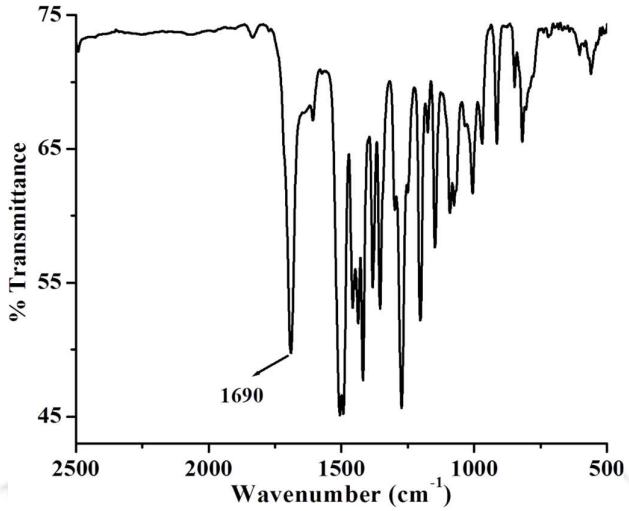

Figure A1.38. FT-IR spectrum of [Fe(DTC^{-})$_2$(NO)] in KBr.

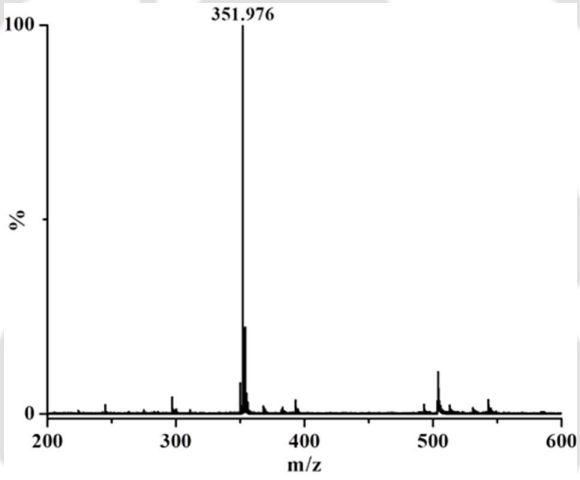

Figure A1.39. ESI-mass spectrum of [Fe(DTC^{-})$_2$(NO)] in CH_3CN (Calculated, 351.986; Found, 351.976, after loss of NO).

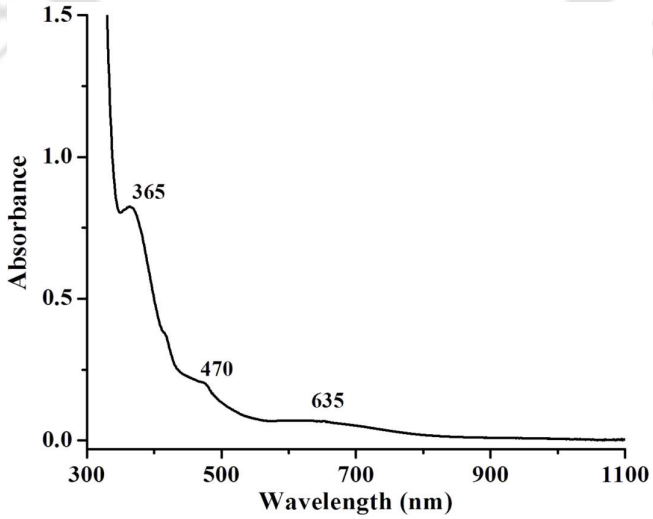

Figure A1.40. UV-visible spectrum of [Fe(DTC^{-})$_2$(NO)] in CH_2Cl_2 at room temperature.

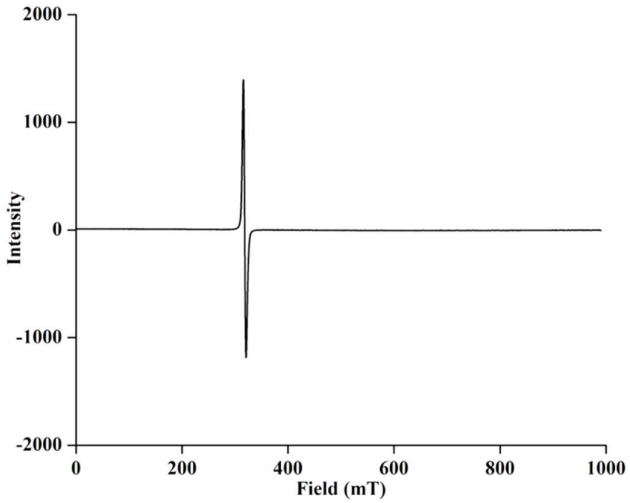

Figure A1.41. X-band EPR spectrum of [Fe(DTC^{-})$_2$(NO)] in CH_2Cl_2 at 77 K.

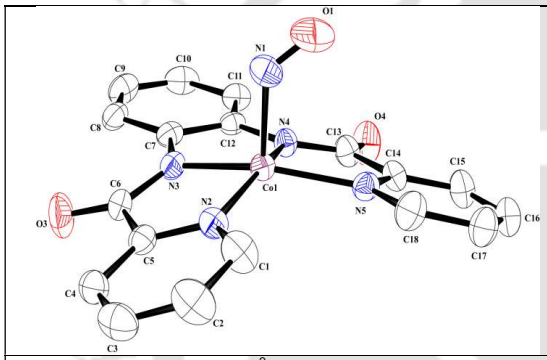

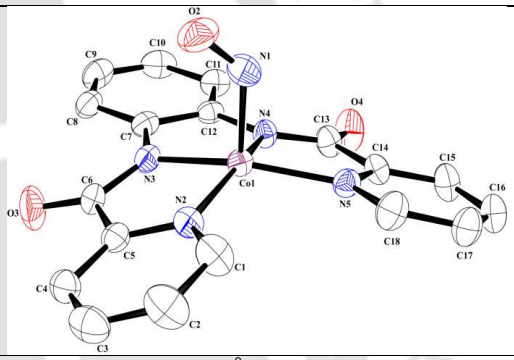

N1-O1 (Å) – 1.045(13)	**N1-O2 (Å)** -1.119(10)
Co1-N1$_{NO}$ (Å) -1.791(6)	**Co1-N1$_{NO}$ (Å)** - 1.791(6)
Co1-N1-O1 (°) -125.2(9)	**Co1-N1-O2 (°)** -130.2(7)

Figure A1.42. Two conformations of complex **2.2**.

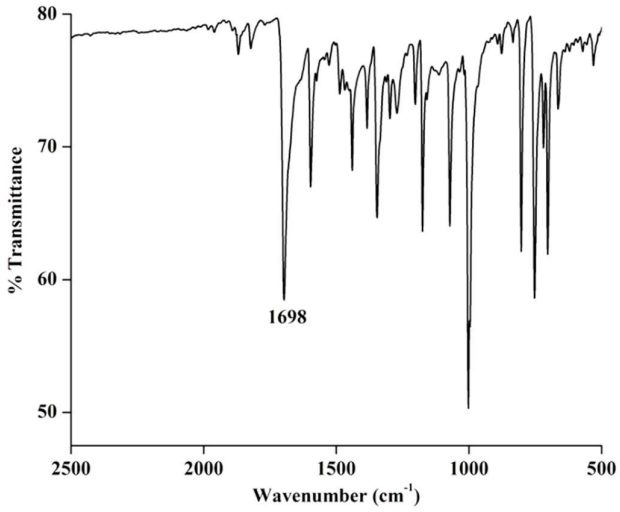

Figure A1.43. FT-IR spectrum of [Fe(TPP^{2-})(NO)] in KBr.

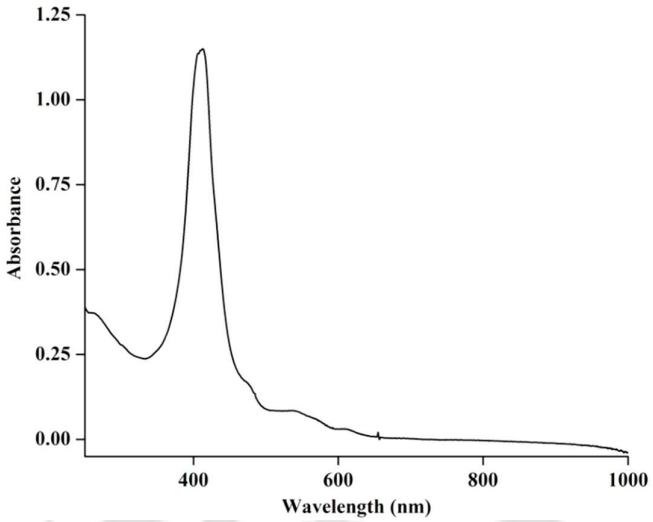

Figure A1.44. UV-visible spectrum of [Fe(TPP^{2-})(NO)] in CH_2Cl_2 at room temperature.

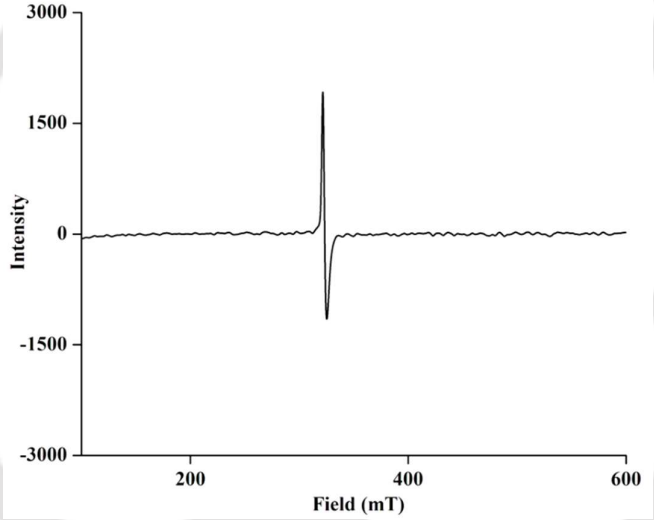

Figure A1.45. X-band EPR spectrum of [Fe(TPP^{2-})(NO)] in CH_2Cl_2 at 77 K.

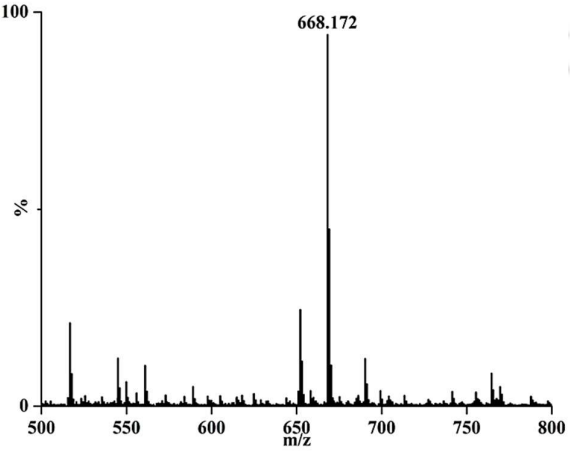

Figure A1.46. ESI-mass spectrum of [Fe(TPP^{2-})(NO)] in CH_3CN (Calculated, 668.166; Found, 668.172, after loss of NO).

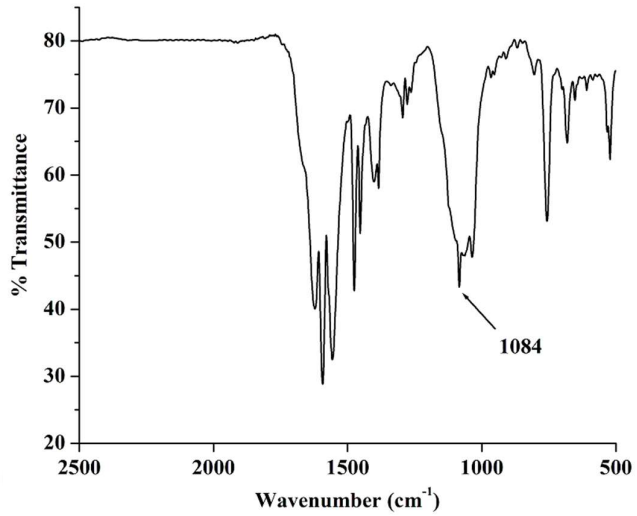

Figure A1.47. FT-IR spectrum of the reaction mixture of $NaBF_4$ and complex **2.2** in KBr.

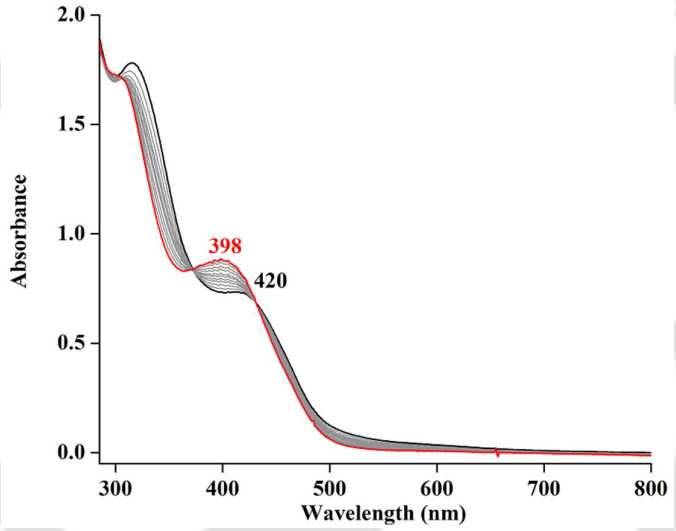

Figure A1.48. UV-visible spectroscopic study of reaction kinetics of complex **2.2** with $NaBF_4$ in CH_3OH at room temperature.

Table A1.1. Crystallographic data for complexes **2.2** and **2.4**.

	2.2	**2.4**
Formulae	$C_{18}H_{12}N_5O_3Co$	$C_{27}H_{32}CoN_5O_4S_2$
Mol. wt.	405.26	613.63
Crystal system	Monoclinic	monoclinic
Space group	P 21	P 21/c
Temperature /K	120(2)	298(2)
Wavelength /Å	0.71073	0.71073
a /Å	6.2778(2)	11.5584(11)
b /Å	13.3612(4)	20.649(2)
c /Å	9.8714(3)	12.1832(12)
α/°	90	90

β/°	91.582(2)	98.591(3)
γ/°	90	90
V/ Å^3	827.69(4)	2875.2(5)
Z	2	4
Density/Mgm^{-3}	1.626	1.418
Abs. Coeff. /mm^{-1}	1.068	0.784
Abs. correction	none	none
F(000)	412	1280
Total no. of reflections	2920	9717
Reflections, $I > 2\sigma(I)$	2610	4333
Max. 2θ/°	25.000	25.00
Ranges (h, k, l)	$-7 \le h \le 7$ $-15 \le k \le 15$ $-11 \le l \le 11$	$-13 \le h \le 13$ $-24 \le k \le 24$ $-14 \le l \le 14$
Complete to 2θ (%)	0.999	0.997
Refinement method	Full-matrix least-squares on F^2	Full-matrix least-squares on F^2
Goof (F^2)	0.937	1.158
R indices [$I > 2\sigma(I)$]	0.0321	0.0467
R indices (all data)	0.0384	0.0596

Table A1.2. Selected bond lengths (Å) of complexes **2.2** and **2.4**.

Atoms	**2.2**	**2.4**
Co1-N1	1.791(6)	1.977(3)
Co1-N2	1.986(4)	1.898(3)
Co1-N3	1.878(4)	1.904(3)
Co1-N4	1.869(5)	1.959(3)
Co1-N5	1.985(4)	
N1-O1	1.045(13)	
N1-O2	1.119(10)	
N2-C5	1.356(6)	
C5-C6	1.511(8)	1.503(4)
C6-N3	1.340(6)	
N3-C7	1.414(6)	
C7-C12	1.414(7)	
C12-N4	1.419(7)	
N4-C13	1.334(7)	
C13-C14	1.509(8)	1.498(5)
C14-N5	1.344(6)	
Co1-S2		2.2609(9)
Co1-S1		2.2797(9)
C19-S1		1.721(3)
C19-S2		1.710(3)

Table A1.3. Selected bond angles (˚) of complexes **2.2** and **2.4**.

Atoms	2.2	2.4
N1-Co1-N2	94.4(2)	107.17(11)
N1-Co1-N3	100.7(2)	107.17(11)
N1-Co1-N4	102.18(19)	96.84(11)
N1-Co1-N5	94.6(3)	
Co1-N1-O1	125.2(9)	
Co1-N1-O2	130.2(7)	
O1-N1-O2	104.6(10)	
S2-Co1-S1		76.16(3)
S1-Co1-N1		86.74(8)

Appendix II

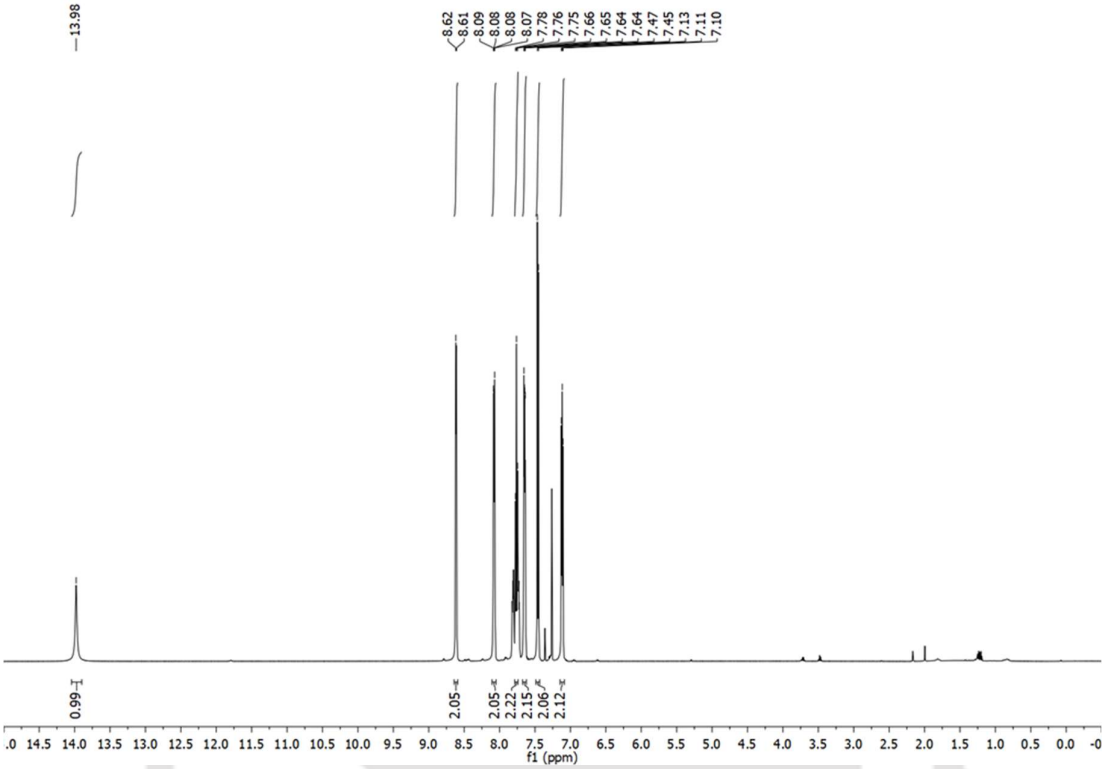

Figure A2.1. ^{1}H-NMR spectrum of ligand HBPI in $CDCl_3$.

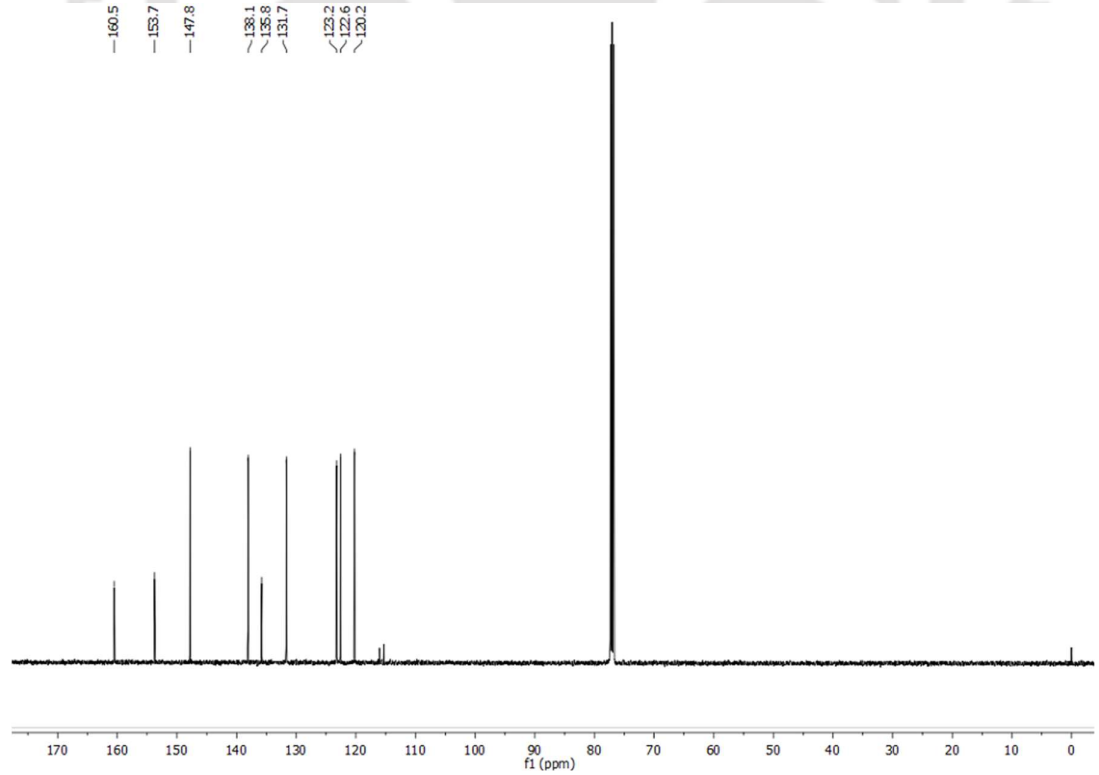

Figure A2.2. ^{13}C-NMR spectrum of ligand HBPI in $CDCl_3$.

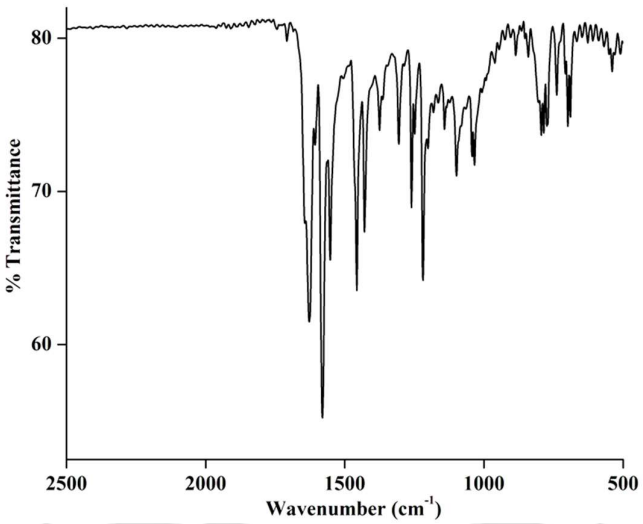

Figure A2.3. FT-IR spectrum of ligand HBPI in KBr.

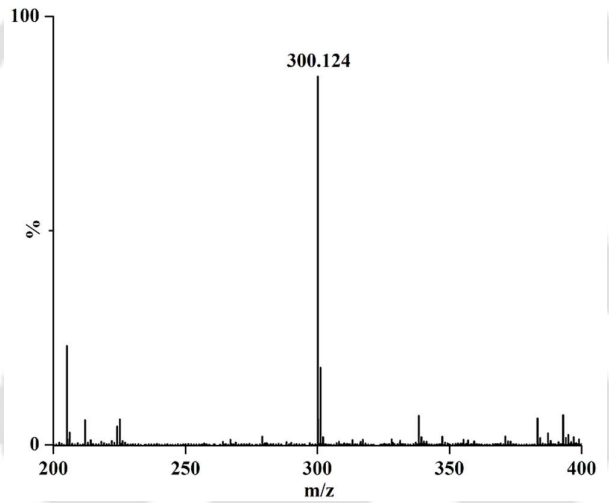

Figure A2.4. ESI-mass spectrum of ligand HBPI in CH_3CN (Calculated: 299.117; Found: 300.124 $[M+H]^+$).

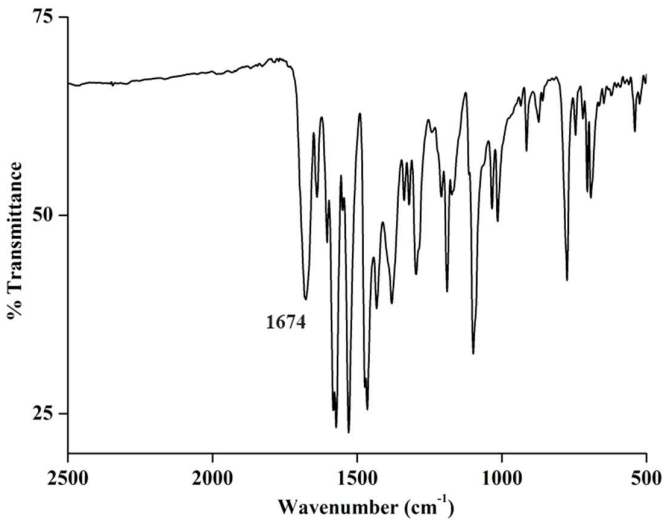

Figure A2.5. FT-IR spectrum of complex **3.1** in KBr.

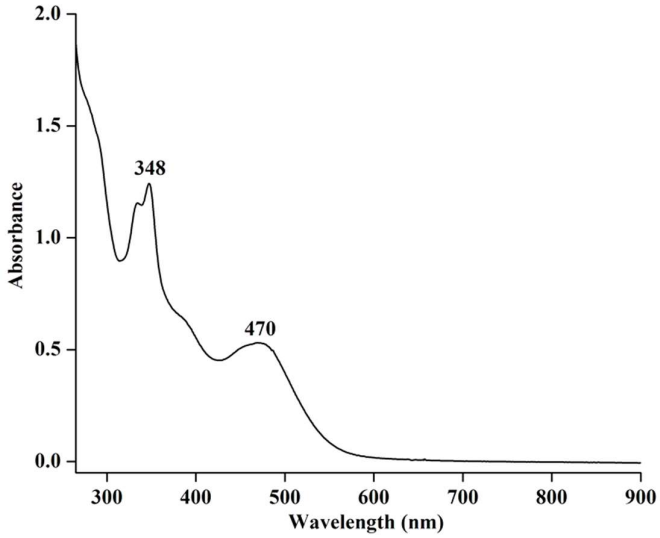

Figure A2.6. UV-visible spectrum of complex **3.1** in CH_2Cl_2 at room temperature.

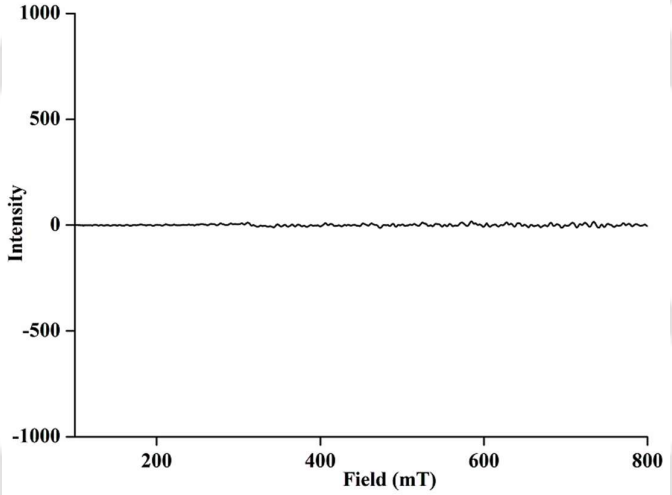

Figure A2.7. X-band EPR spectrum of complex **3.1** in CH_2Cl_2 at 77 K.

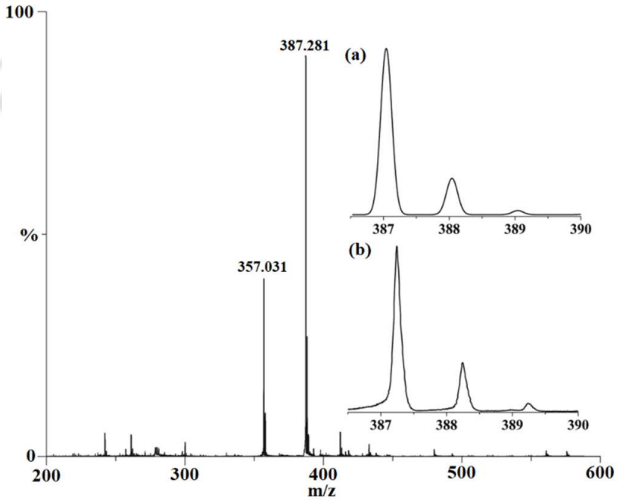

Figure A2.8. ESI-mass spectrum of complex **3.1** in CH_3CN (Calculated: 387.040, Found: 387.281, for $[Co(BPI)(NO)]^+$ unit).

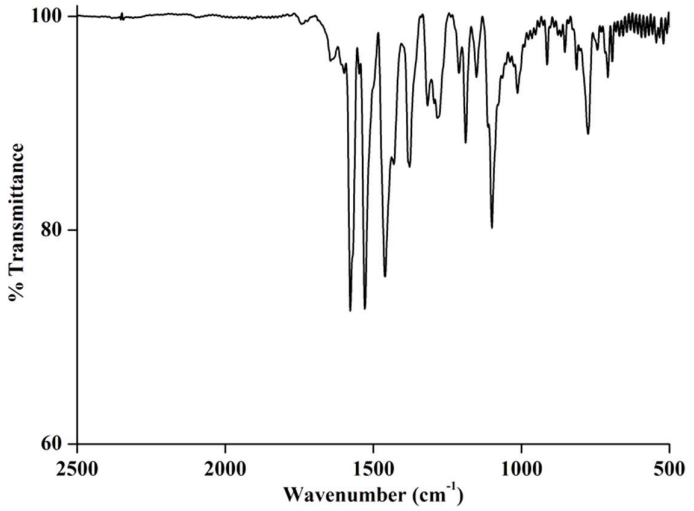

Figure A2.9. FT-IR spectrum of complex **3.2** in KBr.

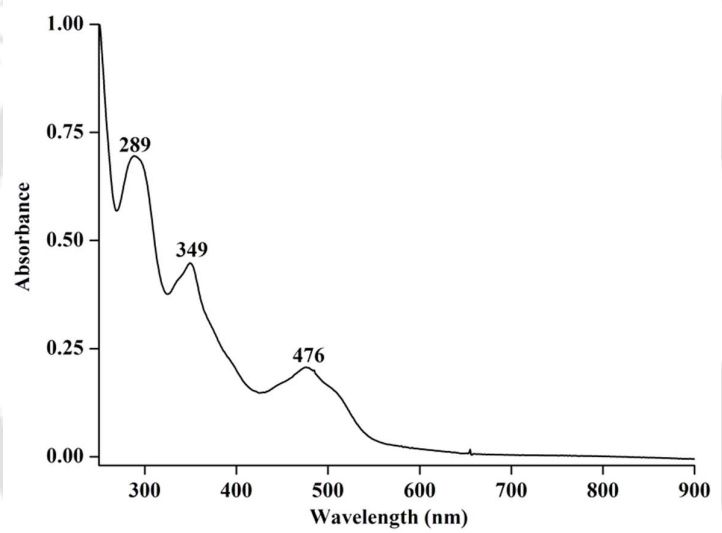

Figure A2.10. UV-visible spectrum of complex **3.2** in CH_2Cl_2 at room temperature.

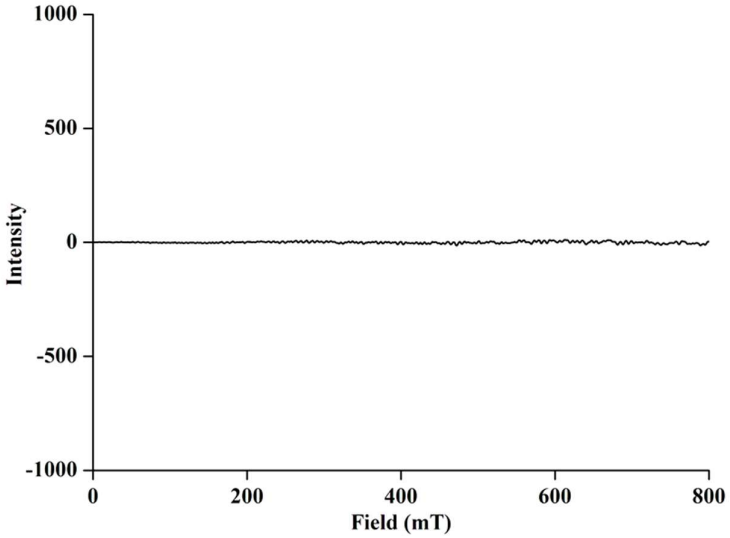

Figure A2.11. X-band EPR spectrum of complex **3.2** in CH_2Cl_2 at 77 K.

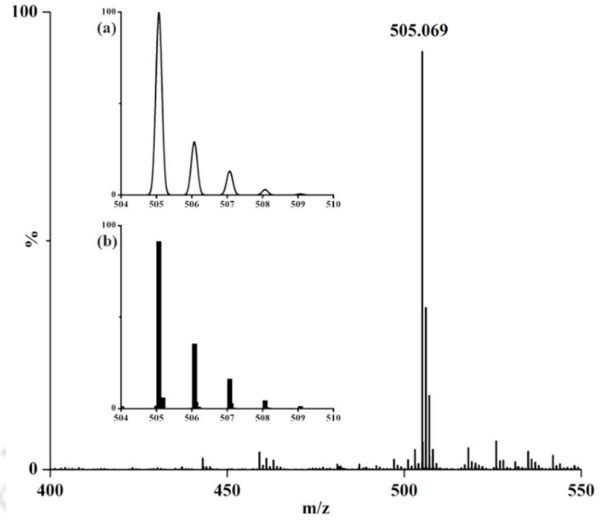

Figure A2.12. ESI-mass spectrum of complex **3.2** in CH_3CN **(**calculated: 505.068; found: 505.069; Inset: Isotopic distribution pattern; (a) Simulated, (b) Experimental).

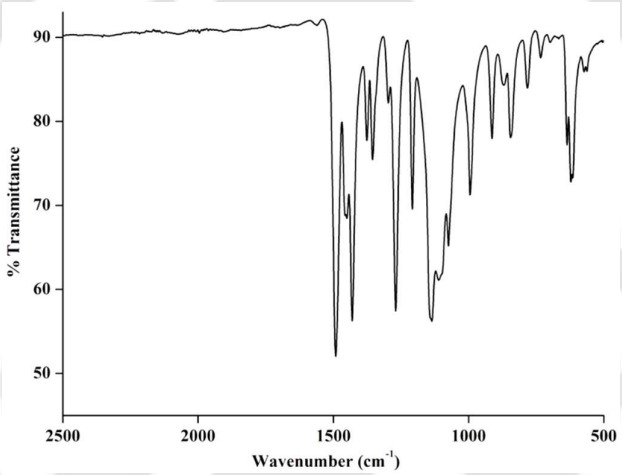

Figure A2.13. FT-IR spectrum of $[Fe^{II}(DTC^{-})_2]$ in KBr after purging head-space gas from reaction mixture.

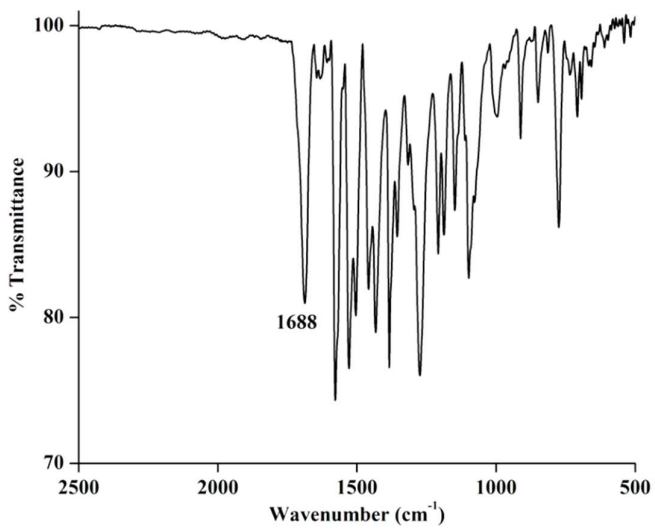

Figure A2.14. FT-IR spectrum of reaction mixture of complex **3.1** and $[Fe^{III}(DTC^{-})_3]$ in KBr.

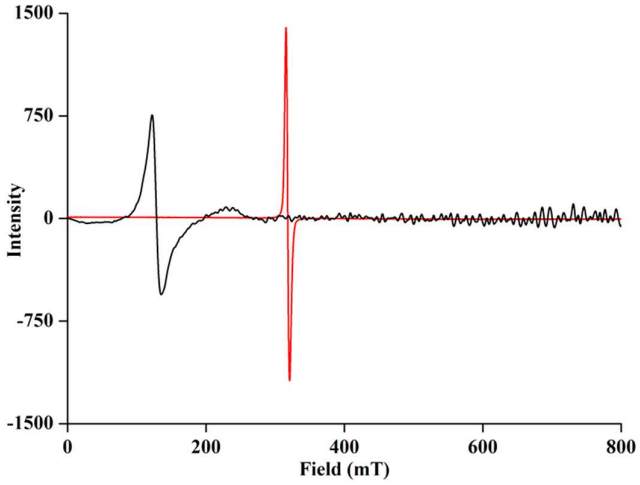

Figure A2.15. X-band EPR spectra of the reaction mixture of complex **3.1** and $[Fe^{III}(DTC^{-})_3]$ (initial (black) and final (red)) CH_2Cl_2 at 77 K.

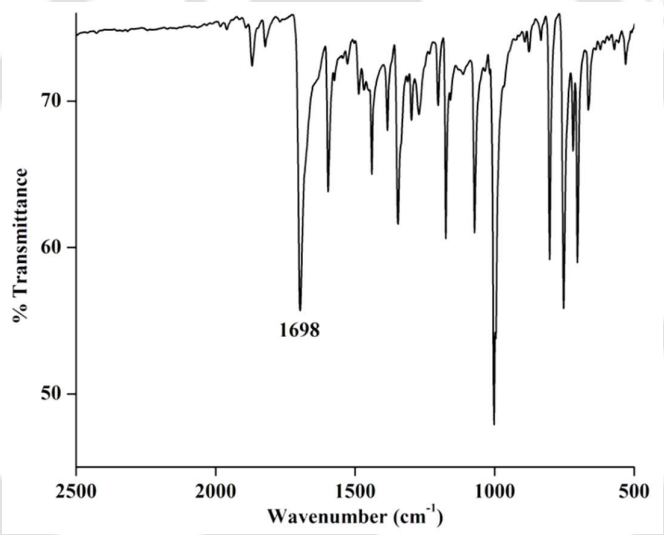

Figure A2.16. FT-IR spectrum of $[Fe(TPP^{2-})(NO)]$ in KBr.

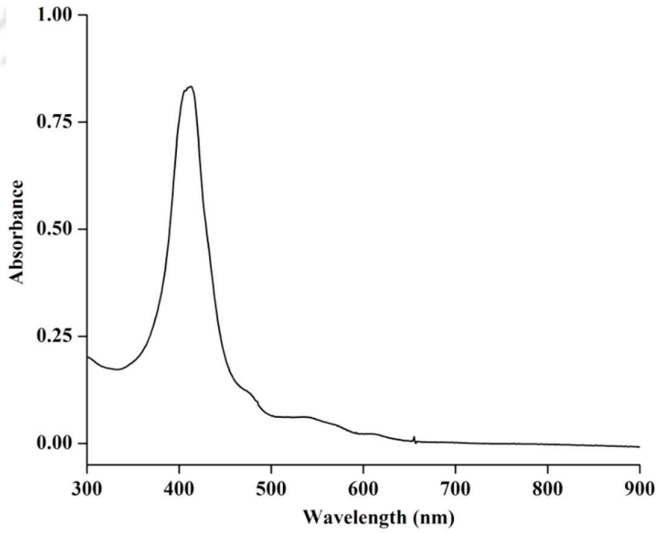

Figure A2.17. UV-visible spectrum of $[Fe(TPP^{2-})(NO)]$ in CH_2Cl_2 at room temperature.

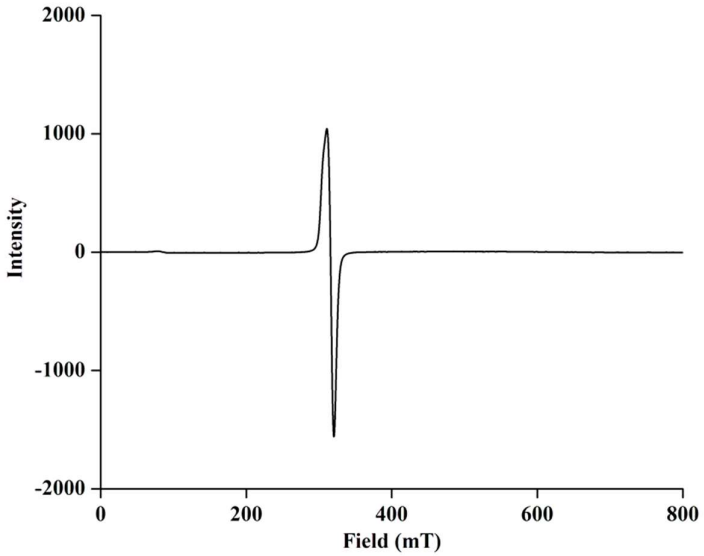

Figure A2.18. X-band EPR spectrum of [Fe(TPP^{2-})(NO)] in CH_2Cl_2 at 77 K.

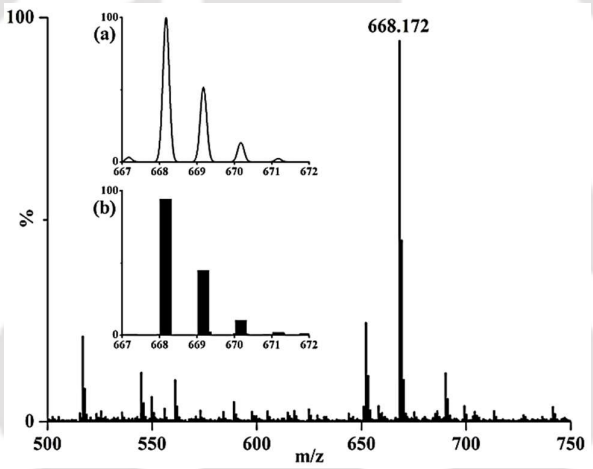

Figure A2.19. ESI-mass spectrum of [Fe(TPP^{2-})(NO)] in CH_3CN (Calculated: 668.166; Found: 668.172, after loss of NO).

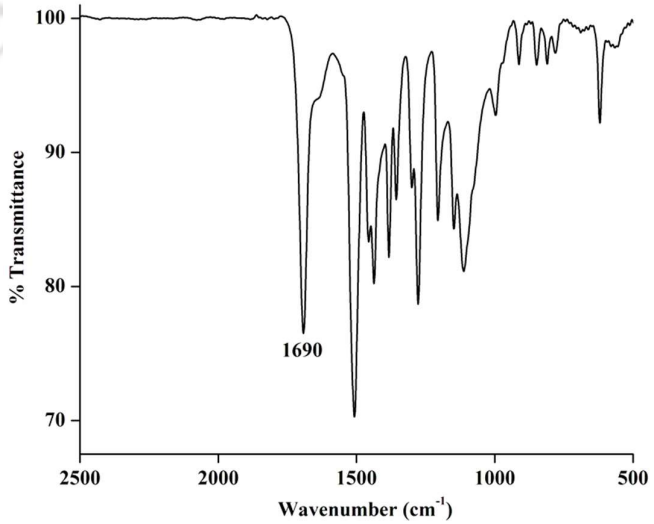

Figure A2.20. FT-IR spectrum of [Fe(DTC^{-})$_2$(NO)] in KBr.

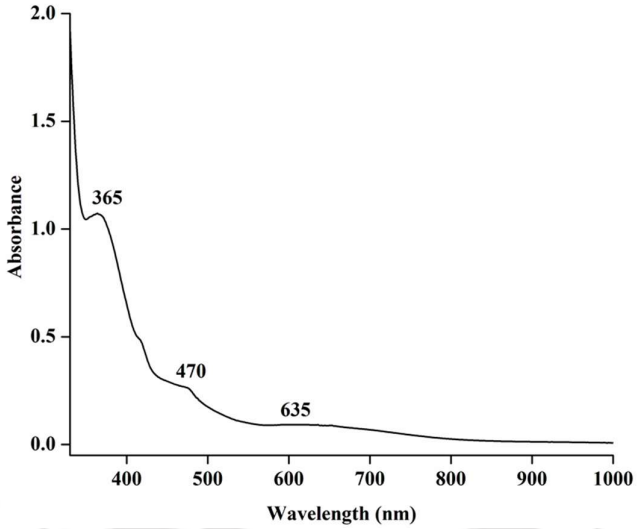

Figure A2.21. UV-visible spectrum of $[Fe(DTC^{-})_2(NO)]$ in CH_2Cl_2 at room temperature.

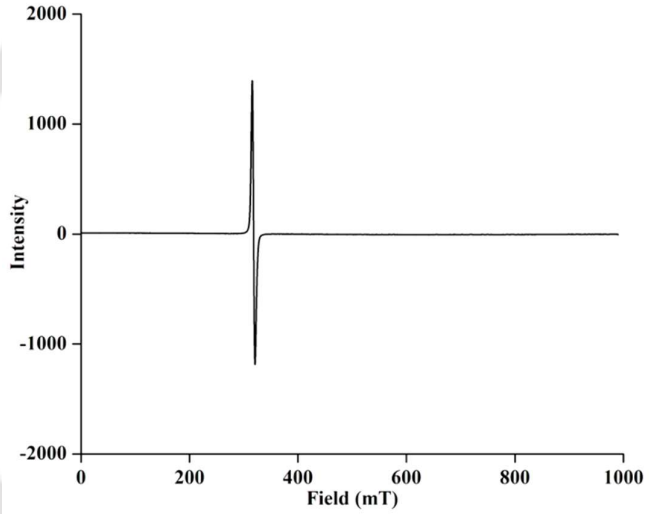

Figure A2.22. X-band EPR spectrum of $[Fe(DTC^{-})_2(NO)]$ in CH_2Cl_2 at 77 K.

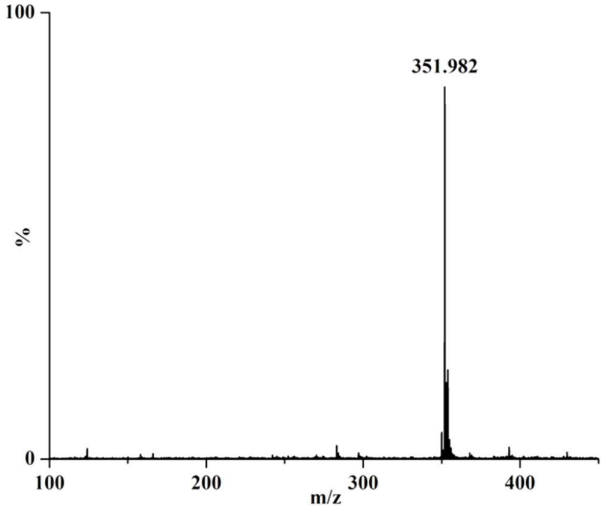

Figure A2.23. ESI-mass spectrum of $[Fe(DTC^{-})_2(NO)]$ in CH_3CN (Calculated: 351.986; Found: 351.976, after loss of NO).

Result File : d:\gc data\bm\shankhadeep\Co(BPI).rst
Sequence File : D:\GC Data\Co(BPI).seq

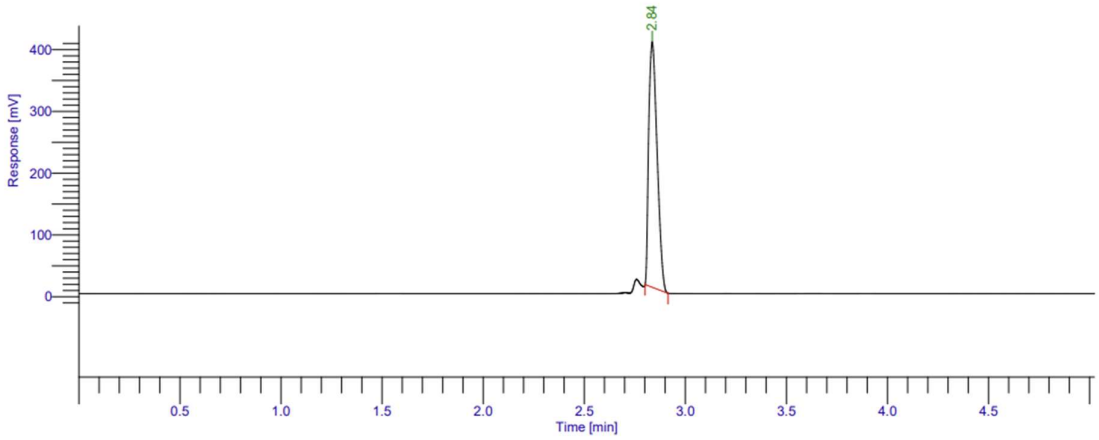

IIT Guwahati Chemistry Dept.

Peak #	Component Name	Time [min]	Area [uV*sec]	Height [uV]	Area [%]
1		2.836	1144118.88	397309.94	100.00
			1144118.88	397309.94	100.00

Figure A2.24. Gas chromatograms of headspace gas of the reaction mixture of complex **3.1** and NaDTC in presence of HBF_4 (retention time = 2.84 minutes).

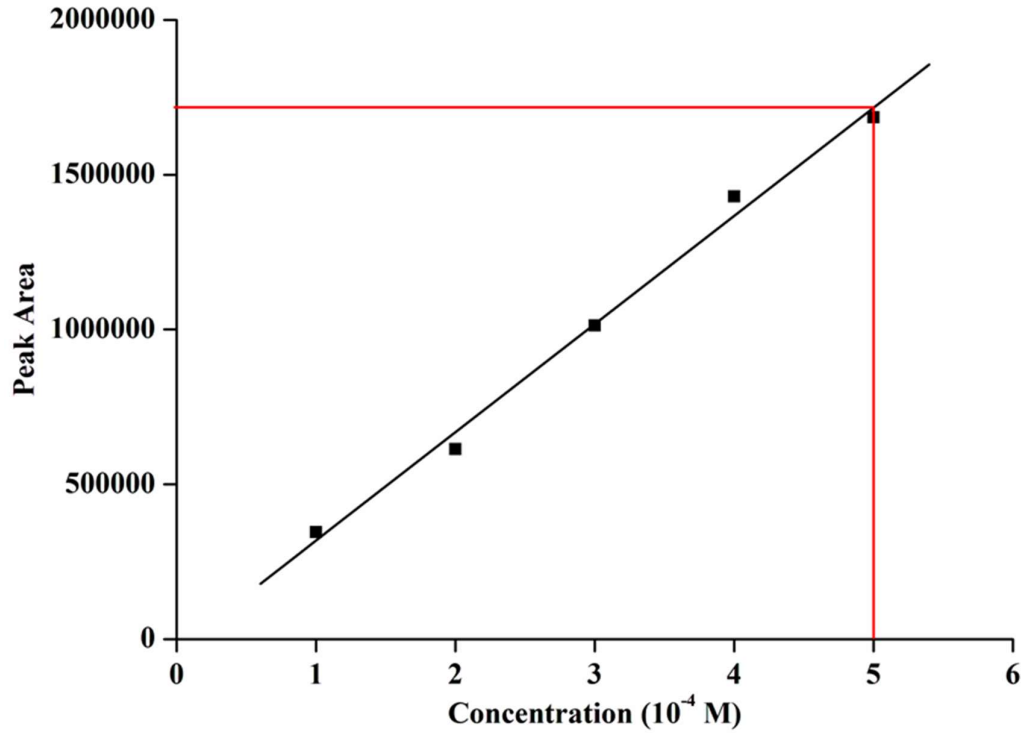

Figure A2.25. GC calibration curve for determination of amount of N_2O (red line corresponds to the sample).

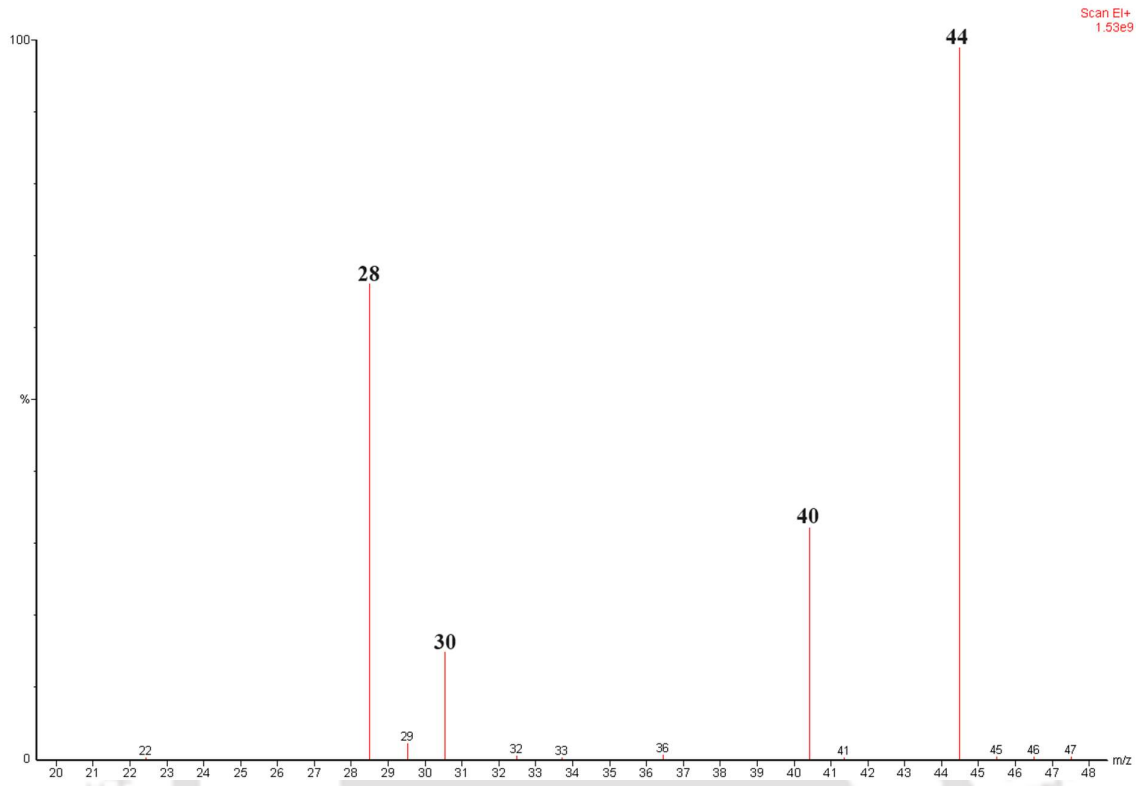

Figure A2.26. GC-mass spectrum of the headspace gas of the reaction mixture of complex **3.1** and NaDTC in presence of HBF_4.

Table A2.1. Crystallographic data for complex **3.1**.

	3.1
Formulae	$C_{20}H_{15}CoN_6O_3$
Mol. wt.	446.31
Crystal system	Monoclinic
Space group	C2/m
Temperature /K	120
Wavelength /Å	0.71073
a /Å	15.6806(13)
b /Å	16.1904(13)
c /Å	8.6708(7)
α/°	90
β/°	106.317(2)
γ/°	90
V/ $Å^3$	2112.6(3)
Z	4
Density/Mgm^{-3}	1.403
Abs. Coeff. /mm^{-1}	0.845

Abs. correction	none
F(000)	912
Total no. of reflections	3655
Reflections, $I > 2\sigma(I)$	3027
Max. 2θ/°	25.242
Ranges (h, k, l)	$-24 \leq h \leq 21$ $-25 \leq k \leq 24$ $-12 \leq l \leq 12$
Complete to 2θ (%)	0.973
Refinement method	Full-matrix least-squares on F^2
Goof (F^2)	1.074
R indices [$I > 2\sigma(I)$]	0.0468
R indices (all data)	0.0608
Largest diff. peak/hole / e Å^{-3}	0.66/-0.52

Table A2.2. Selected bond lengths (Å) of complex **3.1**.

Atoms	**3.1**
Co1-N1	1.842(3)
Co1-N2	1.9828(16)
Co1-N4	1.884(2)
N2-C5	1.357(2)
C5-N3	1.376(2)
N3-C6	1.294(2)
C6-N4	1.373(2)
N1-O1	1.091(5)
Co1-O2	1.937(2)

Table A2.3. Selected bond angles (˚) of complex **3.1**.

Atoms	**3.1**
N1-Co1-N2	89.80(4)
N2-Co1-N4	90.99(4)
N1-Co1-N4	103.30(14)
Co1-N1-O1	129.9(3)
N2-Co1-O2	89.06(4)
N1-Co1-O2	97.18(12)

Appendix III

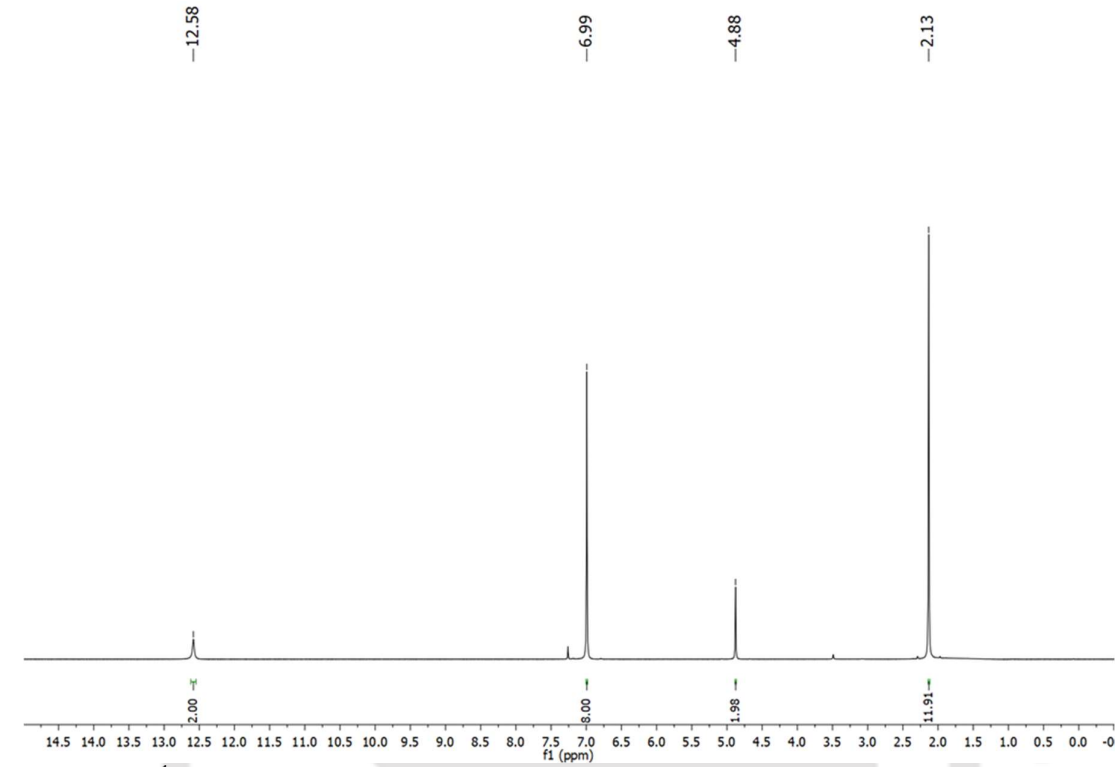

Figure A3.1. ^{1}H-NMR spectrum of H_2TMTAA in $CDCl_3$.

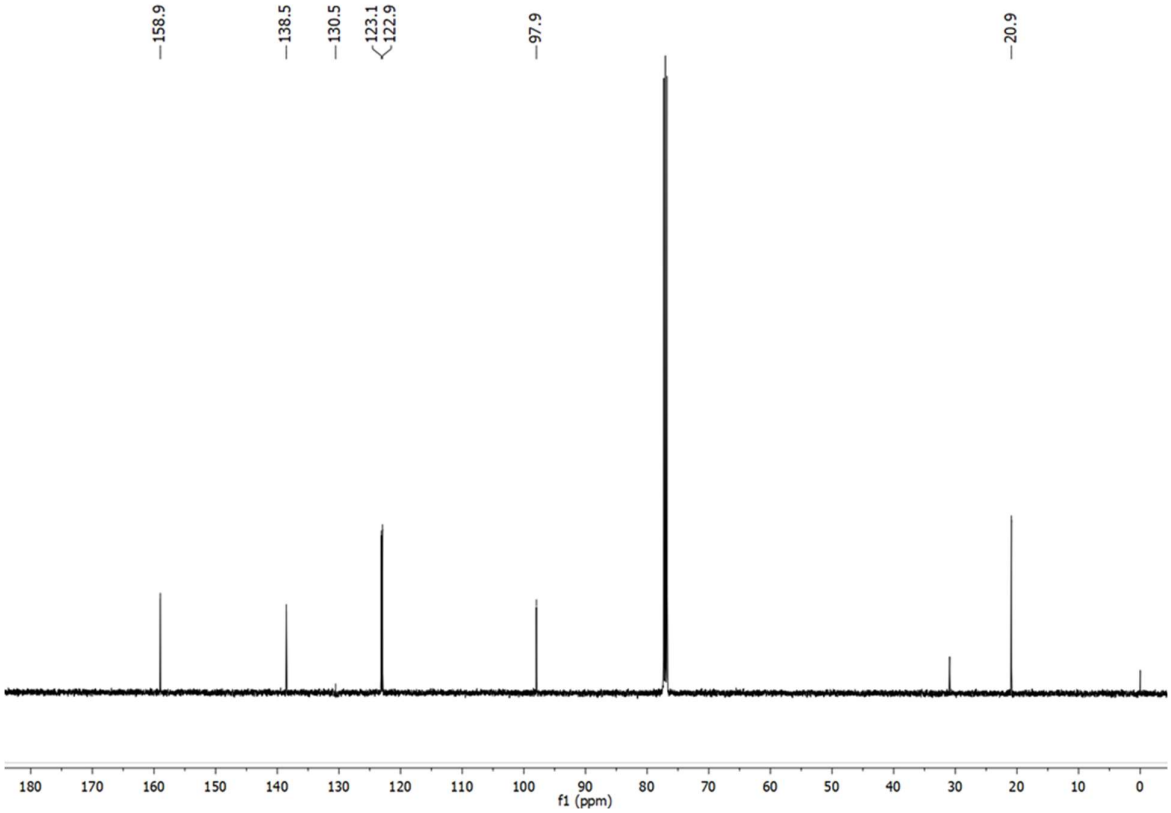

Figure A3.2. ^{13}C-NMR spectrum of H_2TMTAA in $CDCl_3$.

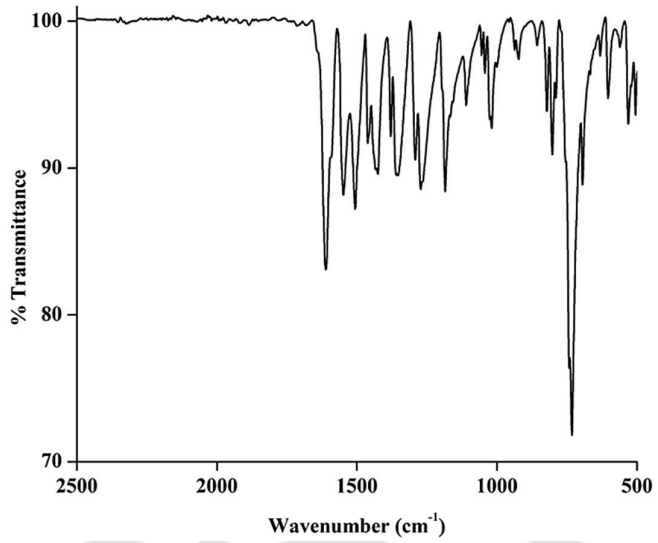

Figure A3.3. FT-IR spectrum of H_2TMTAA in ATR probe**.**

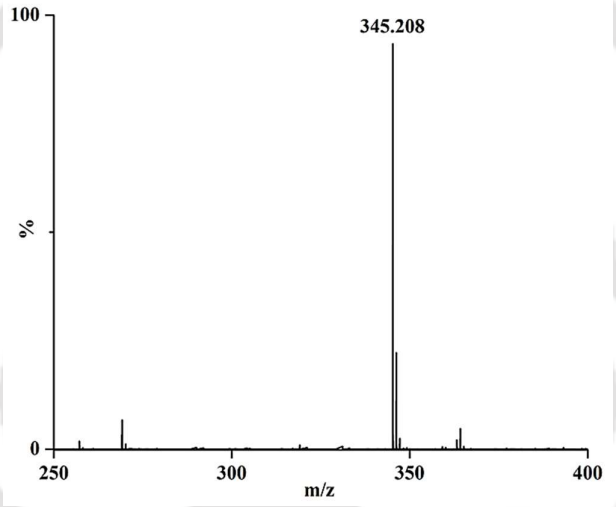

Figure A3.4. ESI-mass spectrum of H_2TMTAA in CH_3CN. **(**Calculated, 345.208; Found, 345.208, for $[M+H]^+$).

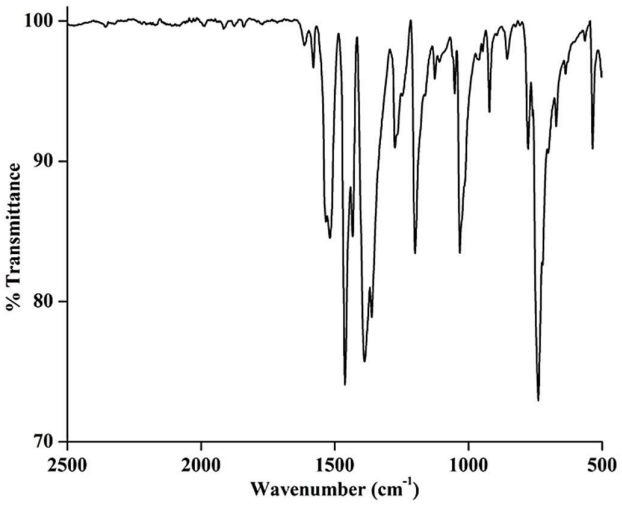

Figure A3.5. FT-IR spectrum of complex **4.1** in ATR probe.

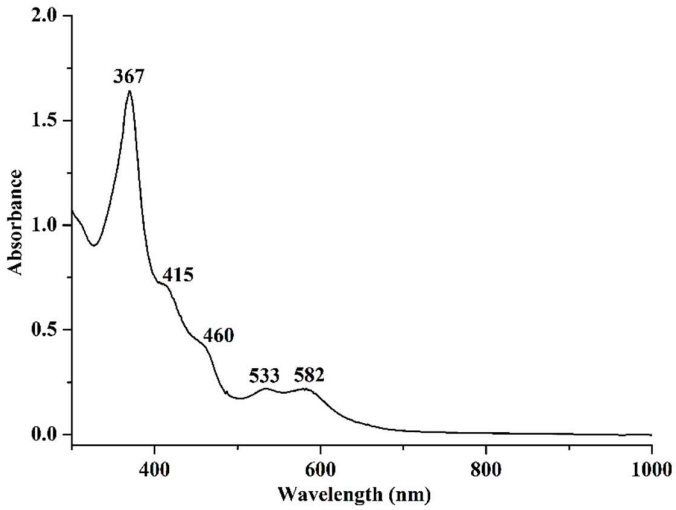

Figure A3.6. UV-visible spectrum of complex **4.1** in CH_2Cl_2 at room temperature.

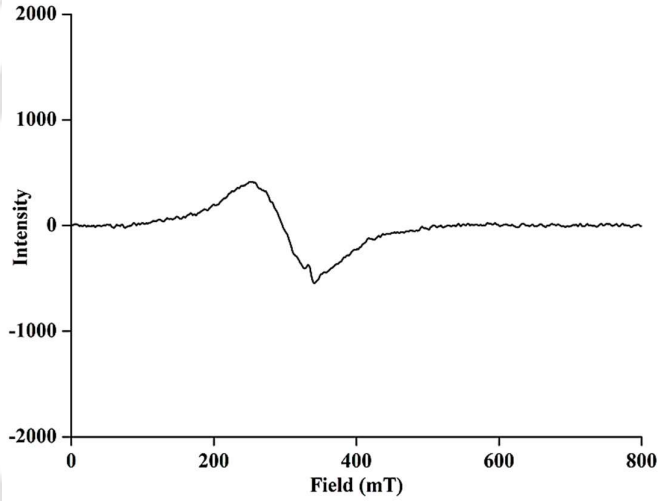

Figure A3.7. X-band EPR spectrum of complex **4.1** in CH_2Cl_2 at 77 K.

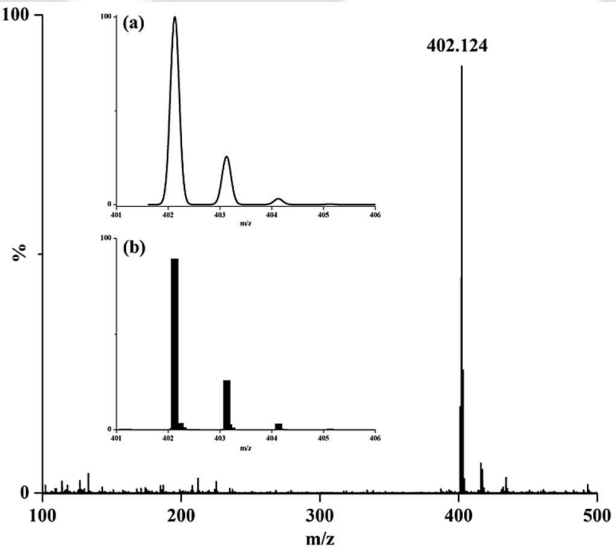

Figure A3.8. ESI-mass spectrum of complex **4.1** in CH_3CN **(**Calculated, 402.125; Found, 402.124; for $[M+H]^+$. Inset: Isotopic distribution pattern; (a) Simulated, (b) Experimental).

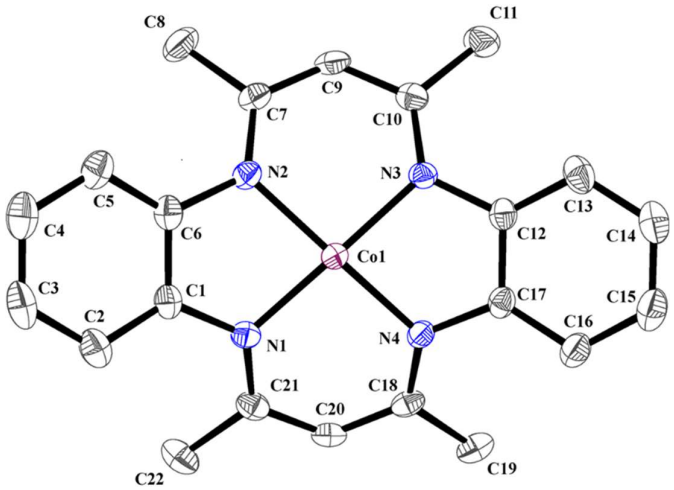

Figure A3.9. ORTEP diagram of complex **4.1 (**30% thermal ellipsoid. H atoms are omitted for clarity).

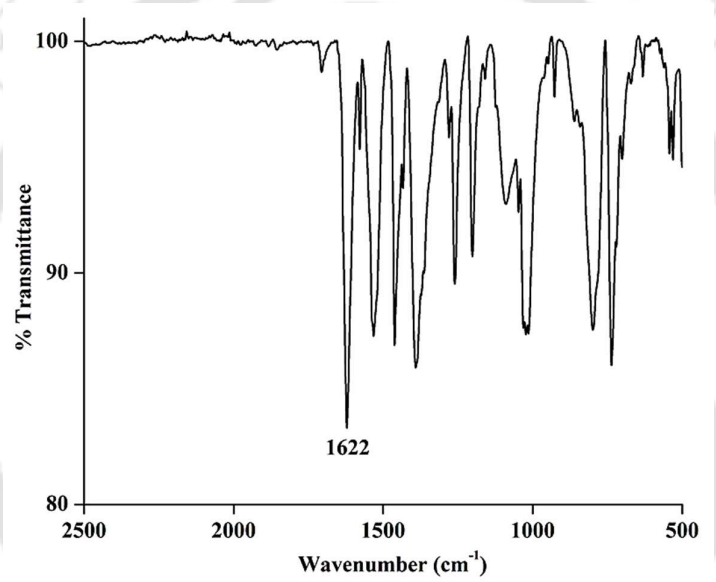

Figure A3.10. FT-IR spectrum of complex **4.2a** in ATR probe.

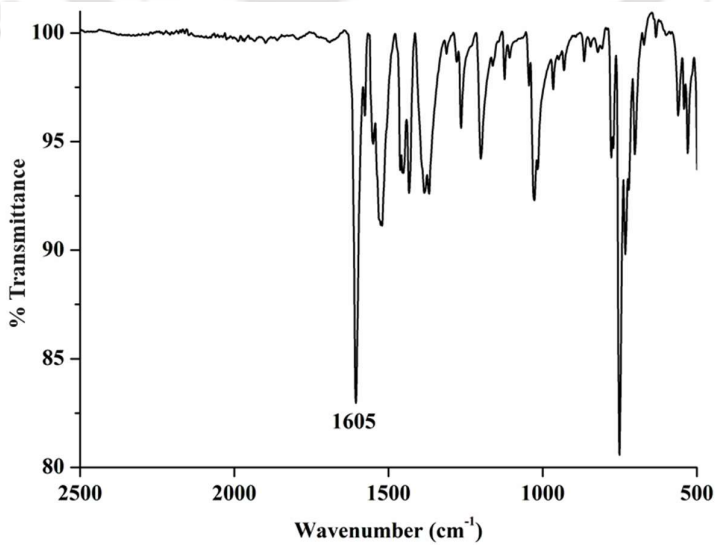

Figure A3.11. FT-IR spectrum of complex **4.2b** in ATR probe.

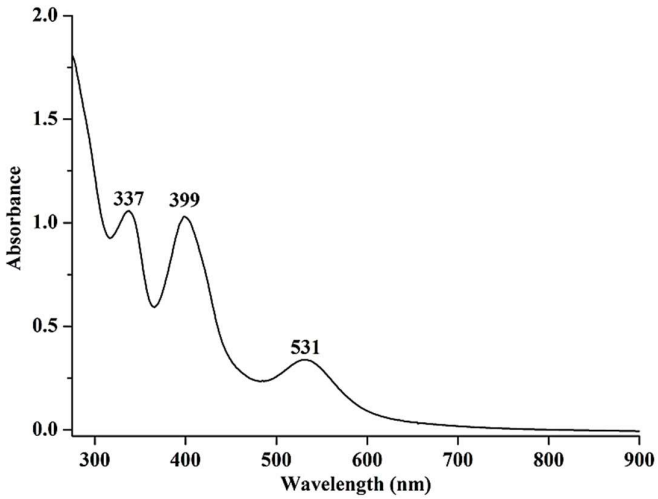

Figure A3.12. UV-visible spectrum of complex **4.2a** in CH_2Cl_2 at room temperature.

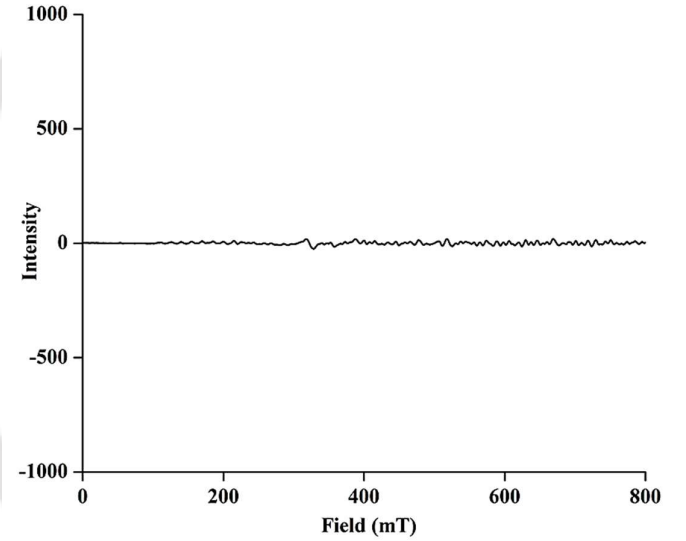

Figure A3.13. X-band EPR spectrum of complex **4.2a** in CH_2Cl_2 at 77 K.

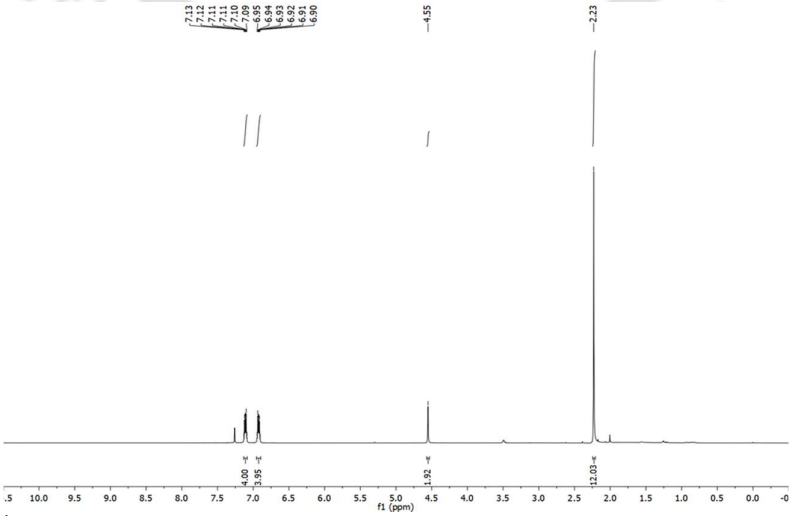

Figure A3.14. ^{1}H-NMR spectrum of complex **4.2a** in $CDCl_3$.

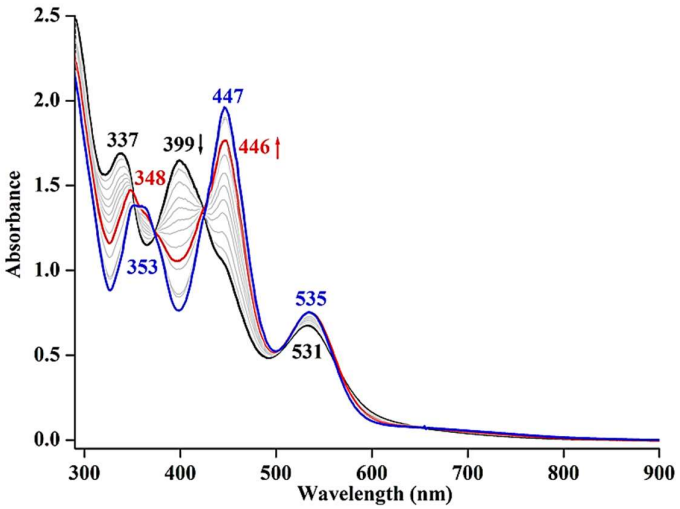

Figure A3.15. UV-visible spectral monitoring of complex **4.2a** (black), followed by addition of imidazole (red) then $NaBPh_4$ (blue) in CH_2Cl_2 at room temperature.

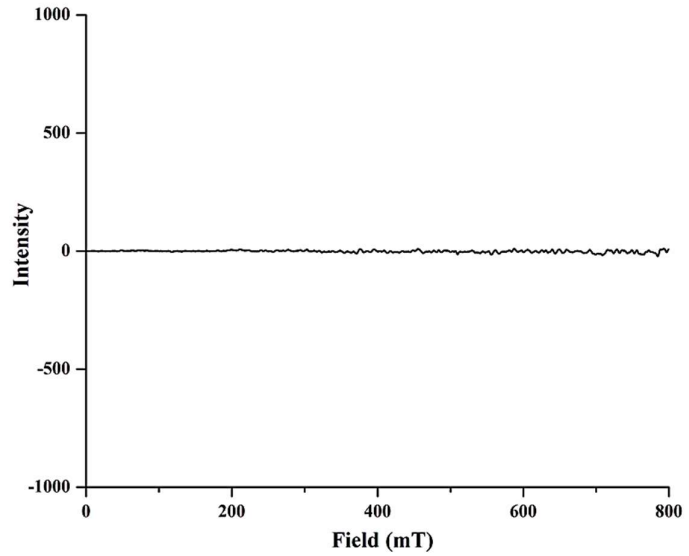

Figure A3.16. X-band EPR-spectrum of $[Co^{III}(TMTAA^{2-})(IM)]^{+}$ in CH_2Cl_2 at 77 K.

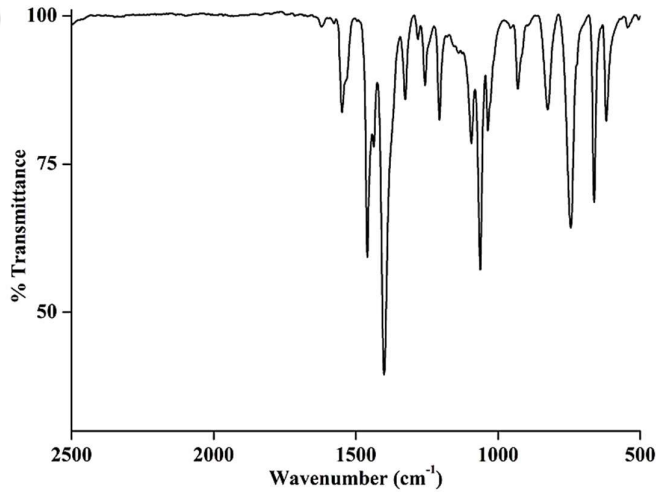

Figure A3.17. FT-IR spectrum of complex **4.3** in ATR probe.

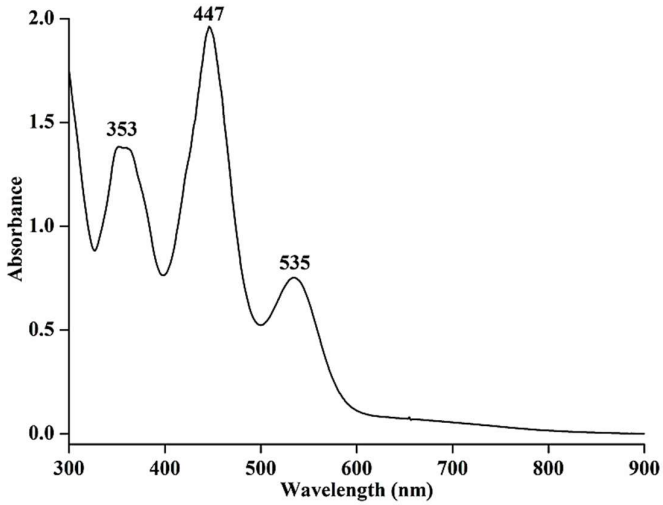

Figure A3.18. UV-visible spectrum of complex **4.3** in CH_2Cl_2 at room temperature.

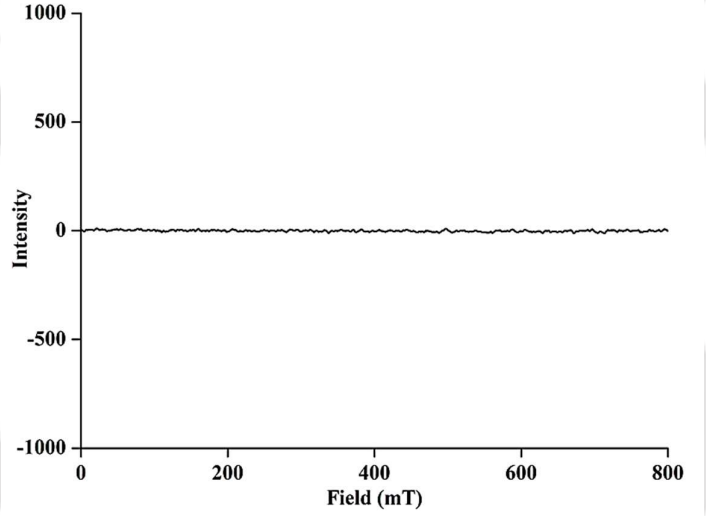

Figure A3.19. X-band EPR spectrum of complex **4.3** in CH_2Cl_2 at 77 K.

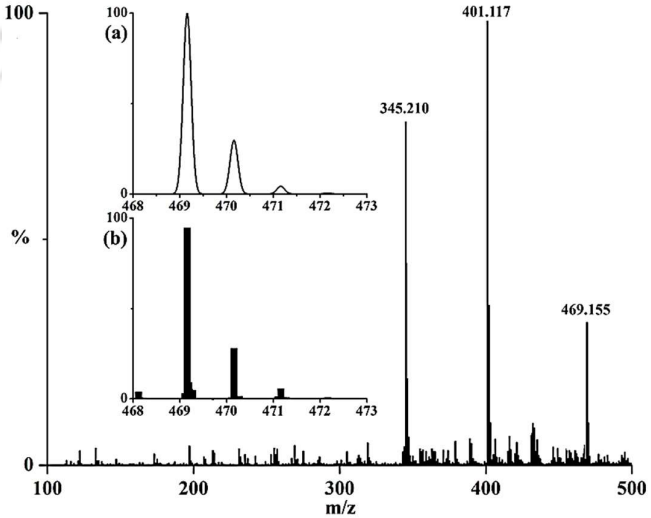

Figure A3.20. ESI-mass spectrum of Complex **4.3** in CH_3CN **(**Calculated, 469.155; Found, 469.155; After loss of BPh_4 unit. Inset: Isotopic distribution pattern; (a) Simulated, (b) Experimental).

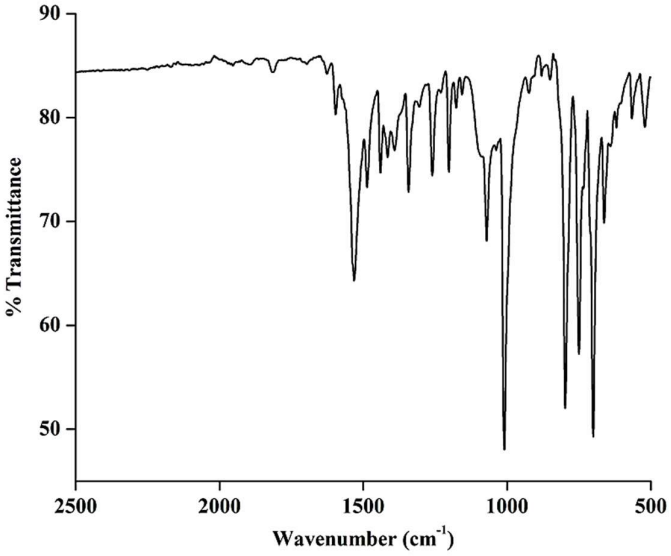

Figure A3.21. FT-IR spectrum of complex $[Mn^{III}(TPP^{2-})Cl]$ in ATR probe.

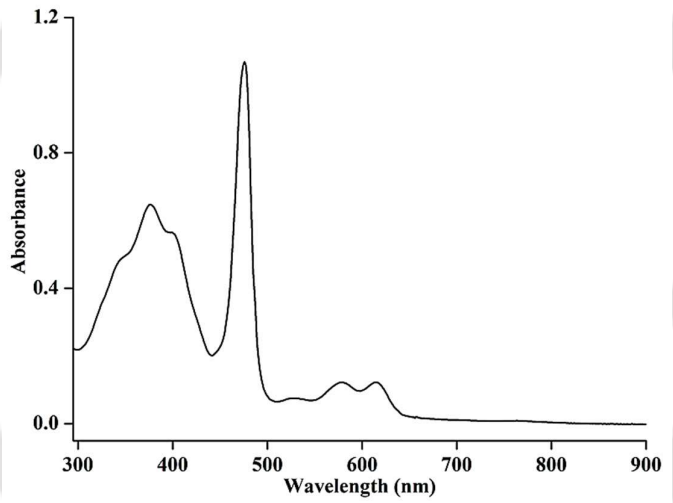

Figure A3.22. UV-visible spectrum of $[Mn^{III}(TPP^{2-})Cl]$ in CH_2Cl_2 at room temperature.

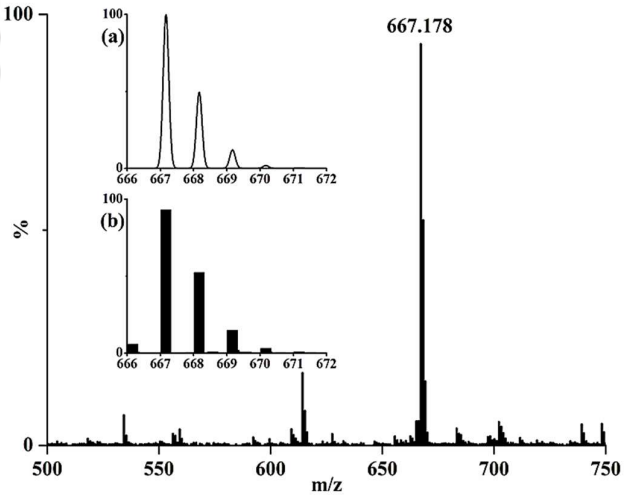

Figure A3.23. ESI-mass spectrum of $[Mn^{III}(TPP^{2-})Cl]$ in CH_3CN **(**Calculated, 667.169; Found, 667.178; after loss of Cl^-. Inset: Isotopic distribution pattern; (a) Simulated, (b) Experimental).

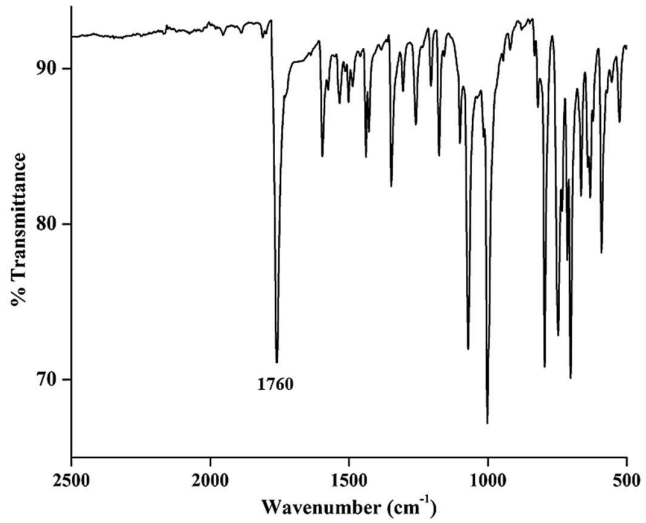

Figure A3.24. FT-IR spectrum of complex [Mn(TPP^{2-})(NO)] in ATR probe.

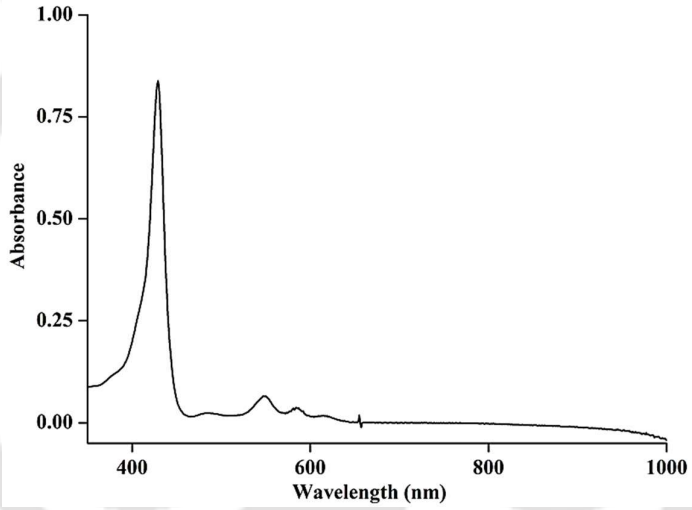

Figure A3.25. UV-visible spectrum of [Mn(TPP^{2-})(NO)] in CH_2Cl_2 at room temperature.

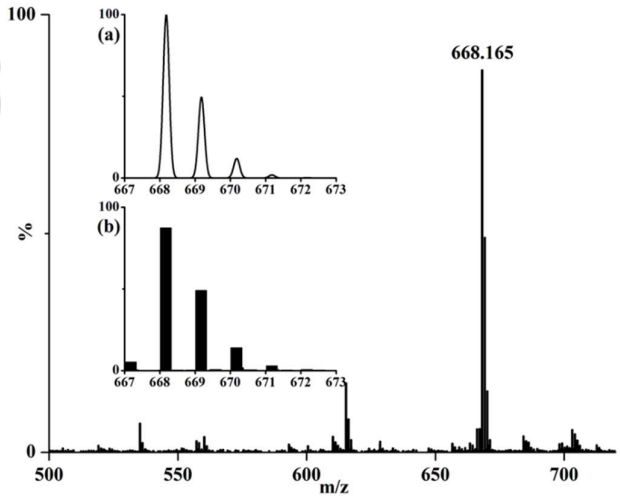

Figure A3.26. ESI-MS spectrum of [Mn(TPP^{2-})(NO)] in CH_3CN **(**Calculated, 668.177; Found, 668.165; After loss of NO, protonated. Inset: Isotopic distribution pattern; (a) Simulated, (b) Experimental).

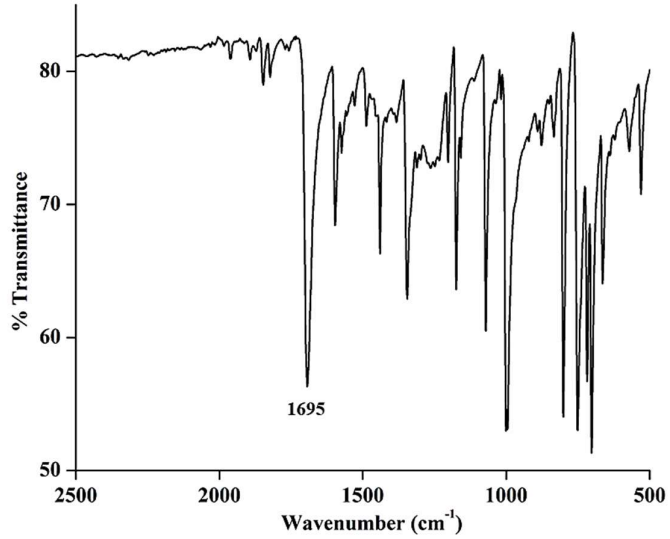

Figure A3.27 FT-IR spectrum of complex [Fe(TPP^{2-})(NO)] in ATR probe.

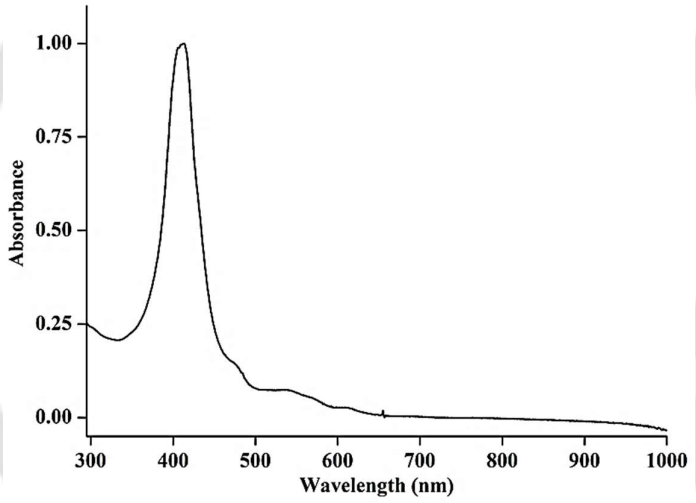

Figure A3.28. UV-visible spectrum of [Fe(TPP^{2-})(NO)] in CH_2Cl_2 at room temperature.

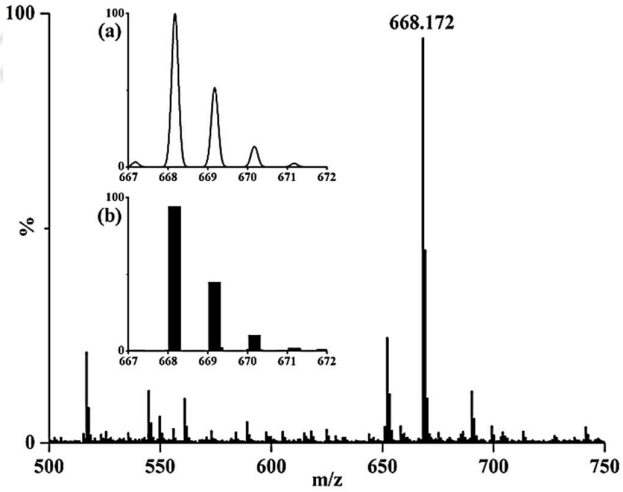

Figure A3.29. ESI-mass spectrum of [Fe(TPP^{2-})(NO)] in CH_3CN **(**Calculated, 668.166; Found, 668.172; After loss of NO, Inset: Isotopic distribution pattern; (a) Simulated, (b) Experimental)

Result File : D:\GC Data\BM\Riya\27-06-23\CoTMTAANO-N2O.rst
Sequence File : D:\GC Data\CoTMTAANO-N2O.seq

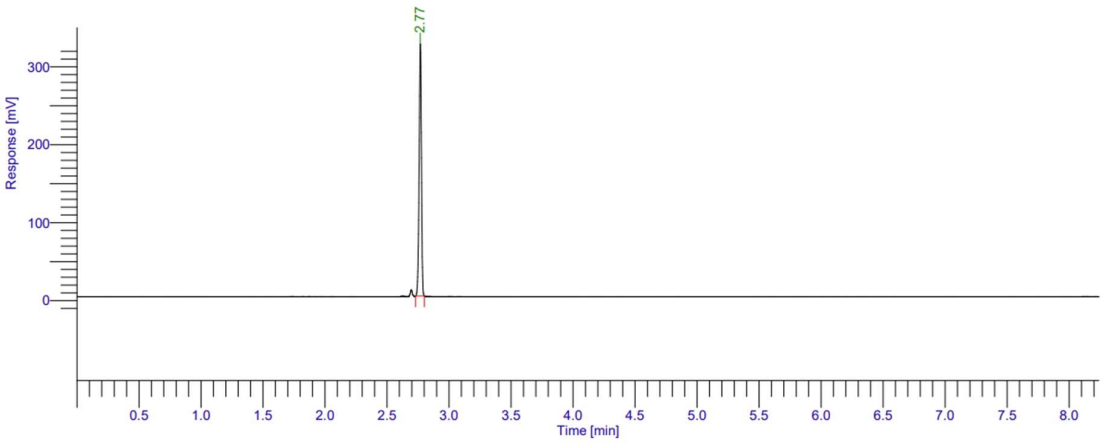

IIT Guwahati Chemistry Dept.

Peak #	Component Name	Time [min]	Area [uV*sec]	Height [uV]	Area [%]
1		2.768	417386.88	323732.56	100.00
			417386.88	323732.56	100.00

Figure A3.30. Gas chromatograms of headspace gas of the reaction mixture of complex **4.2a** and imidazole in presence of HBF_4 (retention time = 2.77 min).

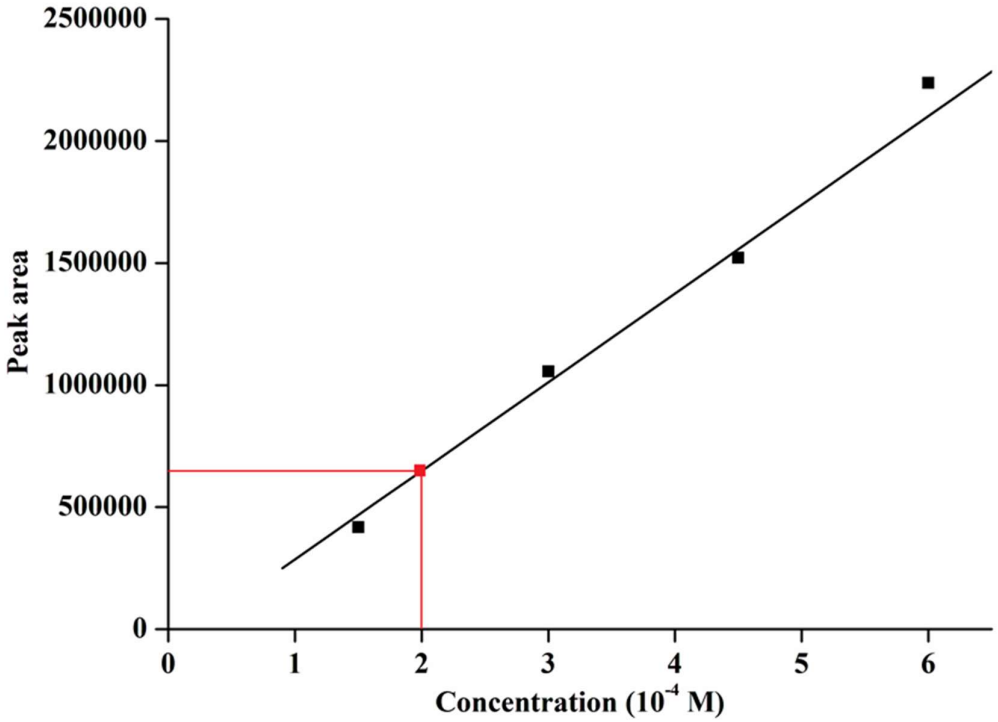

Figure A3.31. GC calibration curve for determination of amount of N_2O (red line corresponds to the sample).

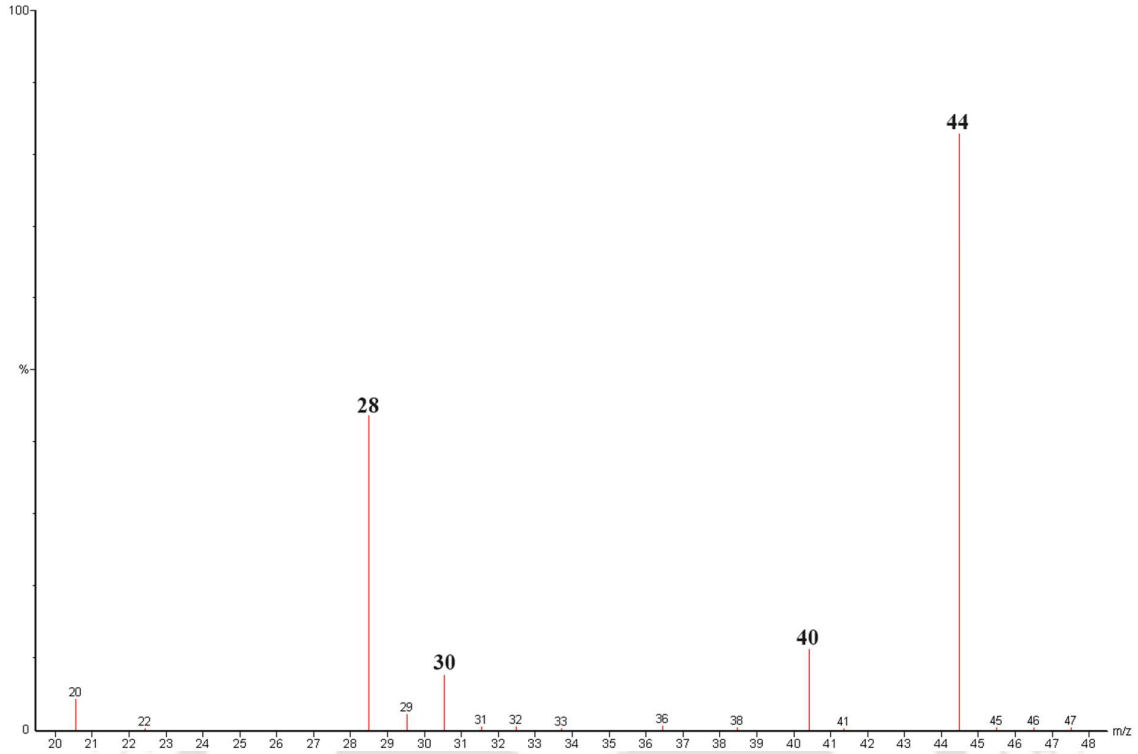

Figure A3.32. GC-mass spectrum of the headspace gas of the reaction mixture of complex **4.2a** and imidazole in presence of HBF_4.

Table A3.1. Crystallographic data for complexes **4.1**, **4.2a** and **4.2b**.

	4.1	**4.2a**	**4.2b**
Formulae	$C_{44}H_{44}Co_2N_8$	$C_{23}Cl_2CoN_5OH_{24}$	$C_{22}H_{22}CoN_5O$
Mol. wt.	802.73	516.30	431.37
Crystal system	Monoclinic	Triclinic	Monoclinic
Space group	$P2_1/c$	P-1	$P2_1/n$
Temperature /K	293(2)	296.0	298.0
Wavelength /Å	0.71073	0.71073	0.71073
a /Å	14.4344(8)	9.1802(8)	7.7663(4)
b /Å	16.4066(5)	11.2850(10)	15.5053(8)
c /Å	16.2778(7)	12.0488(10)	19.3814(10)
α/°	90	102.415(3)	90
β/°	99.840(4)	94.370(3)	90.119(2)
γ/°	90	104.862(3)	90
V/ Å^3	3798.2(3)	1166.81(18)	2333.9(2)
Z	4	2	4
Density/Mgm^{-3}	1.404	1.470	1.228
Abs. Coeff. /mm^{-1}	0.917	0.990	0.755
Abs. correction	none	none	None

F(000)	1672	532	896.0
Total no. of reflections	6684	4111	4108
Reflections, $I > 2\sigma(I)$	5141	3802	3736
Max. 2θ/°	27.9930	27.83	27.83
Ranges (h, k, l)	$-17 \le h \le 15$ $-19 \le k \le 11$ $-14 \le l \le 19$	$-10 \le h \le 10$ $-13 \le k \le 13$ $-14 \le l \le 14$	$-9 \le h \le 9$ $-18 \le k \le 18$ $-23 \le l \le 23$
Complete to 2θ (%)	0.999	1.000	0.999
Refinement method	Full-matrix least-squares on F^2	Full-matrix least-squares on F^2	Full-matrix least-squares on F^2
Goof (F^2)	0.998	1.095	1.164
R indices [$I > 2\sigma(I)$]	0.0453	0.0702	0.0566
R indices (all data)	0.0659	0.0728	0.0604
Largest diff. peak/hole / e $Å^{-3}$	0.51/-0.74	0.81/-0.72	0.41/-0.27

Table A3.2. Selected bond lengths (Å) of complexes **4.1**, **4.2a** and **4.2b**.

Atoms	**4.1**	**4.2a**	**4.2b**
Co1-N1	1.908(2)	1.910(3)	1.910(3)
Co1-N2	1.900(3)	1.910(3)	1.897(3)
Co1-N3	1.901(2)	1.902(3)	1.902(3)
Co1-N4	1.902(3)	1.907(3)	1.892(3)
Co1-N5	-	1.818(3)	1.803(4)
N5-O1	-	1.124(5)	1.138(5)
Co2-N5	1.889(2)	-	-
Co2-N6	1.895(2)	-	-
Co2-N7	1.885(2)	-	-
Co2-N8	1.891(3)	-	-

Table A3.3. Selected bond angles (˚) of complexes **4.1**, **4.2a** and **4.2b**.

Atoms	**4.1**	**4.2a**	**4.2b**
N1-Co1-N2	84.57(10)	83.37(13)	83.84(14)
N2-Co1-N3	95.49(11)	94.59(13)	94.96(14)
N3-Co1-N4	89.46(9)	83.17(13)	83.50(14)
N4-Co1-N1	84.56(10)	94.66(13)	93.79(15)
Co1-N5-O1	-	125.1(3)	125.0(3)
N1-Co1-N5	-	95.98(14)	96.58(16)
N2-Co1-N5	-	97.17(14)	95.69(16)
N3-Co1-N5	-	98.43(14)	97.54(16)
N4-Co1-N5	-	99.59(14)	100.18(17)

Appendix IV

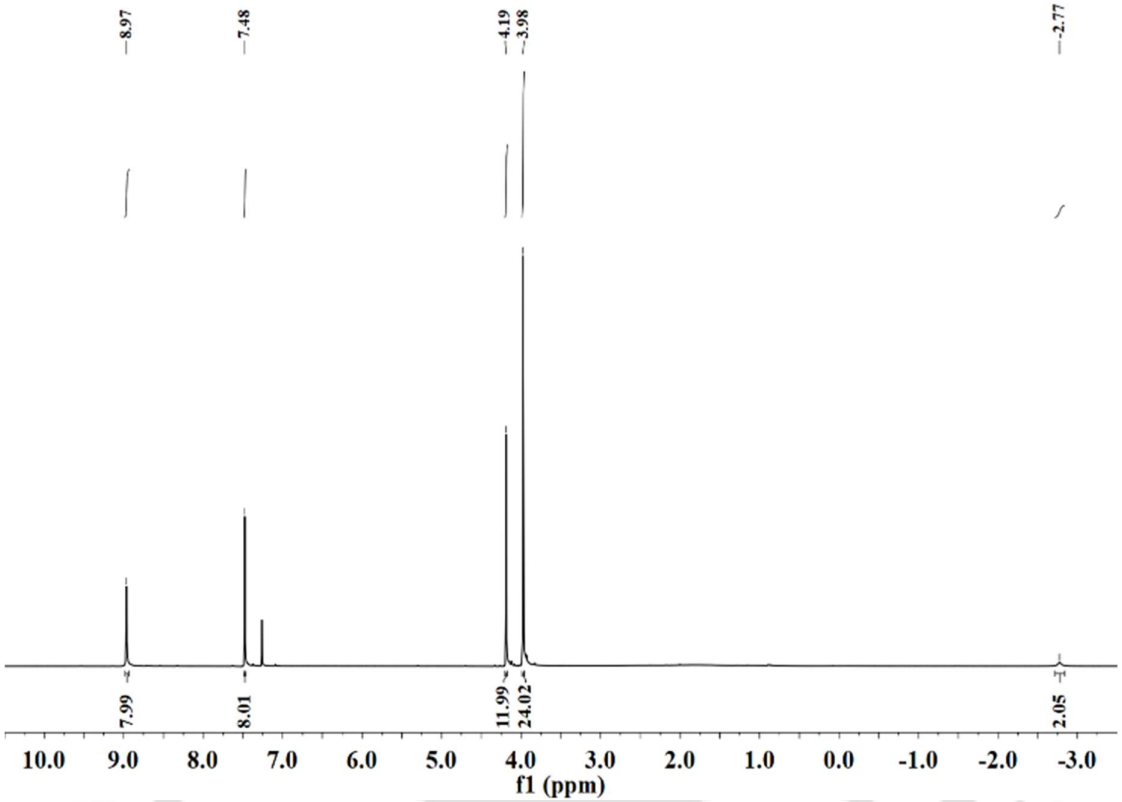

Figure A4.1. ^{1}H-NMR spectrum of H_2TTMPP in $CDCl_3$.

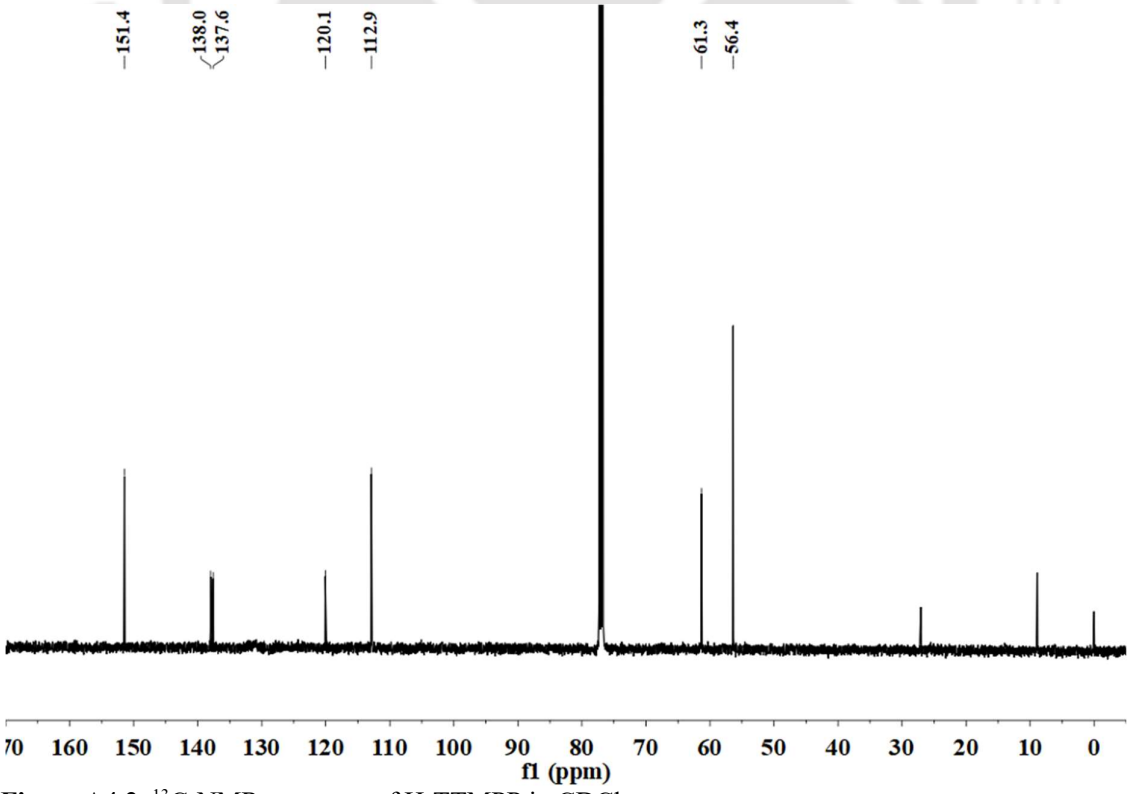

Figure A4.2. ^{13}C-NMR spectrum of H_2TTMPP in $CDCl_3$.

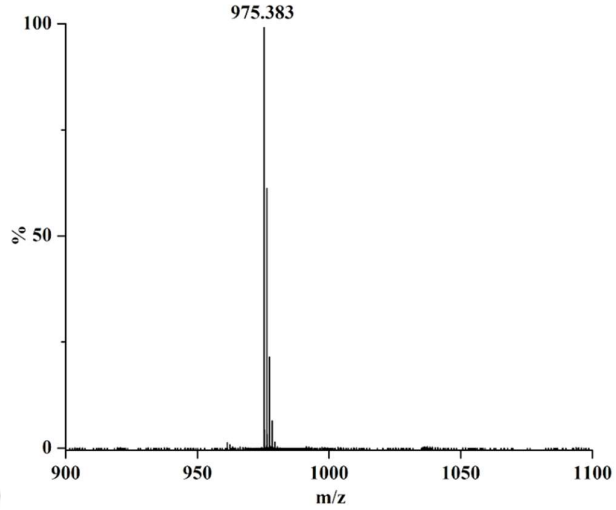

Figure A4.3. ESI-mass spectrum of H_2TTMPP in CH_3OH (Calculated, 975.381; Found, 975.383, $[M+H]^+$ peak).

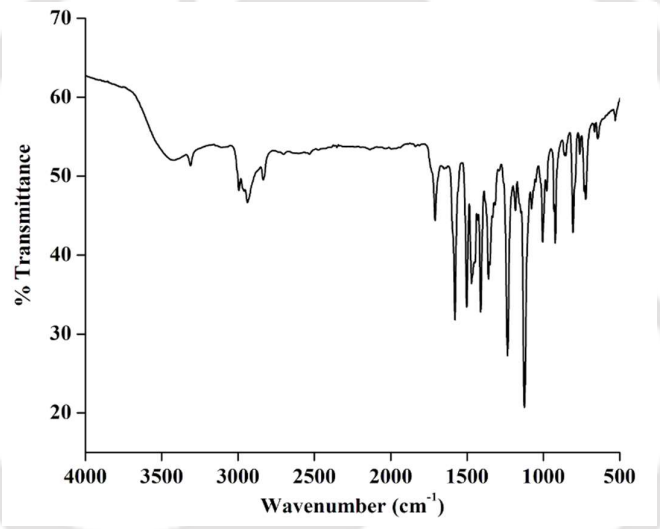

Figure A4.4. FT-IR spectrum of H_2TTMPP in ATR probe.

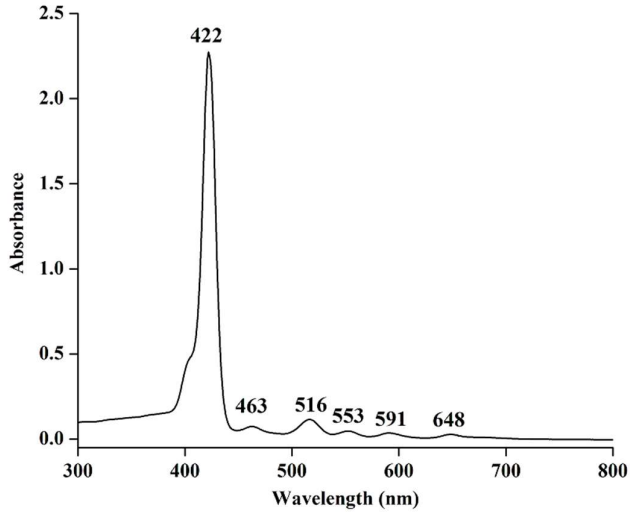

Figure A4.5. UV-visible spectrum of H_2TTMPP in CH_2Cl_2.

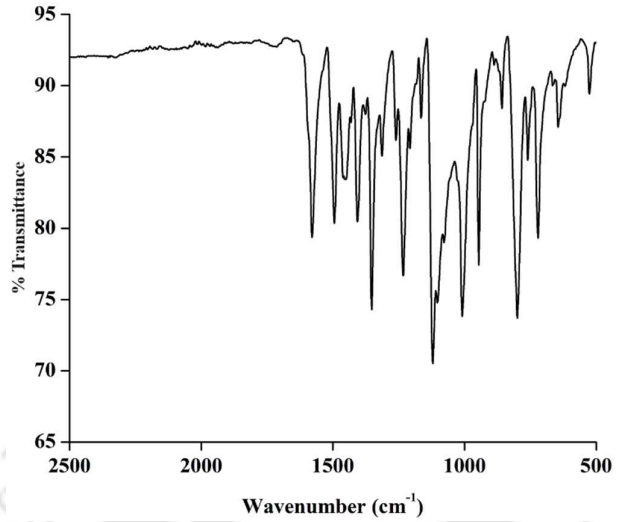

Figure A4.6. FT-IR spectrum of complex **5.1** in ATR probe.

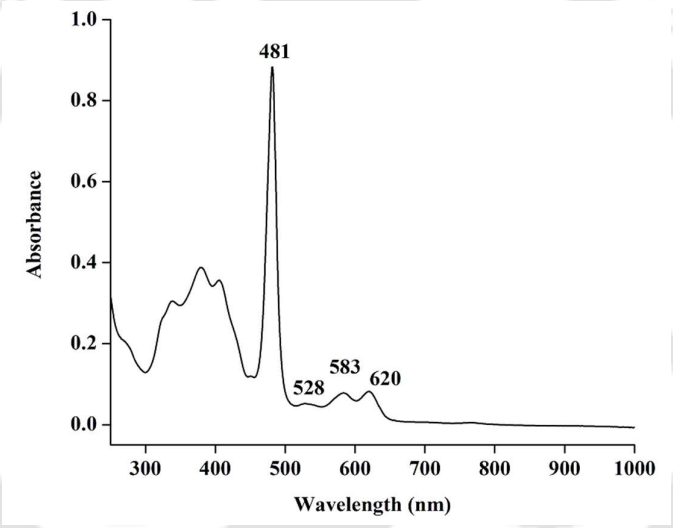

Figure A4.7. UV-visible spectrum of complex **5.1** in CH_2Cl_2 at room temperature.

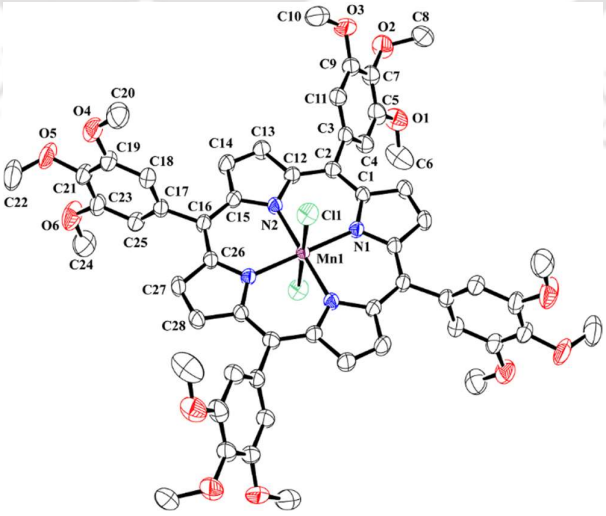

Figure A4.8. ORTEP diagram of complex **5.1** (showing 30% thermal ellipsoid. H-atoms are omitted for clarity).

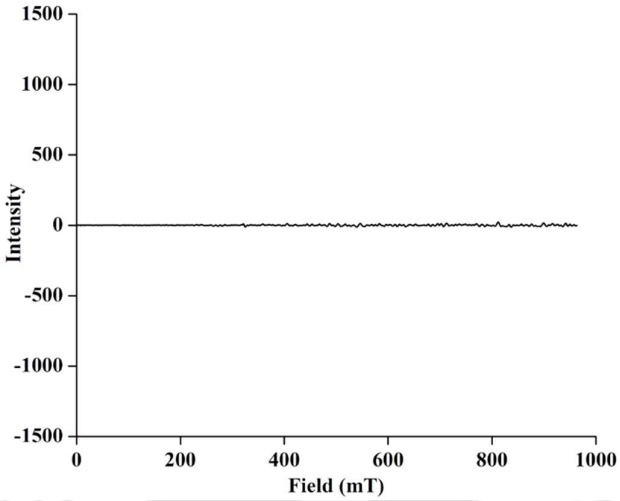

Figure A4.9. X-band EPR spectrum of complex **5.1** in CH_2Cl_2 at 77 K.

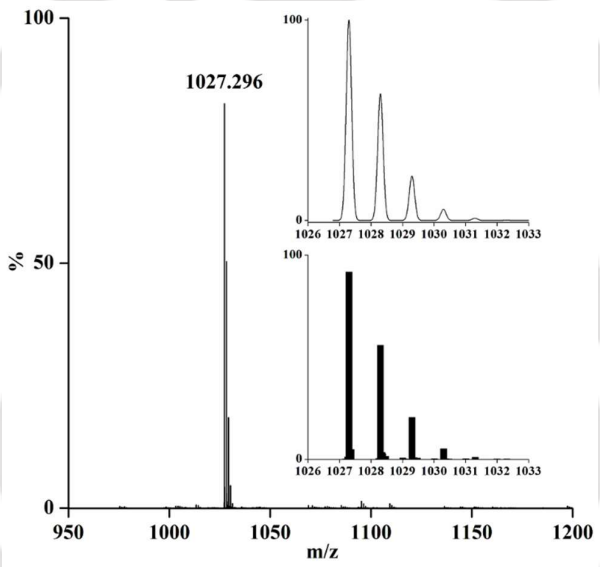

Figure A4.10. ESI-mass spectrum of complex **5.1** in CH_3OH (Calculated, 1027.296; Found, 1027.296, after loss of Cl^-, Inset: Isotopic distribution pattern (a) simulated, (b) experimental).

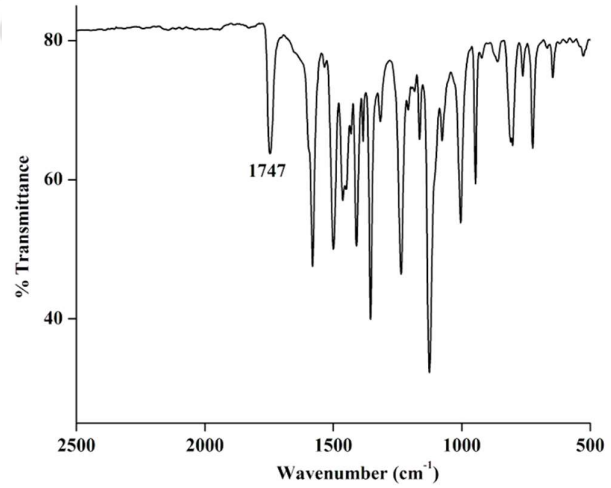

Figure A4.11. FT-IR spectrum of complex **5.2** in ATR probe.

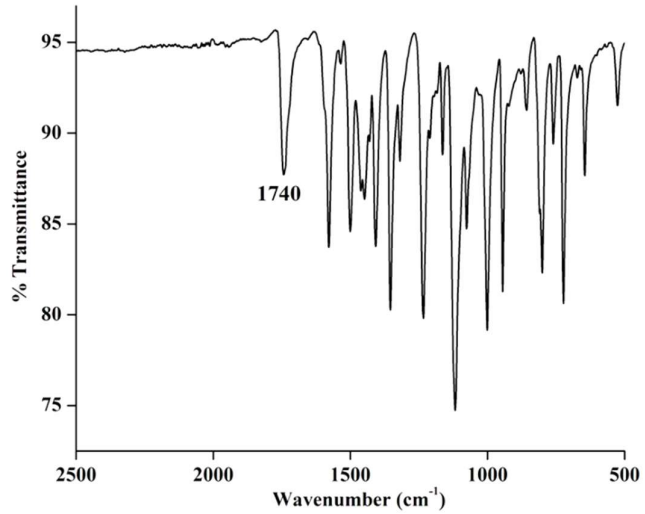

Figure A4.12. FT-IR spectrum of complex **5.2** in CH_2Cl_2 solution.

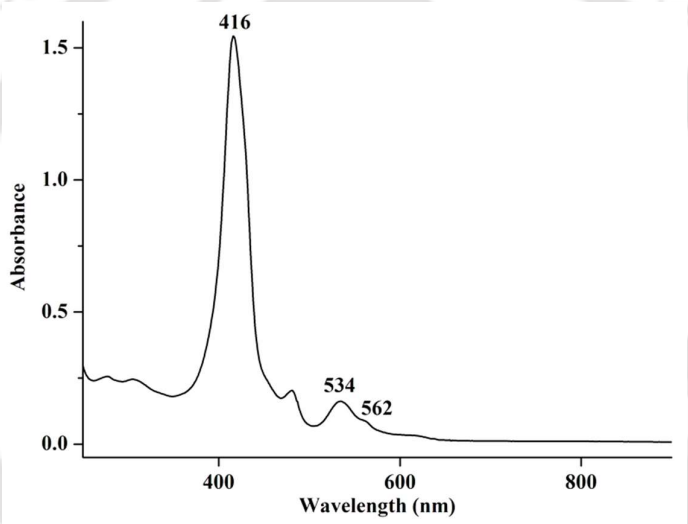

Figure A4.13. UV-visible spectrum of complex **5.2** in CH_2Cl_2 at -40 °C.

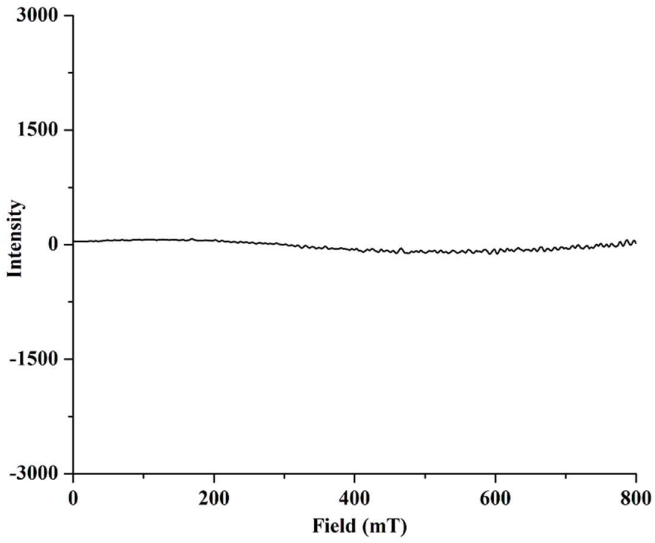

Figure A4.14. X-band EPR spectrum of complex **5.2** in CH_2Cl_2 at 77 K.

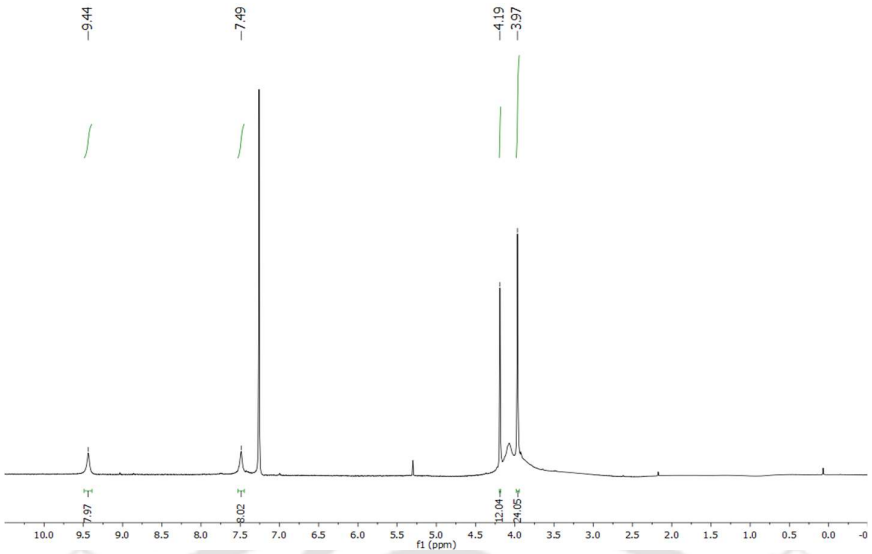

Figure A4.15. ^{1}H-NMR spectrum of complex **5.2** in $CDCl_3$.

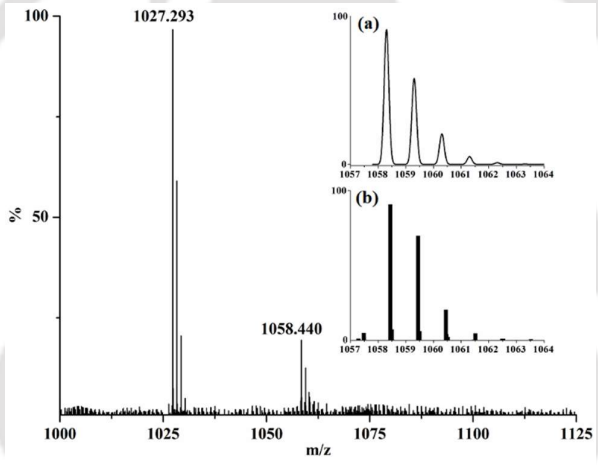

Figure A4.16. ESI-mass spectrum of complex **5.2** in CH_2Cl_2-CH_3OH (20:80) (Calculated, 1058.302; Found, 1058.440, $[M+H]^+$, Inset: Isotopic distribution pattern (a) simulated, (b) experimental).

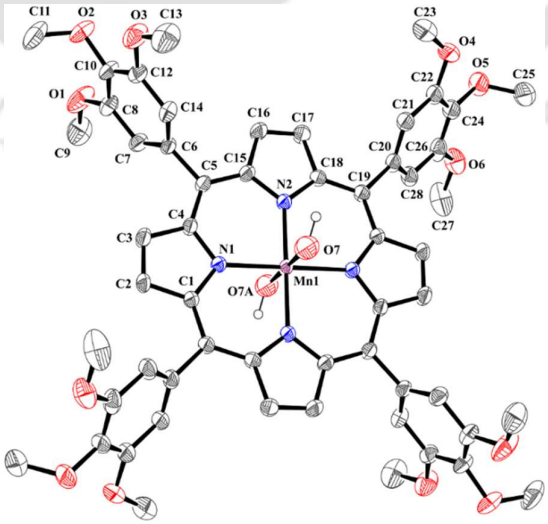

Figure A4.17. ORTEP diagram of complex **5.3** (40% thermal ellipsoid plot, H-atoms (except OH hydrogen) are omitted for clarity).

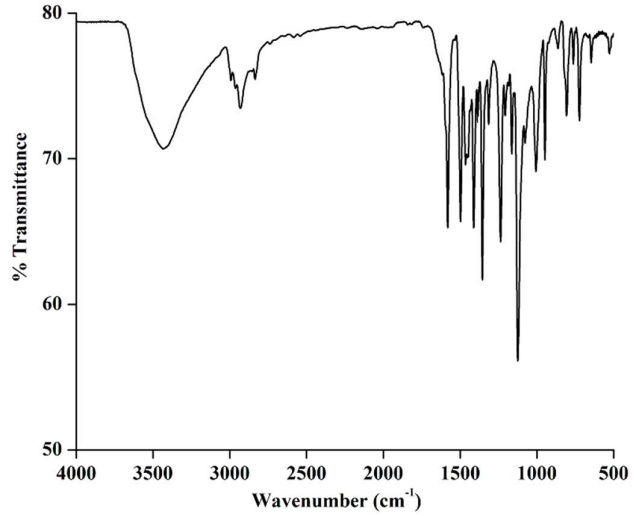

Figure A4.18. FT-IR spectrum of complex **5.3** in ATR probe.

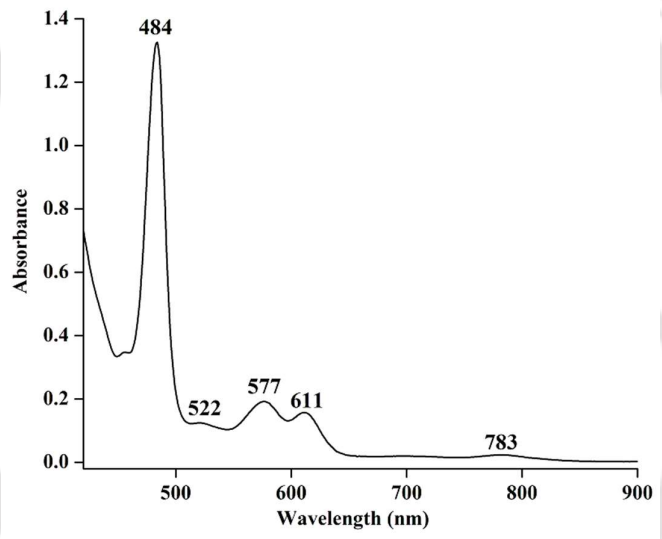

Figure A4.19. UV-visible spectrum of complex **5.3** in CH_2Cl_2 at room temperature.

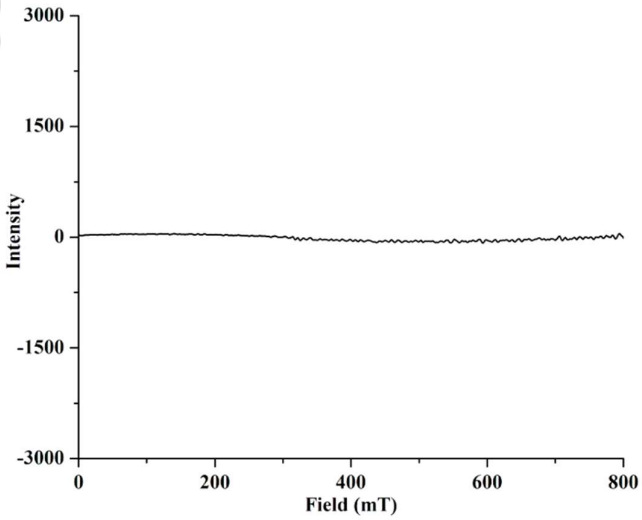

Figure A4.20. X-band EPR spectrum of complex **5.3** in CH_2Cl_2 at 77 K.

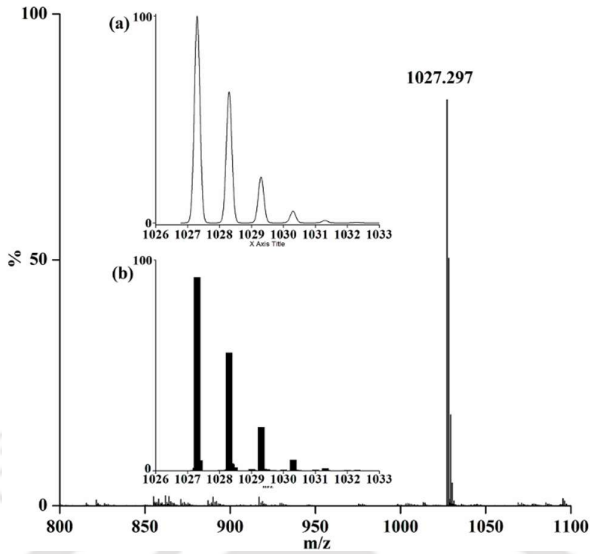

Figure A4.21. ESI-mass spectrum of complex **5.3** in CH_3OH (Calculated, 1027.296; Found, 1027.297. after loss of OH^-, Inset: Isotopic distribution pattern (a) simulated, (b) experimental).

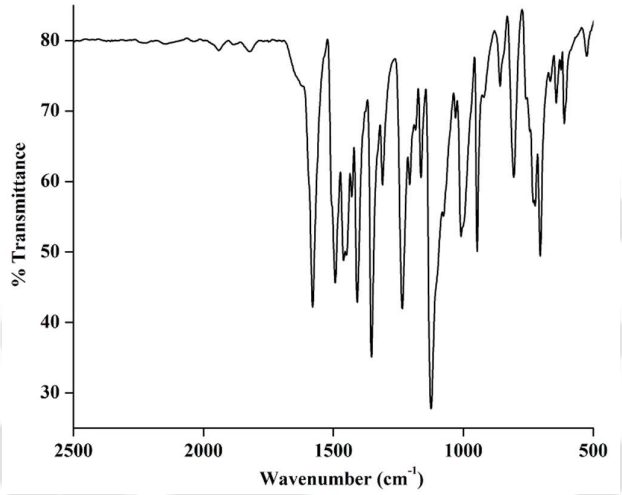

Figure A4.22. FT-IR spectrum of complex **5.4** in ATR probe.

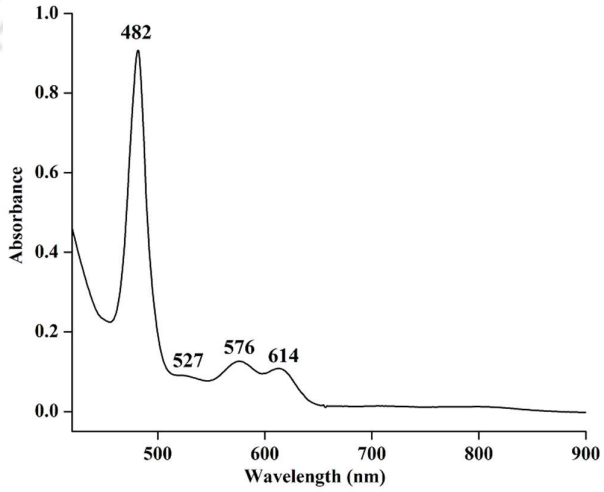

Figure A4.23. UV-visible spectrum of complex **5.4** in CH_2Cl_2 at room temperature.

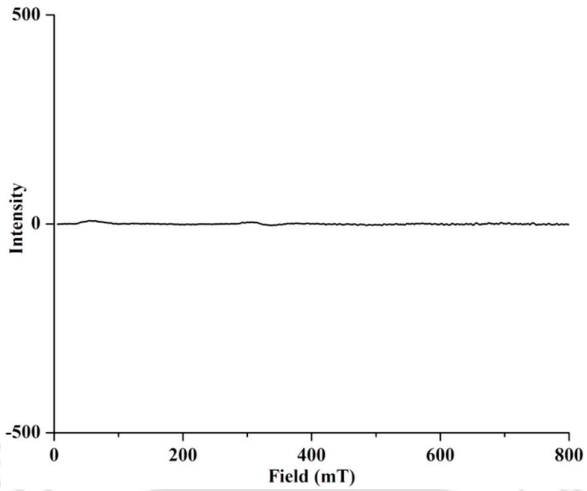

Figure A4.24. X-band EPR-spectrum of complex **5.4** in CH_2Cl_2 at 77 K.

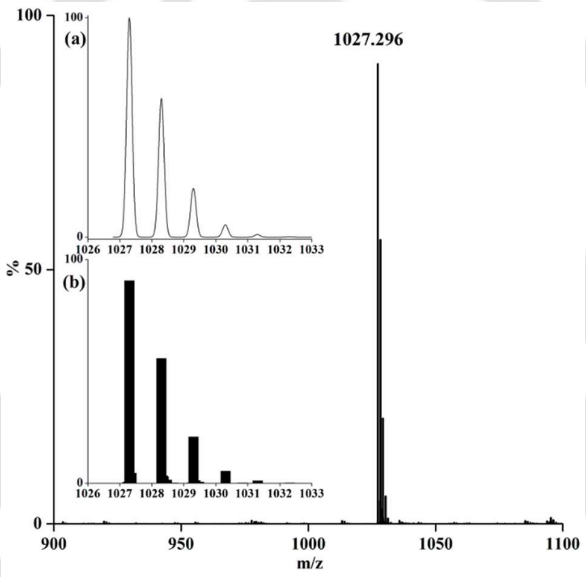

Figure A4.25. ESI-mass spectrum of complex **5.4** in CH_3OH (Calculated, 1027.296; Found, 1027.296, after loss of BF_4^-, Inset: Isotopic distribution pattern (a) simulated, (b) experimental).

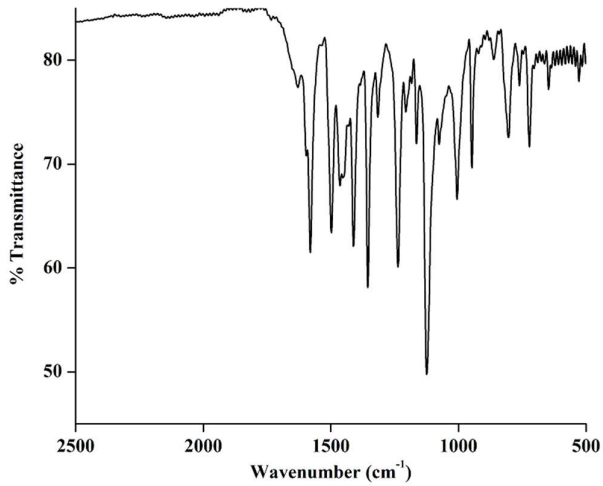

Figure A4.26. FT-IR spectrum of complex **5.5** in ATR probe.

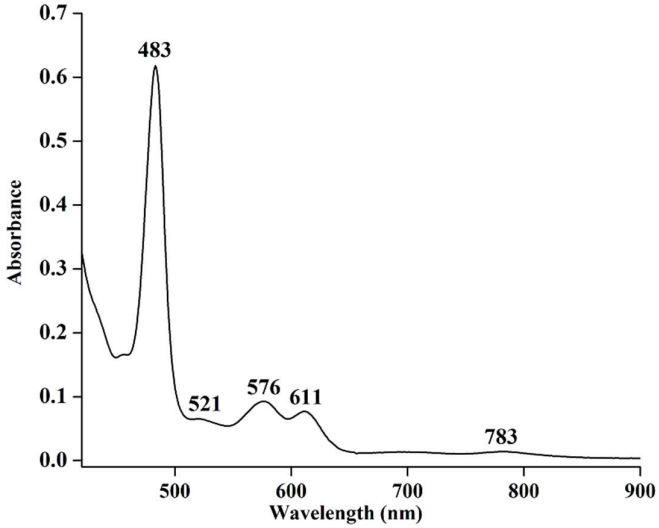

Figure A4.27. UV-visible spectrum of complex **5.5** in CH_2Cl_2 at room temperature.

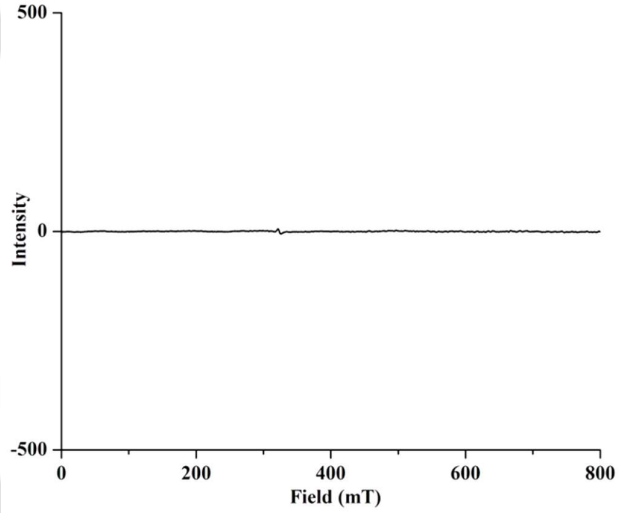

Figure A4.28. X-band EPR spectrum of complex **5.5** in CH_2Cl_2 at 77 K.

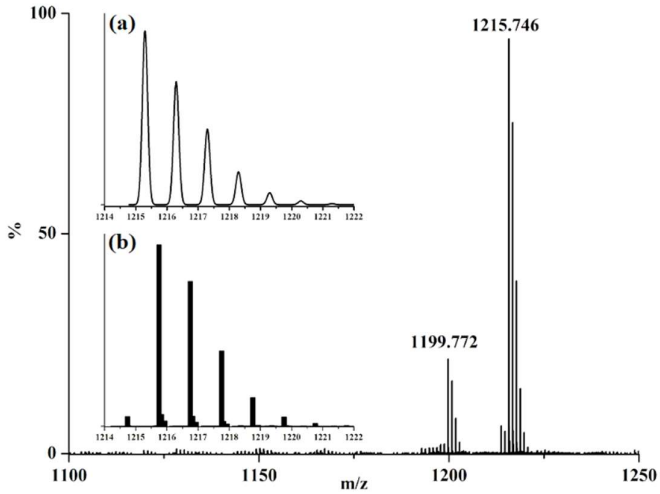

Figure A4.29. ESI-mass spectrum of complex **5.5** in CH_3OH (Calculated, 1215.346; Found, 1215.746 $[M+K]^+$, Inset: Isotopic distribution pattern (a) simulated (b) experimental).

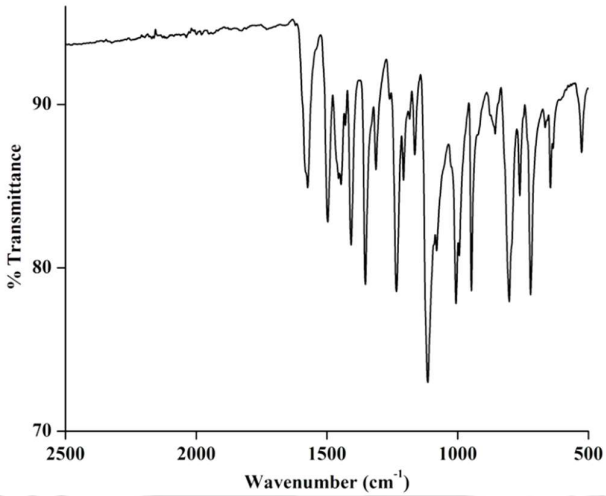

Figure A4.30. FT-IR spectrum of complex **5.1** isolated from reaction mixture in ATR probe.

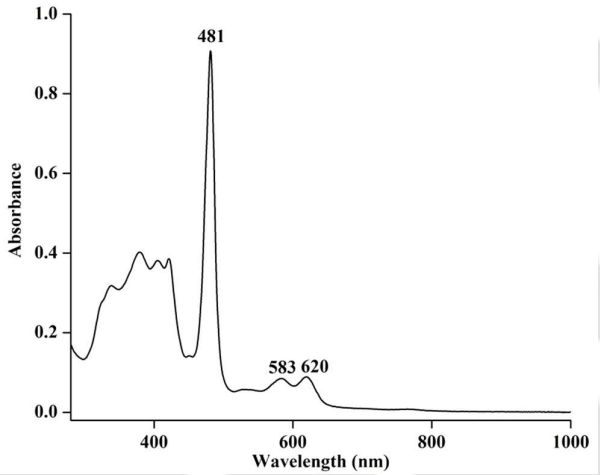

Figure A4.31. UV-visible spectrum of complex **5.1** isolated from reaction mixture in CH_2Cl_2 at room temperature.

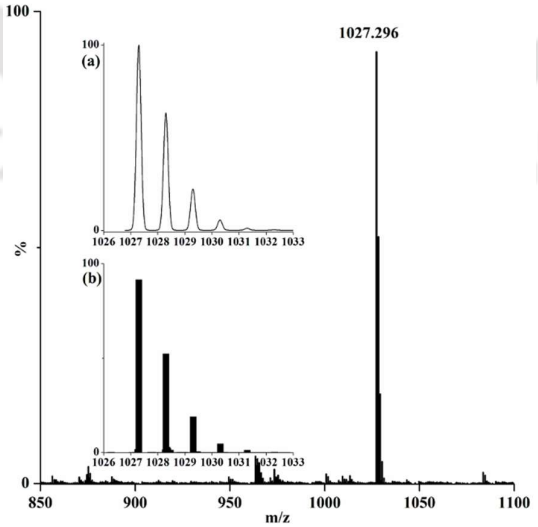

Figure A4.32. ESI-mass spectrum of complex **5.1** isolated from reaction mixture (Calculated, 1027.296; Found, 1027.296. after loss of Cl^-, Inset: Isotopic distribution pattern (a) simulated (b) experimental).

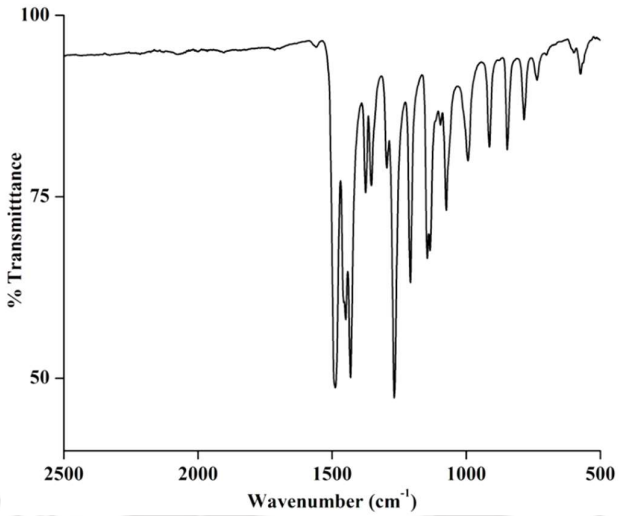

Figure A4.33. FT-IR spectrum of CH_2Cl_2 solution of $[Fe^{III}(DTC^{-})_3]$ after purging the headspace gas in ATR probe.

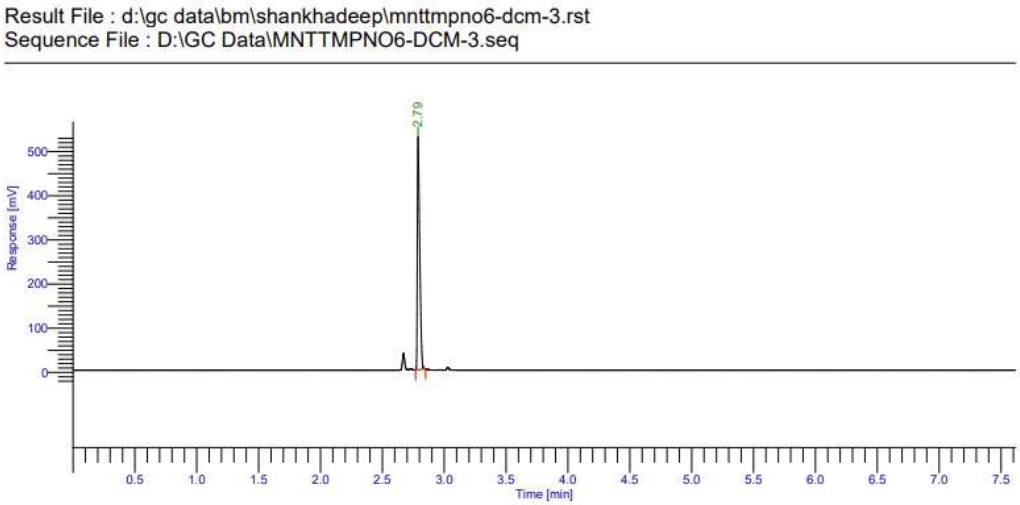

IIT Guwahati Chemistry Dept.

Peak #	Component Name	Time [min]	Area [uV*sec]	Height [uV]	Area [%]
1		2.788	704776.39	527521.17	100.00
			704776.39	527521.17	100.00

Figure A4.34. Gas chromatogram of standard N_2O (retention time = 2.79 minutes).

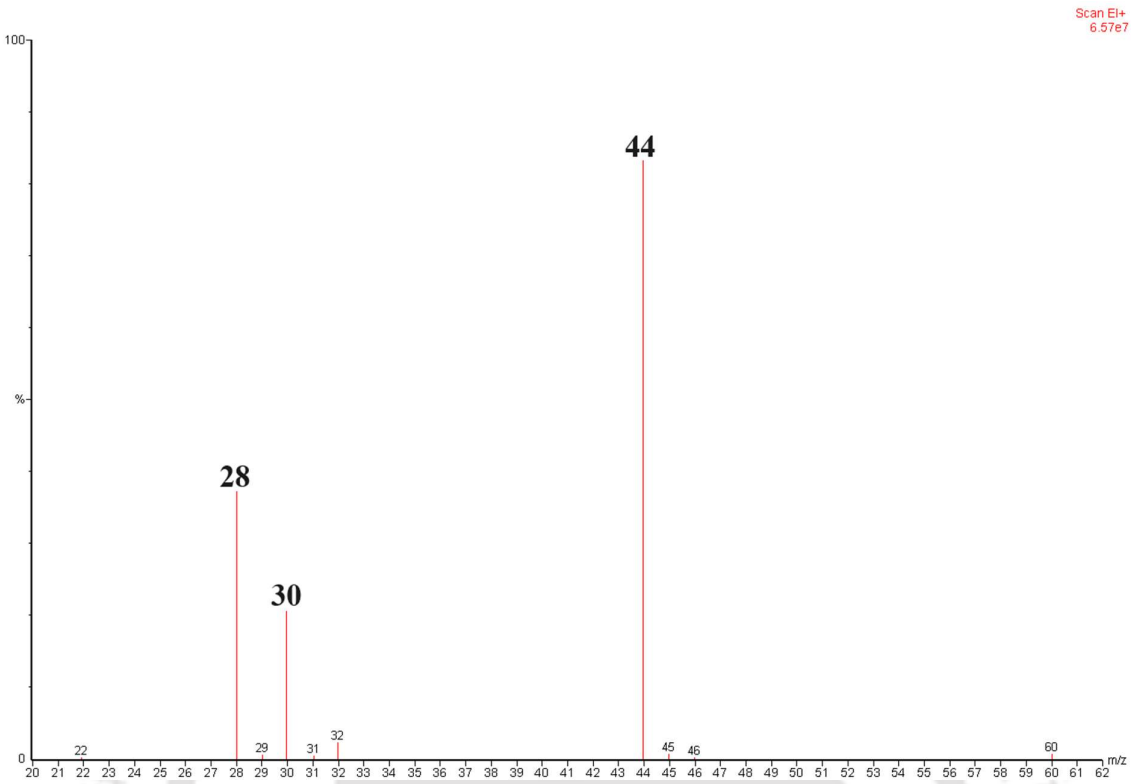

Figure A4.35. GC-mass spectrum of the headspace gas of the CH_2Cl_2 solution of complex **5.2**.

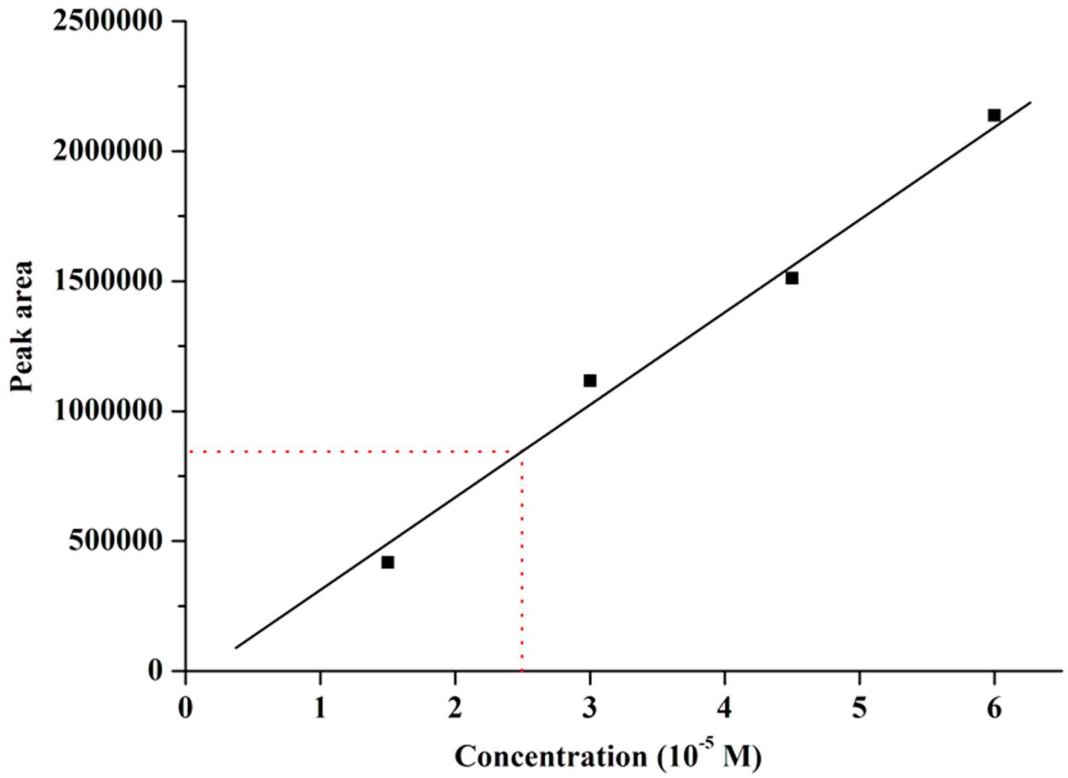

Figure A4.36. GC calibration curve for determination of amount of N_2O (red dot corresponds to the sample).

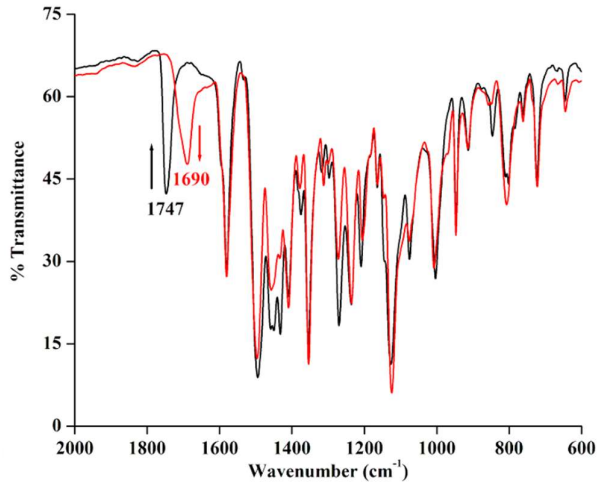

Figure A4.37. FT-IR spectrum of reaction mixture of complex **5.2** and [$Fe^{III}(DTC^{-})_3$] in ATR probe (Initial (Black); Final (red)).

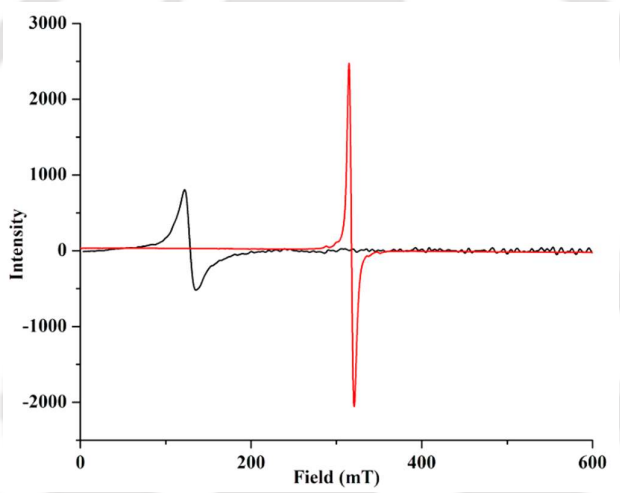

Figure A4.38. X-band EPR spectra of the reaction of [$Fe^{III}(DTC^{-})_3$] and complex **5.2** in CH_2Cl_2 at 77 K. (Initial (black) and final (red)).

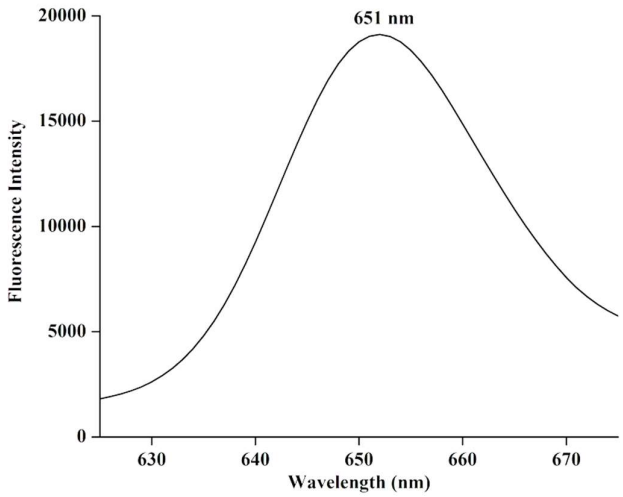

Figure A4.39. Fluorescence response (λ_{ex} = 420 nm) of complex **1** in dichloromethane solution at 298 K.

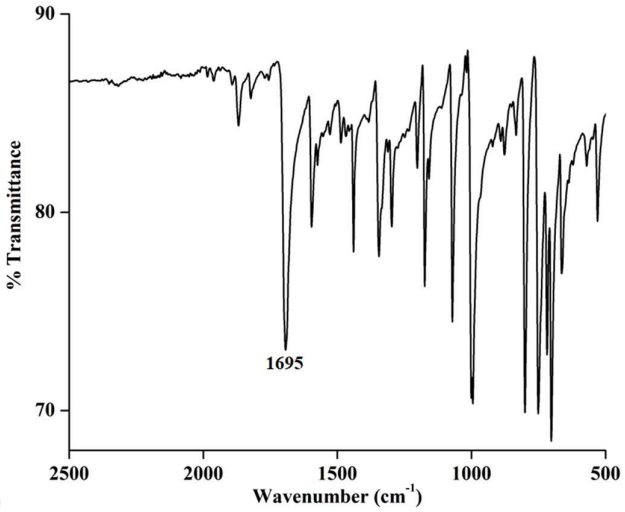

Figure A4.39. FT-IR spectrum of complex [Fe(TPP^{2-})(NO)] in ATR probe.

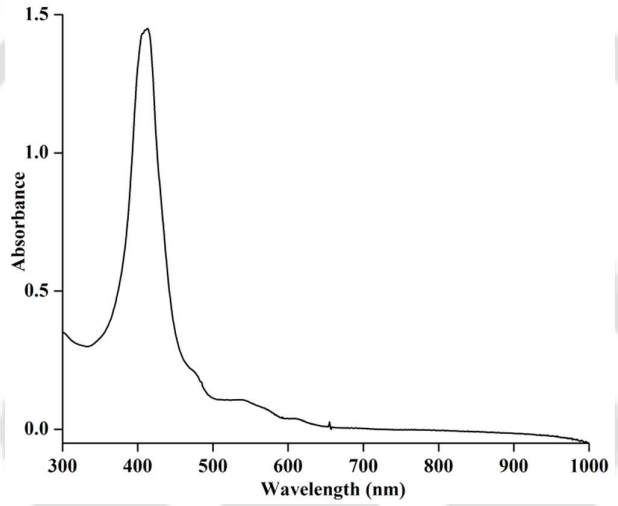

Figure A4.40. UV-visible spectrum of complex [Fe(TPP^{2-})(NO)] in CH_2Cl_2 at room temperature.

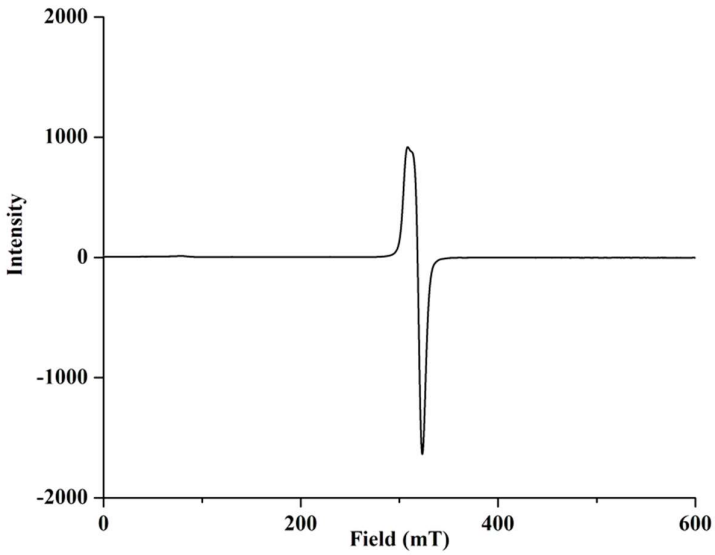

Figure A4.41. X-band EPR spectrum of [Fe(TPP^{2-})(NO)] in CH_2Cl_2 at 77 K.

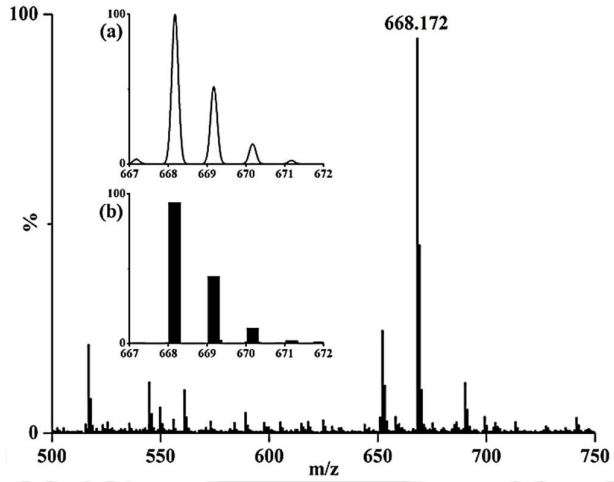

Figure A4.42. ESI-mass spectrum of [Fe(TPP^{2-})(NO)] in CH_3OH (Calculated, 668.166; Found, 668.172. after loss of NO, Inset: Isotopic distribution pattern (a) simulated (b) experimental).

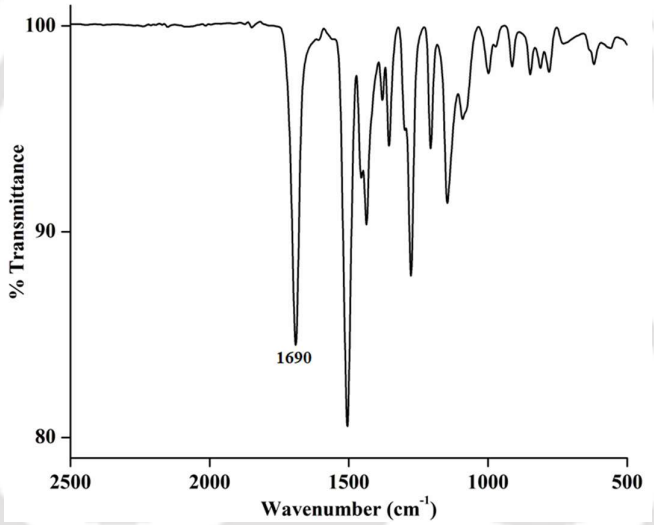

Figure A4.43. FT-IR spectrum of complex [Fe(DTC^{-})$_2$(NO)] in ATR probe.

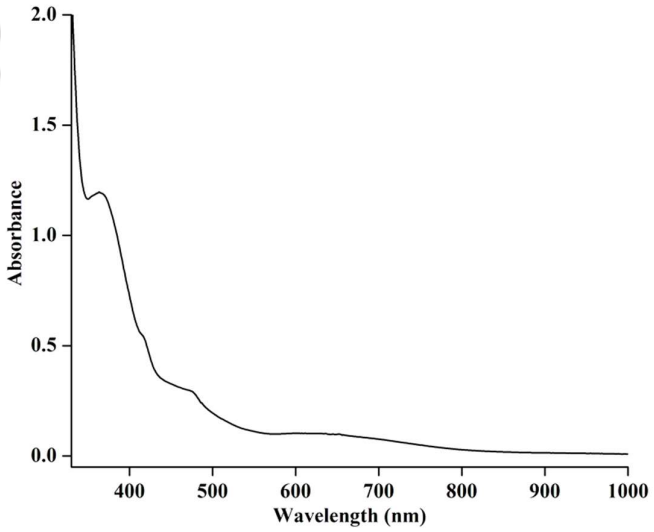

Figure A4.44. UV-visible spectrum of complex [Fe(DTC^{-})$_2$(NO)] in CH_2Cl_2 at room temperature.

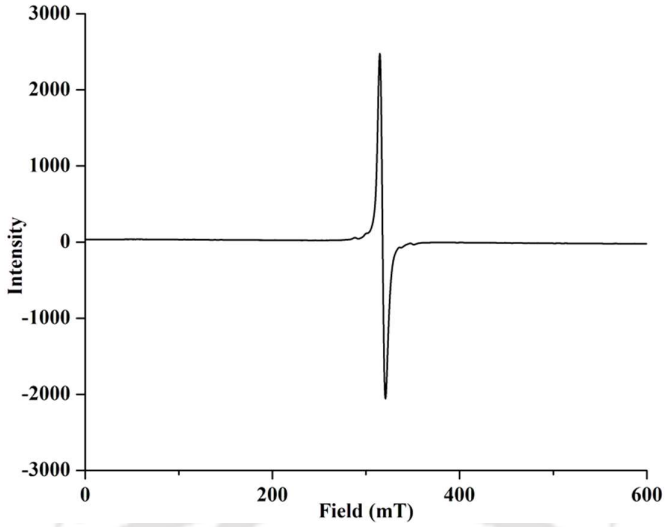

Figure A4.45. X-band EPR spectrum of $[Fe(DTC^{-})_2(NO)]$ in CH_2Cl_2 at 77 K.

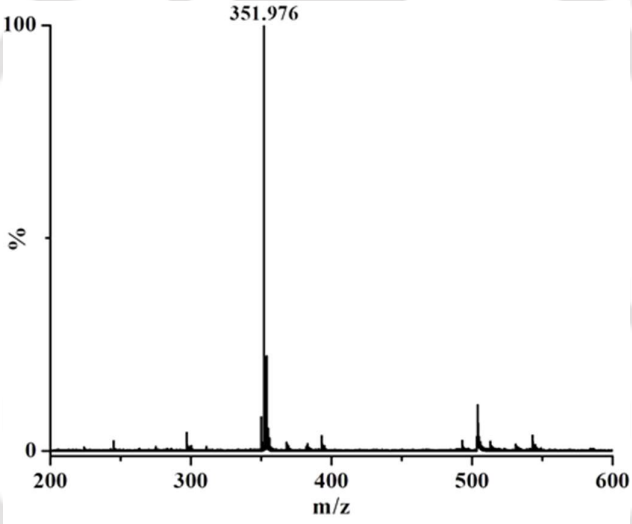

Figure A4.46. ESI-mass spectrum of $[Fe(DTC^{-})_2(NO)]$ in CH_3OH (Calculated, 351.986; Found, 351.976. after loss of NO, Inset: Isotopic distribution pattern (a) simulated (b) experimental).

Table 4.2. Crystallographic data for complexes **5.1**, **5.3** and **5.4**.

	5.1	**5.3**	**5.4**
Formulae	$C_{56}H_{52}N_4O_{12}Cl_2Mn$	$C_{56}H_{54}N_4O_{14}Mn$	$C_{83}H_{81}BN_4O_{14}Cl_3Mn$
Mol. wt.	1098.86	1061.97	1530.62
Crystal system	Triclinic	Triclinic	Monoclinic
Space group	P -1	P -1	P 21/c
Temperature /K	298(2)	298.0	297.00
Wavelength /Å	0.71073	0.71073	0.71073
a /Å	8.0273(4)	7.981(3)	15.425(5)
b /Å	12.4667(6)	12.383(5)	22.911(7)
c /Å	14.3129(7)	14.282(6)	25.451(8)

α/°	86.5190(10)	85.706(12)	90
β/°	75.1190(10)	76.649(12)	105.144(9)
γ/°	88.2800(10)	87.299(13)	90
V/ Å^3	1381.60(12)	1368.9(9)	8682(5)
Z	1	1	4
Density/Mgm^{-3}	1.321	1.288	1.171
Abs. Coeff. /mm^{-1}	0.400	0.309	0.304
Abs. correction	none	none	none
F(000)	571	555	3200
Total no. of reflections	4862	6126	19273
Reflections, $I > 2\sigma(I)$	4109	4129	12494
Max. 2θ/°	25.000	25.242	25.242
Ranges (h, k, l)	$-9 \le h \le 9$ $-14 \le k \le 14$ $-17 \le l \le 17$	$-10 \le h \le 10$ $-15 \le k \le 15$ $-18 \le l \le 18$	$-19 \le h \le 19$ $-29 \le k \le 29$ $-32 \le l \le 32$
Complete to 2θ (%)	0.998	0.976	0.995
Refinement method	Full-matrix least-squares on F^2	Full-matrix least-squares on F^2	Full-matrix least-squares on F^2
Goof (F^2)	1.053	1.059	1.073
R indices [$I > 2\sigma(I)$]	0.0615	0.0728	0.0960
R indices (all data)	0.0741	0.1118	0.1420

Table 4.3. Selected bond lengths (Å) of complexes **5.1**, **5.3** and **5.4**.

Atoms	**5.1**	**5.3**	**5.4**
Mn1-N1	2.011(2)	2.011(2)	2.008(3)
Mn1-N2	2.007(2)	1.992(3)	2.002(3)
Mn1-N3	-	-	2.003(3)
Mn1-N4	-	-	2.008(3)
Mn1-Cl1	2.5277(17)		-
Mn1-O7	-	2.098(5)	-
Mn1-O13	-	-	2.270(3)
Mn1-O14	-	-	2.261(3)

Table 4.4. Selected bond angles (˚) of complexes **5.1**, **5.3** and **5.4**.

Atoms	**5.1**	**5.3**	**5.4**
N1-Mn1-N2	90.86(10)	89.01(10)	90.03(13)
N1-Mn1-Cl1	90.26(9)	-	-
N2-Mn1-Cl1	89.46(9)	-	-
N1-Mn1-O7	-	90.05(12)	-
N2-Mn1-O7	-	88.44(12)	-
N2-Mn1-N3			89.74(13)
N3-Mn1-N4			89.86(13)
N4-Mn1-N1			90.36(13)

Cartesian coordinates of the optimized geometry of complex 5.2.

Mn	-0.000034000	-0.001739000	-0.242167000
N	0.000009000	-2.011752000	0.057420000
N	-2.003195000	-0.008335000	0.087777000
O	-5.928410000	-5.024330000	-2.349619000
O	5.147037000	-6.003362000	2.159715000
O	-5.146208000	-6.002720000	2.162768000
O	-6.400069000	-6.500650000	-0.147273000
O	6.400447000	-6.500106000	-0.150793000
O	5.928058000	-5.022899000	-2.352437000
C	2.840340000	-1.108989000	0.068674000
C	-2.840384000	-1.109069000	0.069127000
C	1.100078000	-2.849890000	0.028434000
C	4.220280000	-0.691008000	0.112759000
H	5.066677000	-1.361547000	0.124789000
C	-3.497168000	-3.502350000	-0.011001000
C	-3.783676000	-4.250110000	1.135852000
H	-3.231210000	-4.048563000	2.044559000
C	4.199065000	-3.730462000	-1.201049000
H	3.958422000	-3.138244000	-2.074533000
C	2.436695000	-2.445559000	0.029648000
C	3.497237000	-3.502189000	-0.012551000
C	-5.189600000	-4.722105000	-1.243062000
C	-2.436686000	-2.445629000	0.030514000
C	-4.199245000	-3.731226000	-1.199234000
H	-3.958864000	-3.139379000	-2.073042000
C	4.781709000	-5.235746000	1.094127000
C	4.221498000	0.669397000	0.139356000
H	5.069462000	1.337083000	0.172767000
C	3.784090000	-4.250434000	1.133899000
H	3.231816000	-4.049351000	2.042824000
C	-1.100053000	-2.849911000	0.028942000
C	5.189508000	-4.721219000	-1.245553000
C	-4.781191000	-5.235552000	1.096750000
C	0.680256000	-4.229414000	-0.018339000
H	1.349005000	-5.076577000	-0.053298000
C	-5.483822000	-5.483270000	-0.096643000
C	5.484101000	-5.482849000	-0.099536000
C	-0.680223000	-4.229427000	-0.017972000
H	-1.348972000	-5.076605000	-0.052572000
C	4.452668000	-5.827668000	3.389070000
H	4.583730000	-4.811645000	3.783960000
H	4.894397000	-6.545273000	4.081743000
H	3.381511000	-6.040371000	3.278868000
C	-4.451433000	-5.826550000	3.391827000
H	-3.380295000	-6.039192000	3.281326000
H	-4.892863000	-6.543959000	4.084894000
H	-4.582454000	-4.810407000	3.786419000
C	-7.767314000	-6.080857000	-0.058501000
H	-7.953397000	-5.571481000	0.895682000
H	-8.369295000	-6.990389000	-0.109147000
H	-8.027768000	-5.420360000	-0.893644000

C	5.655943000	-4.319600000	-3.560350000
H	4.621941000	-4.478815000	-3.891114000
H	6.341159000	-4.732154000	-4.301967000
H	5.842331000	-3.243614000	-3.449437000
C	-5.656639000	-4.321564000	-3.557919000
H	-5.843091000	-3.245543000	-3.447456000
H	-6.341998000	-4.734514000	-4.299183000
H	-4.622703000	-4.480845000	-3.888856000
C	7.767696000	-6.080201000	-0.062591000
H	8.027712000	-5.419555000	-0.897748000
H	8.369727000	-6.989676000	-0.113645000
H	7.954170000	-5.570956000	0.891587000
N	-0.000076000	1.992906000	0.121235000
N	2.003108000	-0.008299000	0.087784000
O	5.948454000	5.036615000	2.487865000
O	-5.075040000	6.008528000	-2.011728000
O	5.075685000	6.009175000	-2.008809000
O	6.364812000	6.518984000	0.280431000
O	-6.364897000	6.519102000	0.276945000
O	-5.949333000	5.037425000	2.484955000
C	-2.841995000	1.090862000	0.126814000
C	2.841863000	1.090914000	0.127388000
C	-1.100192000	2.829487000	0.174852000
C	-4.221616000	0.669301000	0.138840000
H	-5.069610000	1.336970000	0.171852000
C	3.492468000	3.489590000	0.191177000
C	3.750645000	4.241638000	-0.959573000
H	3.183655000	4.035219000	-1.858162000
C	-4.212626000	3.726234000	1.365724000
H	-3.993651000	3.132643000	2.243964000
C	-2.437552000	2.427283000	0.158686000
C	-3.492642000	3.489577000	0.189574000
C	5.192652000	4.727087000	1.394465000
C	2.437382000	2.427314000	0.159611000
C	4.212088000	3.725835000	1.367632000
H	3.992806000	3.131972000	2.245612000
C	-4.737622000	5.237410000	-0.939947000
C	-4.220342000	-0.691118000	0.112966000
H	-5.066714000	-1.361683000	0.125290000
C	-3.750409000	4.241265000	-0.961503000
H	-3.183120000	4.034544000	-1.859835000
C	1.100011000	2.829498000	0.175367000
C	-5.193168000	4.727527000	1.391914000
C	4.737886000	5.237741000	-0.937378000
C	-0.680340000	4.205069000	0.289437000
H	-1.349426000	5.048224000	0.376775000
C	5.458340000	5.492258000	0.243898000
C	-5.458442000	5.492339000	0.241015000
C	0.680087000	4.205071000	0.289788000
H	1.349115000	5.048235000	0.377467000
C	-4.361834000	5.822896000	-3.229347000
H	-4.497828000	4.807840000	-3.624709000
H	-4.783686000	6.544474000	-3.930178000
H	-3.290461000	6.023551000	-3.101078000
C	4.362694000	5.824130000	-3.226642000

H	3.291307000	6.024785000	-3.098483000
H	4.784720000	6.545994000	-3.927073000
H	4.498706000	4.809244000	-3.622437000
C	7.733337000	6.113612000	0.153091000
H	7.899928000	5.613874000	-0.809696000
H	8.327694000	7.028532000	0.196202000
H	8.021318000	5.448835000	0.975835000
C	-5.709482000	4.330103000	3.696733000
H	-4.680609000	4.477486000	4.048705000
H	-6.404816000	4.749249000	4.425171000
H	-5.905462000	3.256228000	3.580933000
C	5.708116000	4.328968000	3.699357000
H	5.904093000	3.255117000	3.583333000
H	6.403196000	4.747881000	4.428171000
H	4.679118000	4.476300000	4.050982000
C	-7.733358000	6.113728000	0.148930000
H	-8.021772000	5.449052000	0.971607000
H	-8.327734000	7.028656000	0.191621000
H	-7.899449000	5.613872000	-0.813882000
N	-0.000042000	0.021054000	-1.840491000
O	-0.000076000	0.042523000	-3.019390000

List of Publications

1. "Can a Nitrosyl of a Mn(II)–Porphyrin Complex Release Nitroxyl/HNO"

   Rakesh Mazumdar, **Shankhadeep Saha**, Bapan Samanta, and Biplab Mondal.

   Inorg. Chem., **2021**, *60,* 18024.

2. "Reaction of a $\{Co(NO)\}^8$ complex with superoxide: Formation of a six coordinated $[Co^{II}(NO)(O_2^{-})]$ species followed by peroxynitrite intermediate"

   Rakesh Mazumdar, Baisakhi Mondal, **Shankhadeep Saha**, Bapan Samanta, and Biplab Mondal.

   J. Inorg. Biochem., **2022**, 228, 111698. (invited article)

3. "Reaction of a nitrosyl complex of Mn(II)–porphyrinate with superoxide: NOD activity is favoured over SOD activity"

   Rakesh Mazumdar, **Shankhadeep Saha**, Bapan Samanta, Riya Ghosh, Sayani Maity, and Biplab Mondal.

   Dalton Trans., **2023**, 52, 7917.

4. "Reaction of a Co(III)-peroxo complex with nitric oxide: putative formation of a peroxynitrite intermediate"

   Bapan Samanta, Riya Ghosh, Rakesh Mazumdar, **Shankhadeep Saha**, Sayani Maity, and Biplab Mondal.

   Dalton Trans., **2023**, *52,* 15815.

5. "Sixth ligand induced HNO/NO^- release by a five-coordinated cobalt(II) nitrosyl complex having a $\{CoNO\}^8$ configuration"

   Shankhadeep Saha, Sayani Maity, Rakesh Mazumdar, Bapan Samanta, Riya Ghosh, Ankur Kanti Guha, and Biplab Mondal.

   Inorg. Chem., **2023**, *62,* 17074.

6. “Insights into oxidovanadium (3,4,5-trimethoxyphenyl) porphyrin: A comprehensive study of synthesis, crystal structure, Hirshfeld surface analysis and computational studies”

   Ijaz Ullah Muzaddadi, Arumugam Murugan, Madhukar Hemamalini, Muhammed Nawaz Tahir, **Shankhadeep Saha**, Bipul Bezbaruah, Mohammad Farid Hussain, Vijay Kumar Mandal and Benzir Ahmed

   J. Mol. Struct. **2024**, 1315, 138764

7. “Photo-induced nitroxyl anion/HNO release from a nitrosyl complex of Mn(II) porphyrinate”

   Shankhadeep Saha, Sayani Maity, Bapan Samanta, Kalishankar Bhattacharyya, and Biplab Mondal.

   (Under revision)

8. “Reaction of a non-heme iron-nitrosyl with dioxygen: Self-killing through NOD-like activity”

   Riya Ghosh, Bapan Samanta, Rakesh Mazumdar, **Shankhadeep Saha**, and Biplab Mondal.

   (Communicated)

9. “Reaction of a Nitrosyl Complex of Co(II)-porphyrin with Hydrogen peroxide: Formation of a Porphyrin Radical Cation”

   Bapan Samanta, **Shankhadeep Saha**, Riya Ghosh, Sayani Maity and Biplab Mondal. (Communicated).